ČESKÉ VYSOKÉ UČENÍ TECHNICKÉ V PRAZE

Fakulta stavební

Experimentální centrum

Investigating the bond behaviour of steel bars in concrete under high loading rates

O soudržnosti ocelové výztuže s betonem při vysokých rychlostech zatěžování

DISERTAČNÍ PRÁCE

Ing. Petr Máca

Doktorský studijní program: Stavební inženýrství

Studijní obor: Fyzikální a materiálové inženýrství

Školitel: prof. Ing. Petr Konvalinka, CSc.
Univ.-Prof. Dr.-Ing. Dr.-Ing. E. h. Manfred Curbach
Ing. Radoslav Sovják, Ph.D.

Praha, 2017

ČESKÉ VYSOKÉ UČENÍ TECHNICKÉ V PRAZE
Fakulta stavební
Thákurova 7, 166 29 Praha 6

PROHLÁŠENÍ

Jméno doktoranda: Petr Máca

Název disertační práce:
Investigating the bond behaviour of steel bars in concrete under high loading rates,
O soudržnosti ocelové výztuže s betonem při vysokých rychlostech zatěžování.

Prohlašuji, že jsem uvedenou doktorskou disertační práci vypracoval/a samostatně pod vedením školitele prof. Ing. Petra Konvalinky, CSc. .
Použitou literaturu a další materiály uvádím v seznamu použité literatury.

Disertační práce vznikla v souvislosti s řešením projektu: "Verbund zwischen Beton und Bewehrungsstahl bei hohen Belastungsgeschwindigkeiten" - Fkz.:150148627

v Praze dne 27.2.2017

podpis

Abstract

Reinforced concrete structures are increasingly subjected to extreme loading events such as impacts, explosions and earthquakes. Because reinforced concrete is a composite material, good load transfer between concrete and reinforcing steel is required. Such load transfer is provided by an adequate bond. The bond stress-slip relationships were studied under quasi-static and high loading rates ranging from 0.01 mm/s to 10 m/s. Only deformed bars were investigated in this dissertation where deep insight into experimental setup and techniques is provided. The theory of wave propagation through an elastic body is used to analyse the measured results. Bond stress-slip relationships for impact loading were obtained during push-in and pull-out tests. A new specimen geometry which is more suitable for impact testing was proposed in this work. The experimental program included setting up a drop-tower which was produced sufficiently long loading pulse which led to the failure of the bond zone. Also, high rate push-in tests were performed in modified split Hopkinson pressure bar. The used experimental setup and the evaluation process of the recorded data were described. Engineering strains measured on the steel rebar were utilised to evaluate the bond stress, which was thereupon put into relation to the slip. Several aspects that influence the bond strength were discussed both for quasi-static and impact loading. The importance of different slip measurement approaches on the overall bond stress-slip relationship was illustrated. In addition, the influence of the inertia of the specimen on the obtained data was discussed. It was shown that in the case of non-direct measurements, the inertial effects must be considered during the data evaluation process. The main focus of this work was on experimental techniques and evaluation methods. Therefore, only one concrete class with an average compressive strength of 51 MPa was studied. The results show that it is not possible to define the bond stress or slip rate as a single value as they change in time. It was concluded that higher loading rates increase the bond strength. However, this increase is only up to 30%, and it is much lower than it was expected. In all investigated cases, the failure mechanism was caused by shearing off the concrete cantilevers between the steel ribs. No change in failure mode was observed based on the loading rate or type of loading. Nearly negligible influence of loading type was observed. In most cases, the bond resistance for push-in loading was higher in comparison to the pull-out type of loading.

Keywords: bond stress; concrete; steel; impact loading; pull-out; push-in; SHB; experimental testing.

Abstrakt

Závislost napětí soudržnosti na prokluzu výztuže vzhledem k betonu byla zkoumána při kvazistatických a vysokých rychlostech zatěžování v rozmezí od 0,01 mm/s do 10 m/s. V této disertační práci, která poskytuje hluboký náhled do experimentálních technik a zkoušení, byla zkoumána pouze výztuž s žebírky. K analýze naměřených výsledků byla použita teorie šíření vln v elastickém prostředí. Vztah napětí soudržnosti a prokluzu výztuže při rázovém zatížení byl měřen na vzorcích, ve kterých je výztuž vtlačována do betonu (push-in) a vzorcích ve kterých je výztuž vytahována z betonu (pull-out). V této práci byl navržen nový válcový typ vzorku, který je vhodnější pro rázové zatěžovací zkoušky. Experimentální program zahrnoval sestavení a odzkoušení padacího zařízení, které by poskytlo dostatečně dlouhý rázový impuls vedoucí k porušení soudržnosti. Kromě toho byly provedeny také push-in zkoušky při vysokých rychlostech zatížení v zařízení zvaném „split Hopkinson bar“. V práci je detailně popsán použitý postup při návrhu a vyhodnocování experimentů. Poměrná deformace měřená přímo na ocelové výztuži pomocí tenzometrů byla použita k vypočítání napětí soudržnosti, které bylo přiřazeno k příslušným hodnotám prokluzu výztuže. Byly zkoumány mnohé vlivy, které mají vliv na soudržnost oceli s betonem a to jak při kvazistatickém tak při rázovém zatěžování. V práci byl objasněn vliv rozdílných přístupů k měření prokluzu výztuže. Kromě toho byl také analyzován vliv setrvačnosti vzorku na výsledky. Bylo ukázáno, že v případě nepřímých měření není možné setrvačnost zanedbat. Hlavním cílem této práce bylo sestavení a kalibrace zkušebních zařízení, jakož i popsání experimentálních technik a metod pro vyhodnocování výsledků. Z důvodu vyloučení vlivu pevnosti betonu, byla studována pouze jedna třída s průměrnou pevností v tlaku 51 MPa. Výsledky ukazují, že při rázových zkouškách není možné definovat rychlost změny napětí soudržnosti nebo rychlost prokluzu jako konstantní hodnotu, protože jsou tyto rychlosti v průběhu experimentu značně proměnné. Z výsledků práce plyne, že při vysoké rychlosti zatěžování dochází k maximálně 30% navýšení soudržnosti, což je podstatně méně, než bylo předpokládáno. Ve všech popsaných případech došlo k porušení soudržnosti vlivem usmýknutí betonových konzolek mezi jednotlivými žebírky. Vzhledem k rychlosti nebo typu zatěžování nebyla pozorována žádná změna v módu porušení. Typ zatěžování se ukázal býti téměř zanedbatelný, nicméně ve většině případů byla naměřena větší soudržnost u vzorků typu push-in ve srovnání se vzorky typu pull-out.

Klíčová slova: soudržnost; beton; ocel; napětí; zatížení rázem; pull-out; push-in; SHB; experimentální analýza.

TO MY WIFE

Table of contents

Acknowledgement

The presented thesis was written as a part of a research programme funded by the German Federal Ministry of Economic Affairs and Energy (BMWi, project no. 1501486) on the basis of a decision by the German Bundestag. Therefore, the author would like to thank the German government for the financial and material support.

The author would like to thank his supervisors Prof. Dr.-Ing. Dr.-Ing. E.h.Manfred Curbach and Prof. Ing. Petr Konvalinka, CSc. for their valuable advice and research ideas, as well as, their support not only on the scientific but also on the personal level. Many thanks go to the supervisor-specialist, Ing. Radoslav Sovják, Ph.D. for many fruitful conversations and valuable input to this work.

This work would not be possible without the staff of Otto-Mohr-Laboratorium, who helped during the preparation of the specimens as well as the testing. Special thanks go to Mrs Dietz and Ms Sonntag for their patience with the author's German skills. Also, the contribution of the students who cooperated on this project is greatly appreciated.

The author would like to thank all colleagues from the Institute of Concrete Structures at the TU Dresden and to colleagues from the Experimental Centre at the CTU in Prague. Special thanks go to Evmorfia Panteki who conducted the numerical simulations of the experimental results. The results of her work allowed to reduce the number of experiments and to choose the optimal experimental setup. Many thanks also go to the author’s colleague Matthias Quast who was always prepared to answer project relevant as well as irrelevant questions and who always brought valuable input during the productive discussions.

Without the financial and moral support of author’s wife and his family, this work would never be possible. They showed a great deal of patience and understanding, while the work was written.

Used symbols

Latin uppercase

A	Area
A_c	Area of concrete cross-section
A_s	Steel rebar cross-section area
E	Modulus of elasticity
E_{cm}	Mean concrete modulus of elasticity
E_s	Steel modulus of elasticity
F	Force
$\dot{F}$	Force rate
I	Geometrical impedance
R_m	Steel ultimate tensile stress
R_p	Steel yielding stress
R_p	Proof plastic strength
V	Volume
Z	Sonic impedance

Latin lowercase

$\vec{a}$	Acceleration vector
$a_m, a_{1/4}, a_{3/4}$	Steel rib height in the middle, in ¼ and in ¾
b_s	Rebar rib width
c	Concrete cover
c	Wave propagation velocity
c_0, c_1, c_2	Wave velocities
c_s	Rib spacing
d_s	Reinforcement bar diameter
dt	Infinitesimal time increase
dx	Infinitesimal length increase
e	Width of longitudinal rib
f_{bd}	Bond design strength

f_c	Concrete compressive strength
$f_{c,cube}$	Concrete compressive strength measured on cubes
$f_{c,cm}$	Mean concrete compressive strength measured on cubes
f_{ck}	Characteristic concrete compressive strength (measured on cylinders)
f_{cm}	Mean concrete compressive strength (measured on cylinders)
f_{ctm}	Mean concrete tensile strength
$f_{ctm,f}$	Mean concrete flexural strength
$f_{ctm,sp}$	Mean concrete splitting tensile strength
f_R or f_r	Relative rib area
g	Gravitational acceleration
h	Height
h_s	Rib height
k	Spring stiffness
k_1	Exponent
l	Length
l_b	Bond length
m	Target (beam) mass, or just mass
m_0	Impactor mass
p	Transverse pressure/radial shear stress
s	Slip
s_{max}	Slip at maximal bond stress
s_{split}	Slip at splitting failure
t	Time or concrete age
u	Displacement
u_s	Steel reinforcement bar circumference
v	Target velocity after impact or just velocity
$\overline{v}$	Target velocity before impact
v_0	Impactor velocity after impact
$\overline{v}_0$	Impactor velocity before impact
v_i	Incident velocity
v_r	Reflected velocity
v_t	Transmitted velocity

Greek letters and symbols

$\emptyset$	Bar diameter
Λ	Compressive pulse length
α	Angle
α, α_1	Coefficient
$\beta, \beta_1, \beta_2, \beta_3$	Transverse rib inclination angle
$\beta_{cc}(t)$	Function to describe the strength development in time
β_w	Concrete compressive strength measured on 200 mm cubes
γ	Coefficient
δ_c	Concrete displacement
δ_s	Steel displacement
ε	Engineering strain
$\dot{\varepsilon}$	Strain rate
ε_c and ε_s	Engineering strain in concrete and steel
ε_i	Incident strain
ε_r	Reflected strain
ε_t	Transmitted strain
ν	Poisson ratio
ρ	Density
σ	Stress
$\dot{\sigma}$	Stress rate
σ_c	Stress in the concrete
σ_i	Incident stress
σ_r	Reflected stress
σ_s	Stress in the steel rebar
σ_t	Transmitted stress
τ	Local bond stress or just bond stress
$\dot{\tau}$	Bond stress rate
τ_m	Mean bond stress
τ_{max}	Maximal bond stress, i. e. bond strength
$\tau_{max,loc}$	Local maximal bond stress
τ_{split}	Bond stress at splitting failure

Notation and Abbreviations

ACI	American Concrete Institute
ASTM	American Society for Testing and Materials
BSt	Bewehrungsstahl (Reinforcing steel)
CEB	Comité euro-international du béton (European Committee for Concrete)
CFC	Channel frequency class
CFRP	Carbon fibre reinforced polymer
DIC	Digital image correlation
DIF	Dynamic increase factor
DIN	Deutsches Institut für Normung (German Institute for Industrial Normalisation)
FIB	Fédération internationale du béton (International Federation for Structural Concrete)
FIP	Fédération Internationale de la Précontrainte (International Federation for Prestressing)
HSSCC	High strength self-compacting concrete
IB1	Incident bar 1
IB2	Incident bar 2
IIR	Infinite impulse response
LVDT	Linear variable differential transformer
LVDT	Linear variable differential transformer (transducer)
MC	Model code
MC2010	Model Code 2010
PhD or Ph.D.	Doctor of Philosophy
PTFE	Polytetrafluoroethylene (Teflon®)
RB or rebar	Reinforcement bar
RILEM	Reunion Internationale des Laboratoires et Experts des Materiaux, Systemes de Construction et Ouvrages (International Union of Laboratories and Experts in Construction Materials, Systems, and Structures)
SAE	Society of Automotive Engineers
SHB	Split Hopkinson bar
SHPB	Split Hopkinson pressure bar

Chapter 1

Introduction

1.1 Motivation

The main motivation of this work is to study the possible increase in bond strength of reinforced concrete when subjected to higher loading rates. The reason for this is very simple. At present, many structures of strategic importance such as nuclear power stations, commercial centres, military as well as government buildings or infrastructure are threatened by terrorist attacks and other types of extreme load events like earthquakes, gas explosions and car or plane impacts. Most of the structures mentioned above are made partly or exclusively of reinforced concrete. It is well known that the behaviour of a composite material such as reinforced concrete depends not only on the behaviour of its components, i.e. steel and concrete, but also on its interaction.

In civil engineering, the bond behaviour is usually described as a bond stress corresponding to a certain value of reinforcement bar slip. In general, three failure mechanisms can be identified: pure pull-out or push-in, splitting of the concrete cover and the combination of the both mechanisms. The local bond stress is usually investigated by the so-called pull-out test [1] on short bond lengths. In the case of small bar diameters and short bond lengths, the test can be modified to push-in setup without significant influence. This test setup is then more suitable for impact loading measurements.

Many research teams reported that the measured strength of concrete [2] as well as the strength of reinforcing steel [3, 4] rise with high loading rates. This phenomenon is usually called the strain rate effect, and it is summarised for instance in the ACI report on Dynamic Fracture of Concrete [5] and CEB report No. 184 [6]. Usually, the strain rate

effect has been studied separately for steel and concrete, and it is significantly different for concrete compressive strength in comparison with tensile strength [7, 8].

In order to take advantage of the increased strengths for the design of impact exposed buildings, as described above, it is important to ensure that the bond between concrete and steel can also withstand the respective loading. In addition, it is important to fully understand the failure mechanisms and other specifics of the bond strength under impact loading. This work, therefore, attempts to make a small contribution in this area of research.

1.2 Hypothesis

The main hypothesis of this work is that the bond strength between steel and concrete will increase with increased loading rates. It is expected that the increase will be proportional to the well-known increase of concrete compressive strength under a high loading rate. However, the different concrete compressive strength and tensile strength dynamic increase factors can have an influence on the failure mode. During the 100 years of concrete research several hypotheses have been formulated to explain the DIF, none of which is experimentally proven to 100%. Firstly, it is the rate dependency of the microcrack growth rate. The fast increase of the applied load leads to multiple cracking, i.e. to increased number of micro-cracks. This comes along with increased energy absorption during failure procedure. In other words, this effect can be defined as the influence of inertia at the micro-crack level [9]. The second effect is the viscous behaviour of the bulk material between the cracks, i.e. creep of concrete or viscosity due to the water content. The last effect is the influence of structural inertia forces, which can significantly change the state of stresses and strains of the material [10]. While the first two effects are hard to separate, it is expected that the structural inertia forces have a significant influence on the bond stress-slip behaviour. An attempt to separate these effects will be made.

1.3 Objectives

The main aim of this work is to analyse the influence of high loading rates on the bond behaviour between reinforcing steel bars and concrete experimentally. For this reason, the bond stress-slip relations between concrete and reinforcing steel for different loading rates need to be measured and compared. Only short bond lengths should be

investigated in order to understand the local bond behaviour. The most pressing questions to be answered within the specific objectives of the work are as follows:

1. Are the geometry of the specimens and the experimental procedures of standard RILEM test [1] appropriate for high loading rate experimental investigations?
2. How can the loading rate be defined in case of pull-out or push-in tests?
3. Are there any significant differences in the load direction?
4. Does the bond strength for higher loading rates increase? What are the limits?
5. How do different dynamic increase factors for concrete compressive and tensile strength influence the bond mechanisms? Does the failure mechanism in case of the impact loading change in comparison to the quasi-static loading?
6. The impact tests will be performed only on specimens having reinforcing steel bars with 10 mm in diameter. What is the influence of the bar diameter in the case of quasi-static loading?

A very important objective of this work was to develop a reliable method for testing bond strength between steel and concrete under impact loading as there are currently no standards addressing this issue.

1.4 Scope of the Work

The work starts with an introduction and an overview of the available literature on the topic of bond stress-slip relationships and material testing under high loading rates (Chapter 2). In the third chapter, the experimental setup is presented. This includes a description of the quasi-static tests as well as the impact tests that were performed in specially instrumented drop-tower and the split Hopkinson bar (SHB). Two modifications of SHB are described, and the influence of the experimental setup on the results is discussed. In addition, the measurement methods, as well as used equipment and data acquisition system, are presented. In the fourth part of the work results of quasi-static and impact testing are provided. Both pull-out and push-in type of tests are compared. Different approaches to defining the loading rate during impact bond tests are discussed. The results are critically analysed, and possible effects that could influence the results are shown. In the case of impact testing results, special attention is paid to proper description and analysis of the experiment on the basis of elastic wave propagation. In the fifth and last chapter, the most important findings are summarised, and the future research needs are identified.

Chapter 2

State of the Art

2.1 Bond stress-slip characterisation

Reinforced concrete is a composite material. On the macroscopic level, it can be viewed as a concrete matrix with reinforcement – in most cases made of steel. The force transfer between concrete and steel depends on the bond properties of these two materials. In modern concrete, to increase the bond capacity, the reinforcing steel is usually deformed. That means that the bars have longitudinal and transverse ribs. The transverse ribs are usually declined. The form and shape of the ribs are normalised for instance by DIN 488 [11] code, as well as by Eurocode [12]. The examples of rib spacing and geometry as defined in DIN 488 [11] is shown in Figure 2-1. From the spacing and arrangement of the ribs, the information about the country of production can be read. The usual ranges for the spacing, height and rib inclination angle of transverse ribs are given in Table 2-1

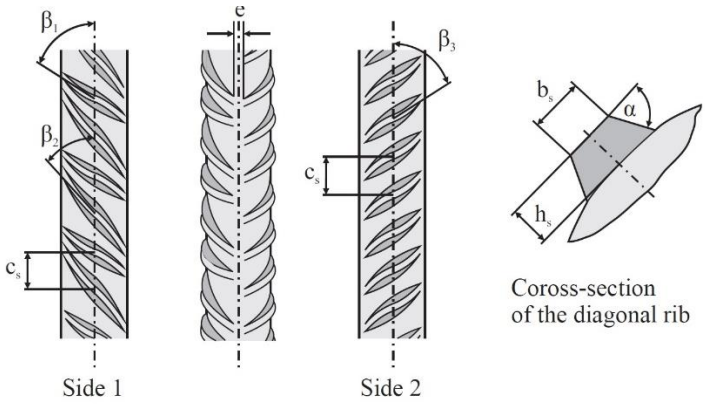

Figure 2-1: Rib geometry of reinforcing deformed bar according to DIN 488 [11].

Table 2-1: Ranges for the rib parameters.

Rib height, h_s	**Rib spacing, c_s**	**Transverse rib inclination angle, β_{1-3}**
0.03d - 0.15d	0.4d – 1.2d	35° - 75°

The bond between concrete and steel is not only influenced by the rib geometry but also by the state of the surface treatment. The surface of reinforcing steel bars that are used in Europe is usually without any corrosion protection. Whereas in the USA an epoxy coating is much more usual, influencing the chemical bond between steel and concrete [13]. In addition, stainless steel bars, as well as non-metallic reinforcement such as carbon fibre reinforced polymers (CFRP), can be used to prevent corrosion. Such bars have naturally different bond behaviour compared to steel bars. This work is therefore exclusively concentrated on steel reinforcing bars (rebars) without any surface treatment. All the investigated steel bars comply with the DIN codes [11]. Only bars with ribs, usually called deformed bars, are investigated throughout the study as plain bars are not used by the construction industry anymore.

The bond between concrete and steel within reinforced concrete structures, allows longitudinal forces to be transferred from the concrete matrix to the reinforcing steel bars. Shang et al. [14] note that concrete and steel reinforcement bars cannot work together successfully without good bond behaviour.

Generally, the bond strength can be calculated using a model based on uniform bond stress distribution [15] as shown in Eq. (1)

$$\tau = \frac{F}{u_s \cdot l_b} = \frac{F}{\pi \cdot d_s \cdot l_b} \tag{1}$$

The bond stress is usually presented in a relationship to relative slip. Such relationships are then used for designing anchorages, calculating expected crack widths and for the creation of numerical and analytical models. An example of such relationship can be seen in Figure 2-2. The bond between steel and concrete during a pull-out test can be divided into three main phases: chemical adhesion, mechanical interlocking and friction. After the chemical adhesion is exploited, micro cracks in the vicinity of the reinforcement bar are formed. The force transfer is realised by small cantilevers sometimes called keys in between the ribs. This phase is connected with increasing relative slip.

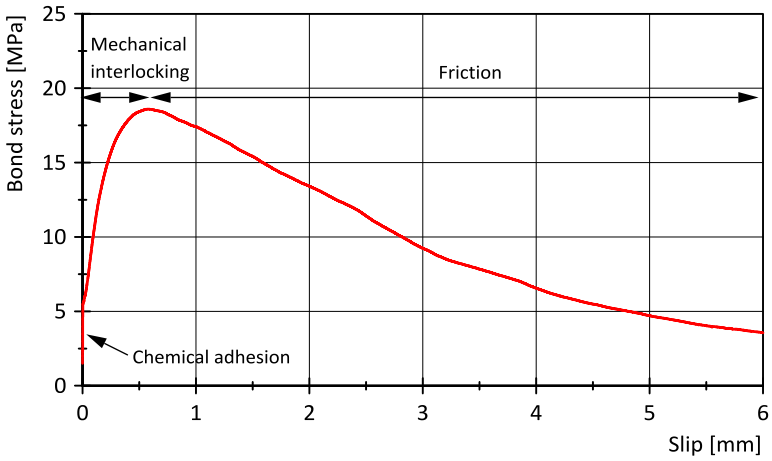

Figure 2-2: Representative example of a pull-out bond stress-slip relationship.

The relative rebar slip or displacement occurs when the strains in the steel reinforcement differ from the strains within the concrete matrix [16]. It can be calculated as an integral from the strain difference along the bar.

$$s(x) = \int_0^x \varepsilon_s(x) - \varepsilon_c(x)\, dx \tag{2}$$

For short bond lengths is the slip experimentally determined as a relative displacement of the bar to the undisturbed concrete mass. There are two forms of slip that contribute to the total measured value [17]. Firstly it is the movement between the reinforcing bar and the concrete-steel interface, as a result of the reinforcing bar moving through the concrete test specimen. In Figure 2-3a) below, the dashed red line represents an accentuated relative slip s_1 of rebar between the concrete-steel interfaces. Secondly it is the deformation of the test specimen, due to the applied forces. Once force is applied, the deformation of the test specimen can be seen to affect the displacement of the steel-rebar relative to the zero reference point of the test specimen. This slip s_2 is indicated by the displacement between the specimen and red dashed line in Figure 2-3b) below. For this reason the relative slip needs to be measured far away from the steel reinforcement where the concrete is undisturbed, especially in the case of steels with large diameters and high bond strengths.

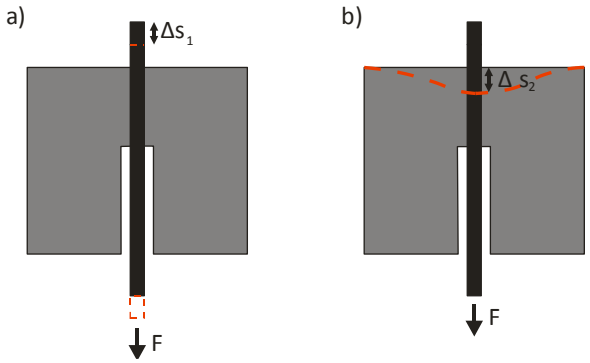

Figure 2-3: Slip due to: a) rebar movement, b) concrete deformation.

2.1.1 Specimen types

In order to analyse various properties relevant to the reinforced concrete structure, several testing methodologies can be implemented. The different testing methods provide an opportunity to understand the relevant failure mechanism for each loading case and scenario. A greater appreciation and understanding of this area allows for a more informed design process, where the relevant failure mechanism can be prevented or mitigated by appropriate design. Many experimental setups for examining the bond stress-slip behaviour were introduced since the invention of reinforced concrete at the beginning of the 20th century [18]. The possible test configurations are shown in Figure 2-4. These type of tests are: a) the tension specimen which is suitable for crack width observations, b) beam and g) beam-end specimens which try to simulate real stress conditions in beams, c) pull-out and d) push-in specimens which are relatively easy to manufacture and by far the most popular, e) splice specimens for investigating anchorage and splice lengths and finally f) cantilever specimens for simulating eccentric loading. The type of the bond specimen has an influence not only on the measured bond strength but also on the nature of the bond response. This is even more pronounced in the case of dynamic or impact testing.

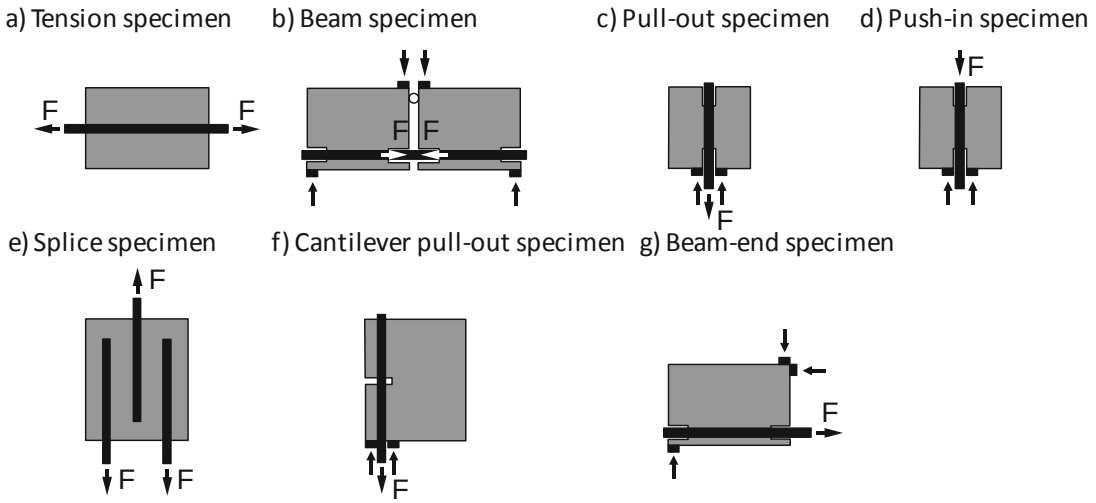

Figure 2-4: Type of bond tests, according to [19].

In Europe, the most widely used type of test is the pull-out test as codified by DIN EN10080, appendix D [20] and other harmonised national codes. The main advantages of this test are ease of sample preparation, ease of testing, relatively small weight of the samples and low production costs. The main criticism of this type of tests is that it doesn't represent the actual stress conditions in most of the reinforced concrete members. Usually, the reinforced concrete member, either slab or beam, is loaded in flexure which means that the concrete is in tension and partly cracked. However, in the pull-out type of the test, the concrete is under compression providing additional confinement to the reinforcing bar. Anke Wildermuth [21] compared in her dissertation pull-out tests specimens with beam-end specimens. She concluded that the beam-end test provides a reasonable alternative to the widely used pull-out test while maintaining rather uncomplicated experimental setup. The advantage of the test is that it better simulates the field conditions and the concrete cover can be more realistic. Anke also studied the influence of the relative rib area on the bond stress of steel in concrete. She stated that in general the pull-out test slightly overestimates the effect of the relative rib area whereas the beam-end specimen slightly underestimates it.

The usage of beam end test for impact testing of bond resistance is extremely complicated. There are several reasons for that. Firstly the samples are heavier, and thus the inertial effect of the sample can't be neglected. Secondly, the test itself is more complicated on preparation. Because the beam-end is supported by several places, the path of loading stress wave propagation cannot be easily determined. For the reasons mentioned above, it was decided to use a modified pull-out type of tests in this research.

The following chapter will mainly concentrate on this type of tests and several aspects as discussed in the literature will be presented.

2.1.2 Failure mechanisms

In general, there are two ways of performing the bond stress test. According to the code, the steel rebar is pulled out of a concrete cube with an edge of 200 mm. This is the most conventional test and will be referred to as **pull-out** in the further text. It is also possible to modify the test and push the rebar through the concrete specimen. This type of test is more suitable for drop-tower and split Hopkinson bar (SHB) testing [22, 23]. In this work, it will be referred to as **push-in**. In the following sections, the differences between the two types of tests will be discussed in the context of state of the art.

The basic failure mechanisms are valid for both types of tests. Two main modes of failure within pull-out and push-in testing can be identified according to [24] as splitting failure and pulling failure. Simplified stress-slip diagrams are presented in Figure 2-5 to demonstrate the difference in the mode of failure. The red line represents pulling failure, whereas the blue line represents splitting failure.

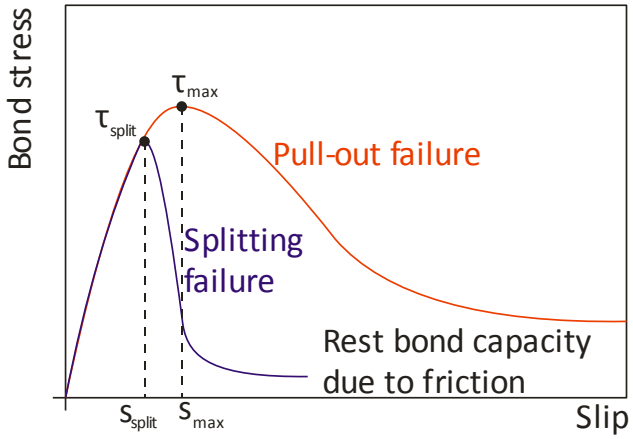

Figure 2-5: Splitting and pulling type of failure

In the deformed steel reinforcement bar, the ribs transfer the bearing forces into the surrounding concrete. These forces are inclined by angle α and can be decomposed to radial and tangential component which is perpendicular with the steel axis as shown in Figure 2-6. The radial shear stress p within the specimen is dependent upon the tangential shear stress τ developed along the concrete steel interface, and the angle α of the rib to the concrete-steel interface or upon the direction that the pull-out load is

applied [25]. The radial components must be balanced by the tensile ring stresses in the surrounding concrete, otherwise longitudinal cracks will form. The parallel component is equal to the bond force.

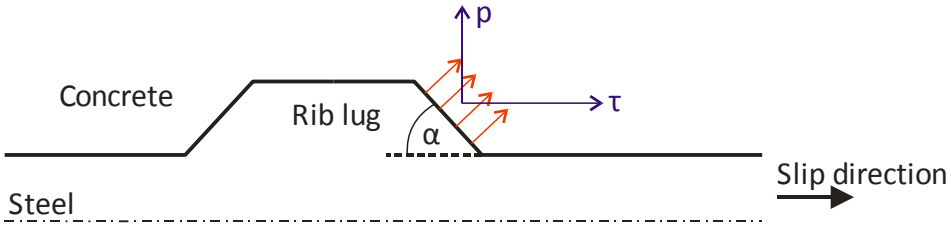

Figure 2-6: Radial and tangential components of shear stress, [25].

Pulling failure occurs when the reinforcing bar is pulled out of the concrete specimen in a way that no visible cracks are apparent on the specimen surface. This type of failure is usually associated with specimens having a concrete cover greater than 4.5 times the diameter of the reinforcing bars [19, 26]. The forces acting on concrete and steel during pull-out failure mode are sketched in Figure 2-7. The upper limit of bond strength is determined in this failure mechanism, as a result of the shear cracking of small concrete cantilevers between adjacent ribs of the deformed steel reinforcement bar [27, 28]. This crushing of the concrete cantilevers is also an explanation why is the bond strength so closely dependent on concrete compressive strength. This and other factors influencing the bond strength will be discussed in more detail in chapter 2.1.4.

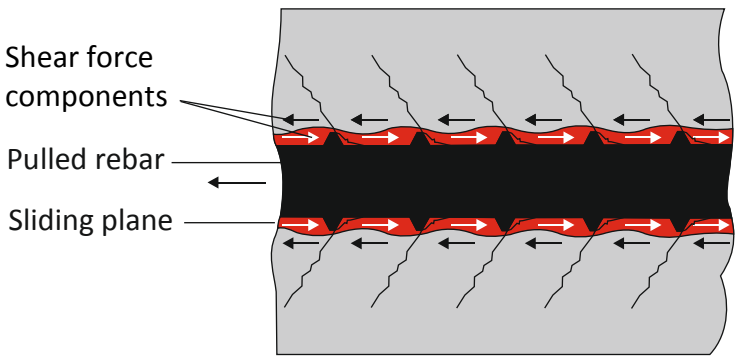

Figure 2-7: Cracks around the rebar for pull-out bond failure, after [29].

Splitting failure occurs when radial cracks propagate through the entire concrete cover which is insufficient to prevent the spread of these cracks. This happens when the tensile strength capacity of the concrete is reached. The tensile capacity is influenced by the stress state in the concrete body which is usually multiaxial. That means that the splitting

failure can occur even before uniaxial tensile strength is reached. When the cracks reach the outer concrete surface, a sudden drop in bond stress follows. An example of splitting failure as observed on pull-out specimens with a concrete cover of $2\times d_s$ is shown in Figure 2-8.

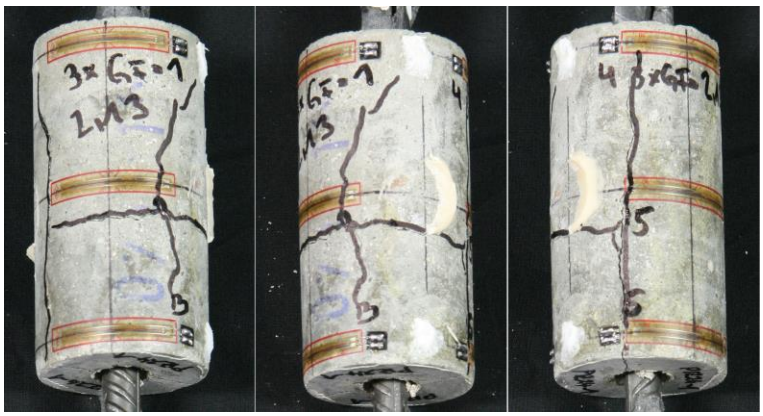

Figure 2-8: Example of splitting failure.

2.1.2.1 Pull-out

When looking on pull out type of failure in more detail, we can identify four main stages of the failure. According to the state-of-the-art report on a bond of reinforcement in concrete that was conducted by CEB-FIP [17], there are four different stages characterising an interaction between the concrete and a bar subjected to a pull-out force. These stages (Figure 2-9) are as follows [17]:

1) **Un-cracked concrete:** for low bond stress values, the bond is maintained by the chemical adhesion between the steel and concrete along the interface. No slip between the reinforcing bar and the concrete occurs, and as a result, no cracks are formed. This stage is associated with the micromechanical interaction between the microscopically rough steel surface and the concrete. In general, however, the chemical adhesion and micromechanical physical interactions do not contribute a great deal to the bond performance of the bar, hence the relatively small forces and stresses associated with this stage. This stage of bar slip occurs for both plain and deformed reinforcing bars.

2) **First cracking:** after the chemical adhesion breaks down, the ribs induce large localised bearing stresses onto the concrete cantilevers between the ribs. At these points, transverse microcracks begin to form and permit the reinforcement bar to

slip. The forces are not great enough at this stage to allow wedging action to initiate full concrete splitting.

3) **Partial splitting:** as higher bond stresses are induced within the test specimen, longitudinal cracks appear, and radial cracks form. The cracks develop due to the wedging action of the concrete stuck in front of the rib of the deformed bar. The wedging action resulting from the stuck concrete produces an outward component of pressure, which is resisted by the surrounding concrete providing a confinement effect upon the reinforcing bar. The bond strength and stiffness are governed by the interlocking with reinforcement, the concrete keys radiating from the reinforcing bar, and finally the undamaged outer concrete ring. Depending upon the presence and levels of transverse reinforcement, the failure mechanisms can vary between test specimens. For example, heavy transverse reinforcement within a sample may prevent the formation of the splitting cracks to the surface, and result in the sample failing in pull-out mode.

4) **Failure:** when it comes to the failure mode there are three main possibilities for bond failure for plain and deformed bars depending on the confinement level and support conditions.

   a) **Through splitting:** for plain bars, this failure mode occurs immediately after the depletion of the chemical adhesive bond capacity. The frictional bond is dependent mainly on the dry friction between the plain bar and concrete. It is strongly affected by transverse pressure.

   b) **Splitting-induced pull-out:** this failure mode occurs when light to medium transverse reinforcement is provided. The longitudinal cracks break through the whole cover and bond tends to fail suddenly. In the reinforced concrete structural members such as beams, the sufficient amount of stirrups can assure bond efficiency in spite of concrete splitting. During this stage, the bond stress as high as 0.3 to 0.5 of concrete compressive strength can be developed. However, this is associated with unacceptably high values of relative slip ($s/\emptyset > 0.05$). After the maximal bond strength is reached, the bond stress still remains significant even at very large slip values. This post peak behaviour is associated with shearing off and crushing of the concrete cantilevers between the ribs. In the end, the bond behaviour tends to become a dry-friction type.

c) **Pull-out:** this failure mode is in effect very similar to the splitting induced pull-out. The main difference is that it doesn't come to the splitting of the concrete cover because of the heavy transverse reinforcement, high concrete cover or the additional confinement provided by specimen support. The associated bond stresses are even higher than in the previous two cases (4a and 4b). The bond failure is caused by bar pull-out. The force transfer mechanism changes from rib bearing to dry friction. After the peak, the interface is smoothened due to wear and compaction. This leads to further decrease of bond stress.

The failure stages 1 to 4 refer to the local behaviour of bond, while the global behaviour results from the superimposition of the various stages. The local behaviour applies to the ideal segment of the bar, but it is possible to use the local bond stress results to predict or model the global behaviour. The pull-out failure (4c) is typical for tests which are done according to RILEM [1] recommendations. For the reasons of high confinement, this test tends to overestimate the bond stress. On the other hand, the failure mode is very well described, and other influencing factors can be eliminated. The main limitation of using a pull-out test is that it fails to accurately replicate or reproduce the actual conditions in a reinforced concrete member [30]. Anchorage lengths within pull-out testing are normally short, between 2 and 5 times the bar diameter, to allow for uniform stress distribution. However, in reality, the bond zone within reinforced concrete structures is the entirety of the bar length, and it is not uncommon for these lengths to be of several meters. The contrast between 50 mm and 5 m bond lengths and the effect on the bond zone properties is therefore obvious.

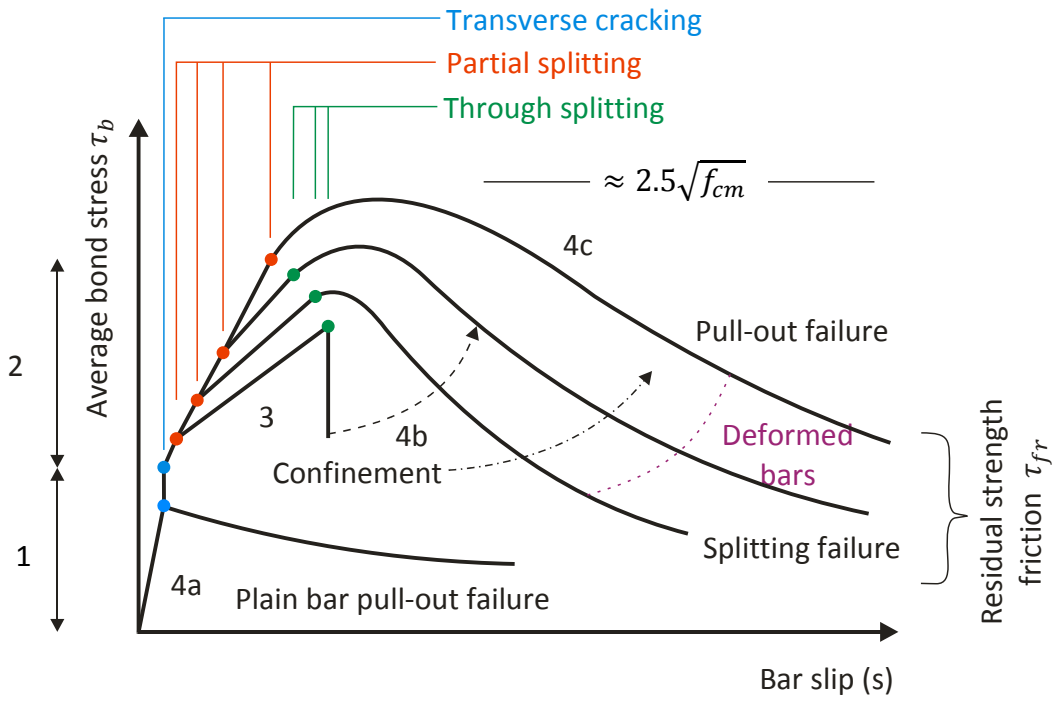

Figure 2-9: Local bond stress-slip law, after [31]

2.1.2.2 Push-In

The standard test for determining the bond stress-slip relationships is the pull-out test as described in the previous chapter. This test is however not always suitable for impact testing. Therefore some researchers such as Yan [22], Wensauer [32] or Michal [33] used a push-in type of test. In this test, the same or similar specimen as in the case of the pull-out test is used. The main difference is that the reinforcement steel is pushed into the concrete body and is therefore under compression. The principal **failure mechanism** is independent of the load direction and was described in the previous chapter. The main difference arises from the so-called Poisson effect, the phenomenon in which a material tends to contract or expand in directions perpendicular to the direction of tension or compression. For a long isotropic elastic bar with a diameter d_s and for small deformations it is possible to write:

$$\Delta d_s = -d_s \cdot \nu \cdot \varepsilon \tag{3}$$

where

Δd_s is change in the bar diameter
ν is Poisson ratio
ε is axial strain in the bar (positive for axial tension).

This can be rewritten in terms of force by using one-dimensional Hook's law as:

$$\Delta d_s = -d_s \cdot \nu \cdot \frac{F}{A \cdot E} \tag{4}$$

That means that the change in the steel diameter is dependent on the force required to push-in the bar into the concrete. This force is relatively small for bars with small diameters and for short bond lengths. After combining with Eq. (1) we can write the Equation (4) in terms of bond stress:

$$\Delta d_s = -\nu \cdot \frac{4 \cdot \tau \cdot l_b}{E} \tag{5}$$

It can be seen that the change of the diameter of the bar is dependent predominantly on the bond length as the bond stress is more or less constant for varying bar diameter. In case an average bond stress of 20 MPa, the bond length of 20 mm and Poisson ratio 0.27 is assumed, the diameter contraction or expansion is 2.16 µm. In the case of push-in tests, such lateral expansion shouldn't influence the bond stress-slip relationship. To the same conclusion came Wensauer [32] and Michal [33] who didn't observe any significant differences between push-in and pull-out results for steel reinforcement with short bond lengths. The difference between average pull-out and single push-in bond stress-slip results as measured by Wensauer [32] is shown in Figure 2-10. With the exception of one specimen which failed by splitting no significant difference was observed between push-in and pull-out behaviour.

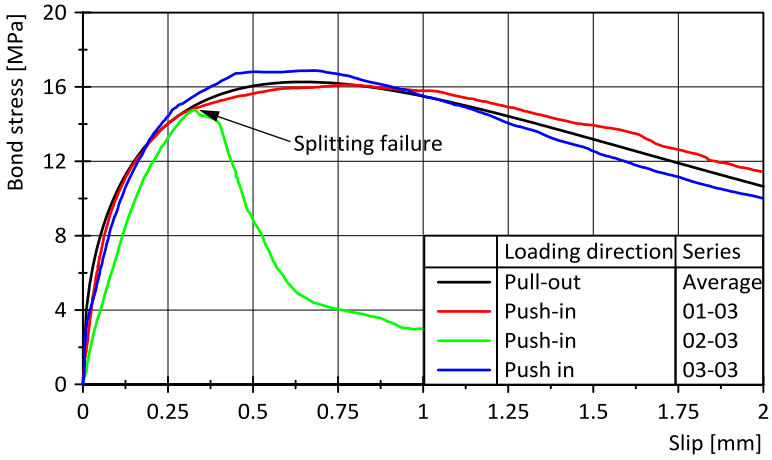

Figure 2-10: Difference between push-in and pull-out loading, after [32].

Eligehausen et al. [34] reported that the bond stress-slip relationship for monotonic loading in tension was almost identical to that in compression. Also, Uijl and Bigaj [29] report that Poisson effect can be neglected as long as the force transferring mechanism

is the rib-bearing, i.e. until τ_{max}. They report that the local transverse deformation cannot be disregarded during the friction phase of failure. In this case, the Poisson effect may considerably influence the development of the radial compressive stress and, hence, the bond stress. This is even more pronounced for very long bond lengths or concretes with high bond strength. In this case, the steel yields and the lateral contraction in tension or lateral expansion in compression is not negligible. This was observed for instance by Ruiz et al [35].

In his PhD thesis, Yan [22] used specimens with a reinforcement bar centrally embedded in concrete prisms with dimensions 152.4 × 152.4 × 63.2 mm. He concluded that under both static and impact loading conditions, push-in loading direction always produced greater bond stress in comparison with pull-out direction. The stress development along the steel rebar is shown in Figure 2-11.

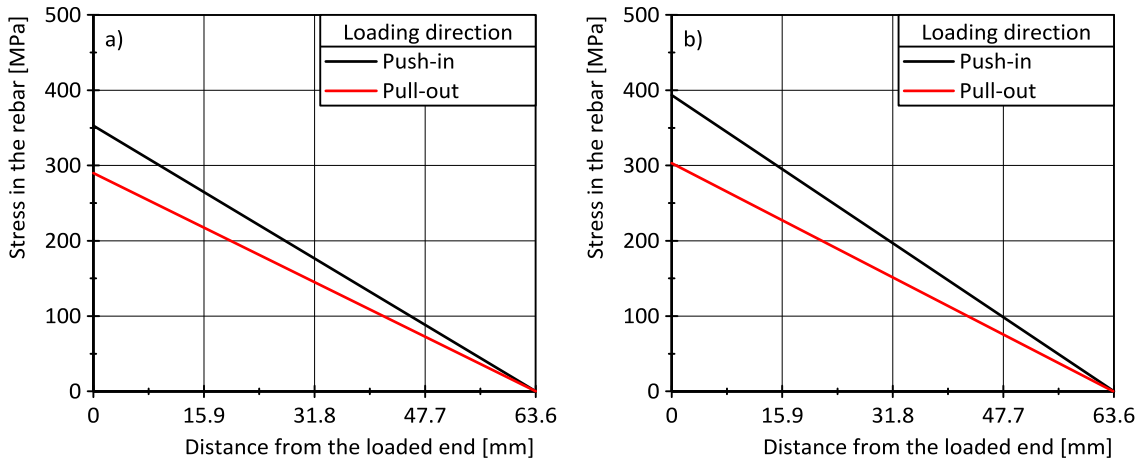

Figure 2-11: Stresses in the deformed rebar for pull-out and push-in a) static tests and b) impact tests, after [22]

2.1.3 Types of loading based on the loading rate

2.1.3.1 Quasi-static

Under quasi-static loading is understood loading which can be characterised as a series of steps in which the sum of forces acting on every part of the structure is nearly equal of zero. In experimental testing, it is characterised by slow loading rates of around 0.01 mm/s. The time dependent behaviour of materials, such as creep and relaxation or fatigue and impact loading, for very slow or very fast loading rates does not have much effect on the results of quasi-static experiments. The quasi-static loading case is the most investigated one. The bond mechanics was investigated by numerous researchers,

and it is summarised by several state-of-the-art reports. Because this work concentrates on impact loading, the quasi-static case will not be discussed in detail. Comprehensive information can be found for instance in the report of ACI Committee 408 on Bond and Development of Straight Reinforcing Bars in Tension [36], in the above-mentioned Model Code 2010 [16], in the report by fib Commission 4 on Bond Mechanics Including Pull-out and Splitting Failures [17] and many others. The basis for bond strength investigations was discussed by Rehm [37] in 1961. The pull-out investigations on the bond stress behaviour of reinforcing steel were performed by Martin and Noakowski [24]. The way towards the harmonised European bond test was described by Cairns and Plizzari [38]. The possibilities of using beam-end test for investigating the bond behaviour were studied by Wildermuth [21]. The influence of lateral tensile stress on the bond between concrete and steel was in detail studied by Laura Ritter [19]. This list could go further on as there are many others who investigated the bond between the steel and concrete.

2.1.3.2 Dynamic-cyclic

Loading rate effects are investigated in this work, and therefore it is important to make a clear distinction between cyclic and impact loading because both types of loading are sometimes referred to as dynamic loading. The main difference is in the duration of the loading and its reoccurrence. While cyclic loading is obviously reoccurring, it is relatively slow in comparison to the impact loading. Generally, cyclic loadings are divided into two categories [39]. The first category is the so-called *low-cycle* loading. For this type of loading the load, history contains less than one thousand cycles, but the range of applied bond stress is very wide. The typical example of such low-cycle loading is an earthquake or extreme wind loading. The second category is the so-called *high-cycle* or fatigue loading. For this type of loading typically thousands or millions of cycles are typical. On the other hand, the bond stress range is relatively narrow. Bridge structural parts, offshore structures, and structures supporting vibrating machinery are often subjected to high-cycle or fatigue loading. High-cycle loadings are considered a problem at service load levels, while low-cycle loadings produce problems at the ultimate limit state. The bond behaviour under cyclic loading can further be subdivided according to the type of applied stress. The first is unidirectional loading, which implies that the rebar bond stress value doesn't change a sign during a load cycle. Throughout the load history, the bond stress is either positive (tension) or negative (compression). This is typical for instance of bridge beams subjected to cyclic loading from traffic. The second is reversed cycle loading, where the bar is subjected alternatively to tension and compression. The

stress reversals are the typical for seismic loading. Cycles with reversed loading produce degradation of bond strength and bond stiffness that is more severe than for the same number of load cycles with unidirectional loading.

Most commonly, direct pull-out tests as defined in RILEM RC 6-1994 [1] for cyclic testing of bond behaviour are preferred. The reason for that is the relative simplicity of the test setup and procedure and the ability to isolate the effects of different investigated parameters. Because the concrete and steel are not in the same state of stress, alternative experimental methods have been developed such as the beam bending test [20] or simplified beam-end test [21]. The following authors [40–43] studied the bond behaviour of reinforcing steel under cyclic loading. The topic itself is fairly complicated and will be discussed very briefly in this chapter.

The development of the bond stress during cyclic loading is, similarly to the quasi-static loading, dependent on the friction and mainly mechanical interlocking between the reinforcing steel ribs and the surrounding concrete. According to Leonhardt [44], the bond between reinforcing steel and concrete is the weakest link of the reinforced concrete structural members under cyclic loading. Analogically to fatigue loading of unreinforced concrete the cyclic fatigue loading of the rebar-concrete bond can be divided into three phases as shown in Figure 2-12. Phase one is characterised by a non-linear fast growth of the rebar to concrete slip. Gylltoft [45] here notes that upon initial loading of a pull-out test specimen non-reversible slipping will occur causing a better fit between concrete and steel. This better-fit results in an improved interaction and consequently the steel-concrete bond zone behaves much stiffer upon secondary loading. In phase 2 the slip growth is fairly constant and linear, and in phase 3 the slip increases disproportionally to the number of cycles. Ultimately the total bond failure can occur during the phase 3.

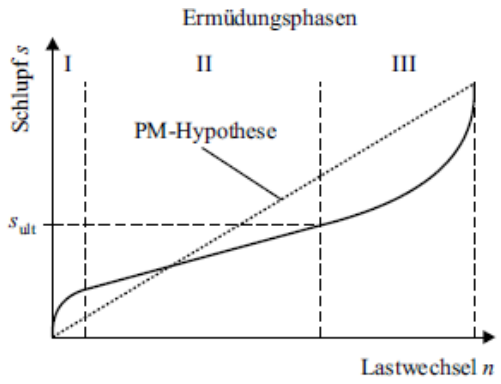

Figure 2-12: Phases of slip growth under cyclic loading according to [43]

The bond behaviour under cyclic loading was in the 70ties extensively studied by Rehm and Eligehausen. They studied both short [46] and long [47] bond lengths up to 10^6 loading cycles. The short bond lengths were studied using cylindrical specimens with a bond length equal to $3 \times d_s$ which was located in the middle of the specimen. Their experimental results showed that the cyclic loading leads to attenuation of the bond stress. From the results measured on specimens with long bond lengths [47] can be concluded that it comes to redistribution of the load during the cyclic loading because of the changes in local stiffness. Similar behaviour can also be observed for a sustained load of the same magnitude.

Zuo and Darwin [42] investigated the behaviour of high relative rib area bars under cyclic loading. They conclude that reverse cyclical loading can result in severe deterioration of bond between concrete and steel, especially in the beam to column joints. Darwin and Graham [48] used ASTM A 944 beam-end specimens to evaluate the bond strength of reinforcing bars with a wide range of relative rib areas f_R under monotonic loading. They observed that, under all conditions of confinement, the initial stiffness of bond stress-slip curves increases with an increase in relative rib area. This means that bars with high f_R exhibit less bond deterioration than conventional bars. Therefore, it can be expected that reinforced concrete members and frame joints that are affected by bond deterioration under seismic loading will exhibit better performance if reinforced with high f_R bars than if reinforced with conventional bars.

In work presented by Soleymani [49] a performance of ribbed bars under reversed cyclic loading beam test is presented. Because of the complexity of the test setup, special attention is paid to eliminate unwanted forces that could be generated in the system during the test. In their work, they tested beams made of high-strength self-compacting concrete (HSSCC) with compressive strength around 100 MPa with embedded reinforcement bars with a diameter of 16 mm. The testing procedure could be described as low-cyclic loading with several reversed cycles with increasing amplitude. The researchers conclude that the bond stress-slip relationships obtained from the reversed cyclic bending test are not inconsistent with the traditional RILEM pull-out test. However, the bond stress in the beam test was found to reduce considerably after reaching the maximum strength. Therefore, as opposed to the ductile bond–slip envelope observed under monotonic loading, a substantial deterioration of bond stress occurred under cyclic loading which can potentially have a marked influence on the seismic performance of reinforced concrete structures.

There is a significant amount of data on the frequency influence for concrete [50] and steel [51] separately, however, only a few researchers have studied the bond itself. Mainly Koch and Balázs [52, 53] in the 90ties studied the influence of the loading frequency on concrete-steel bond behaviour. They investigated frequencies ranging from 0.5 Hz to 8 Hz. Based on their results there are only minor influences of the loading frequency on bond behaviour.

2.1.3.3 Dynamic-impact

Dynamic impact loading will be in detailed discussed in Chapter 2.2. This chapter here is included only for completeness. It is also important to make a clear distinction between dynamic cyclic loading (as described in the chapter above) and impact loading. The main difference is that in the case of impact loading the loading is very rapid - it lasts several microseconds and shock wave propagation theory needs to be taken into consideration. This is in more detail discussed in chapter 2.2.1. The typical loading time studied in this work ranged between 0.2-0.3 ms. The loading also lasts until the failure is reached. On the contrary, the cyclic loading studies bond stress-slip relationships under millions of loading cycles. These cycles are from the point of view of impact loading relatively slow. Usually, 1-15 Hz which corresponds to loading times of 1000 to 66 ms.

2.1.4 Factors influencing bond strength

The bond strength between the steel reinforcing bar and concrete is influenced by many boundary conditions and factors [43]. In Table 2-2 these boundary conditions are divided into categories based on the material influence, the experimental setup and type of loading. These boundary conditions influence for instance the chemical adhesion between concrete and reinforcing elements, the gripping effect of concrete shrinkage which improves the shear interlock along the reinforcement, the frictional resistance to sliding, as tensile stresses are placed upon the test specimen, the resistance of concrete to cracking and so on. The factors which are relevant to the performed experimental work, as described in Chapter 4, are discussed in more detail in this chapter.

Table 2-2: Factors influencing bond stress according to Lindorf [43].

Material	**Experimental setup**	**Type of loading**
Concrete	Bond length	Tensile
• Composition	Concrete cover	Compressive
• Manufacturing	Transverse reinforcement	Long-term
• compressive strength	Concreting direction	Static
• tensile strength	Position of the rebar	Cyclic (dynamic)
• load deformation behaviour	Cracks	Impact
Steel	Temperature	Lateral compressive stress
• yielding strength	Number of ribs in the bond zone	Lateral tensile stress
• tensile strength		
• stress-strain behaviour		
• rebar diameter		
• ribs geometry		

2.1.4.1 Concrete strength

The concrete compressive strength is the most important property that defines concrete. The general trend is to put all other concrete properties to the relation with concrete compressive strength. As shown in Chapter 3.1.1 this can be very accurate for modulus of elasticity and less accurate for concrete tensile strength. Because of the many influencing factors (Table 2-2) prediction of maximal bond stress based solely on concrete compressive strength is somewhat complicated. The general idea behind this relation is that the maximal bond stress, especially during the pull-out failure mode is dependent on the strength of the concrete cantilevers (keys) that are formed between the steel ribs. The influence of concrete compressive strength was heavily investigated in the past, and several analytical models based on compressive and tensile strength were formulated. The overview of analytical models is provided in Table 2-3.

Table 2-3: Analytical models for predicting maximal bond stress based on concrete compressive strength, according to [21, 54].

Source	Relationship
Rehm (1961) [37] Martin (1973) [55]	$\tau \sim \beta_w$
Martin and Noakowski (1981) [56]	$\tau \sim \beta_w^c$ for deformed bars is c - 1 to 1.2
CEB Bull. No. 151 (1982) [57]	$\tau \sim$ concrete tensile strength by splitting failure $\tau \sim$ concrete shear strength by pull-out failure
Martin (1982 and 1984) [58, 59]	$\tau \sim \beta_w$ by $\Delta < 0.01\ mm$ and by $\Delta > 1.0\ mm$
Paschen et al. (1974) [60]	$\tau \sim$ concrete tensile strength
Untrauer/Henry (1965) [61] Eligehausen et al. (1982)[34] Robins/Standish (1984) [62] Soroushian et al. (1991) [63]	$\tau \sim \sqrt{f_c}$
Nagatomo/Kaku (1985) [64]	$\tau \sim f_c^{\frac{2}{3}}$
Nykyri (1986) [65]	$\tau \sim \beta_w$ depending on the ribs type $\tau \sim c_1 \beta_w^{0.469} + c_2 \beta_w$
DIN ENV 1992 [66]	$f_{bd} \sim f_{ck}^{\frac{2}{3}}$
CEB-FIP MC 2010 [16]	$\tau(\Delta) \sim f_{ck}^{\frac{1}{2}}$
Huang et al. (1996) [67]	$\tau \sim f_{cm}$

As can be seen from Table 2-3, according to the most authors the maximal bond stress τ_{max} is exponentially dependent on the concrete compressive strength. Generally it can be written:

$$\tau_{max} = a_1 \cdot f_{cm}^{k_1} \tag{6}$$

where $k_1 > 0$. Depending on the value of the exponent k_1 different coefficients a_1 arise. In her dissertation Laura Ritter [19] compared her own results with maximal bond strength values that can be found in literature. Only short bond lengths until the ratio $l_b/d_s = 5$ were considered. From 165 single values she calculated weighted average of a_1 as 3.99 and k_1 0.5. In case that all results are evaluated with predefined $k_1 = 0.5$, then $a_1 = 3.14$. These coefficients are higher in comparison to MC 2010 where the following equation for calculating maximal bond stress under good bond conditions is recommended:

$$\tau_{max} = 2.5 \cdot \sqrt{f_{cm}} \quad (7)$$

It is important to stress that because of the many influencing factors it is very hard to predict the maximal bond stress based just on one factor such as concrete compressive strength. However, Eq. (7) provides a very good approximation of expected maximal bond strength. According to the MC 2010 [68], the bond stresses between concrete and the reinforcing bar for pull-out failure can be calculated as a function of the relative displacement s parallel to the bar axis as follows:

$$\tau(s) = \tau_{max}\left(\frac{s}{s_1}\right)^{\alpha} \quad \text{for} \quad 0 \le s \le s_1 \quad (8)$$

$$\tau(s) = \tau_{max} \quad \text{for} \quad s_1 \le s \le s_2 \quad (9)$$

$$\tau(s) = \tau_{max} - \left(\tau_{max} - \tau_{fr}\right) \cdot \frac{s - s_2}{s_3 - s_2} \quad \text{for} \quad s_2 \le s \le s_3 \quad (10)$$

$$\tau(s) = \tau_{fr} \quad \text{for} \quad s_3 < s \quad (11)$$

where the parameters for pull-out or push-in failure mode are given by Table 2-4

Table 2-4: Parameters defining the mean bond stress–slip relationship of ribbed bars

	Good bond conditions	**Other bond conditions**
$\tau_{\max}$	$2.5 \cdot \sqrt{f_{cm}}$	$1.25 \cdot \sqrt{f_{cm}}$
s_1	$1.0\ mm$	$1.8\ mm$
s_2	$2.0\ mm$	$3.6\ mm$
s_3	$c_s = 4.93\ mm$[1]	$c_s = 4.93\ mm$[1]
α	0.4	0.4
τ_{fr}	$0.4 \cdot \tau_{max}$	$0.4 \cdot \tau_{max}$

[1] c_s is the clear distance between ribs. The value was taken for mostly investigated steel in this research ($d_s = 10\ mm$) from Table 3-6.

2.1.4.2 Reinforcement diameter

The generally adopted assumption is that the bar diameter has a negligible effect on the maximal bond stress. In engineering praxis usually, a larger number of small bars rather than a smaller number of large bars is preferred. In terms of force, according to Equation (1), larger bars require larger forces to cause either a splitting or pull-out failure for bars not confined by transverse reinforcement. The result is that the total force developed at bond failure is not only an increasing function of concrete cover, bar spacing, and bonded length but also of the bar area. The bond force at failure, however,

increases slower than the bar area, which means that a longer embedment length is needed for a larger bar to fully develop a given bond stress.

When it comes to results presented in the literature, some authors reported increasing bond strength with decreasing steel diameters [69, 70], while others found an opposite effect [71]. Generally, it is very hard to separate all different parameters that influence the bond behaviour. The problem is that with the change of a bar diameter also the relative rib area changes. Also, the relation between rib spacing and the size of aggregate in the concrete plays an important effect.

2.1.4.3 Relative rib area

According to the literature the relative rib area f_R and rib pattern does not have influence on the overall deflection of a beam. On the other hand, the relative rib area influences the bond stress-slip behaviour. This parameter is particularly important for the crack width, splice and anchorage lengths. When comparing deformed bars to plain bars the bond behaviour is approximately the same until the pull out failure of plain bars which according to Abrams [72] occurs at a slip of 0.25 mm. For deformed bars, the ribs increase the bond resistance be bearing directly on the adjacent concrete. Abrams observed that the ratio of the bearing area of the projections (projected area measured perpendicular to the bar axis) to the entire surface area of the bar in the same length could be used as a criterion for evaluating the bond resistance of deformed bars. Thirty years later, Clark [73, 74] found that bond performance improved for bars with lower ratios of shearing area (bar perimeter times center-to-center distance between ribs) to bearing area (projected rib area normal to the bar axis) and recommended that the ratio of shearing area to bearing area be limited to a maximum of 10 and, if possible, 5 or 6. In current practice, this criterion is described in terms of the inverse ratio as shown in Equation (12). That is, the ratio of the bearing area to the shearing area, which is known as the relative rib area.

$$f_R = \frac{projected\ rib\ area\ normal\ to\ bar\ axis}{nominal\ bar\ perimeter \cdot center\ to\ center\ rib\ spacing} \tag{12}$$

Generally speaking, bond strength increases with increasing rebar surface roughness, i.e. f_R. According to Rehm and Martin [75] small relative rib area of approximately 0.02 leads to an increase of the crack width of about 50 % in comparison with crack widths for $f_R \approx 0.065$. In case the relative rib area is further increased to 0.1 it leads to decreased crack widths only by 20 % in comparison to $f_R \approx 0.065$. The ultimate anchorage capacity is, however, limited by microcracking and splitting of the

surrounding concrete. That means that there is no point of increasing f_R over 0.2. It can be concluded that crack widths decrease with the increase in relative rib area. This is valid for structural members with and without stirrups.

2.1.4.4 Specimen shape, concrete cover and bond zone position

The **shape** of the pull-out specimens, as well as the position of the bond zone, were changing during the time. Already in the year 1905 investigated Bach [76] the bond stress-slip relationships on smooth bars without ribs. The bar was completely embedded in the concrete, and spiral reinforcement was used to provide lateral reinforcement. In the early sixties, a cubical specimen with a short bond zone located in the middle was developed by Rehm [37]. Cubes with a side of 100 mm were used for smaller steel diameters (14 mm), and cubes with a side of 200 mm were used for steel with a diameter of 24 mm. Similar test shape was later adopted by other researchers. For testing bond strength under dynamic loading usually, cylindrical specimens were used. More details are presented in Chapter 2.2.4. Rehm and Eligehausen [77] used relatively oblong cylinders for cycling testing where the friction between the bearing plate and the arch effect are minimised. Possible examples of pull-out tests are shown in Figure 2-13.

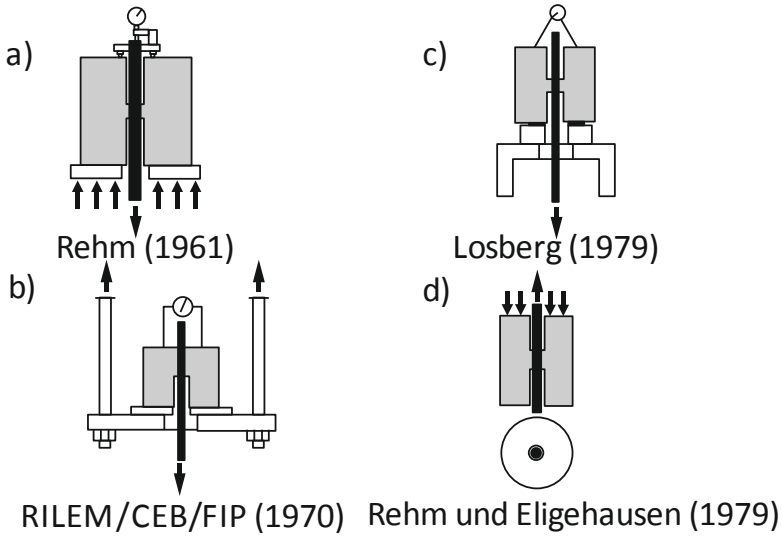

Figure 2-13: Possible examples of pull-out tests, after [78].

The magnitude of **concrete cover** is very important for the failure mode of the specimen. Large concrete covers provide enough confinement to prevent the splitting cracks from propagating to the outer surface of the specimen. In the case of splitting failure, the concrete cover has a direct influence on the maximal bond strength, which increases with increase in the cover. From a certain thickness of the concrete cover, a change of

failure mode is observed, and the concrete cover does not further influence the maximal bond strength. The thickness of concrete cover is usually defined as a ratio between concrete cover and reinforcement diameter c/d_s as these two properties are connected. For instance Abrishami and Mitchell [79] reported that for the ratio of $c/d_s = 3$ pulling mode of failure occurs whereas for the ratio of $c/d_s = 2.1$ splitting type of failure occurs. Eckfeldt [80] for high strength concrete reported the following limits:

- For shear off of the concrete cantilevers: $c/d_s > 2.9 \dots 4.8$
- Splitting initiated by pull-out: $c/d_s \approx 2.9 \dots 4.8$
- Splitting failure mode: $c/d_s < 2.9 \dots 4.8$

Laura Ritter in her dissertation [19] provides limits for minimal c/d_s for pull-out type of specimen in dependence on concrete class and reinforcement bar diameter. In case of C40/50 the minimal c/d_s was 2.65 to 3.25 for rebar diameter of 16 to 25 mm. In case of C20/25 the minimal concrete cover ratio c/d_s was 1.48 and 2.77 for rebar diameter of 16 and 20 mm respectively. Other researchers [81] usually report for normal strength concrete the minimal c/d_s ratio around 2.5. The confinement ratio c/d_s is also used in model for predicting maximal bond strength for instance by Uijl and Bigaj [29]. According to the RILEM [1] recommendations for performing pull-out tests, the minimal confinement ratio c/d_s should be greater than 5.

The **position of the bond zone** is very important for the results of bond strength testing. Should the bond zone be too near to the support plate, splitting would occur. That's why bond free length for pull-out tests is required by RILEM [1]. Also, the position of the bond zone in the middle of the specimen is not optimal. The weak point of the Rehm's test was the friction between the support plate and specimen which caused compressive arch formation in the middle of the specimen. This is the reason why the bond zone was moved to the top in the RILEM specimen [1], and an anti-friction pad was inserted between the bearing plate and the specimen. The eccentricity of the distributed reaction force with respect to the axis of the bar can be reduced by using a support ring with a small diameter that is inserted between the specimen and the bearing plate similarly to the research performed by Losberg [82].

2.1.4.5 Bond zone length

The length of the bond zone is a very important factor that influences the bond strength. There is a fundamental difference between the bond stress distribution along rebars

with long embedment length $l_b > 20d_s$ and short embedment lengths $l_b \approx 5d_s$. This is schematically shown in Figure 2-14. While the long embedment length correspond to the real situation in the structural member, the maximal bond strength is usually investigated in samples with short embedment lengths. From Figure 2-14 it is evident that the mean bond stress for short embedded lengths correspond to the maximal bond strength. Whereas for the mean bond stress for longer embedded length is lower than the local maximal bond strength $\tau_{max,loc}$. For more details about long embedment lengths and anchorages, the background to the fib Model Code for Concrete Structures 2010 [83] can be referred to. The bond length however influences the results of pull-out tests (short embedment lengths) as well. This will be discussed in this chapter.

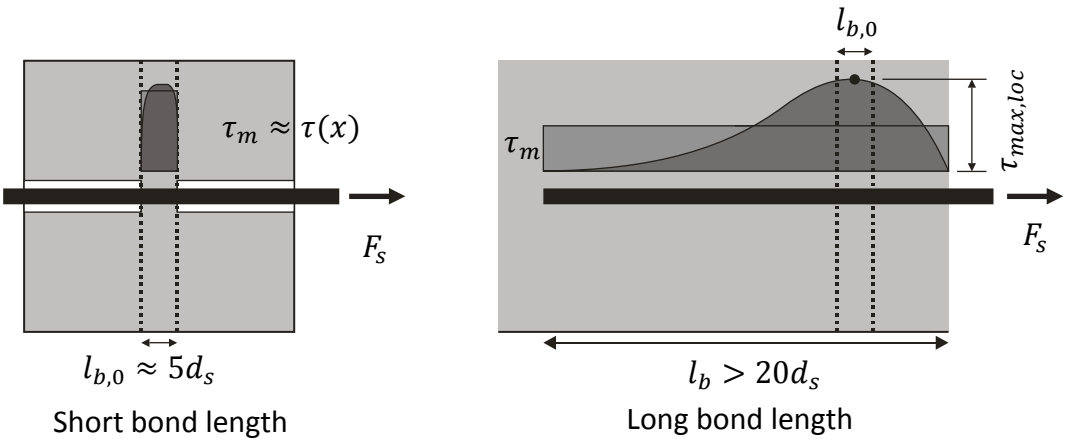

Figure 2-14: Bond stress distribution along a rebar for short and long bond lengths, after [19]

For short bond lengths, the bond stress is calculated according to Eq. (1). It is assumed that the bond stress is evenly distributed along the circumference of the bar. In the case of pull-out failure mode, the amount and position of ribs in the bond zone are very important, because each rib provides additional interlocking action. If the first rib is located at the beginning of the bond zone, the first concrete cantilever (key) nearly immediately fails because of stress concentration. The force is then mainly resisted by the remaining ribs. In case of very short bond lengths of $2d_s$ only 3 cantilevers are present in the bond zone. If one cantilever fails it has much larger effect than if the bond zone is $5d_s$ long and 6 cantilevers are present in the bond zone. The short bond zones of $2d_s$ are also much more sensitive to local inhomogeneities in concrete which cause in general larger scattering in results. They are also more sensitive to the size of aggregate used. The opinion on bond zone length is not consistent in literature. For instance Martin and Noakowski [56] investigated embedment lengths of $5d_s$, $10d_s$ and

$15d_s$. For a slip of $s = 0.1\ mm$ they concluded, that the bond stress increases with increasing bond length. The observed this trend independently on the concrete compressive strength. To a different conclusion comes Ritter [19] in her dissertation. She compared her measurement results with results in literature [67, 70, 84–86] and formulated the following Equation(13) for normalized bond strength.

$$\tau_{max,30} = 23.6 \cdot \left(\frac{l_b}{d_s}\right)^{-\frac{1}{3}} \tag{13}$$

where $\tau_{max,30}$ is the maximal bond strength normalized on concrete compressive strength of 30 MPa according to Eq. (14). This normalization assumes second root dependency of the bond strength on the concrete compressive strength. This is reasonable and in agreement with the MC 2010 [16] recommendations.

$$\tau_{max,30} = \tau_{max} \cdot \sqrt{\frac{30}{f_{cm}}} \tag{14}$$

She concluded that with increasing embedment length the average bond strength decreases. This is graphically shown in Figure 2-15. It is important to note that different authors use different specimens and test configurations. Therefore it is extremely hard to compare between each other.

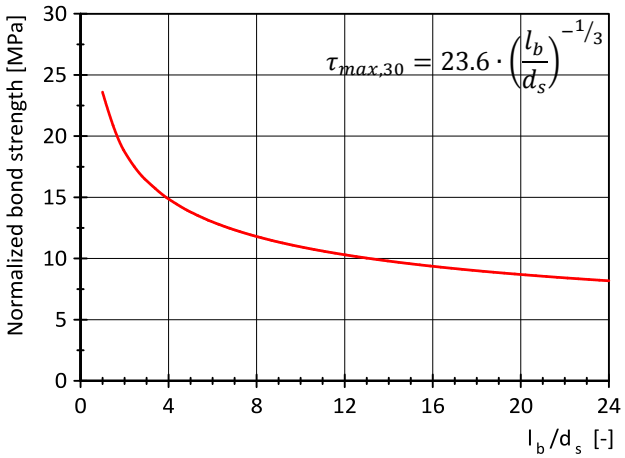

Figure 2-15: Bond zone length influence on bond strength for the pull-out test.

2.1.4.6 Loading rate

The loading rate influences the bond strength as well. However, because it is the main topic of this work, it will be discussed in the following Chapter 2.2 in more detail.

2.1.5 Variation of the results

The simple pull-out specimens with short embedded are accompanied by a quite significant variation or scatter of the test results. Because of the short bond length, an influence of weak point in the concrete is increased, which is reflected in a larger variation of the test results. Such weak points can be for instance (See [37]):

- Microstructure non-uniformity due to the pores in the concrete,
- Different position of aggregates under the ribs,
- Different rib height,
- Local differences in matrix mechanical parameters,
- The different chemical bond of the steel parts without ribs,
- The position of the bar during concreting,
- Bending of the bar due to eccentric loading,
- Impairment of the bond during handling and installation.

Very important role plays the number of ribs in the bond zone and their position, especially for short bond lengths. In their research Hawkins et al. [84] stated that the scattering of the results decreases from four ribs in the bond zone. The normal variation of the results can be as high as 20% from the average. For instance, Eligehausen [87] reported for their pull-out tests with a bond zone of $5d_s$ a scattering of the bond stress of 18% from the average. They studied twelve specimens and different concrete matrixes.

In general, the scattering of the bond stress is highest for small slip values. With increasing slip the scattering decreases. This was for instance confirmed by Martin [58] who performed pull-out tests with a bond length of $5d_s$. He observed a decrease of the coefficient of variation from 20% to 10% for slip values of 0.1 mm and 2 mm respectively. For their experimental program, they used specially manufactured ribbed steel with minimal deviation in the rib geometry.

2.2 High loading rate review

Concrete and other brittle materials behave differently when subjected to high strain rates. Already in his research Abrams in 1917 discovered that the concrete material properties change with the change of loading rate. This was later on called Dynamic Increase Factor (DIF), and it will be discussed in more detail in this chapter. The DIF can

be characterised as an increase of a mechanical property then the specimen is subjected to impact loading in comparison with the same property as measured during quasi-static loading. Various types of loading result in various strain rates which are shown in Figure 2-16.

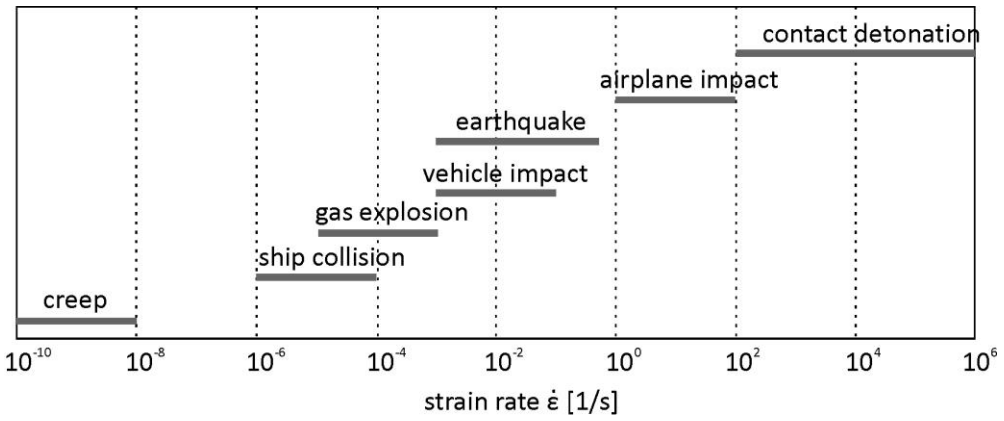

Figure 2-16: Different types of loading and corresponding strain rates.

In order to study the loading rate effects, it is first important to discuss the wave propagation theory and its difference to the theory of rigid bodies that is usually used in civil engineering.

2.2.1 Wave propagation theory

2.2.1.1 Rigid bodies vs. wave propagation

Impact problems are usually solved in Civil Engineering by using the spring-mass model. This method is very effective and good for studying the global behaviour of structures. Each structural element can then be represented by its dynamic mass and by spring which characterises its stiffness. This is sketched in Figure 2-17. For every impact incident, a momentum equation is valid, and we can write:

$$m_0\bar{v}_0 + m\bar{v} = m_0 v_0 + mv \tag{15}$$

Based on the Newtonian collision rule we can define a coefficient of restitution as:

$$\varepsilon_{res} = \frac{-v_0 - v}{\bar{v}_0 - \bar{v}} \; ; \varepsilon_{res} \in \langle 0; 1 \rangle \tag{16}$$

if $\varepsilon_{res} = 1$ the impact is ideally elastic and if $\varepsilon_{res} = 0$ it is ideally plastic. For steel the usual value of ε_{res} is 0.98. From the knowledge of the velocity before the impact we can calculate the velocity after impact by using Eq. (15) and (16). Then we can add the calculated velocity as a boundary condition in the equation of motion.

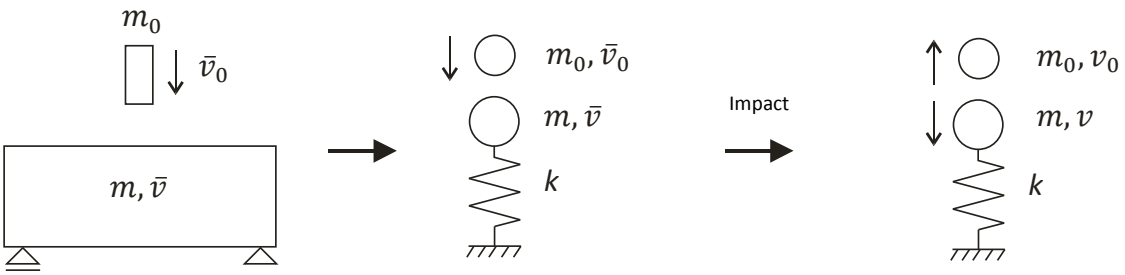

Figure 2-17: Typical simplification of impact problem in civil engineering.

The problem is that this approach assumes that the bodies are rigid and that the structural member can be represented by the simplified mass model. In addition, the impact duration needs to be separable from vibration which follows. According to some authors [88], the impact duration needs to be shorter than 1/4 of the eigen-period of the mass-spring system. Normally, the damping of such system should be considered. The mass-spring model does not take into account shock waves that propagate through the objects during the impact itself. Such situation is shown in Figure 2-18. The waves in impactor and the primary and secondary waves propagate with their specific velocities c_0, c_1 and c_2. In the case of a long bar, the primary waves are the longitudinal waves and the secondary waves are the transversal waves. These velocities are dependent on the type of material in which they propagate and on the type of the wave. As can be seen from Figure 2-18 the situation even in a simple sample can be quite complicated as the waves overlap each other. Therefore long thin bars are usually used to study dynamic characteristics of materials, because one dimensional longitudinal waves are predominant in long bars. From the above it, is clear that for the detailed analysis of bond strength between steel and concrete the approach of wave propagation theory needs to be used. The basics of the wave propagation theory work are explained for instance in books written by Graff [89] or Meyers [90].

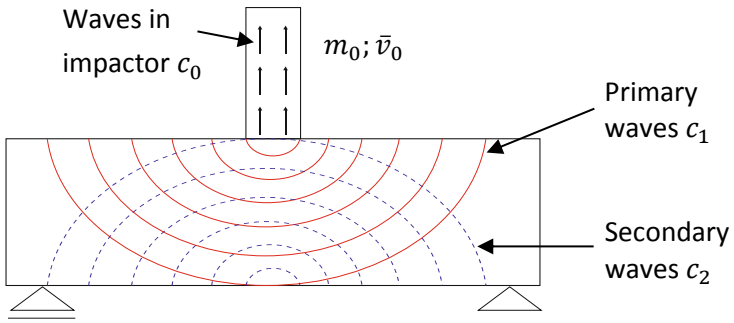

Figure 2-18: Primary and secondary waves in a beam after an impact.

2.2.1.2 Impedance

To be able to analyse bond problems the concept of impedance needs to be briefly explained. In the following text, only longitudinal waves will be considered. Whenever a wave reaches some discontinuity, it gets refracted (transmitted) and reflected at the boundary. This is caused by the different sonic impedance of the materials. The sonic impedance can be denoted as Z and is defined as a product of its medium density and by its sound or elastic wave velocity. We can write:

$$Z = \rho \cdot c \tag{17}$$

The sonic impedance is, therefore, a material property and it is applicable to any continuum. If the discontinuity is also geometrical, we can define geometrical impedance as:

$$I = \rho \cdot c \cdot A \tag{18}$$

Equation (18) is used for instance if two elastic bars with different diameters impact each other. To be able to define the stress during the impact we need to solve the momentum equation which can be written as:

$$\int F(t)dt = m \cdot v \tag{19}$$

In stress wave calculations, two different velocities must be considered. The velocity of the stress wave travelling at wave speed c and the particle's motion velocity designated with symbol v. The uniaxial elastic wave propagation velocity c within homogenous and isotropic material can be calculated:

$$c = \sqrt{\frac{E}{\rho}} \tag{20}$$

The particle velocity is the velocity of the material as the stress wave transmits energy through the medium. In the case of an impact, the particle velocity is the striker's initial impact speed, usually designated as v_0. As the stress wave passes, the particle's velocity changes from zero to v_0. All the material behind the stress wave is now at v_0. If we consider an elastic wave propagating with a wave velocity c in elastic material (Figure 2-19) we can rewrite Eq. (19) in terms of stress for infinitesimal element with a length of dx and impact time dt as:

$$F \cdot dt = d(m \cdot v) \tag{21}$$

Equation (21) tells us that impulse is equal to change in momentum. The volume of the infinitesimal part under consideration is $V = A \cdot dx$. We can then write:

$$\sigma \cdot A \cdot dt = \rho \cdot A \cdot dx \cdot v \tag{22}$$

$$\sigma = \rho \cdot \frac{dx}{dt} \cdot v = \rho \cdot c \cdot v \tag{23}$$

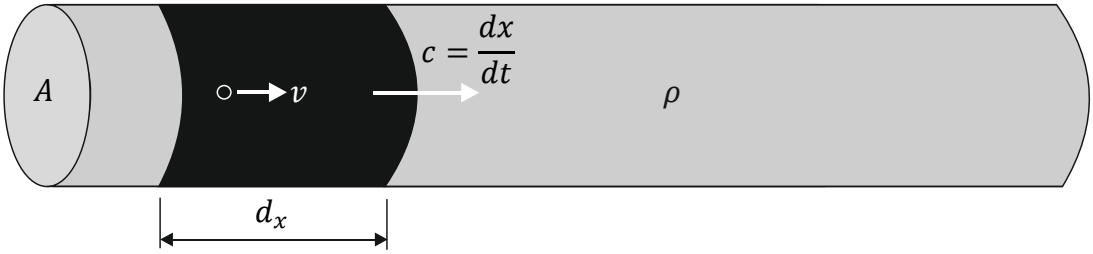

Figure 2-19: Change in momentum for a longitudinal wave in a thin rod.

In case the wave reaches an interface with an impedance mismatch a part of the wave will get transmitted and part of the wave will get reflected. This is shown in Figure 2-20, where impedance $I_1 > I_2$.

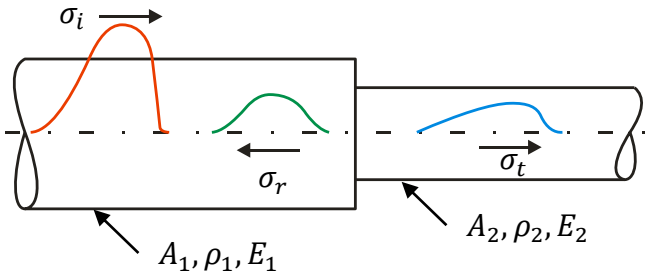

Figure 2-20: Impact of two infinite rods with different impedances.

At the interface an equilibrium of forces need to exist:

$$A_1 \cdot (\sigma_i + \sigma_r) = A_2 \cdot \sigma_t \tag{24}$$

where σ_i is the incident stress, σ_r is the reflected stress and σ_t is the transmitted stress. In addition a continuity of velocity need to exist:

$$v_i + v_r = v_t \tag{25}$$

The signs of the stresses and particle velocities can be derived from Figure 2-20. By using Eq. (23) we can write:

$$v_i = \frac{\sigma_i}{\rho_1 \cdot c_1} \qquad v_r = \frac{-\sigma_r}{\rho_1 \cdot c_1} \qquad v_t = \frac{\sigma_t}{\rho_2 \cdot c_2} \tag{26}$$

Substituting Equations (26) into (25) yields:

$$\frac{\sigma_i}{\rho_1 \cdot c_1} - \frac{\sigma_r}{\rho_1 \cdot c_1} = \frac{\sigma_t}{\rho_2 \cdot c_2} \tag{27}$$

After combining equations (24) and (27), we can write:

$$\sigma_t = \frac{2A_1\rho_2 c_2}{A_1\rho_1 c_1 + A_2\rho_2 c_2}\sigma_i \tag{28}$$

and

$$\sigma_r = \frac{A_2\rho_2 c_2 - A_1\rho_1 c_1}{A_1\rho_1 c_1 + A_2\rho_2 c_2}\sigma_i \tag{29}$$

Using Eq. (18) for impedance we can write:

$$\sigma_t = \frac{2A_1\rho_2 c_2}{I_1 + I_2}\sigma_i \qquad\qquad \sigma_r = \frac{I_2 - I_1}{I_1 + I_2}\sigma_i \tag{30}$$

From Eq. (30) is apparent that the impedance of the material influences the amplitude of the stress waves. When $I_1 > I_2$ the reflected wave has the same sign as the as the incident pulse. In the case that $I_1 < I_2$ the reflected wave has an opposite sign. In case that geometrical impedance is not considered Eq. (30) can be simplified to:

$$\sigma_t = \frac{2\rho_2 c_2}{\rho_1 c_1 + \rho_2 c_2}\sigma_i \qquad\qquad \sigma_r = \frac{\rho_2 c_2 - \rho_1 c_1}{\rho_1 c_1 + \rho_2 c_2}\sigma_i \tag{31}$$

When the transmitted and reflected stress wave amplitudes are known it is possible to evaluate what happens in two extreme cases: 1) free and 2) fixed (rigid) end. For the first case, we can write $\rho_2 c_2 \approx 0$ and for the second case we can write $\rho_2 c_2 \to \infty$. For the second case we assume that the end is rigid and that means the modulus of elasticity of the second material is infinitely large. By using Eq. (20) the elastic wave propagation velocity is then:

$$c_2 = \sqrt{\frac{\infty}{\rho}} = \infty \tag{32}$$

For the free surface - the first case - we see from Eq. (31) that the transmitted wave is $\sigma_t = 0$ and $\sigma_r = -1 \cdot \sigma_i$. For a rigid boundary Eq. (31) yields:

$$\sigma_t = \frac{2\rho_2 c_2}{\rho_1 c_1 + \rho_2 c_2}\sigma_i = \frac{2}{\frac{\rho_1 c_1}{\rho_2 c_2} + 1}\sigma_i \approx 2\sigma_i \tag{33}$$

and

$$\sigma_r = \frac{\rho_2 c_2 - \rho_1 c_1}{\rho_1 c_1 + \rho_2 c_2}\sigma_i = \frac{1 - \frac{\rho_1 c_1}{\rho_2 c_2}}{\frac{\rho_1 c_1}{\rho_2 c_2} + 1}\sigma_i \approx 1\sigma_i \tag{34}$$

The behaviour of a stress wave (in blue), as well as particle velocity (in grey) when it reaches the free end and rigid end of the bar, is graphically shown in Figure 2-21 a) and b) respectively.

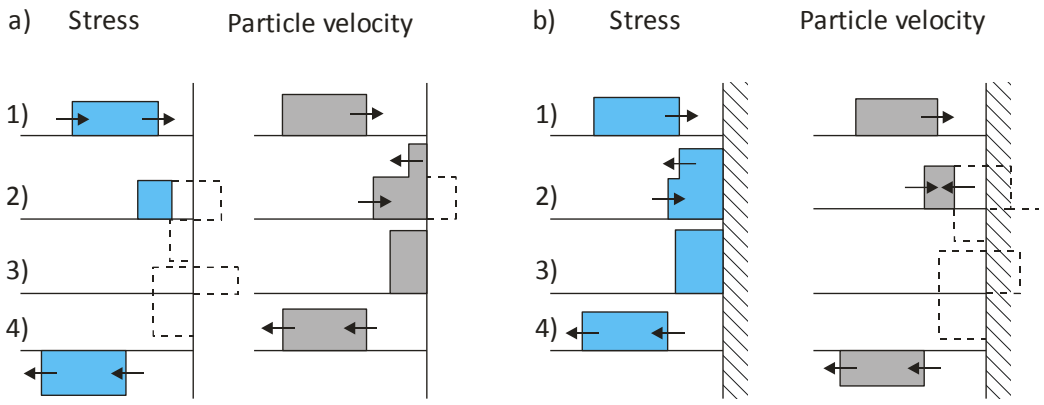

Figure 2-21: Reflection of a rectangular stress pulse at a) free end and b) rigid support. After [90].

For this work, it is very important to discuss Figure 2-21 in more detail. At the free end boundary condition, Figure 2-21 a), it comes in the second and third step to the interaction between the incident and reflected stress pulse. The stress at the free end must be therefore zero to satisfy the boundary condition. From the fourth step, it is seen that the reflected pulse has opposite sign as the incoming one. That means that at it comes to stress reversal at the free end. It can also be seen from Figure 2-21 a) that it comes to particle velocity and displacement doubling at the free end. See steps 2 and 3. The exact opposite situation arises in the case of the rigid boundary as shown in Figure 2-21 b). During the steps 2 and 3, it comes to stress doubling. For instance, if the incident wave is compressive, the reflected wave is compressive as well and the both waves superimpose each other. The particle velocity and displacement are obviously zero at the rigid support. The following results of this simple analysis are of practical importance:

a) At free end, it comes to:
   - stress neutralisation during the interaction,
   - stress reversal after interaction and
   - deflection doubling during the interaction.

b) At rigid support, it comes to:
   - stress multiplication and
   - stresses become identical after the interaction.

For instance, the stress reversal can be utilised when testing the tensile dynamic behaviour of materials during spallation tests [91]. In his dissertation, Wensauer [32] described a concept in which the concrete spallation can be utilised for pull-out bond strength testing (see Chapter 2.2.4).

2.2.1.3 Longitudinal impact of two bars

The basis of the experimental work presented in this thesis is the longitudinal impact of two flat-ended bars which is used to analyse the bond stress behaviour of steel and concrete under impact. In the most basic impact scenario, an impactor of a finite length L and flying with a velocity v is impacting a long thin semi-infinite bar which is not under motion. Both impactor and bar are characterized by the same material properties and cross-sectional areas as shown in Figure 2-22. When the impactor and bar collide, two stress waves starts to propagate to the right and left from the interface. The waves have analytically predictable rectangular shape and are both compressive. Because of the same material the wave propagation velocity is $c_1 = c_2 = c$ for both bars. When the stress pulse in the impactor reaches it's free end it comes to stress reversal and tensile wave propagates towards the bar. After this wave reaches the interface of the impactor and the semi-infinite bar, it comes to separation because the contact can transfer only the compression. Because the impedances of the impactor and the bar are the same, the impactor is brought to rest after the separation. This separation occurs at time:

$$T = \frac{2 \cdot L}{c} \tag{35}$$

From the contact time, the length of the compressive pulse in the bar can be calculated.

$$\Lambda = 2 \cdot L \tag{36}$$

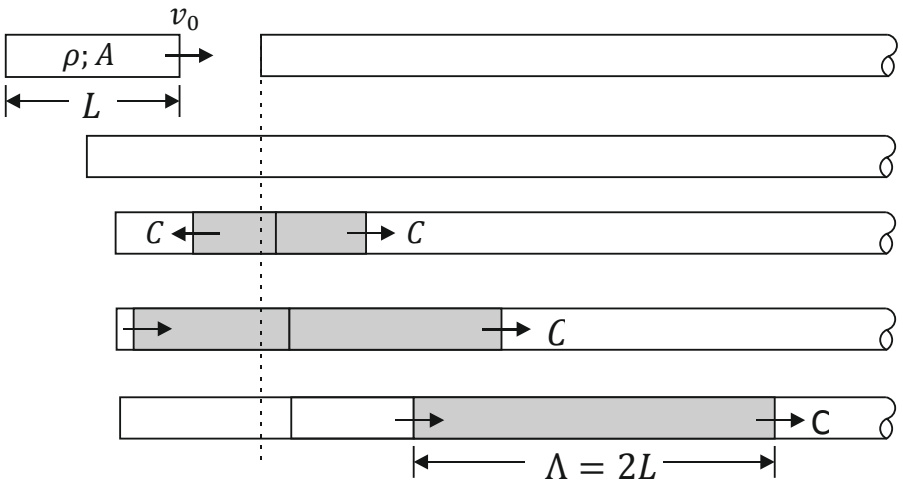

Figure 2-22: Impactor hitting a long thin bar, after [90].

The particle velocity in the bar after impact v_p can be calculated from the conservation of momentum, i.e. momentum before impact is equal to momentum after impact. The mass of particles under motion after impact is:

$$m_p = \rho \cdot A \cdot \Lambda = \rho \cdot A \cdot 2L \tag{37}$$

where *2L* is the length of the stress pulse. We can when write

$$\begin{gathered} m\bar{v}_0 = m_p v_p \\ \rho \cdot A \cdot \bar{v}_0 = \rho \cdot A \cdot 2L \cdot v_p \\ v_p = \frac{\bar{v}_0}{2} \end{gathered} \tag{38}$$

From the particle velocity, it is easy to calculate the stress intensity σ_0 of the generated pulse using Eq. (23) as:

$$\sigma_0 = \frac{1}{2} \cdot \rho \cdot c \cdot \bar{v}_0 \tag{39}$$

In reality, the stress pulse is not entirely rectangular, but it shows oscillations that are caused by lateral inertia. This is usually called dispersion effect and was studied by Pochhammer [92] and Chree [93] as well as Rayleigh [94].

2.2.2 Concrete behaviour under high strain rates

The influence of strain rate on concrete compressive and tensile strength is a very complex topic. It becomes even more complicated when the multiaxial behaviour of

concrete is considered. It is important to realise, that dynamic impact loading cannot be considered simply as an extreme case of high-stress rate application. The complex energy transfer mechanisms associated with impact loading appear to be different from those under quasi-static loading. Thus, according to Banthia et al. [95], it is not possible to predict the behaviour of concrete under impact loading solely on the base of quasi-static tests. However, a consensus among researchers exists, that high loading rates lead to increase in mechanical properties. The question is, how big this increase is and what part of the increase can be attributed to the influence of inner material inertia and what part is the actual material behaviour. For detailed information, an ACI report on dynamic fracture of concrete can be referred to [5], as well as many other publications. The increase in a mechanical property is usually presented in relationship to either stress or strain rate which is defined as stress or strain increase in time:

$$\dot{\varepsilon} = d\varepsilon/dt \tag{40}$$

$$\dot{\sigma} = d\sigma/dt \tag{41}$$

The unit is in both cases 1/s. An increase in a mechanical property is defined as a dynamic increase factor (DIF) which is a ratio between the dynamic property and its quasi-static reference value. Because of inertial and crack propagation considerations, it is not possible to directly link strain rates and loading rates. It is recognised that various concrete mechanical properties have different strain rate sensitivity. The DIF of concrete in tension, flexure, and compression is schematically shown in Figure 2-23. The strain corresponding to the maximum strength also increases with an increase in the loading rate. The increase in strain is due to the development of multiple cracks in the failure zone, and the value of the maximum strain is strongly dependent on the width assumed for the failure zone.

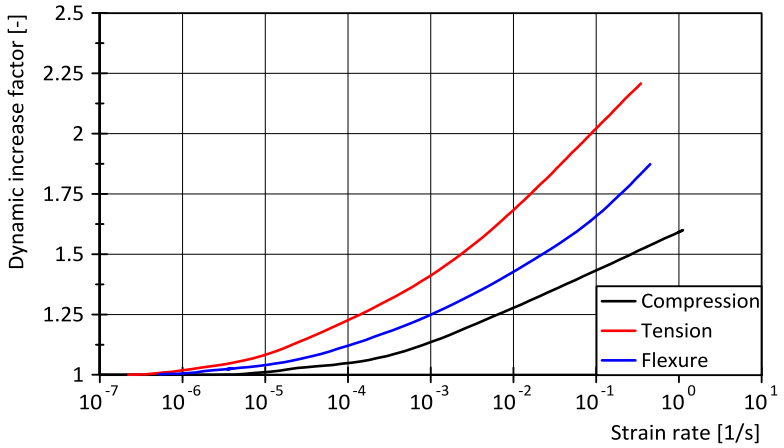

Figure 2-23: Strain rate behaviour of plain concrete under different types of loading, after [96].

In the case of the bond between concrete and deformed bars it can be expected that it will be greater at high loading rates in comparison to low rates because the bond strength depends on two effects:

1. Concrete-rebar shear, and microfracture within the concrete.
2. Bearing between the concrete and the ribs of the rebar.

Because the compressive strength of concrete in both the shear and bearing modes increases with increased loading rate, it will be discussed in more detail. In their work, Bischoff and Perry [7] summarised the most important findings on strain rate effects on the concrete compressive strength. Extensive work on biaxial concrete compressive strength was performed for instance by Quast [97]. A significant increase in the concrete compressive strength under dynamic loading was observed at strain rates higher than 30 s^{-1}. This is reflected in the MC 2010 [16], where for a given strain and stress rate, respectively, the compressive strength under high rates of loading can be estimated from:

$$\frac{f_{c,imp,k}}{f_{cm}} = \left(\frac{\dot{\varepsilon}_c}{\dot{\varepsilon}_{c0}}\right)^{0.014} \quad \text{for } \dot{\varepsilon}_c \leq 30\ s^{-1} \tag{42}$$

$$\frac{f_{c,imp,k}}{f_{cm}} = 0.012\left(\frac{\dot{\varepsilon}_c}{\dot{\varepsilon}_{c0}}\right)^{1/3} \quad \text{for } \dot{\varepsilon}_c > 30\ s^{-1} \tag{43}$$

with $\dot{\varepsilon}_{c0} = 30 \cdot 10^{-6}\ s^{-1}$

$$\frac{f_{c,imp,k}}{f_{cm}} = \left(\frac{\dot{\sigma}_c}{\dot{\sigma}_{c0}}\right)^{0.014} \quad \text{for } \dot{\sigma}_c \leq 10^6\ MPa/s \tag{44}$$

$$\frac{f_{c,imp,k}}{f_{cm}} = 0.012\left(\frac{\dot{\sigma}_c}{\dot{\sigma}_{c0}}\right)^{1/3} \quad \text{for } \dot{\sigma}_c > 10^6\ MPa/s \tag{45}$$

with $\dot{\sigma}_{c0} = 1\ MPa/s$.

Above 85 % of the experimental data are above the MC formulas. This is graphically shown in Figure 2-24 where also increase in compressive strength as measured by various authors in dependence on the strain rate is shown.

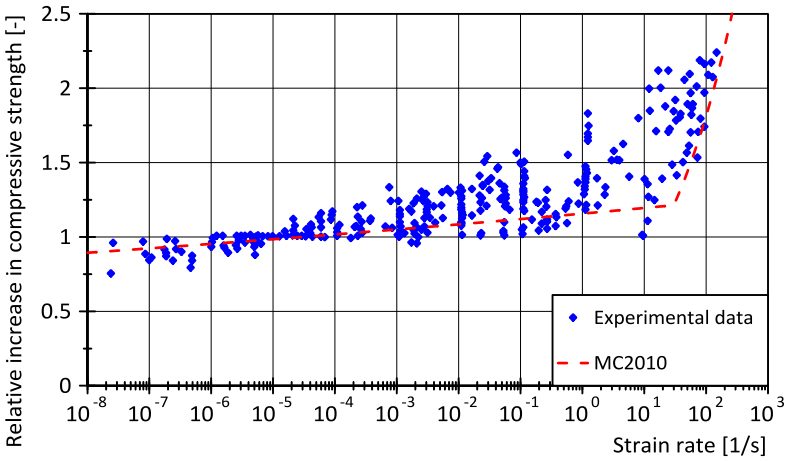

Figure 2-24: Compressive strength vs. strain rate, after [98].

Takeda [99] stated that the strain rate sensitivity of concrete led to two different effects: on the stress-strain relationships, and on the fracture criterion. The distributed area of strain was much narrower under dynamic loading than under static loading. In real structures, the increased bond strength of the reinforcement in concrete could lead to a brittle failure because the deformation is limited only to a short length of the reinforcing bar. For instance, Bentur, Mindess and Banthia [100] and Banthia [101] showed that, under certain circumstances, the steel reinforcement itself might fail under impact loading of reinforced concrete beams. The enhanced concrete-steel bond limited the deformations to the small area under the point of impact, leading to ductile fracture of the steel.

2.2.3 Steel behaviour under high strain rates

The reinforcing steel in the elastic area doesn't show great sensibility to the loading rate. This changes when the steel yields as then the tensile strength, as well as the elongation without necking increases by increasing loading rate. This was described for instance by Lin [102] in his dissertation. Hjorth [103] measured stress-strain relation of reinforcing steel for three different strain rates $\dot{\varepsilon} = \varepsilon \,/\, t$ of 0.00128, 0.128 and 12.8 1/s. The results for BSt 42/50 (K) steel are shown in Figure 2-25. He concluded that the ultimate tensile stress R_m increases with increasing strain rate and that fracture strength is independent on the strain rate. The strain at steel yielding seems also to be unaffected by the strain rate which agrees with the research conducted by Lin [102].

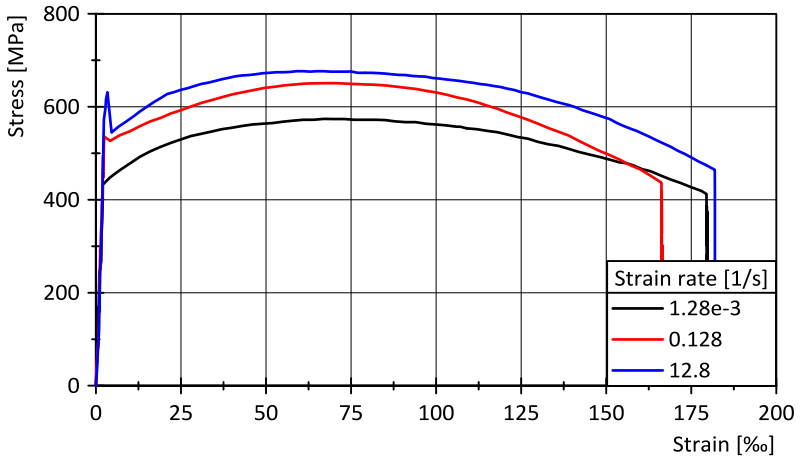

Figure 2-25: Stress-strain diagrams for BSt 42/50 (K) steel under high strain rates, after [103].

2.2.4 Bond behaviour under high strain rate loading

The available literature regarding the bond stress-slip behaviour under impact loading is relatively limited. In the past research groups from the USA, Holland, Germany and Japan studied the topic. Generally, it is believed that bond strength is sensitive to loading rate similarly as in the case of just concrete. The strain rate effect is more pronounced for concretes of lower strength classes. The problem which arises during analysis of various research results is that no standardised test for high loading rates exists. There are basically three categories in which the high loading rate experimental work can be divided into:

1) Tests in conventional servo-hydraulic machines with high loading crosshead velocity.
2) Experimental work based on free fall such as drop-tower experiments.
3) Studies involving split Hopkinson bar and its modifications.

The results can then be evaluated from the point of rigid body elementary theory or from the point of wave propagation theory. When it comes to specimens, usually push-in or pull-out specimen types (Figure 2-4) are used. The problem is that the approach of every research group is very different which makes the results very hard to interpret. Details such as sampling rate, type of used sensors and filtration of noise from the measured signals can significantly influence the results. These boundary conditions are not always presented in the literature. In the following paragraphs, an overview of works known to the author is presented. An attempt is made to evaluate these results critically with respect to each other.

First studies about the influence of high loading rates on the bond behaviour of steel and concrete were published by Hansen and Liepins [104] and by Shah and Hansen [105]. In their research, they used deformed steel of various diameters that was embedded in concrete with varying compressive strength. Their research programme has covered the following categories of tests:

1. Specimens with the concrete compressive strength of 13.8 MPa, 24.1 MPa and 41.4 MPa.
2. Specimens with reinforcing steel diameter of 25.4 mm, 32.3 mm and 43.0 mm.

The used steel diameter was quite large in comparison with other studies. Pull-out specimens were used for the tests, both of static and dynamic loads. The dynamic load was of a triangular pulse type with a rise time of about 15 to 20 ms. The test specimen was relatively complicated and consisted of a reinforced concrete block as shown in Figure 2-26. Always two reinforcement bars were embedded into the concrete specimen. The bond length was $3 \times d_s$ whereas the bond free zone was made by using cast iron pipes with rubber stops. The slip was measured at the unloaded end of the bars with LVDT (linear variable differential transformer) sensors. The pull-out force was measured using two strain gauges that were glued on both sides of the rebar before the bond zone as well as a load cell attached to the loading frame. The acceleration of the test bock was measured by accelerometers with a range of ±40 g.

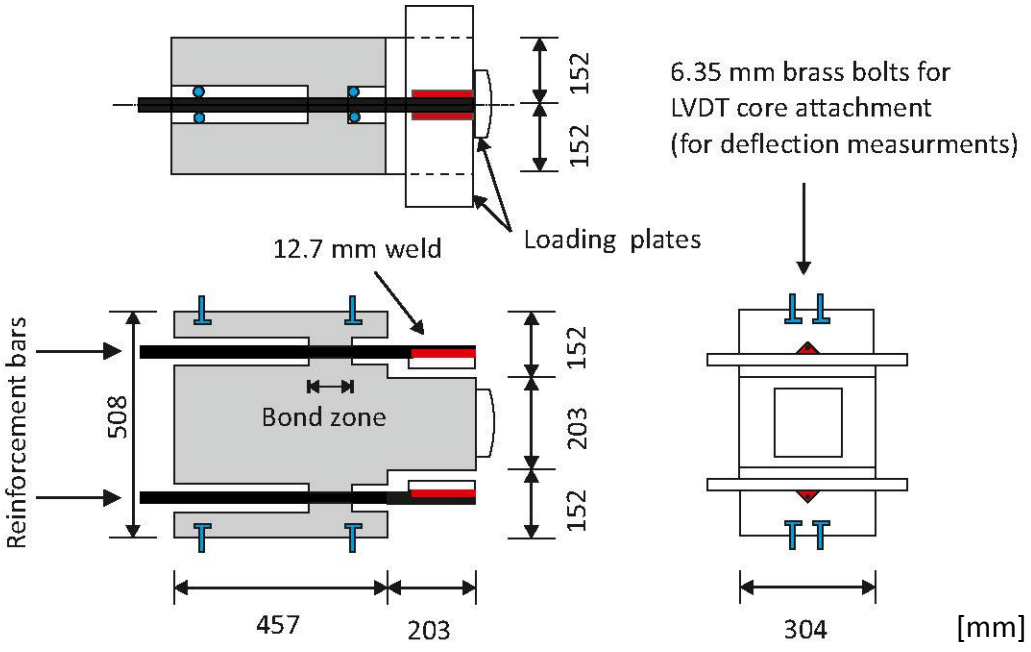

Figure 2-26: Test specimen as used by [105]

They concluded that static ultimate bond strength of concrete is of the order on 0.5 to 0.6 f_c, while the corresponding dynamic ultimate bond strength of concrete varies from 0.6 to 0.9 f_c. The dynamic increase factor is larger for concretes of lower strengths. They also concluded that splitting and cracking are important factors that influence the bond failure.

Unfortunately, their report doesn't provide details about results evaluation and the way how the inertia of the sample was eliminated from the measurements. If the results were to be analysed from the wave propagation theory point of view, then the strain gauge as well as the load measurements before the bond zone capture the loading tensile wave introduced into the reinforcement steel. However, the portion of load transferred into the specimen can be diametrically different from these measurements. This will be shown in this work in Chapter 4.2. In addition, symmetric loading of both rebars seems to be problematic in dynamic case.

A great number of pull-out tests under dynamic loading conditions was performed by Hjorth [103]. He studied not only the effect of the loading rate but also the effects of the bond zone length and the steel diameter influence. The investigated steels had diameter d_s = 8, 16 and 26 mm. He used cylindrical specimens with minimal concrete cover of $5d_s$ and 16 to 160 mm long bond zone located in the middle of the specimen. Pull-out type of test was performed in hydro-pulse loading machine with a load rise from 500 s to 5 ms. Pull-out force was measured with a load cell, and relative slip was measured with LVDT's. The results were evaluated based on the average bond stress rate until failure $\dot{\tau} = \tau/t$ in [MPa/s]. He concluded that short bond lengths until $3.5 \times d_s$ are not very suitable for bond testing as the results scattering was too high and that in some cases the steel was loosen even before the start of the experimental work. Based on the bond stress slip behaviour of plain bars he concluded that chemical bond and steel-concrete friction does not contribute to the increase of bond strength under high rate loading. The results of Hjorth were redrafted by Wensauer [32] in his dissertation and are presented in Figure 2-27. Only results of steel with a diameter of 16 mm and bond lengths $5 \times d_s$ and $7 \times d_s$ are presented. The average cubical concrete compressive strength was $f_{c,cm} = 25\ MPa$. Very high scattering which is typical for pull-out tests is apparent form Figure 2-27. The results show an increase of the bond strength up to 30 % in average for loading rates as high as 3 000 MPa/s. Hjorth attributed the increase in dynamic bond strength to the increased concrete compressive strength under high loading rates. Similarly to other researchers, he concluded that with an increasing concrete compressive strength the sensitivity to the loading rate is lower.

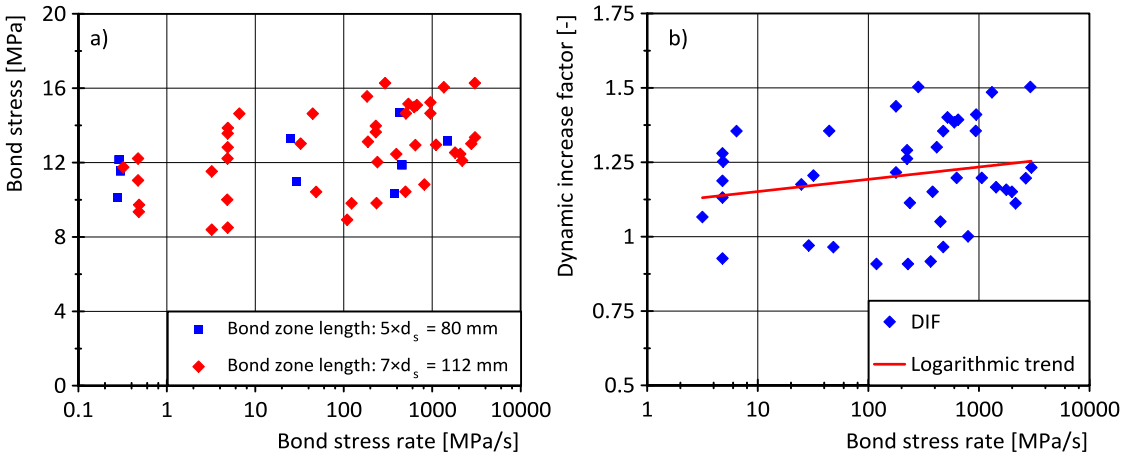

Figure 2-27: Results for deformed bars: a) bond stress and b) DIF in dependence on the bond stress rate. After [32], original data from [103].

The influence of loading rate on average bond stress-slip relationship for a relatively long bond length of $7 \times d_s$ as measured by Hjorth is presented in Figure 2-28. The concrete average compressive strength was $f_{cm,c} = 25.5MPa$.

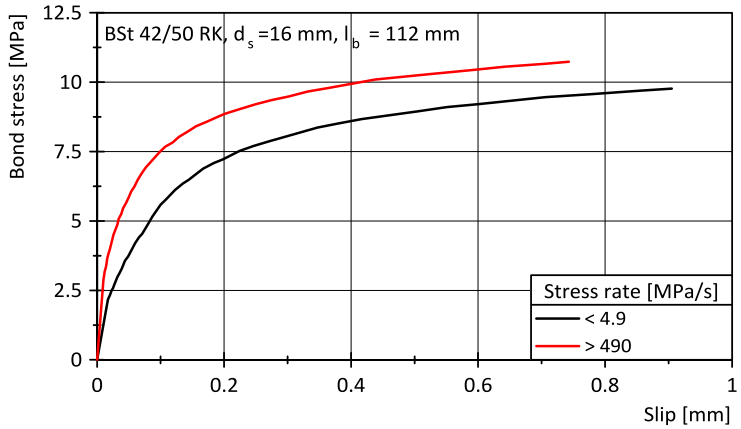

Figure 2-28: Typical bond stress-slip relations for two loading rates. After [103].

The pull-out resistance on cylindrical specimens was measured by Vos and Reinhardt [106, 107]. They were the first research team that used a method based on the split Hopkinson bar (SHB) for bond strength determination under impact loading. Their SHB was vertically arranged, and they measured the tensile wave induced by a steel impactor that strikes a stopper (anvil) attached to the end of the incident bar. In this respect, their experimental setup was very similar to the drop-tower setup used in this experimental work (Chapter 3.6.1). By using damping material between the stopper and impactor, they were able to produce loading rates ranging from 20×10^3 to 160×10^3 MPa/s. The sample built in the testing rig as used by Reinhardt [108] is shown in Figure 2-29.

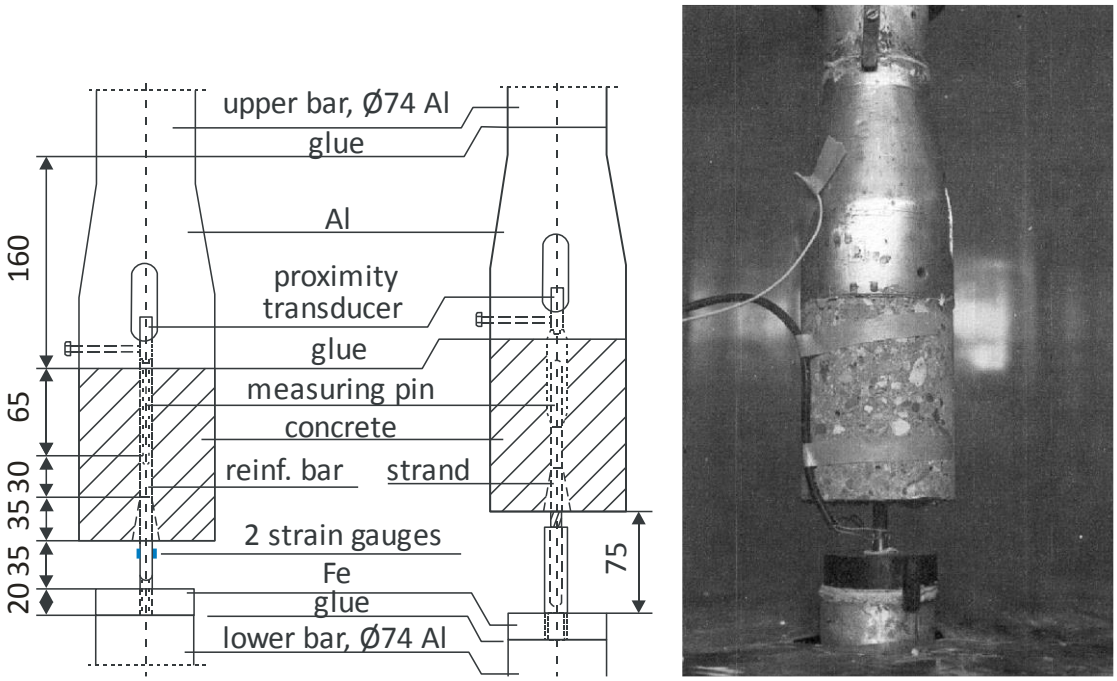

Figure 2-29: Pull-out test setup as used by Reinhardt [80].

The concrete cylinders for pull-out testing were 104 mm in diameter and 130 mm in height. The reinforcing bars had a diameter $d_s = 10\ mm$ and bond length was $3 \times d_s = 30\ mm$. The slip of the rebar was measured with the aid of proximity transducer, and the force is determined through the strain gauge signal evaluation. They used very good sampling rate of 2 MHz. In their research they accounted for material and geometrical impedance of the sample and of the incident and transfer bar. The main goal of the work was to study the influence of concrete strength on bond strength DIF. Three concrete were investigated with a mean compressive strengths of 23, 45 and 55 MPa. Plain bars as well as deformed bars and pretensioning tendons were investigated. The bond stress rate was calculated as the slope of $\tau - t$ curve for a displacement of 0.01 mm. Bond stress-slip relationships or two different concrete grades as measured by Reinhardt [108] are presented in Figure 2-30.

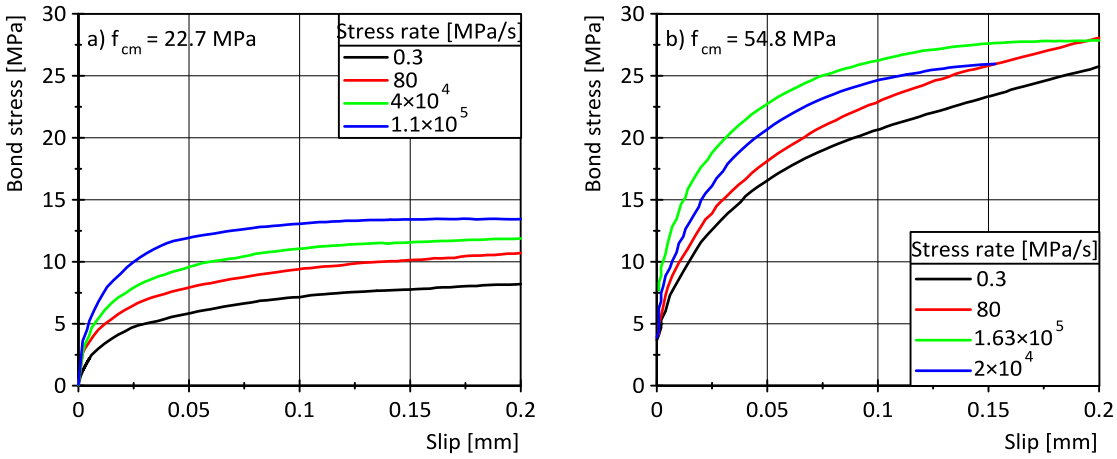

Figure 2-30: Bond stress-slip relationships at four loading rates for concrete with a cubical strength of a) 22.7 MPa and b) 54.8 MPa.

Similarly, to all other researchers, it can be seen that the DIF is higher for concretes with low compressive strength. From Figure 2-30 a) it can be seen that the increase in bond strength is up to 60%. For the concrete of higher compressive strength ($f_{cm} = 54.8\ MPa$) the increase is not so significant Figure 2-30 b). At the slip value of 0.2 mm the maximal dynamic bond strength is even lower than the quasi-static one. The failure mechanism was directly connected with the shearing off of the concrete cantilevers (keys) between the ribs. Therefore, the increase of the dynamic bond strength was attributed to the concrete compressive strength. Based on their results Reinhardt formulated an equation which can be used to predict the DIF which is defined as a ratio of dynamic bond stress τ to the static one τ_0.

$$\frac{\tau}{\tau_0} = \left(\frac{\dot{\tau}}{\dot{\tau}_0}\right)^{\frac{0.7(1-2.5\delta)}{f_c'^{0.8}}} \tag{46}$$

This equation is however only valid until a very small slip of 0.2 mm. The equation (46) expresses the fact that the bond stress for a certain displacement and a certain concrete compressive stress increases with the rate of loading. It is valid only for deformed bars with a relative rib area f_R from 0.065 to 0.1. The loading rate has the greatest effect in the case of low strength concretes, especially at small slip between reinforcing steel and concrete. This result can be interpreted as that the effective bond length of a deformed bar decreases with increasing loading rate. In case of plain bars and prestressing strands the strain rate effect was found to be negligible which is in agreement with the findings of Hjorth [103].

In 1982 studied Eligehausen et al. [34] local bond stress-slip relationships under generalised excitations. They concluded that the bond stress-slip relationship was influenced by the rate of slip increase, however slightly less than predicted in [31]. Their results are presented in Figure 2-31. They observed an increase in maximal bond strength of around 24 % for slip rate $\dot{s} = s/t$ that was increased from 0.034 mm/min (0.00057 mm/s) to 170 mm/min (2.8 mm/s). It is interesting to observe, that the loading rate effect is already observable by relatively slow loading rates. Similar effect was observed also in this work, where the rate sensibility was observable at the loading rate of 50 mm/s which correspond to 3 000 mm/min.

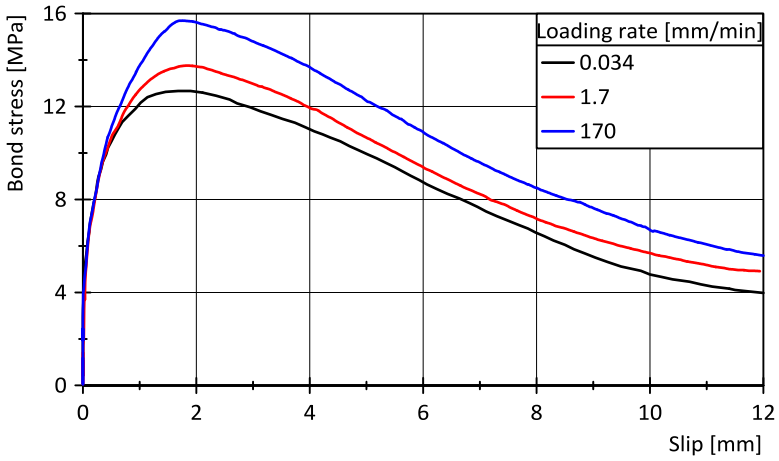

Figure 2-31: Loading rate influence under monotonic increasing slip, after [34].

Contradictory results to the ones of Eligehausen were presented by Rußwurm [109] et al. They studied bond stress-strain behaviour under relatively low loading rates until the slip value of 1 mm. Under the investigated bond stress rates $\dot{\tau} = \tau/t$ between 0.002 to 0.2 MPa/s no increase in bond strength was observed. Similar behaviour was observed by Martin and Noakowski [24] for bond stress rates from 0.5 to 50 MPa/s.

Both push-in and pull-out behaviour of steel plain and deformed reinforcement bars were studied by Yan in his dissertation [22]. The most important findings are summarised in [110, 111] and [112]. In total, the bond strength of 420 test specimens for static, medium and impact loading rates was measured. The loading rates used by Yan are shown in Table 2-5.

Table 2-5: Steel and bond stress rates used as used by Yan [22].

Load type	Stress rate		Testing machine	Loading velocity
	Steel [MPa/s]	Bond [MPa/s]		[mm/s]
Static	$10^{-7} – 10^{-5}$	$0.5\times10^{-8} – 0.5\times10^{-6}$	Instron	$8\times10^{-4} – 8\times10^{-2}$
Medium	$10^{-5} – 10^{-3}$	$0.5\times10^{-6} – 0.5\times10^{-4}$		$8\times10^{-2} – 8$
Impact	$10^{-3} – 10^{-1}$	$0.5\times10^{-4} – 0.5\times10^{-2}$	Impact	8 – 100

The test specimens were concrete prisms 152.4 × 152.4 × 63.5 mm with either smooth bar 12.7 mm in diameter or deformed reinforcing bar 11.3 mm in diameter. The bars were completely embedded in concrete, which yields bond zone lengths $5 \times d_s$ and $5.6 \times d_s$ for plain and deformed bars respectively. Confinement against radial cracks was provided by two concentric spirals 63.5 mm and 127 mm in diameter, that were embedded in the concrete. Both push-in and pull-out tests were performed and concrete compressive strength was varied throughout the experimental work. Plain, polypropylene fibre reinforced concrete as well as steel fibre reinforced concrete was investigated. The strain distribution along the embedded rebar was measured on 5 locations. The average local bond stress $\tau_{i,j}$ was calculated from the axial stresses in the steel σ_s between the ith and jth location as:

$$\tau_{i,j} = \frac{\sigma_{s,i} - \sigma_{s,j}}{4 \cdot \Delta x} \cdot d_s \tag{47}$$

Where Δx is the distance between ith and jth location. The corresponding stresses in the concrete σ_c across the cross section, were calculated from the strain equilibrium equation,

$$\int_{l_i}^{l_j} \pi \cdot \tau_{i,j} \cdot d_s \cdot dl = \gamma \cdot \sigma_c \cdot A_c \tag{48}$$

Where

γ is coefficient that accounts for the nonuniform distribution of stress in the concrete across the section; $\gamma = 0.30$ in their study.

A_c is the area of concrete cross-section.

The strain in the concrete ε_c was always found through the stress σ_c, according to three dimensional Hook's law. The slip $s(x)$ between the rabar and the concrete at any point between the ith and jth location along the rebar was determined by the compatibility condition between the two materials:

$$s(x) = \int_0^x (\varepsilon_s - \varepsilon_c) dl \tag{49}$$

where x is the distance from i[th] point.

The major criticism of Yan's work are the consequences of Equation (48). Here an equilibrium of strains between concrete and steel is assumed. This is certainly true for the quasi-static state. However, this assumption is invalid for impact loading. The strains in concrete ε_c change in time and space based on the way how the loading wave passes through the specimen. There is no equilibrium of strains during the first wave pass. The strain in concrete is influenced by wave reflections from the concrete surface and from the steel-concrete interface. On the other hand, it is probably the best possible way how to approximate the concrete strain as it can't be measured directly without interference in the bond zone area. The relationship between the peak bond stress and the loading rate for normal strength (40 MPa) and high strength concrete (75 MPa) as measured by Yan, is given in Figure 2-32.

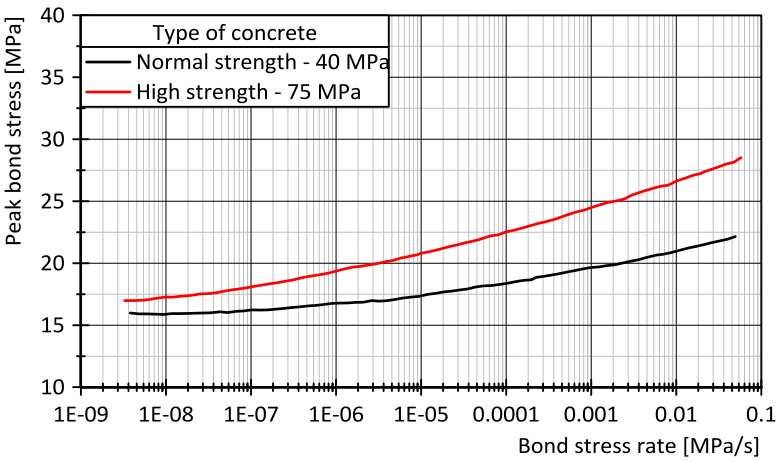

Figure 2-32: Effects of loading rate on the peak bond stress for normal and high strength concrete, from [110].

From Figure 2-32 it can be seen that the peak bond stress increases considerably with an increase in loading rate. In addition, it can be seen that this effect is more pronounced for high strength concrete. This is, however, contradictory to results reported by other studies mentioned above. Yan and Mindess [110] also state that the increase in bond strength is more pronounced for push-in tests compared to pull-out tests. This can, however, be an indirect effect of utilisation of load reversal system rather than actual material behaviour. The results of Yan and Mindess [110] need to be interpreted with a great caution. Even though the impact bond stress rate is suspiciously low in comparison to other researchers, the measured DIF is remarkable. Similarly to other researchers,

they concluded that the strain rate effect is negligible for plain bars. The main conclusions as summarised by Yan and Mindess [110] are as follows:

1. A higher loading rate significantly increases the bond resistance capacity;
2. Higher stresses, both in the rebar and in the concrete, greater slips, higher bond stresses, and larger fracture energies during the bond failure were developed with an increase in the loading rate;
3. Higher loading rate significantly changes the bond stress-slip relationship; and
4. These effects are especially noticeable for high strength concrete, steel fibre reinforced concrete, and for the push-in loading case.

The reason for the test specimens being able to withstand greater bond stress with increased loading rates is primarily due to the velocity of crack propagation. With increased rate, the stress does not have sufficient unloading time to dissipate the forces throughout the concrete matrix to the point of weakness. The cracks are therefore less able to form at higher loading rates than at lower loading rates.

Another series of pull-out tests on cylindrical specimens was performed by Weathersby [113]. Similarly to this work he studied three loading rates with the following loading durations: static (97–713s), dynamic (31–200 ms) and impact (4–7.4 ms). The loading duration was defined as the time from the beginning of the loading to the failure of the specimen. For the deformed bars he measured 100 % increase in the bond strength in case of the impact loading. The concrete cover of the tested specimens was however very small, and the dominating failure mechanism was concrete splitting. The resistance of the concrete to splitting is dominated by its tensile strength which is more sensitive to strain rates. This could explain the exceptionally high DIF. This was also confirmed by the research of Solomos and Berra [86] who showed that in the case of splitting failure the increase of bond strength is up to 90 % whereas in the case of pull-out failure mode the increase is only 30 %. In their research, they used short unconfined and long confined rebar specimens. They investigated Dywidag bars with a diameter of 20 mm and bond length of 100 or 200 mm. They used a modified split Hopkinson bar that consisted of a 100 m long pre-stressed bar that was abruptly released. This lead to nearly rectangular loading pulse of 40 ms duration and a rise time of 400 µs. The incident bar was of 72 mm in diameters and the transmitter bar of 25 mm in diameter. A 1.1 m long load-inversion canister was used, which housed the rebar specimen as shown in Figure 2-33.

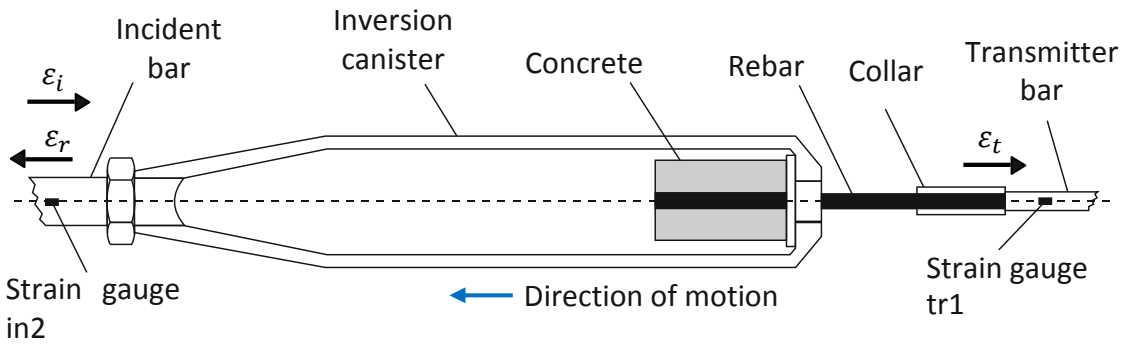

Figure 2-33: Details of mounting of the rebar specimen in the inversion canister between the incident and transmitter bars, from [86].

The pull-out force was calculated from the strain measured in transmitter bar, and the slip was measured as a relative movement of point C on Figure 2-33 to the canister's surface by an optical extensometer. She slip was subsequently corrected by the elastic elongation of the segment AC of the rebar. That means that the slip was measured by the loaded end of the specimen. The slip measured by optical extensometer was also compared to the slip calculated from the Hopkinson bar analysis. For more details refer to [86]. Splitting of unconfined specimens and pull-out failure of the confined specimens was observed. In addition, post installed, and cast-in-place specimens were compared. The focus of this review is only on the confined cast-in-place as they are relevant to this work.

As could be expected, the confinement effect minimised the radial expansion of concrete, prevented cracking and increased the rebar friction and mechanical interlocking. A smaller DIF was observed for pull-out specimens in comparison to the splitting specimens. The DIF factors were 22% for the 100 mm and 11% for the 200 mm embedment length, respectively. The moderate increase in DIF was attributed to lower strain sensitivity of the concrete compressive strength. The authors assume that the strain rate in the concrete is in order of 10 s^{-1}, although they state that it's impossible to measure it directly. The average maximal bond stress as measured by Solomos and Berra [86] for two different concrete classes and two types of failure for static and impact loading is presented in Table 2-6.

Table 2-6: The average maximum bond stress of rebar specimens under static and impact testing, after [86].

Concrete class	Bond length [mm]	Failure type	Loading rate	Bond strength [MPa]	DIF [-]
C25/35	100	Pull-out	Static	16.9	-
			Dynamic	20.6	1.22
		Splitting	Static	6.4	-
			Dynamic	12.3	1.91
	200	Pull-out	Static	15,5	-
			Dynamic	17,3	1.11
		Splitting	Static	6,4	-
			Dynamic	9,0	1.39
C50/60	100	Pull-out	-	-	-
		Splitting	Static	10.0	-
			Dynamic	13.2	1.32

That means that the components exhibit more ductility under impact loading. As expected, the pull-out bond strength is greater than the splitting strength. Increase in the bond length from 5×d_s to 10×d_s leads to a slight decrease in maximal bond strength both in the static as well as in the dynamic case. This is caused by uneven bond stress distribution and is discussed in Chapter 2.1.4.5 for quasi-static loading. In agreement with all other research presented in the current chapter, the DIF for concretes of higher strength if lower in comparison to the DIF for low strength concretes.

The influence of high strain rates on the bond behaviour of reinforced concrete was investigated by Wensauer [32] in his dissertation. He proposed a measurement method that was based on split Hopkinson bar in spallation configuration. Cylindrical specimens with 75 mm in diameter and length of 300 mm were tested. The 10 mm in diameter reinforcement bar was placed in the middle of the specimen. Only a small part of the rebar protruded into the last third of the specimen (segment II). The length of the protrusion corresponded to the bond length l_b and was varied from 10 to 40 mm. The sketch of the specimen as used by Wensauer [32] is shown in Figure 2-34. The segments I and II were divided by foil or demoulding oil.

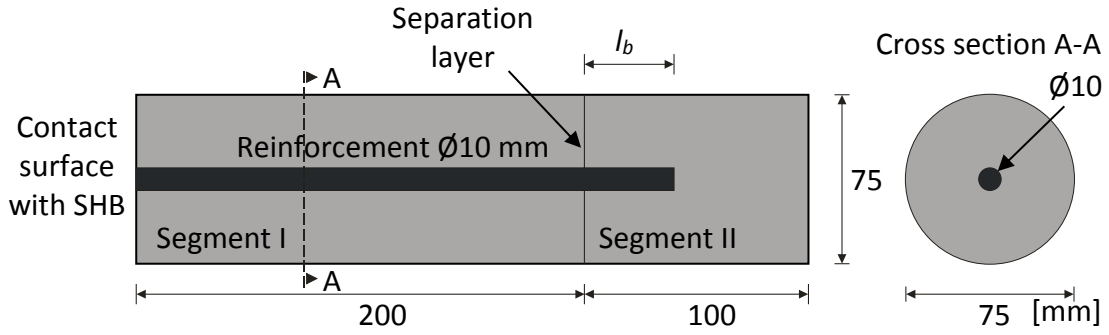

Figure 2-34: Specimen geometry, from [32].

The specimen shown in Figure 2-34 was attached to the end of the incident bar. After a compressive wave had been induced by an impactor into the incident bar, it got transferred into the specimen. At the free end of the specimen, this compressive wave was reflected as a tensile wave travelling in the opposite direction. The theory behind this was explained in Chapter 2.2.1 and sketched in Figure 2-35 a). In case that the bond strength is lower in comparison to the dynamic concrete tensile strength, the stress reversal cause bond failure, which is shown in Figure 2-35 b). In case that the bond strength is greater than the tensile strength of concrete it comes to concrete spallation as shown in Figure 2-35 c).

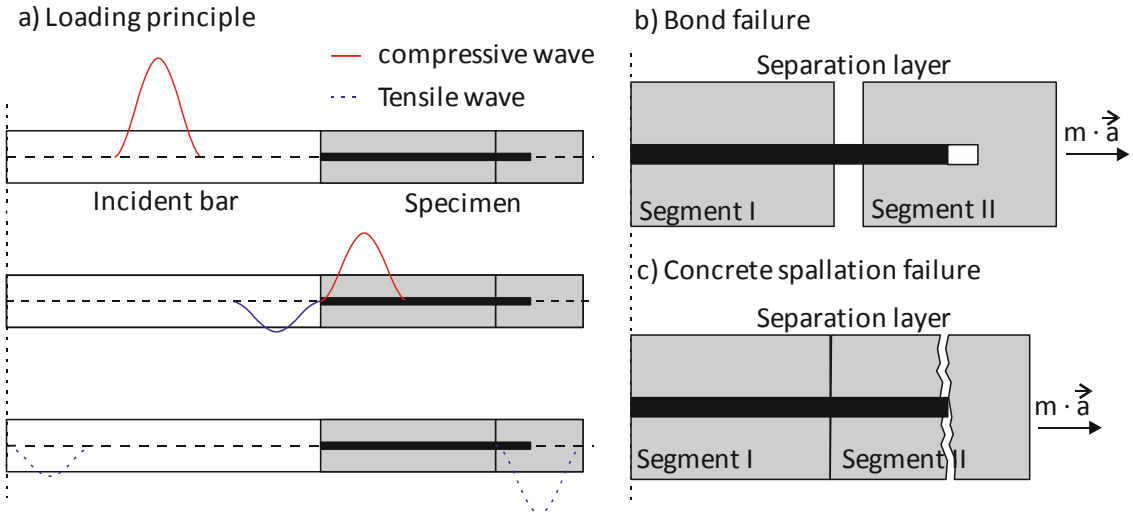

Figure 2-35: Loading principle and expected modes of failure, after [32].

The acceleration of the flying part can be measured, and equilibrium of dynamical forces can be calculated according to:

$$F_{dyn}(t) = m_{segII}\vec{a}_{segII}(t) + F_{bond} \quad (50)$$

The slip can be measured with an optical extensometer on the transition between segments I and II. The time lag that the wave needs to travel through the segments needs to be taken into consideration. In his dissertation Wensauer [32] actually does not provide any bond stress-slip relationships under impact loading for the following reasons:

1. In all investigated cases it came at least to partial cracking of the specimen. This makes Equation (50) invalid because the specimen can no longer be considered as a rigid body.
2. The additional forces were impossible to measure. Therefore it was not possible to calculate more elaborate equilibrium equation.
3. The necessary perfect connection between the incident bar of the SHB and the specimen could not be guaranteed during part of the experiments.
4. Because of multiple wave reflections in the specimen, it was not possible to define an exact moment of failure and to calculate the stress state in the concrete body.
5. Because of the high speeds and complexity of the measured signals, it was not possible to synchronise the measurements to the time of specimen failure.

In the case of the pull-out mode of failure, Wensauer assumes, that the dynamic bond stress increases similarly to concrete compressive strength under high strain rate loading. This assumption is very reasonable, based on the results of this literature review. Wensauer suggests to calculate the increased dynamic compressive strength according to equation published by Hartmann [114]:

$$f_{c,dyn} = f_{c,stat} \cdot 0.5 \cdot \left(\frac{\dot{\varepsilon}}{\dot{\varepsilon}_0}\right)^{0.13} + 0.9 \quad (51)$$

where $\dot{\varepsilon}$ is concrete strain rate and $\dot{\varepsilon}_0 = 1\ s^{-1}$. The calculated dynamic concrete compressive strength can then be used in one of the equations that are used to predict maximal bond strength under quasi-static loading conditions.

The work of Wensauer [32] was continued by Michal et al. In [115] they introduced a bond model and a modified approach to bond testing in the SHB. This concept was further developed in [23]. They used cylindrical specimen with a diameter of 70 mm that was placed in SHB in compression configuration. The bond stress was calculated from the reaction force as measured in the transmitter (output) bar. The relative slip of the

rebar was measured as a difference between reinforcement displacement and the displacement of the concrete sample. The experimental setup is shown in Figure 2-36.

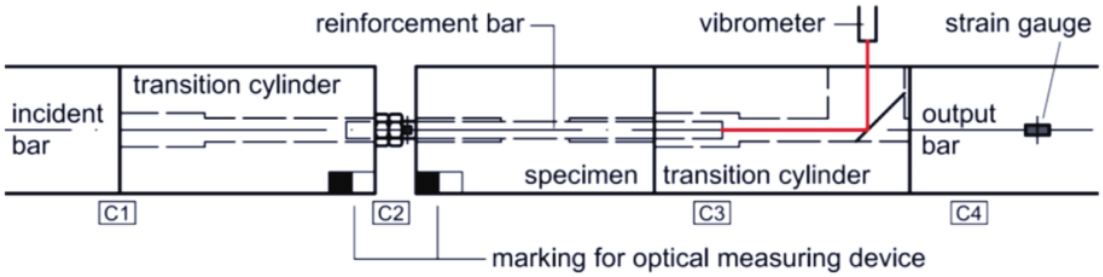

Figure 2-36: Schematic configuration of push-in test, as used by [23].

The rebar relative slip was measured by two independent methods. Firstly, the optical extensometer was used to measure the slip directly on the loaded end of the specimen as is apparent from Figure 2-36. Secondly, the relative slip was calculated according to Eq. (52) by subtracting the displacement of the transmitter bar Δu_{TB} from the displacement of unloaded rebar end measured by vibrometer.

$$s(t) = u_{vibrometer}(t) - \Delta u_{TB}(t) \tag{52}$$

The displacement of the transmitter bar Δu_{TB} was calculated from strain measurements ε_{TB} in the transmitter bar by using the Hopkinson analysis:

$$\Delta u_{TB}(t) = C_{0,TB} \cdot \int_0^t \varepsilon_{TB}(t)dt \tag{53}$$

A very good correlation between the two methods of slip measurement was observed. In the experimental work presented in this Thesis, a similar methods conclusions are reached.

In the research of Michal et al., the bond behaviour of reinforcing steel with a diameter of 10 and 14 mm was compared under static and dynamic loading conditions. The results were classified according to bond stress rate which was in the case of SHB loading in the range of 1×10^5 to 4.5×10^5 MPa/s. In terms of slip rate, the loading range was between 6.22 to 8.60 m/s. Two concrete classes with an approximate strength of 50 and 70 MPa were investigated. The results as reported by Michal et al. [23] are summarised in Table 2-7.

Table 2-7: Results of Michal et al. [23].

Series	Concrete compressive strength [MPa]	Rebar diameter [mm]	Bond length [mm]	Maximal dynamic bond stress [MPa]	DIF
Ch.1	50.5	10	80	18.1	1.42
Ch.2	50.5	10	40	20.2	1.45
Ch.3	72.6	10	40	28.7	1.63
Ch.4	52.0	14	40	31.9	1.83

The failure mode of the quasi-static tests from series 1 to 3 was pull-out. The samples from series 4 failed by splitting, which was caused by larger rebar diameter of 14 mm. This resulted in a decrease of the concrete cover from $3\times d_s$ to $2\times d_s$. The doubling of bond length in series 1 led to 6% lower average quasi-static bond stress. The effect of bond length is discussed in Chapter 2.1.4.5. The maximal bond stress measured during impact loading was always reported higher in comparison with the quasi-static bond stress. The DIFs are shown in Table 2-7. In all cases, the failure mode was by splitting of the specimens. That means that for series 1-3 change in failure mode was observed after the loading velocity was increased. The DIF was highest for series 4. The authors explain this by a quicker increase in dynamic tensile strength of concrete in comparison to the increase in dynamic compressive strength. The authors assume that the strain rate in concrete was in the order of 1 to 10 1/s.

In paper [33] introduced Michal at al. very interesting concept for bond strength testing under dynamic conditions. It is conceptually based on the experimental work done by Solomos et al. [86]. The loading pulse is to be induced by an abruptly released pre-tensioned steel bar. This produces relatively long rectangular tensile impulse which is transferred directly into the reinforcement. The principles of wave propagation can be utilised to analyse such experimental results. The authors also mention that this experimental loading rig could be used for testing other specimen types such as beam specimen or beam-end specimen (Figure 2-4). In this case, specimen inertia needs to be taken into consideration.

2.3 State-of-the-art summary and relevance to current research

It was shown in the FIB state-of-art report on Bond of reinforcement in concrete [78] as well as in the work of Laura Ritter [19] and other authors that very extensive research was performed on bond behaviour under static loading conditions. Various experimental and numerical investigations were conducted to investigate the various bond influencing factors as summarised in Table 2-2. Unfortunately when it comes to bond strength under impact loading relatively little experimental work is available. In addition, some results are contradictory, and it is very hard to compare the results directly as different groups used diametrically different test methods. Nevertheless, based on the literature review as presented in Chapter 2.2 it is possible to draw some general conclusions:

1. The bond behaviour under dynamic loading is quite different from that under static loading. Loading rate influences the bond behaviour, especially for deformed (ribbed) reinforcement bars.
2. Shearing off the concrete cantilevers that are formed between the ribs is the main failure mechanism in case of pure pull-out or push-in failure similarly to the quasi-static tests. The DIF, in this case, is predominantly connected with the concrete compressive strength.
3. The sensitivity of bond strength between steel and high strength concrete to high loading rates is lower in comparison with the bond strength of steel and low strength concrete.
4. In the case of splitting failure mode, the DIF of maximal bond strength is predominantly connected with the rise of concrete splitting tensile strength under impact loading.
5. The DIF for the splitting mode of failure is in general greater than that of the pull-out type of failure.
6. The strain distribution along the reinforcing bar is the most important parameter for understanding the bond phenomenon. In the case of dynamic loading, the strain distribution is much more complicated due to multiple loading wave reflections and impedance mismatch between concrete and steel as well as impedance mismatch inside of the testing rig.

7. Some authors use the classic mechanic of rigid bodies to analyse the bond strength problems, while the more recent works prefer to use analysis based on wave propagation in the elastic body (split Hopkinson bar analysis).
8. It is unclear to what extent inertia of the concrete sample, as well as the bar inertia, influence the results. With harder impacts and from the resulting high accelerations, inertial effects play more important role.
9. The bond strength measurement and analysis under dynamic loading conditions is much more complicated than in the static case.
10. The average DIF for bond strength lies between 1.1 to 1.8 [-].
11. Based on the reviewed works more research is needed to provide a reliable method to measure bond strength under impact loading.

Chapter 3

Experimental investigations

The description of concrete and steel material properties as well as experimental setups of quasi-static, drop-tower and split Hopkinson bar impact tests is provided in this chapter. Only one type of concrete matrix was used to eliminate the effects of concrete compressive strength. Special focus was placed on the detailed description of the experimental setup which was one of the main goals of this work. In many cases, several test rig configurations had to be tried before the optimal experimental setup was reached. The optimisation process is described in more detail where relevant. The main goal of this part of the work was to create a repeatable a reliable test rig which would allow testing bond stress-slip relationships under impact loading. The split Hopkinson bar (SHB) experiments were designed in a way so that the bond zone was loaded only by one compressive wave before any unwanted reflections smear the results.

3.1 Material characterisation

3.1.1 Concrete mix

Throughout the experimental investigations normal concrete with a target average cube compressive strength of 50 MPa was used. The investigation of the concrete compressive strength influence on the bond stress-slip relationship was not one of the objectives of this work as it is relatively well described in the literature (see Chapter 2.2). The focus was on creating a reliable method to measure the bond stress-slip relationship. For this reason, only one concrete class was used, but even though special care was taken in the preparation of the samples, compressive cubical strength ranged from 40 to 60 MPa. Such scattering is, however, normal for concrete as it is a

heterogeneous material. Other reasons, such as different cement quality, varying aggregates quality and a varying amount of entrapped air influence the concrete compressive strength. In addition, deviations in the sample preparation and vibration need to be counted with. The average concrete compressive strength of 51.7 MPa was very close to the target strength of 50 MPa. The coefficient of variation was 8%. The exact concrete composition is shown in Table 3-1. The consistency of the fresh concrete of each batch was measured with a so call flow table test following DIN EN 12350-5 [116]. The flowability varied from 400 to 500 mm.

Table 3-1: Concrete composition in kg per m³.

Cement CEM I 42,5N	Sand 0/2	Aggregates 2/8	Plasticizer FM 30	Water
409	942	771	3.07	203

To be able to classify the used concrete, basic mechanical properties were measured at the beginning of the experimental program before the start of bond testing (Table A-1). The average properties determined on 6 samples are presented in Table 3-2. In addition, the standard deviations and coefficient of variations are presented in Table 3-2. To monitor the concrete quality throughout the experimental work concrete cubical compressive strength as well as splitting tensile strength were determined with every batch of specimens for bond strength testing.

Table 3-2: Basic mechanical properties of the investigated concrete

Property	Symbol	Value	Standard deviation	Coefficient of variation
Cubical compressive strength [a]	$f_{cm,c}$	51.7 [MPa]	3.9 [MPa]	8 %
Cylindrical compressive strength [a]	f_{cm}	47.4	1.4	3 %
Density	ρ	2 300 [kg/m³]	14.1 [kg/m³]	1 %
Flexural strength [b]	$f_{ctm,f}$	4.7 [MPa]	0.2 [MPa]	4 %
Splitting tensile strength [a]	$f_{ctm,sp}$	3.5 [MPa]	0.5 [MPa]	14 %
Modulus of elasticity [c]	E_{cm}	33.6 [GPa]	1.1 [GPa]	3 %

[a] 150 × 150 × 150 mm cubes, [b] 100 × 100 × 400 mm prisms, [c] cylinder Ø 150 mm and 300 mm high

Based on the results presented in Table 3-2 the concrete class can be determined from mean compressive strength measured on cylinders. The control material properties,

measured with every batch of bond specimens, were however measured on cubes. To determine the cylindrical compressive strength, the relationship according to Eq. (54) can be used. This equation was recommended by Ritter [19] in her dissertation and is in good agreement with DIN EN 1992-1-1 [66].

$$f_c = 0.85 \cdot f_{c,cube} \tag{54}$$

After applying Eq. (54) on mean concrete compressive strength as measured on cubes $f_{cm,c} = 51.7\ MPa$ we get a value of cylindrical mean compressive strength of $f_{cm} = 43.95\ MPa$. After comparing this value to the measured cylindrical compressive strength as presented in Table 3-2 a slight underestimation of the actual value can be seen. However, the difference is in the limits given by the measurement uncertainties.

In analysis and design of concrete structures, the characteristic compressive strength f_{ck} is applied. This value may be derived from strength tests by the criterion that 5 % of all possible strength measurements for the specified concrete are expected to fall below the value of f_{ck}. The value of f_{ck} can be estimated from Eq. (55)

$$f_{ck} = f_{cm} - \Delta f \tag{55}$$

Where $\Delta f = 8\ MPa$. The Δf value is independent on concrete compressive strength as discussed in detail in Müller at al. [117]. For the concrete investigated in this research the characteristic concrete compressive strength is $f_{ck,cube} = 43.7\ MPa$ and $\mathrm{f_{ck}} = 39.4\ \mathrm{MPa}$ for cubical and cylindrical compressive strength respectively. These values correspond to the concrete class C32/40.

The mean modulus of elasticity E_{cm} at the age of 28 days can be according to EN 1992-1-1 [66] specified from the concrete compressive strength using:

$$E_{cm} = E_{c0} \cdot \alpha_E \cdot \sqrt[3]{\frac{f_{cm}}{10}} \tag{56}$$

Where $\mathrm{E_{c0}} = 21\ 500\ \mathrm{MPa}$ and $\alpha_\mathrm{E} = 1.0$ for quartzite aggregates.

A similar equation was used by Ritter [19] in her work:

$$E_{cm} = 9840 \cdot \sqrt[3]{f_{cm}} \tag{57}$$

The determination of direct tensile strength f_{ct} is relatively complicated even in laboratory conditions. The reason for this is, that the introduction of tensile force needs

to be without any influences of eccentricity which could cause bending moments in the tested samples. Normally steel plates glued on the top and bottom of a prism are used. According to Model Code 1990 [118] for concrete grades ≤ 50 MPa the mean tensile strength can be estimated from characteristic compressive strength f_{ck} as follows:

$$f_{ctm} = 0.3 \cdot {f_{ck}}^{2/3} \tag{58}$$

The direct tensile strength f_{ctm} can be also calculated from measured splitting tensile strength as shown in Eq. (59)

$$f_{ctm} = \alpha_{sp} \cdot f_{ctm,sp} \tag{59}$$

Traditionally the coefficient α_{sp} can vary from 0.65 to 1. New comprehensive research [119], however, showed that the factor could go beyond 1. For this type of concrete a factor $\alpha_{sp} = 0.9$ as in CEB-FIP MC1990 [118] was used. The comparison between directly measured and calculated values is provided in Table 3-3.

Table 3-3: Measured and calculated concrete mechanical properties.

Property	Measured value	Calculated	
		Equation used	Value
f_{cm}	47.4	(54)	43.9
f_{ck}	N/A	(55)	39.4
E_{cm}	33.6	(56)	36.1
		(57)	35.6
f_{ctm}	N/A	(58)	3.47
$f_{ctm,sp}$	3.5	(59)	3.86

To compare the experimentally measured splitting tensile strength with the mean cubic compressive strength Eq. (58) and (59) can be rewritten utilising Eq. (54) and (55).

$$f_{ctm,sp} = 0.9^{-1} \cdot 0.3 \cdot (0.85 \cdot f_{cm,c} - 8)^{2/3} \tag{60}$$

The dependence between the measured splitting tensile strength and the measured cubical compressive strength is depicted in Figure 3-1. The best fit for the experimental results is provided by a logarithmic equation (61) and also shown in Figure 3-1. In addition, values calculated according to Eq. (60) are shown in the figure. The results show that Eq. (60) gives a very good prediction of the value of splitting tensile strength.

$$f_{ctm,sp} = 1.656 \cdot \ln(f_{cm,c}) - 2.71 \tag{61}$$

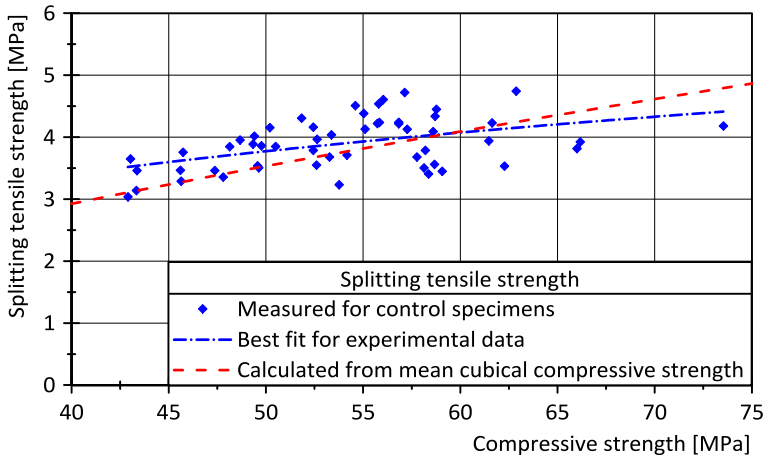

Figure 3-1: Dependence of mean splitting tensile strength on the mean concrete compressive strength – measured and calculated values.

3.1.1.1 Development of strength with time

The compressive strength of concrete in time t depends on many factors such as the type of cement used, amount of admixtures and additions, the water/cement ratio and environmental conditions such as temperature and humidity. For each batch of bond specimens, control compressive and splitting tensile strength were measured after 28 days. Because it was not always possible to perform the dynamic bond stress tests at the age of 28 days more control cubes were casted. These cubes were then used to determine the compressive and tensile splitting strength at the time of bond testing. It is interesting to compare the measured values with the values predicted by Model Code 2010 [16]. For the mean temperature of 20°C the relevant compressive strength of concrete at various ages $f_{cm}(t)$ may be estimated from:

$$f_{cm,c}(t) = \beta_{cc}(t) \cdot f_{cm,c} \tag{62}$$

with:

$$\beta_{cc}(t) = exp\left\{s \cdot \left[1 - \left(\frac{28}{t}\right)^{0.5}\right]\right\} \tag{63}$$

where:

$f_{cm,c}(t)$ is mean cubical compressive strength in MPa at an age t in days;
$f_{cm,c}$ is the mean cubical compressive strength in MPa at an age of 28 days;
$\beta_{cc}(t)$ is a function to describe the strength development with time;

t is the concrete age in days;

s is a coefficient which depends on the reactivity of cement as given in Table 3-4.

Because the concrete tensile strength is dependent on the concrete compressive strength with an exponent of 2/3 (see Eq. (58)) the function $\beta_{cc}(t)$ can be modified accordingly:

$$\beta_{ctm,sp}(t) = \beta_{cc}(t)^{\frac{2}{3}} \tag{64}$$

This allows to predict concrete splitting tensile strength development in time as:

$$f_{ctm,sp}(t) = \beta_{ctm,sp}(t) \cdot f_{ctm,sp} \tag{65}$$

Table 3-4: Coefficients to be used in Eq. (63) for different types of cement

$f_{cm}[MPa]$	Strength class of cement	s
≤ 60	32.5 N	0.38
	32.5 R, 42.5 N	0.25
	42.5 R, 52.5 N, 52.5 R	0.20
> 60	all classes	0.20

The comparison of the measured compressive strength in time with the theoretical values calculated based on Eq. (62) is shown in Figure 3-2a) and similarly the dependence of the concrete splitting tensile strength on time together with the calculated value according to Eq. (65) is shown in Figure 3-2b). The average values of $f_{cm,c}$ and $f_{ctm,sp}$ that are used in Eq. (62) and (65) were taken from Table 3-2 where measured material properties are presented. After comparing Figure 3-2, it can be seen that the Eq. (62) and (65) give a very good prediction of the concrete strength development in time. In addition, the scattering of results around the age of 28 days, for which most of the results exist, can be seen. This scattering is however normal for concrete and the coefficient of variation was 8% and 14% for compressive and splitting tensile strength respectively.

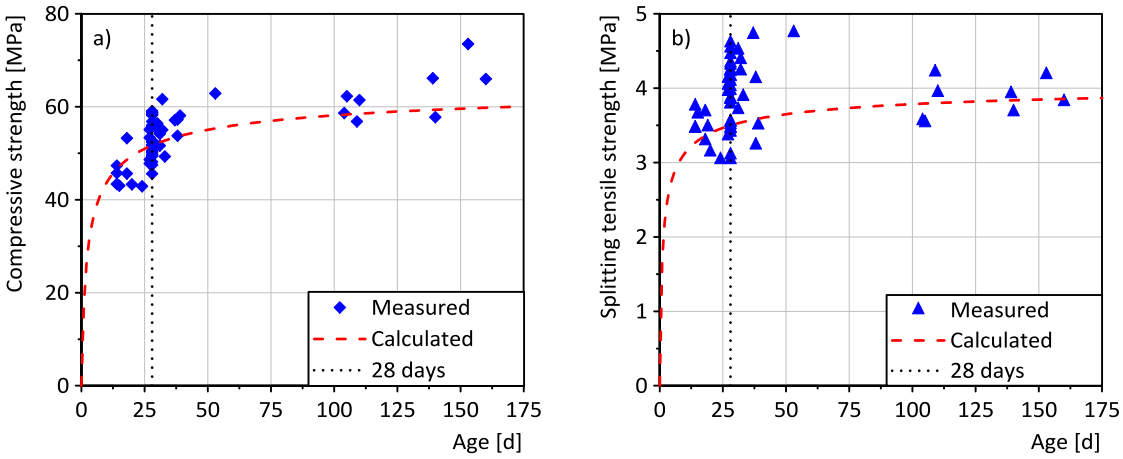

Figure 3-2: Comparison of measured and calculated development of concrete strength in time.

3.1.2 Steel properties

The steel reinforcing bars (rebars) used in this experimental work were conforming to DIN 488-2 [11]. At the beginning of the experimental work, the steel mechanical properties were tested according to DIN EN ISO 6892-1 [120], and the results are shown in Table 3-5. Because of the constant steel quality, the reinforcement bar mechanical properties were not measured for every test series as in the case of concrete.

Table 3-5: Steel mechanical properties

Rebar	d_s [mm]	E_s [GPa]	R_p [MPa]	R_m [MPa]
1	10	208.1	566.3	605
2	10	198.0	555.4	602
3	10	191.4	560.3	602
4	10	198.5	564.3	602
Average	**-**	**199**	**561.6**	**602.8**

The so-called **relative rib area** of the reinforcing bar is a very important parameter for bond testing. The influence of the relative rib area, as well as the formulae how to calculate it, are discussed in Chapter 2.1.4.3. As already described in Chapter 2.1.4.3 the relative rib area is influenced by rib angle pattern, rib height, rib spacing as well as rib width. The relative rib area of used types of steel is shown in Table 3-6 and was calculated according to the following equation:

$$f_R = \left(2 \cdot a_{1/4} + a_m + 2 \cdot a_{3/4}\right) \cdot \left(\pi d - \sum e_i\right) \cdot \frac{1}{6\pi dc} \qquad (66)$$

The process of measuring a reinforcing bar with a small diameter is rather difficult. Because the ribs have a relatively small height, the error caused by inaccurate measurement can be high. This was partly eliminated by taking the measurements repeatedly in several places – each bar was measured on 6 independent places and for one type of bar 3 bars were measured. The dimensions of the ribs as well as their arrangement on a reinforcement bar with a nominal diameter of 10 mm is shown in Figure 3-3. Detailed photos of the reinforcement are shown in Appendix C.

Table 3-6: Geometrical properties of used reinforcing steel

d_s mm	h_s mm	$a_{1/4}$ mm	$a_{3/4}$ mm	c_s mm	β_1 °	β_2 °	β_3 °	b_s mm	e_1 mm	e_2 mm	f_R -	A_s mm^2
8	0.58	-	-	5.49	49	-	-	1.56	1.73	1.7	0.079	50.3
10	0.67	-	-	6.5	65	45	65	1.63	1.8	1.85	0.096	78.5
12	0.68	-	-	7.0	45	-	-	2.34	3.08	2.14	0.074	113.1
14	0.91	-	-	7.24	46	-	-	1.93	2.85	1.78	0.096	153.9
16	1.1	0.75	0.76	8.82	53	-	-	2.77	3.99	3.28	0.063	201.1
20	1.18	1.19	1.24	9.92	48	-	-	2.5	3.42	2.43	0.092	314.2
25	2.09	1.19	1.15	15.25	68	49	58	3	3	-	0.081	490.9
28	2.56	1.65	1.65	17.99	67	46	57	3.13	2.7	-	0.084	615.8

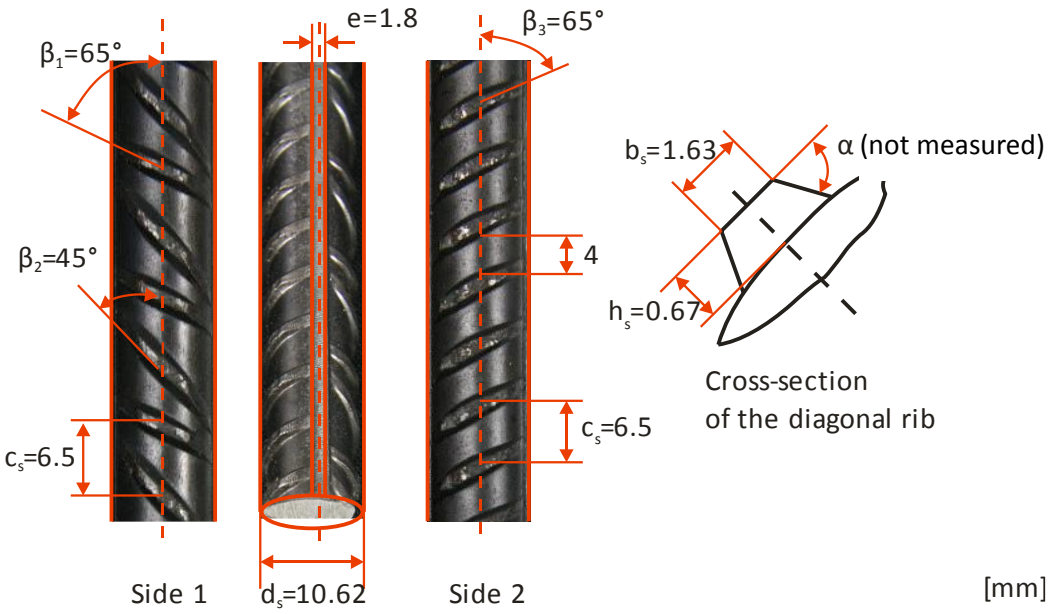

Figure 3-3: Dimensions of the mostly used steel with a nominal diameter of d_s = 10 mm.

3.2 Specimen geometry, preparation and casting procedures

3.2.1 Specimen geometry

Throughout the experimental work, specimens of two geometries were used. The first geometry was a cube with an edge of 200 mm as recommended by RILEM RC6 [1] and shown in Figure 3-4. The second geometry was a cylinder with a diameter of 100 mm and height of 100 mm (Figure 3-5). The cylinders were used as they are more suitable for impact testing and easier to handle. Strain gauges were applied on the rebar only in case of impact testing. For quasi-static tests, conventional load cells were used. For the purpose of this experimental work further changes in comparison to the standard pull out the test as defined in DIN 488-3 [20] were made:

1. The bond length was reduced from $5\times d_s$ to $2\times d_s$.
2. The bond zone was moved from the top to the middle of the specimen.
3. In the case of the cylinders, the concrete cover was just $4.5\times d_s$ instead of $5\times d_s$.

The changes in the specimen geometry and size are mainly arising from the demands of high loading rate testing. The more detailed explanation follows.

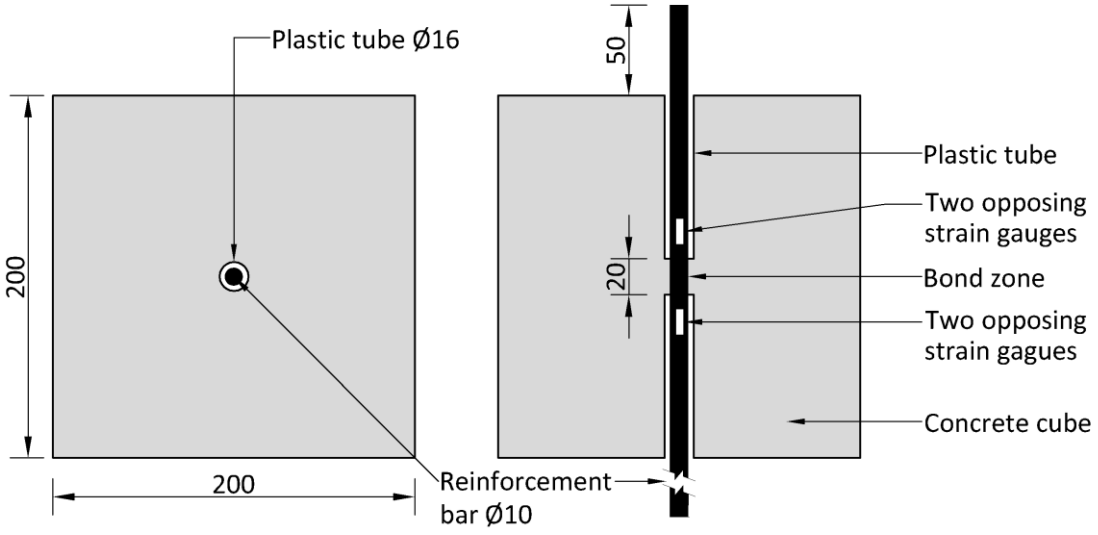

Figure 3-4: Cubical specimen.

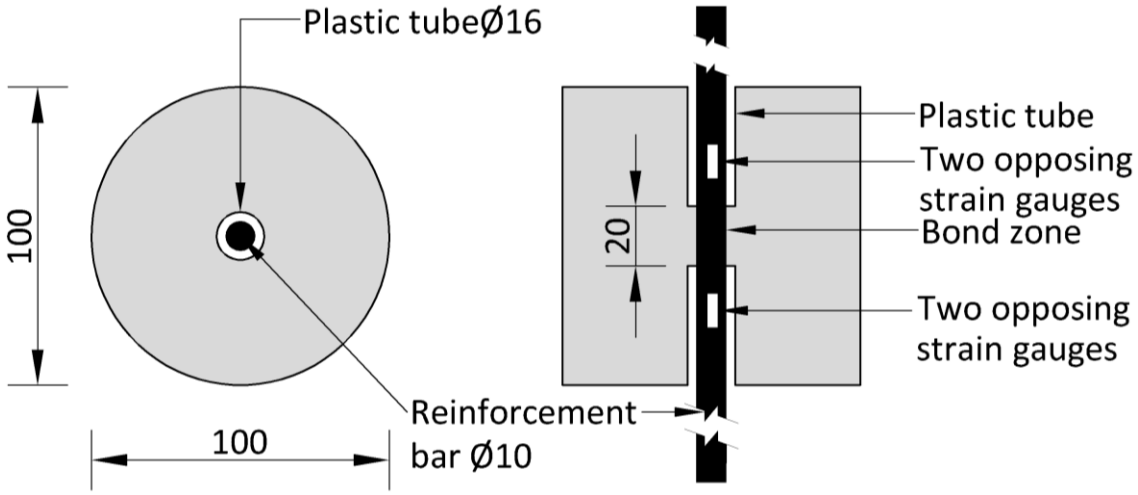

Figure 3-5: Cylindrical specimen.

Ad 1: Reduction of the bond length

The bond length was reduced for two reasons. Firstly, the bond stress is not constant along the rebar for longer bond lengths as shown in Figure 3-6. Experimentally only the average bond stress can be determined and therefore the local maximum in bond stress can be missed. Secondly, for calculating the bond stress from strain measurements before and after the bond zone (Eq. (74) and (75)), it is assumed that the bond zone is very short. In addition, the wave dispersion would influence the measurement results should the distance between the strain gauges be too long.

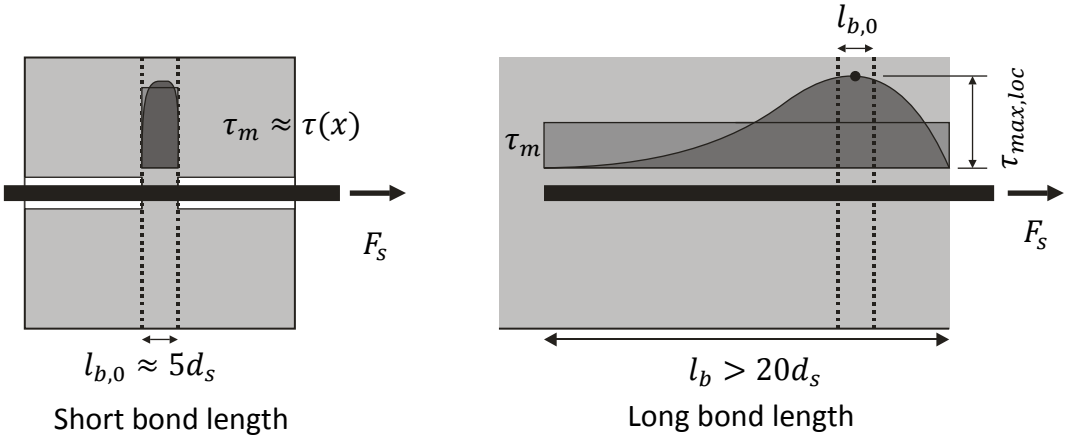

Figure 3-6: Bond stress distribution for short and long bond lengths. After [19].

Ad 2: Location of the bond zone

It is recommended in the code DIN 488-3 [20] that the bond zone is located at the top of the specimen. The reason for that is, that area around the bond zone is as far as possible from the support plate, thus minimising the confinement effect from the friction between the specimen and the plate. For the purpose of this research, the bond zone was moved to the centre of the specimen. Because the bond zone is shorter ($2d_s$) than the code requirement and only steel with a diameter of 10 mm is used the distance to the support plate is sufficient enough. However, a slight influence of the confinement due to the support plate is still present. This effect is further discussed in Chapter 4.1.3. The main advantage in moving the bond zone to the middle of the specimen if that, in the case of impact loading, there are no reflections of the loading wave from the free top surface. The confinement effect of the support plate is negligible in the case of impact testing because only the first pass of the impact loading wave is of interest. That means that by the time, the wave reaches the support plate the bond zone is already damaged, and thus the confinement due to the support plate have no effect on the measured maximal bond stress.

Ad 3: Reducing the concrete cover

After the trial tests, it was observed that reduction of the concrete cover to $4.5 \times d_s$ has no significant effect on the failure mode of the specimens. Throughout the whole experimental work, only pull-out or push-in failure mode by shearing-off of the concrete cantilevers was observed. The influence of concrete cover on the experimental results is discussed in Chapter 4.1.5.

3.2.2 Specimen casting

The 200 mm cubes were cast in standard steel forms as can be seen in Figure 3-7. That means that the testing direction was perpendicular to the concrete casting direction. Due to this casting configuration, small air bubbles can get entrapped under the reinforcement which can influence the results. At the beginning of the experimental work, the specimens were compacted on the vibrating table with a frequency of 50 Hz. However, such specimens had very small or zero bond. During the deeper investigation, it was found out, that the Eigen-frequency of the reinforcement bar in the current configuration is approximately 56 Hz which is very near to the frequency of the vibrating table. This causes excessive vibration of the rebar and thus pushing all coarse aggregates away from the bond zone. To eliminate this effect and because it was not possible to

change the frequency of the vibration table, it was decided to use a standard hand-held concrete vibrator with a much higher vibrating frequency of 300 Hz. The vibrator head immersed into fresh concrete can be seen in Figure 3-7 b). The influence of compaction method is shown in Figure 3-8. Curves for good and bad bond conditions determined according to MC 2010 (Table 2-4) are also shown in Figure 3-8.

In most series for bond testing, six cubes were cast. To provide the bond free zone, plastic tubes with a diameter of 16 mm and with a wall thickness of 1.5 mm were used. Before concreting the plastic tubes were covered with grease to allow easy removal from the specimen before testing. This was done to eliminate any influence of the tube – especially on the first concrete cantilever (key) formed between the tube and the first rib.

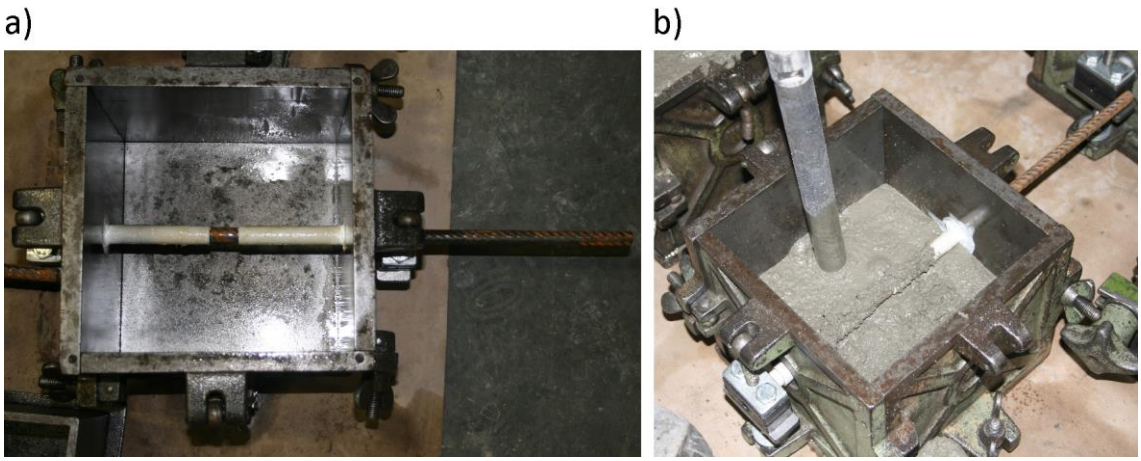

Figure 3-7: 200 mm cubes a) before and b) during casting.

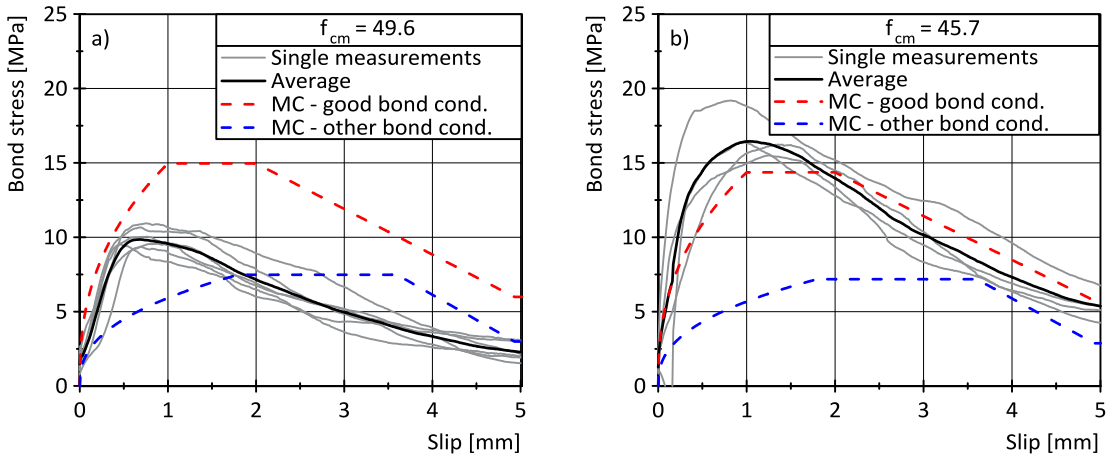

Figure 3-8: Bond stress-slip relationship for specimens compacted on a) vibrating table b) with a vibrator.

The casting of cylindrical specimens was done in specially developed formwork for a series of 8 specimens. Due to the cylindrical shape of the specimen, the concreting direction was parallel to the testing direction. It was decided, that the testing will follow in the direction of placing concrete. That means that the specimen was not rotated and that during the testing it was standing on the smooth bottom surface formed by the formwork. The longer free end of the rebar was pointing out of the base plate of the formwork as seen in Figure 3-9. For this reason, the formwork had to be cantilevered from the vibrating table. The use of the vibrating table ensured the same degree of compaction for all specimens. The specimens were compacted at a frequency of 50 Hz, and because the rebars were in this configuration in the direction of vibration, no problem with the Eigen frequency arose. This concreting setup causes small air bubbles to be entrapped under the rebar ribs thus worsening the bond conditions. However, this effect wasn't found to be significant, and all specimens were concreted in the same way. However, when comparing the results presented in this study to other researchers, this phenomenon needs to be taken into consideration.

Two types of formwork were used. The first type is shown in Figure 3-9. It is relatively lightweight, but the main problem is, that it produces samples which are slightly elliptical. This is no problem when the samples are tested upright in the servo-hydraulic machine or in the drop-tower. However, it is problematic to test such sample in the horizontal direction in Split Hopkinson Bar - SHB (see Chapter 3.6.2). For this reason more robust formwork, as can be seen in Figure 3-10, was developed. Such formwork produced ideal cylinders which were used in all SHB tests. The formwork allowed 8 specimens to be cast simultaneously. Similarly to the cubes, before the actual testing, the plastic tubes were removed so that they couldn't influence the measured results.

Figure 3-9: First type of formwork for casting cylindrical specimens.

Figure 3-10: Second type of formwork for casting cylindrical specimens.

3.2.3 Specimen curing

The curing regime of the specimens was following. Usually, the specimens were concreted on Friday and then covered with plastic foil to eliminate water evaporation. On Monday the specimens were demoulded and stored in the laboratory covered in a wet rug. The reason why the specimens were left in the moulds over the weekend is that the concrete had a higher compressive strength at demoulding. If the samples were demoulded after 24 h, there was a big chance of destroying the bond during the demoulding process as the concrete strength is not fully developed, and the bond zone is very short. That means that only small force is necessary to destroy the bond. The control specimens for concrete compressive strength testing undergone the same procedure as the bond specimens. The control specimens for splitting tensile strength

were, after demoulding, cured in a climatic chamber at a temperature of 20°C and relative humidity of 65%.

3.3 Loading regimes

The main focus of this work is to investigate the influence of the loading rate on the bond stress-slip relationships. For this purpose, the experimental program was divided into three main steps based on the loading velocity. This is summarised in Table 3-7. The loading velocity was chosen as the main variable as it can be easily defined. It is important to note that the loading velocity can be different to the loading rate or stress rate in the sample. This is more detail discussed in the results section in Chapter 4.2.1. In the case of quasi-static tests, the velocity was 0.01 mm/s until the slip of 6 mm. After that, the velocity was increased to 0.5 mm/s to reduce the duration of the test. In the case of impact testing, the velocity of 8.3 m/s corresponds to the maximal possible drop height of 3.5 m calculated from the potential energy according to the following equation:

$$v = \sqrt{2gh} \tag{67}$$

Table 3-7: Loading velocities.

Loading type	Testing machine	Velocity of crosshead	Impactor velocity
Quasi-static	Hydropuls Schenck	0.01 mm/s	-
Medium rate		50 mm/s	-
Impact	Drop-tower	-	8.3 m/s
	SHB	-	10 m/s

The actual impactor velocity in the drop-tower was measured by a set of light barriers eliminating the influence of friction and other effects. Overall it can be stated that the real impactor velocity is around 1-2% smaller compared to the theoretical velocity calculated according to Equation (67). Similarly to the drop-tower, the actual impactor velocity in the SHB was measured with a set of light barriers, and it corresponds to a pressure of 2 to 5 bar in the air gun which is used to launch the impactor. The measuring procedure in detail is shown in Chapter 3.6.2.

3.4 Evaluation of the data

3.4.1 Data acquisition and filtering

The sampling rate for quasi-static tests was 100 Hz and for medium rate tests 9.6 kHz. To reduce the data amount in the post processing phase a 4th order Butterworth low-pass filter with a cut-off frequency 1 Hz and 100 Hz were applied on the results respectively. It was proven that the filters do not influence the shape of the curves, just reduce the electrical noise of the sensors.

All impact loading tests were sampled with a data acquisition rate of 1 MHz which in line with the recommendation of Chen and Song [121] who recommend a minimal sampling frequency of 100 kHz. The minimal resolution of the presented data is therefore 1 ns, and it needs to be taken into account when interpreting the results that are presented in Chapter 4. Because it was necessary to filter the high-frequency noise from the signal, it was decided to use a low pass filter during the post-processing. No electrical filters were used to get uninfluenced raw data. In general, extreme caution needs to be taken when applying filters. Figure 3-11 shows a comparison of different filters according to [121]. It is shown that low-pass filters with frequencies 3 kHz and 100 Hz significantly distort the measured signal. It is unfortunately not uncommon in the literature that researchers use filters as low as 1.2 kHz. Another very common mistake is that the maximal working frequency of strain gauge amplifiers is too low. In this work, the strain gauges amplifiers were capable of working at the rate of 1 MHz. As stated before in the current research a low-pass Channel Frequency Class (CFC) 50 000 filter was used. The mathematical definition of such a filter can be found in SAE J211-1 [122, 123]. In principal it is a low-pass digital IIR 4th order Butterworth filter with a zero phase shift. The minimal sampling frequency for a CFC 50 000 filter is 500 kHz, and the filtering frequency is 83 kHz. The effect of such filter on strain gauge signal is shown in Figure 3-12. It is clearly visible that signal is not distorted by the filter.

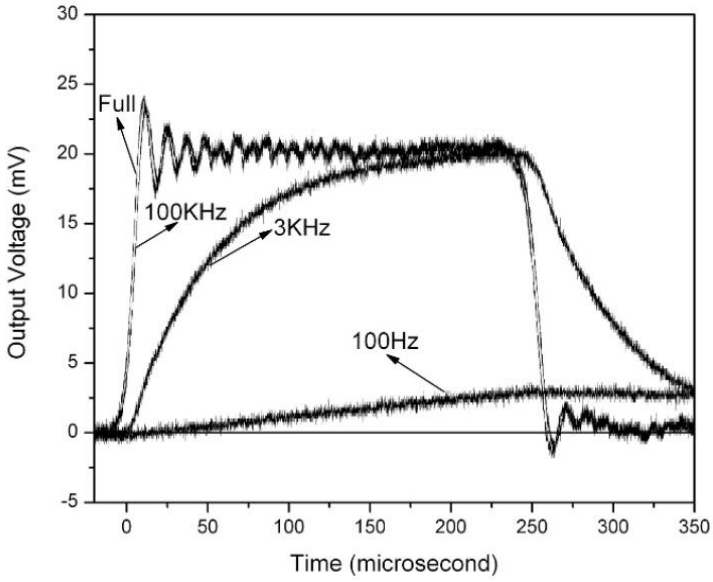

Figure 3-11: An effect of filters on recorded signals [121].

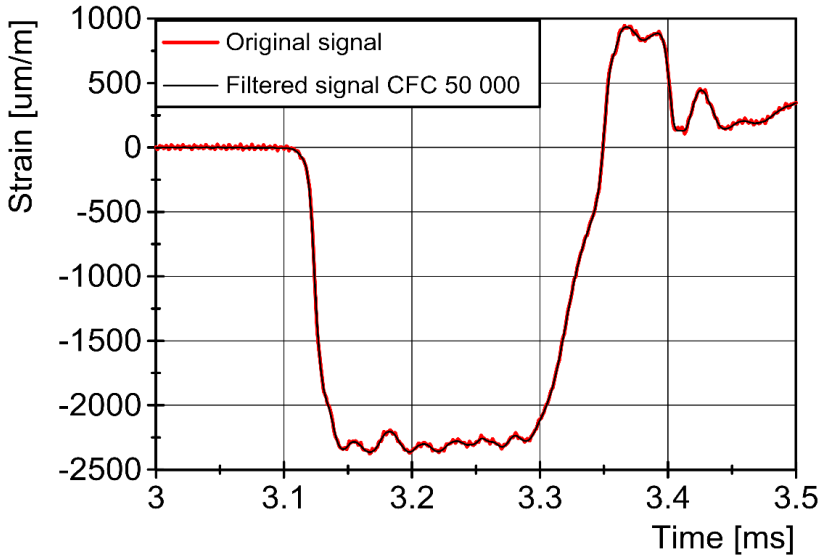

Figure 3-12: Effect of CFC 50 000 filter on recorded strain gauge data.

3.4.2 Time lag correction

In the case of dynamic events such as impact, it is necessary to correct the time lag between signals measured at different places. The time lag is simply corrected by calculating the time which is a need for the mechanical wave to travel through a certain material according to:

$$\Delta t = \frac{l}{c_0} \tag{68}$$

In this research, all the measured signals were moved in time to the middle of the bond zone. Figure 3-13 shows the importance of correcting time lag. In this figure, slip measurements were taken at different positions along the bar and time lag was not corrected. A significant influence on the bond stress-slip relationship can be seen.

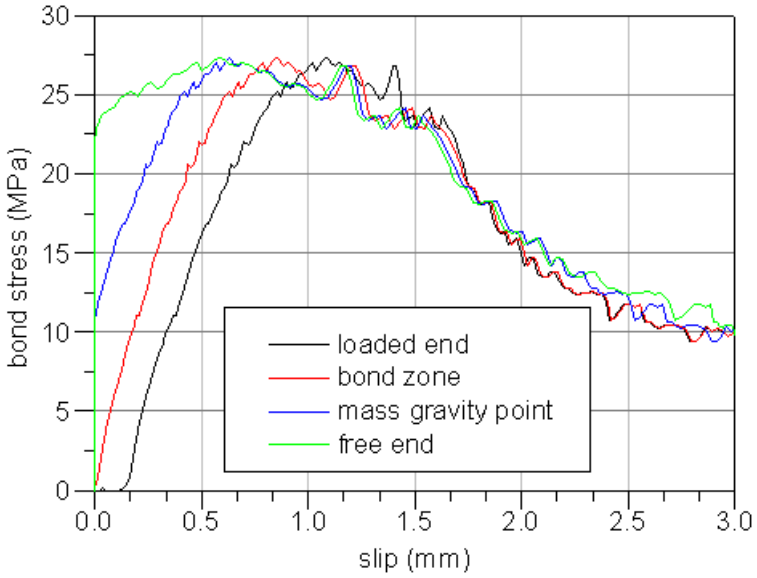

Figure 3-13: The influence of time lag on the bond stress-slip relationship [124].

3.4.3 Averaging

To be able to interpret the measured bond stress-slip relationships average curves need to be built. The procedure is the same for both quasi-static and impact results. In general, there are two possibilities how to make an average curve. The first possibility is to make an average over slip values. That means that for every slip value an average is made of corresponding bond stress values. This procedure is sketched in Figure 3-14a). This method has a disadvantage, that the average maximal bond stress is not an average of maximal bond stress values of each curve because the maximal bond stress doesn't necessarily occur at the same value of slip, as exaggerated shown in Figure 3-14a). The main advantage of this method is that it is relatively straight forward and the bond stress-slip relationships are not deformed. It is especially useful when showing or comparing the average results with the single curves of each and every specimen. The second method of making an average is that the actual slip values are normalised by the slip at maximal bond stress s_{max}. That means that all curves have a maximum at the

same normalized slip of 1 as shown in Figure 3-14b). After the slip values are normalized, the average bond stress is calculated for each normalized slip value in a same manner as in the previous method. The advantage of this method is, that the average maximal bond stress is an average of maximal bond stress of each specimen. The disadvantage is, that the bond stress-slip relationships are deformed, and information about their stiffenes and curve progress is lost.

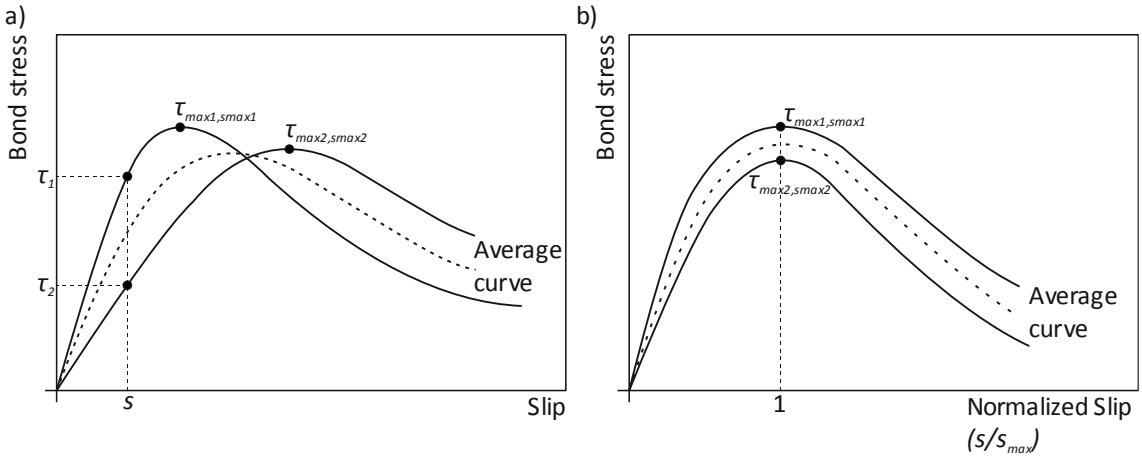

Figure 3-14: Possibilities of making an average.

Luckily the real bond stress-slip relations are not as different as in the exaggerated Figure 3-14 because only specimens with the same geometrical and material properties are averaged together. Only concrete mechanical properties vary between the concrete batches and these variations maximally 10%. The two approaches for making an average of measured data are shown in Figure 3-15. In Figure 3-15a) the average was made following the first method the average bond stress is the mean of measured bond stresses at a given slip value. In Figure 3-15b) the slip values were firstly normalised so that all peaks of maximal bond stress appear at the relative slip of 1. Afterwards, an average was made over the normalised slip values. Figure 3-16 shows the comparison between the average calculation over a) the measured slip (the first method) and b) the normalised slip (the second method). In addition, for the comparison of the two methods, the normalised average was de-normalized by the average value of slip at the maximal bond stress of each curve, and it is shown in Figure 3-16. It can be seen from Figure 3-16 that the difference between the de-normalized and original average constructed according to the method a) is negligible. Therefore, it was decided to use the first method only (Figures 3-31a) and 3.32a)) because the actual progress of individual curves of the bond stress-slip relationship is maintained.

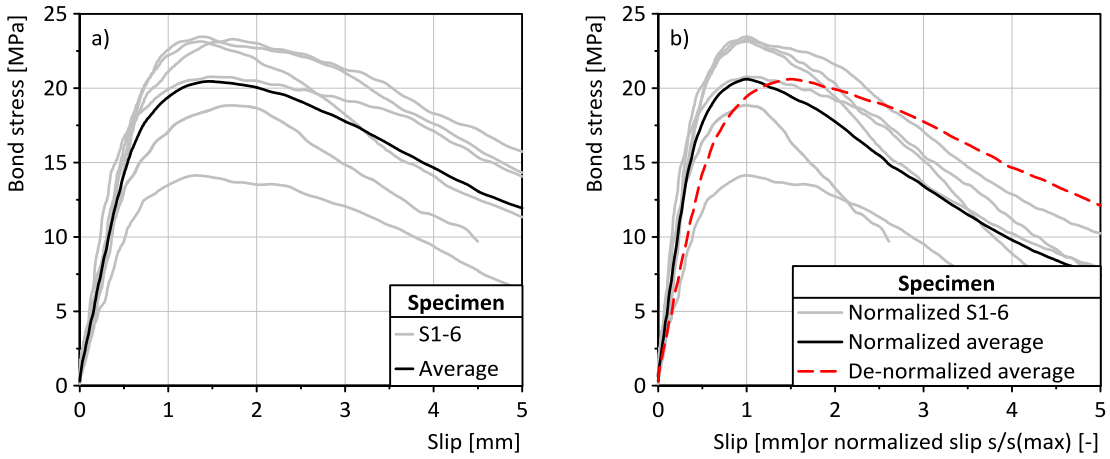

Figure 3-15: Two methods of making a bond stress average: a) over measured slip b) over normalised slip.

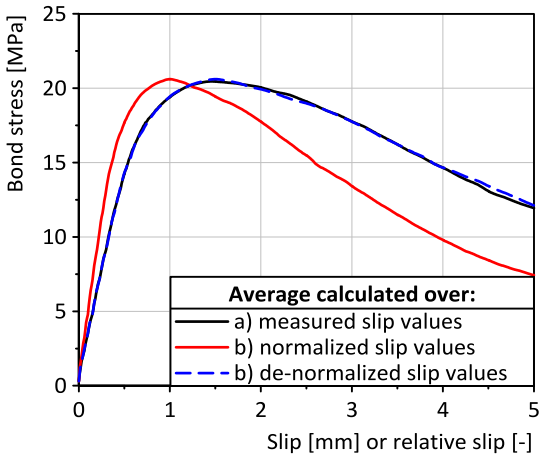

Figure 3-16: Comparison of the two methods of making bond stress average.

3.5 Quasi-static and medium rate experimental setup

The quasi-static and medium rate tests were performed in Schenck Hydropulse loading machine. The loading was displacement controlled according to Table 3-7 both pull-out and push-in type of tests were performed. Cubes, as well as cylinders, were tested to provide a reference for the impact testing. The experimental setup is shown in Figure 3-17. The test setup for the **pull-out** type of test was as follows: A steel frame holding a support plate was connected to the machine frame. The reinforcement rebar was led through a hole in the support plate, and it was hydraulically clamped to the machine crosshead. For the first couple of series, a load cell was located between the sample and the support plate. The comparison between the machine force and load cell signal is

shown in Figure 3-18 for loading rate of 50 mm/s. It can be seen that even for this highest possible rate the load cell signal corresponds to the machine force signal. Later on in the research, the load cell was excluded from the experimental setup, and only machine force signal was used to calculate the bond stress.

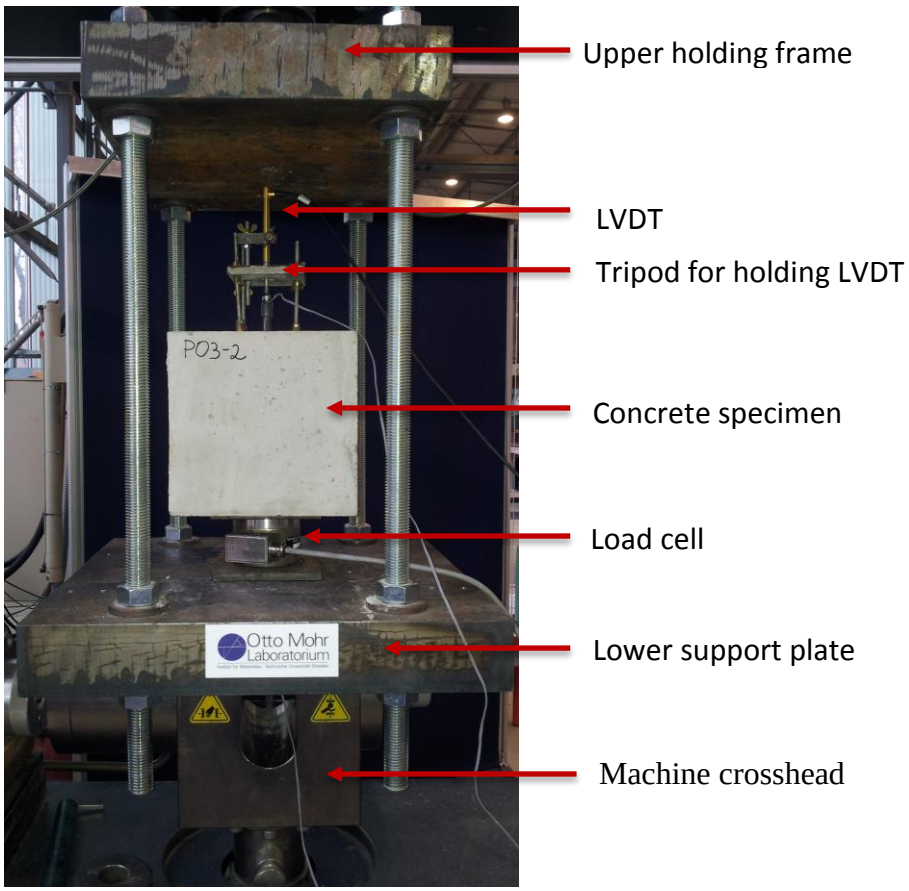

Figure 3-17: Experimental setup: pull-out.

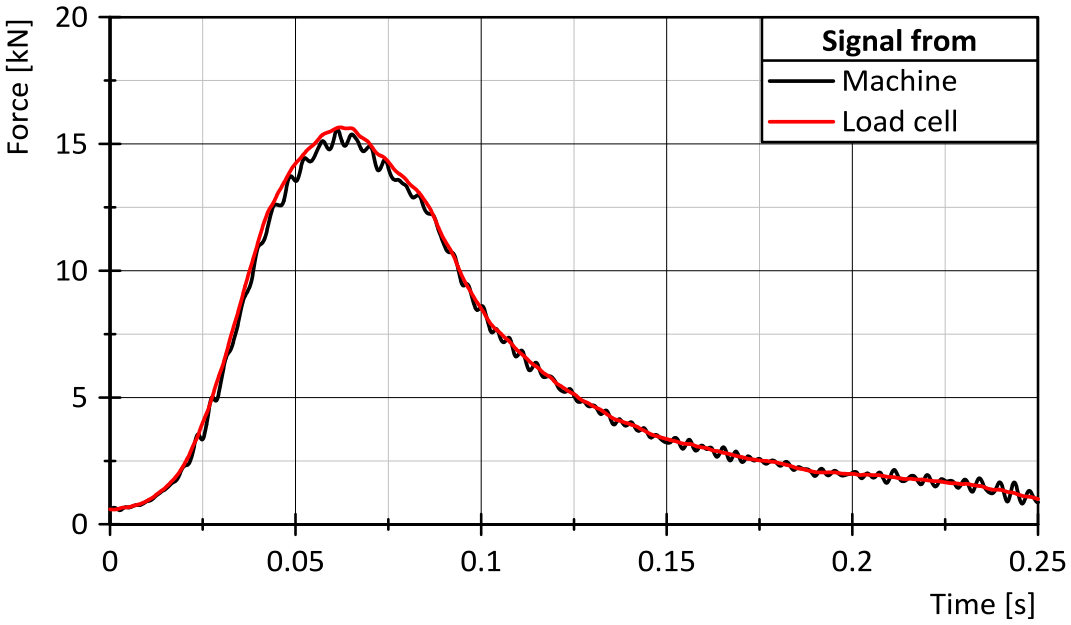

Figure 3-18: Comparison of the machine and the load cell signal.

Instead of the load cell, a hemispherical joint – calotte was used. This joint allowed the sample to adjust and centre itself under applied load so that there was no bending moment in the reinforcement steel. To eliminate the friction, a sheet made of PTFE was placed between the sample and the load cell or calotte. Because the support area influences the compressive stress distribution, the geometry of the used calottes is depicted in Table 3-8. The relative slip of the unloaded end of the rebar was measured using an LVDT. It was mounted on a tripod on top of the concrete specimen far enough from the bar (see Figure 2-3b)). The displacement measured by the LVDT corresponds then directly to the relative slip between bar and concrete. The bond stress was calculated following Equation (1) from the measured force.

Table 3-8: Calotte sizes for cylindrical and cubical specimens.

Specimen type	Outer diameter [mm]	Inner diameter [mm]
Cylinder	76	34
Cube	154	72

In the case of the **push-in** type of test the experimental setup was very similar and is shown in Figure 3-19. The main difference was that the steel rebar was pushed by the upper crosshead of the machine into the concrete specimen. LVDTs on both sides of the

specimen were used to measure the displacement of the specimen and of the reinforcement steel. The averaged displacements of concrete δ_c and rebar δ_s were then calculated. The relative slip was determined as a difference between the specimen displacement and the displacement of the unloaded end of the reinforcement bar:

$$s = \delta_s - \delta_c \tag{69}$$

Calotte and PTFE sheet were placed under the specimen. The force was measured by the machine load cell and calculated according to Eq. (1).

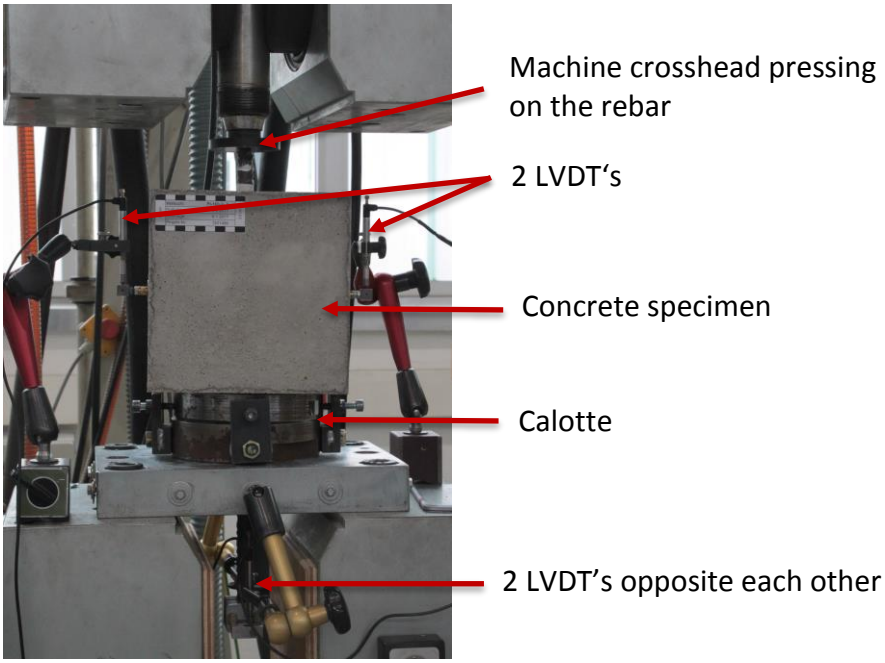

Figure 3-19: Experimental setup: push-in.

3.6 Impact loading experimental setup

The impact loading experimental setup is somewhat more complex in comparison to the quasi-static setup as different measurement techniques were used. In addition, every measurement method was independently checked by an alternative method. The experimental setup is described in more detail as every part can potentially influence the overall result due to its inertia. In addition, capturing accurately such fast loading is very challenging with a there is a high potential to make errors. Many calibrations and trial tests were performed to develop the experimental stand to the state presented in this work. The author is aware of the limitations of each setup and will try to provide ideas for the improvement.

3.6.1 Drop-tower configuration

Both pull-out and push-in tests under impact loading were performed in a specially developed and instrumented drop-tower. The drop-tower was 6 m high and is in both pull-out and push-in test configuration capable of dropping an impactor from a maximal height of 3.5 m. In both configurations, the sample is placed on an instrumented support assembly which consists of two steel plates and a piezoresistive ring load cell (PCB M205C). The opening in the steel plates and ring load cell has a diameter of 20 mm and allows the reinforcement to protrude from the bottom of the assembly. The support assembly is shown in Figure 3-20. The load cell needed to be pre-loaded to at least 54 kN for which initially four screws were used. Even though, the load cell itself is calibrated from the manufacturer, the new assembly needed to be recalibrated. During the calibration process, it was found out, that it is very hard to pre-load the load cell evenly with four screws. Therefore the configuration was changed, and only three Allen screws were used as presented in Figure 3-20. Two semiconductor strain gauges were glued longitudinally on each screw to check the pre-load and to measure the amount of force which is going through the screws. The strain gauges were electrically connected in a diagonal half bridge so that possible bending of the screw was eliminated. Theoretically, no force should go through the Allen screws when the platform is loaded in compression. However, it was not possible to avoid eccentricities and bending of the assembly plates. In addition, it is not possible to avoid multiple reflections from the steel plate due to the geometrical impedance mismatch between the plate and the load cell. Therefore the data from the load cell as well as the strain gauges on the screws were used just as supplemental information, even though that at the beginning of the research it was thought that these data could be reliably used.

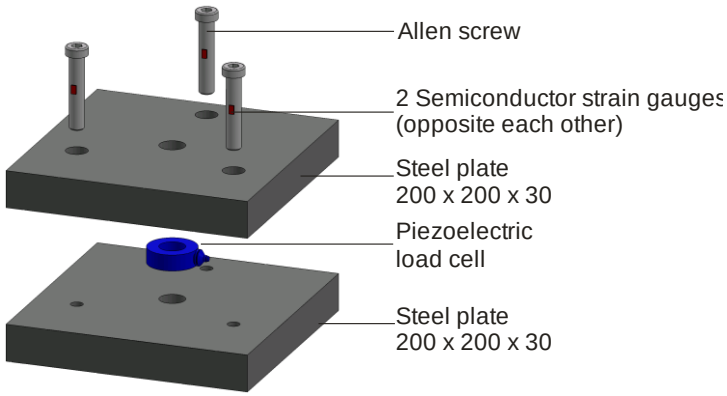

Figure 3-20: Support assembly.

The drop-tower in **pull-out** configuration is presented in Figure 3-21. The support platform was mounted on crossbeams in the height of 6 m. The sample was placed on top of the support plate. To be able to perform a pull-out test a reinforcement bar with a female metric screw from Pfeifer continuity system was used as shown in Figure 3-22a). The reinforcement bar was connected to a 5 m long transfer steel bar with a diameter of 20 mm. For the connection, right-left coupling bolt was used (Figure 3-22b). The long steel transfer bar was used to transfer the loading impulse into the rebar. The impactor was a hollow cylinder made of Cf53 steel with an outer diameter of 50 mm and the inner diameter of 29 mm. The length of the impactor was 500 mm, and its weight was 5.1 kg. The sketch of the impactor is shown in Figure 3-23a). During the experiment, the impactor was released from an electromagnetic holder attached to the end of a hoist. After that the impactor was sliding along the long transfer bar inside of an aluminium tube until it hit the stopper Figure 3-23b). Because the impactor was guided by the aluminium tube, it didn't come into contact with the transfer bar which is very important for repeatability of the experiments. The cylindrical shape of the impactor was chosen in order to produce nearly rectangular loading impulse which travels along the transfer bar and then through the coupling into the rebar. In all investigated cases, only one hit of the impactor was needed for the complete failure of the bond zone.

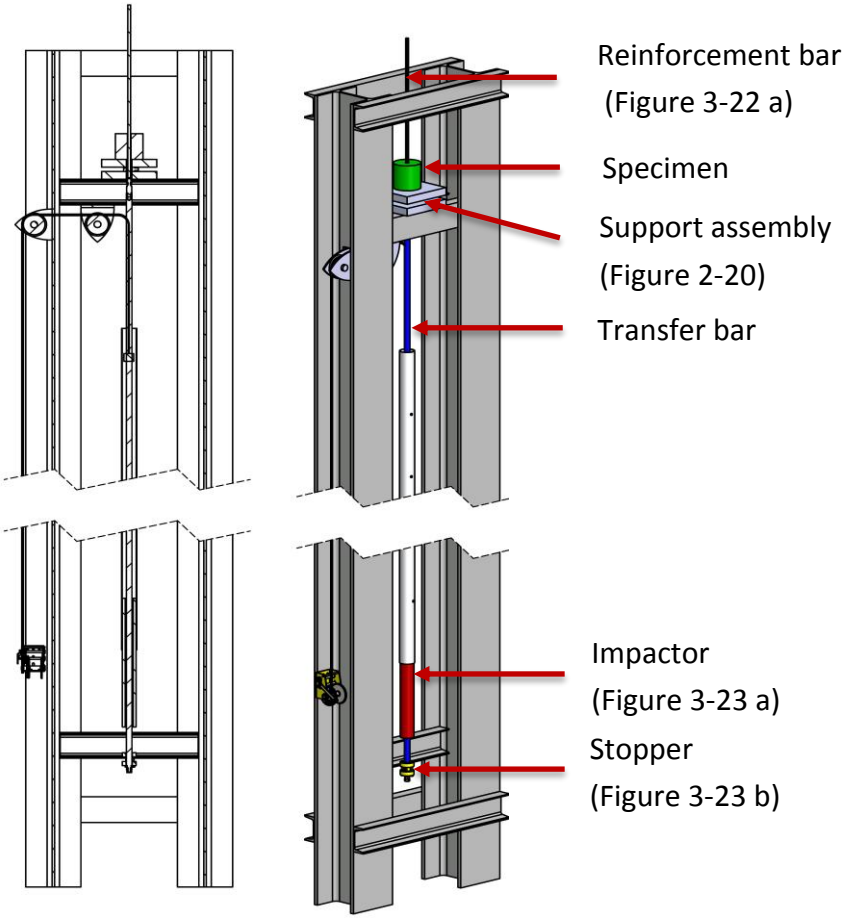

Figure 3-21: Drop-tower in pull-out configuration.

a) b)

Figure 3-22: a) steel rebar with coupling, b) bolt connecting the rebar to the transfer bar.

a) b)

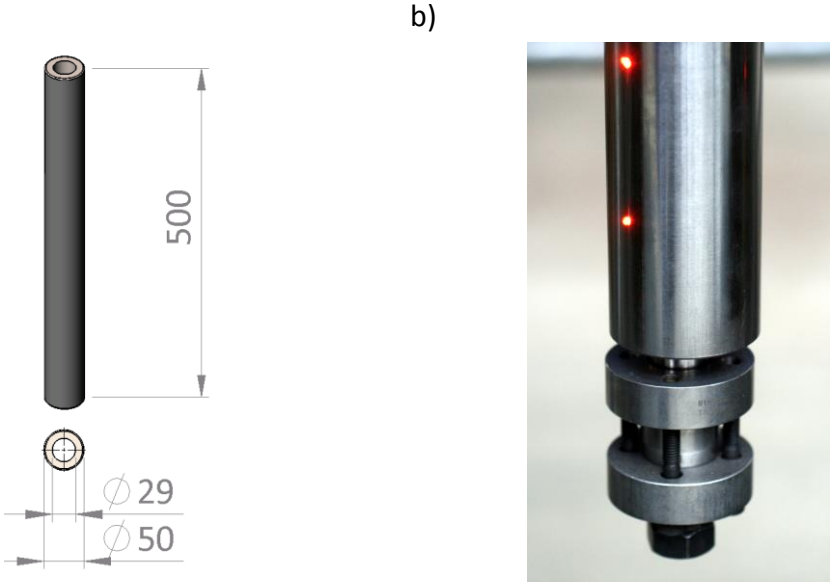

Figure 3-23: a) impactor sketch, b) stopper with an impactor just before impact (red dots are the light barriers).

The configuration of the drop-tower in the **push-in** mode was very similar. The main difference was that the support platform was mounted on the crossbeam near to the bottom of the base of the drop-tower. For the push-in tests, a solid cylindrical impactor with a diameter of 40 mm and a height of 500 mm was used. These dimensions were chosen in order to match the impactor weight (4.9 kg) as closely as possible to the weight of impactor used during pull-out tests (5.1 kg). The impactor was made of Cf53 hardened steel. At the beginning of each test, the impactor was pulled up by a manual pulley system and afterwards it was released from an electromagnetic holder to avoid any interference during the release process. Similarly to the pull-out configuration, the impactor fell down in an aluminium tube with holes to minimise the air friction due to the tunnel effect. The sample was placed on the support platform (Figure 3-20), and the impactor hit the free end of the rebar directly. The drop-tower in push-in configuration is sketched in Figure 3-24.

A data acquisition system capable of sampling the strain gauge amplifiers at the frequency of 1 MHz was used. To eliminate the high-frequency electrical noise in the strain gauge signals a CFC 20,000 low-pass filter was used. The mathematical definition of the CFC filters can be found in SAE J211-1 [122, 123].

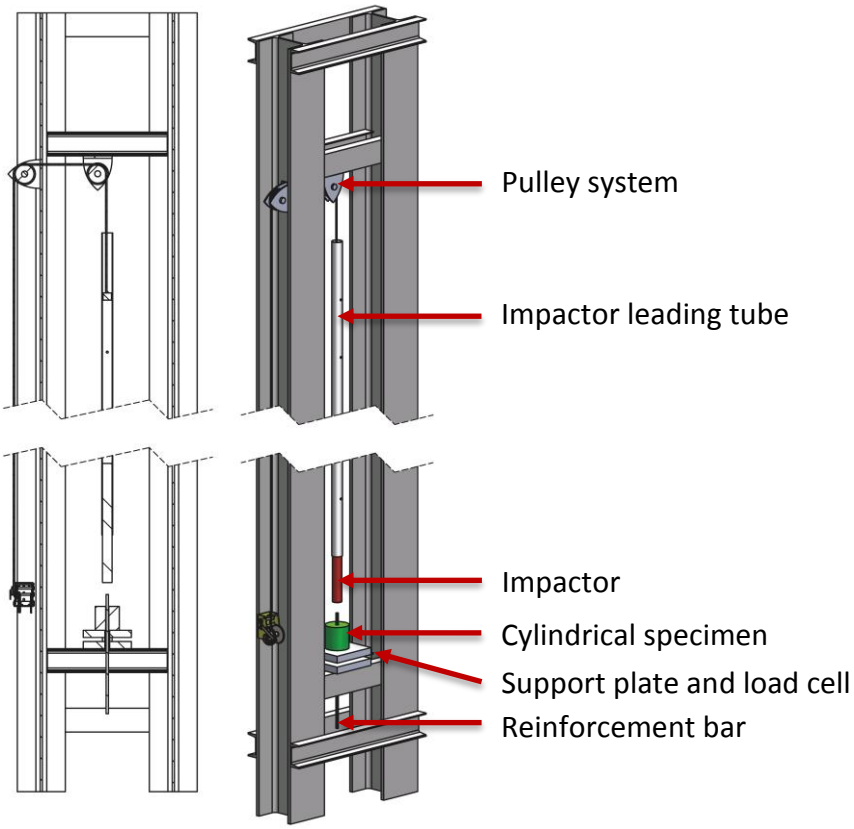

Figure 3-24: Drop-tower sketch in push-in configuration.

3.6.2 Split Hopkinson bar configuration

For investigating the steel-concrete bond stress under high loading rates, split Hopkinson pressure bar was used. Further on, it will be referenced to as simply split Hopkinson bar or SHB. The SHB didn't allow to test samples in pull-out mode; therefore **only push-in tests were performed.** During the experimental work, the SHB was adjusted several times to the research needs and to yield reproducible experimental results. Therefore several configurations exist. The basic configuration consists of a pressure vessel from which an impactor is released. The basic working principle of SHB is to study incident, reflected and transmitted loading wave. The theoretical background was briefly explained in Chapter 2.2.1. In this chapter, the SHB as modified for the purpose of this project will be described.

The size of the impactor was governed by the available pressure vessel. Therefore it had to have 50 mm in diameter. The impactor length was chosen to be 500 mm, so the loading impulse length of 1 m is exactly the same as in the drop-tower tests. The sketch of the SHB is shown in Figure 3-25.

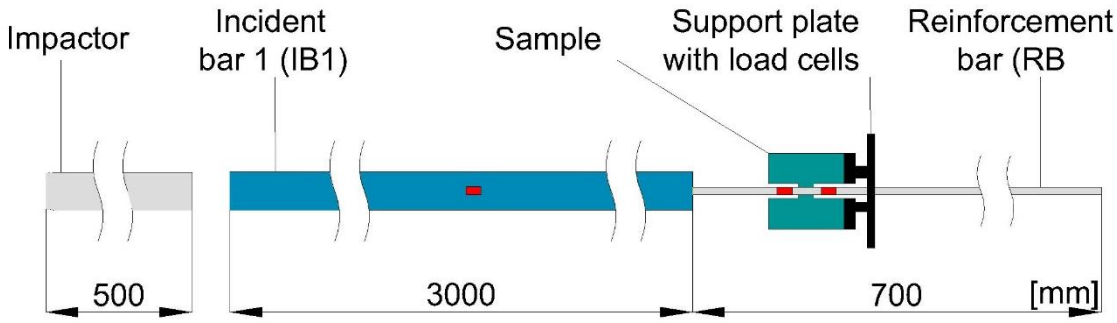

Figure 3-25: SHB sketch. Strain gauges are marked in red.

Several sizes of an incident bar were modelled in LS-Dyna, and it was decided that an incident bar with a length of 3 m and a diameter of 50 mm gives the best results. The incident bar, the reinforcement bar as well as the impactor were made of steel to avoid material impedance mismatch. The geometrical impedance mismatch between the incident bar Ø50 and the reinforcement bar Ø10 was however unavoidable. For more information about impedance, please refer to Chapter 2.2.1. The sample was placed horizontally, after an incident bar, on a half cylindrical holder. The reinforcement bar was in contact with the incident bar, and the other end of the rebar protruded through the support assembly. It was decided to use a different type of load cell assembly for the SHB in comparison to the drop-tower configuration. This new assembly, shown in Figure 3-26, consisted of three piezoelectric load cells (PCB 208C05) that did not have to be pre-stressed. It was, therefore, possible to eliminate the influence of the Allen screws and all the load had to pass through the load cells. The total load is then calculated as the summation of the three load cell signals. Because only cylindrical specimens were tested in the SHB, the support plate had a diameter of 100 mm.

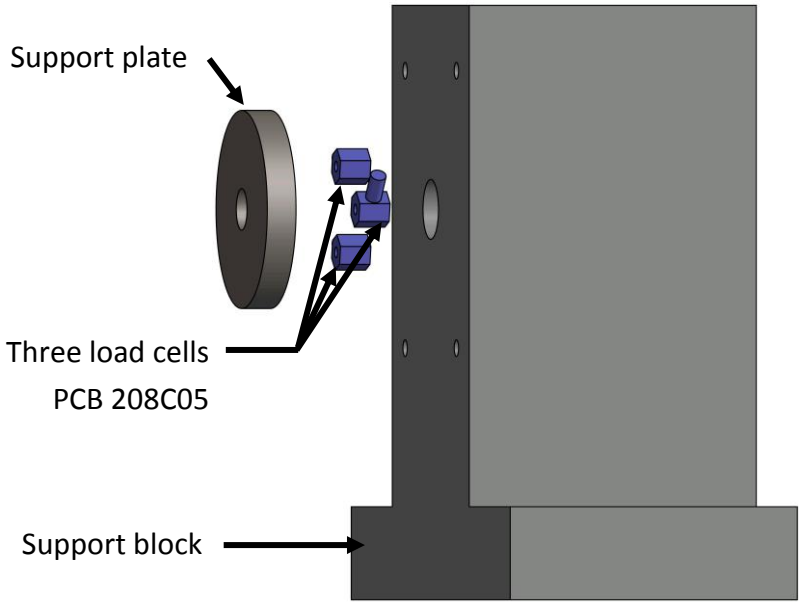

Figure 3-26: Support assembly for SHB.

No transmission bar was used in a push-in configuration as it is possible to measure the strains directly on the reinforcement steel. However, it was necessary to ensure that the reinforcement bar is sufficiently long (700 mm) so that the reflection of the front of the impulse wave from the free end of the rebar doesn't overlap the back end of the impulse.

In the improved SHB setup a second incident bar with a diameter of 10 mm was introduced between the incident bar 1 (IB1) and the reinforcement bar (RB) as can be seen in Figure 3-27. The purpose of this second incident bar is to measure a reflection of the impact wave from the bond zone. Without IB2, the wave reflection from the bond zone reflects from the interface between IB1 and RB due to the impedance mismatch. This second reflection influenced the strain gauge readings before the bond zone, and this was not desirable. Therefore, this improved experimental setup was used in later stages of the experimental work. The isometric model of the SHB is shown in Figure 3-28, and the detail of sample placed in the SHB is shown in Figure 3-29. To minimise wave dispersion caused by the lateral inertia of the bar a so-called pulse shaper was used in some of the experiments. A pulse shaper is, in fact, a mechanical filter which was placed between the impactor and IB1 as seen in Figure 3-30. It was made of copper and had a diameter of 22 mm and thickness of 1 mm. The green clamp on Figure 3-30 is used to stop the motion of the IB1 after displacement of approx. 100 mm by an impacting a damping system.

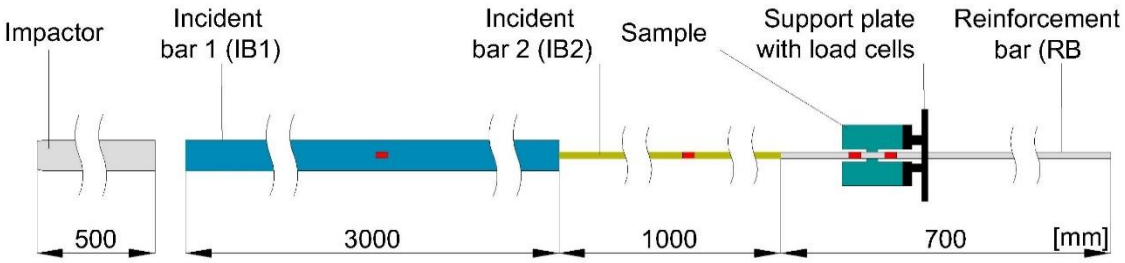

Figure 3-27: SHB with incident bar 2 (IB2).

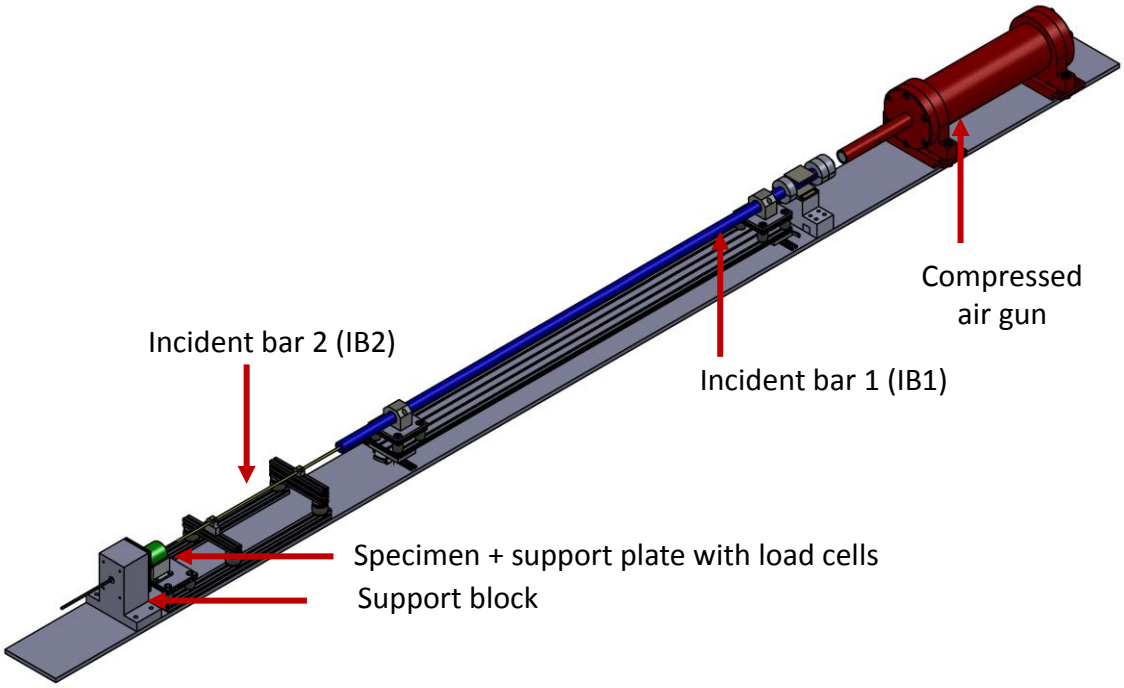

Figure 3-28: Isometric view of the SHB model.

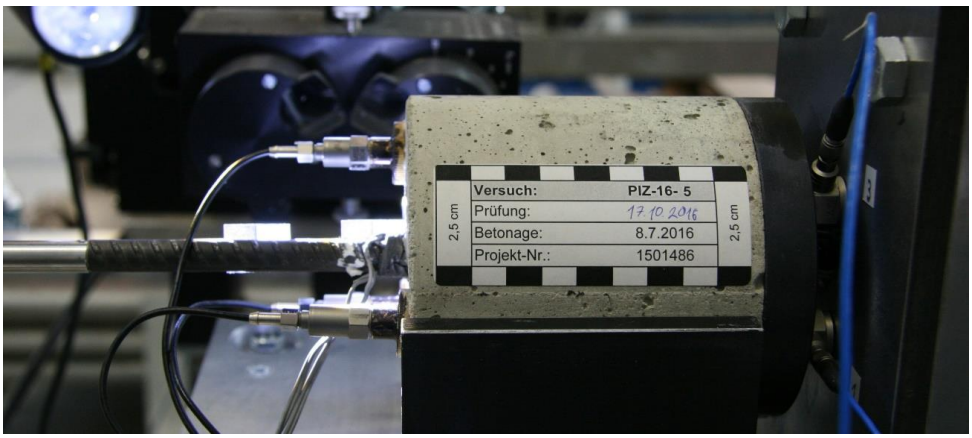

Figure 3-29: Specimen in the SHB.

Figure 3-30: Pulse shaper attached to IB1 with a green clamp for stopping the IB1 after 100 mm.

3.6.3 Instrumentation and measurement methods

Similarly to the data acquisition system, the used sensors and measuring methods have a potential to influence the results in the case of impact events significantly. For this reason, several types of measurement techniques were used throughout the experimental research. To increase accuracy and reliability of the results every value was measured by two independent methods as discussed in this chapter.

Impactor velocity measurement: The measurement of impactor velocity was relative forward and was calculated from the time that the impactor needs to pass between two light barriers at a given distance. The measured velocity was then checked with the theoretical free-fall velocity (drop-tower) or from energy provided by the compressed air (SHB). As expected, very good agreement was found between the measured and theoretical values.

Reinforcement bar slip measurements: In the case of quasi-static tests, the slip was measured on the unloaded end with an LVDT. However, using LVDT's for slip measurement during impact loading is not advisable. The reason for that is that LVDTs measuring principle is based on soft iron core moving in hollow cylinder surrounded by a coil. In the case of a dynamic event, the measurement result is influenced by the pin and spring inertia which makes the LVDTs unsuitable for measuring frequencies above 500 Hz. At the beginning of the research, it was thought that an accelerometer can be attached to the free and of the rebar and that the slip can be calculated by double

integration of acceleration. While this is theoretically possible, in reality, the acceleration at the end of the rebar is very high (due to stress reversal at the free end). Even though, the used accelerometers had a resolution of 50 000 m/s^2 they became easily overloaded. For this reason, it was decided to measure the slip by two contactless optical methods. Namely optical extensometer produced by company Rudolph and laser or vibrometer. The optical extensometer as seen in Figure 3-31a) is capable of tracking a motion of two black-and-white targets. The analogue output signal is then proportional to the measured movement of the black-and-white transition. To get a relative slip of the rebar, one target was glued on the top concrete surface of the sample, and another target was glued directly on the reinforcement, Figure 3-31b). Again, it's very important how the measurement is performed. In one of the trial series, the target was glued on a plastic shell that was tightly screwed on the reinforcement. It was shown, that the influence of the plastic shell inertia is very significant. This was only discovered by using an alternative method of slip measurement – laser and vibrometer.

a) **b)**

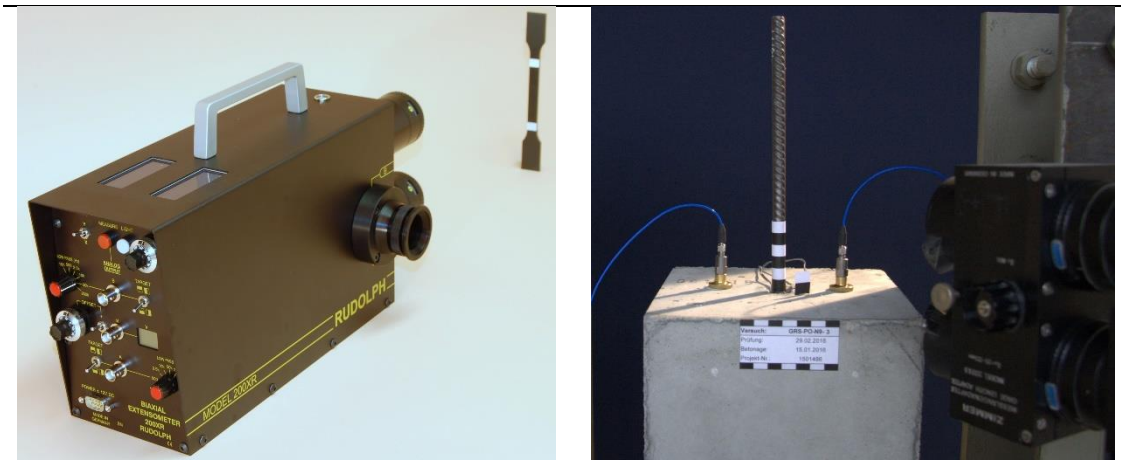

Figure 3-31: a) Optical extensometer 200XH and b) black-and-white targets glued on the specimen.

The slip of the free end of the reinforcement bar was measured using laser deflection meter and later on in the experimental work by vibrometer. The disadvantage of the laser deflection meter was its low accuracy for dynamic measurements. The resolution by 100 kHz sampling frequency was only 0.33 mm which was unsatisfactory. Therefore, this method was used for control measurements only. Later in the project, it was possible to use a more precise Laser-Doppler-Vibrometer to measure the movement of the end of the reinforcement. It has to be taken into consideration, that the response of the rebar at the ends differ from the response in the middle of the rod owing to the

deflection doubling that occurs during the stress reflection and reversal at the free end. This behaviour is seen in Figure 3-32 where the bar movement as measured by the extensometer (approximately in the middle of the rebar) is compared to the bar movement at the end of the rebar as measured by vibrometer. The time lag between the two signals corresponds to the time that the wave needs to travel between the two measuring points which were 650 mm apart. Assuming speed of sound in steel to be 5048 m/s and using Equation (70) the time lag should be 0.13 ms which perfectly corresponds to Figure 3-32. The distance between the measuring points was 650 mm. Due to the friction in the bond zone, the deflection in the middle of the rebar and at its end becomes the same after the first wave pass. Therefore, only the first rising segment of the red curve is influenced by the displacement doubling. The red curve divided by 2 corresponds to the blue line. When comparing the blue and black line, we get a very good match of displacement for the first wave pass.

$$t = \frac{s}{v} = \frac{0.65}{5048} = 0.13 \times 10^{-3}[s] \tag{70}$$

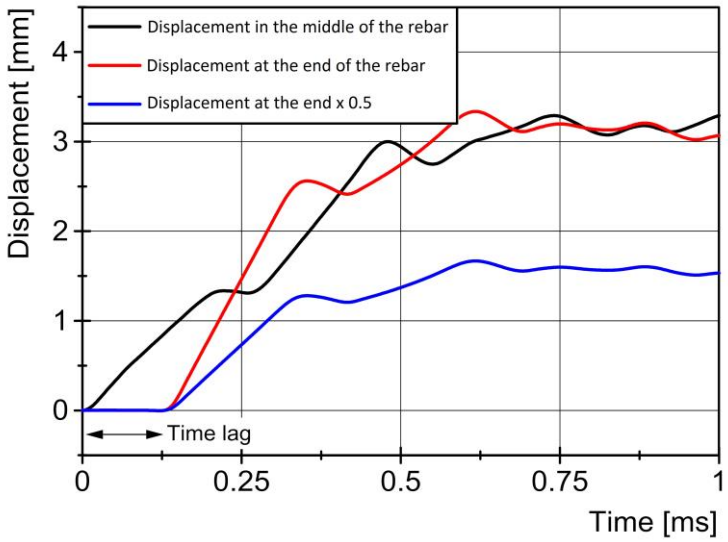

Figure 3-32: Displacement doubling at the end of the rebar.

The impact push-in and pull-out tests were also recorded on a high-speed camera with a sampling frequency of 100 000 fps. Because of the limited resolution, the video from the high-speed camera was mainly used for a qualitative check of the impact incident. However, it is possible to use digital image correlation (DIC) method to evaluate the displacement of the bar. The results very well matched the displacements measured by the optical extensometer. The relative reinforcement bar slip is then calculated as a difference from concrete top surface and rebar displacement.

Bond stress measurement: Calculating the bond stress in the quasi-static case is very easy. As described in Chapter 3.4 the force needed to pull-out/push-in the rebar out of/into the concrete is measured. The bond stress is then calculated from Equation (1) as all other parameters are known.

On the other hand, it is relatively complicated to measure the bond stress during impact loading correctly. The review of methods used by other researchers is provided in Chapter 2.2.4. For the purpose of this research, a novel method was used: strain histories before and after the bond zone were measured. The bond stress state between the reinforcing steel and concrete is shown in Figure 3-33 on the infinitesimally small element. From the equilibrium of forces on this differential element, the Equation (72) can be written.

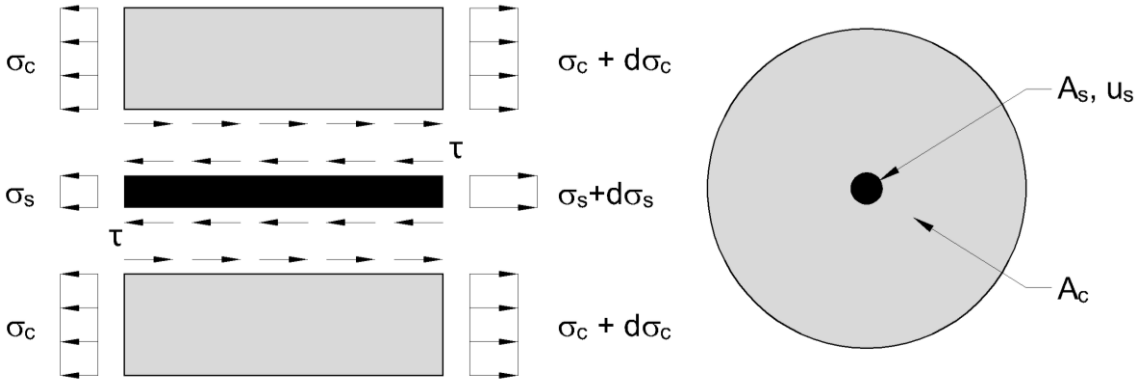

Figure 3-33: Differential element for bond stress between steel and concrete after [125].

$$A_s \frac{d\sigma_s}{dx} = -u_s \cdot \tau(x) \tag{71}$$

This can be rewritten as:

$$A_s \cdot d\sigma_s = -\tau(x) \cdot u_s \cdot dx \tag{72}$$

After substituting A_s, u_s and $d\sigma_s = E d\varepsilon_s$ in the Eq. (72) we get the following relationship:

$$\pi \cdot \frac{d_s^2}{4} \cdot E_s \cdot \frac{d\varepsilon_s}{dx} = -\tau(x) \cdot \pi \cdot d_s \tag{73}$$

After rearranging we get:

$$\tau(x) = -\frac{d_s \cdot E_s}{4} \cdot \frac{d\varepsilon_s}{dx} \tag{74}$$

Under the assumption of constant bond stress for short bond length we can substitute the differential terms by $d\varepsilon_s = \varepsilon_{s,1} - \varepsilon_{s,2}$ and $d_x = l_b = 2 \cdot d_s$ and we get an equation for mean bond stress:

$$\tau_m = -\frac{E_s}{8} \cdot (\varepsilon_{s,1} - \varepsilon_{s,2}) \tag{75}$$

Under the assumption of stress distribution as shown in Figure 3-33, $\varepsilon_{s,2}$ is larger than $\varepsilon_{s,1}$ and therefore the difference $(\varepsilon_{s,1} - \varepsilon_{s,2})$ will be negative which gives positive bond stress. During the evaluation of impact experimental results, the measured strain gauge signals $\varepsilon_{s,1}$ and $\varepsilon_{s,2}$ with a corrected time lag are inserted into Equation (75) and bond stress is calculated. The Equation (75) is of course valid for the quasi-static case as well. In Figure 3-34 a schematic pull-out test setup is shown. The force direction corresponds to the differential element. Because the test is quasi-static the strain in the reinforcement bar before the bond zone is zero $(\varepsilon_{s,1} = 0)$ as there is no load.

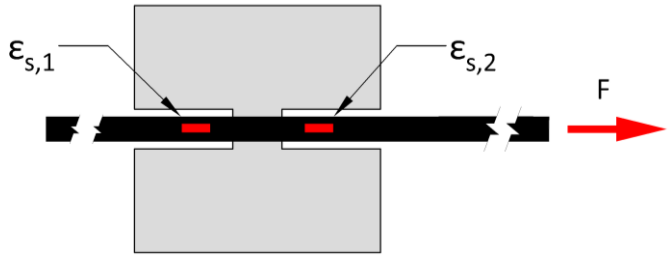

Figure 3-34: Schematic sketch of a pull-out test. Force direction corresponds to the stress state corresponding to the differential element.

After substituting $\varepsilon_{s,2} = F/(A_s \cdot E_s)$ into Eq. (75) we get Eq. (1) valid for the bond length $l_b = 2 \cdot d_s$.

$$\tau_s = -\frac{E_s}{8} \cdot (-\varepsilon_{s,2}) = \frac{E_s \cdot F}{8 \cdot E_s \cdot A_s} = \frac{F}{2 \cdot \pi \cdot d_s^2} \tag{76}$$

For strain measurements, semiconductor strain gauges were used. The advantage of such strain gauges is their high k-factor which is more than 60 times higher than the k-factor of normal (constantan) strain gauges. The high k-factor reduces the necessity for amplification, as well as the noise to signal ratio, making them more suitable for high sampling rates. The main disadvantage of semiconductor strain gauges is their temperature sensitivity and smaller measuring range. In the case of an impact event, the temperature sensitivity is not a big problem, as maximally 1 ms of measurement is of interest. The duration of the loading wave is as short as 0.2 ms. During this time the temperature can be considered as constant. Throughout the experimental work, it was

made sure that the steel does not reach the plastic deformation. Therefore, the limited measuring range of the strain gauges was not a disadvantage. However, the steel yielding proved to be limiting factor for increasing the loading velocity. This is in more detail discussed in Chapter 5.

The strain gauges were glued on the longitudinal rib, and they were covered with varnish and silicone as a protection against humidity. This can be seen in Figure 3-35 and Figure 3-36. On each reinforcement bar, four strain gauges were used. Two before the bond zone and two after the bond zone. A sketch with strain gauge location along the bar for SHB cylindrical specimens is shown in Figure 3-37. For the reason that the bond zone length was not varied, the strain gauge location was the same for all types and sizes of specimens.

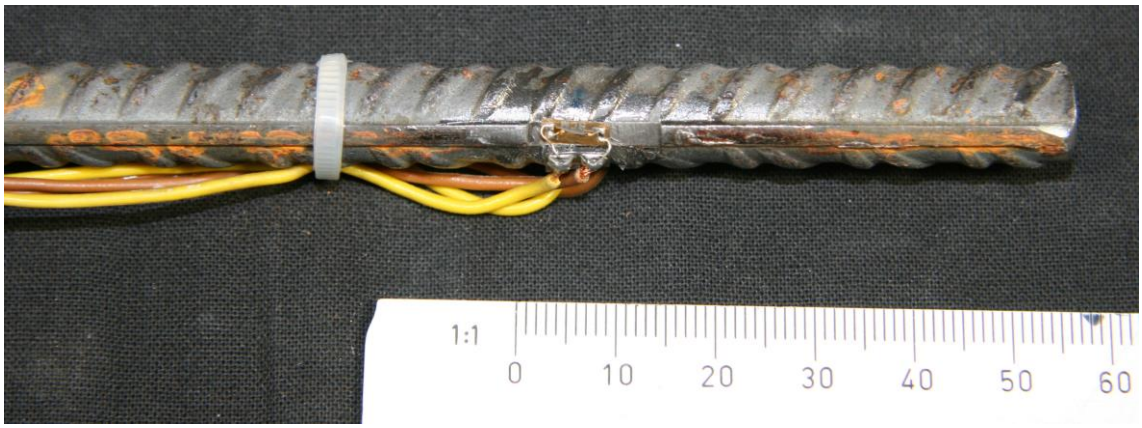

Figure 3-35: Strain gauge glued on the reinforcement bar-without silicone layer.

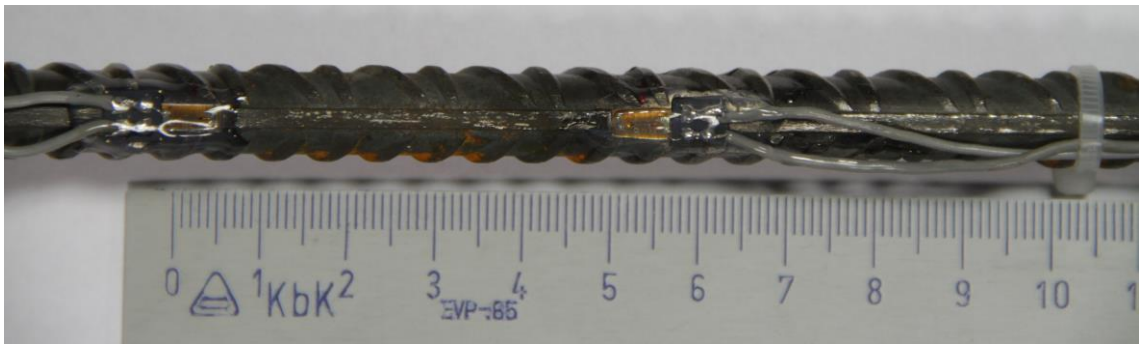

Figure 3-36: Strain gauges glued on the reinforcement bar including the silicone layer.

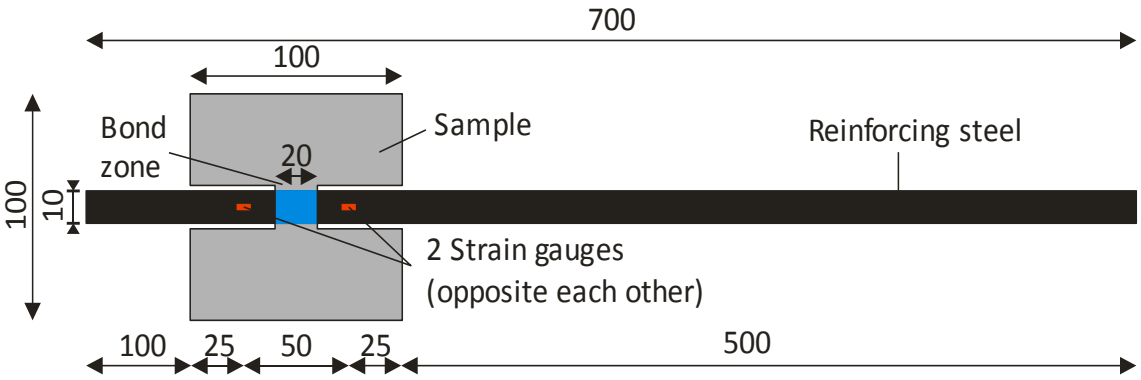

Figure 3-37: Location of strain gauges along the bar.

The results of strain measurement are two waves: before and after the bond zone. These two waves along with the initial impact wave, as measured on the IB2, are shown in Figure 3-38. In this figure, time lag was not corrected, and it corresponds to the distance between the strain gauges. From Figure 3-38 it can be seen, that strains before the bond zone are higher than the initial pulse. This is caused by a compressive wave that is partially reflected from the bond zone and superimposed on the incoming pulse. The strain gauge signal after the bond zone is lower compared to the initial pulse because a part of the wave gets transferred through the bond zone into the concrete body.

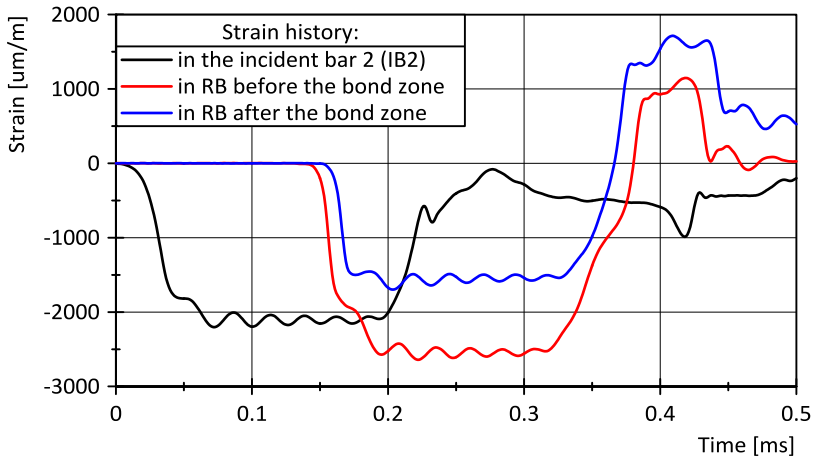

Figure 3-38: Result of strain measurement – time lag not corrected.

Another way how to determine the bond stress is to measure the force needed to pull-out/push-in the reinforcement from the specimen and subsequently use Eq. (1). The biggest problem with this approach is to determine the correct force that needs to be measured. At the beginning of the research, it was thought that simply measuring the reaction force will be satisfactory. For this reason, two types of load cells were constructed, and they are presented in Figure 3-20 and in Figure 3-26. However,

throughout the experimental work, it was shown that the reaction force contains a contribution of sample inertia. Therefore, it was decided to measure the acceleration of the specimen on its surface. The inertial force was then calculated from its mass and acceleration. The bond force was then calculated by subtracting the inertial force from the reaction force following Equation (77):

$$F_{bond} = F_{support} - m \cdot \vec{a}(t)_{specimen} \quad (77)$$

Where F_{bond} is the force required to destroy the bond, $F_{support}$ is the reaction force measured by the load cell and $\vec{a}(t)_{specimen}$ is the acceleration of the specimen. The problem is, that the acceleration in equation (77) needs to be the whole body acceleration. This is, however, impossible to determine experimentally, as only the surface acceleration can be measured. Because of the wave reflections that happen on the surface, this measurement method is not so accurate. The reflections cannot be mathematically eliminated as waves of many frequencies travel through the concrete specimen. Numerical simulation in LS-Dyna showed that the body acceleration was significantly different from the surface acceleration. For this reason this method of calculating bond stress slip was considered only as supplementary method. It was used only in the case when one or more strain gauges were defect. The force measured by the load cell (reaction force) is compared with the inertial force in Figure 3-39. The inertial force is multiplied by -1 in Figure 3-39. The blue curve is the true contact force that is acting in the bond zone. The problem is, that although the time lag of all signals was corrected, the inertial force and reaction force doesn't have the same waveform. This is caused by the reasons described above, mainly by the impossibility to measure the whole body acceleration.

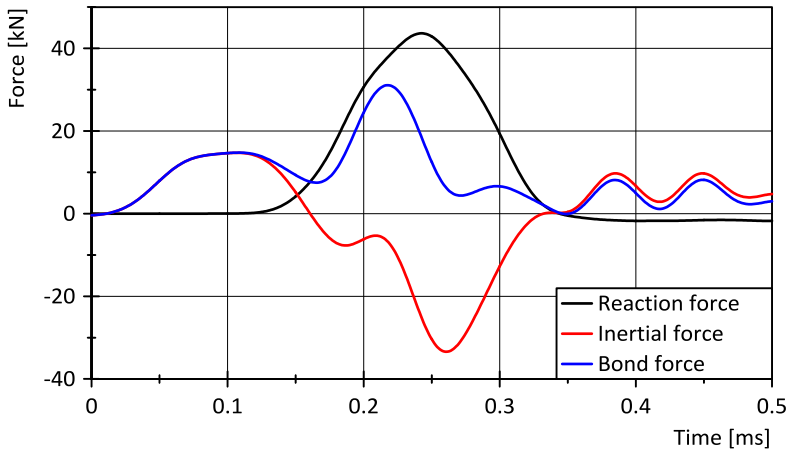

Figure 3-39: Determination of true bond force (compression is positive).

The Figure 3-39 clearly shows that it would be incorrect to say that the bond force is equal to the reaction force because the reaction force is mainly dependent on the mass of the sample. The maximal reaction force of 43.6 kN from Figure 3-39 corresponds to the bond stress of 68.8 MPa which is very unrealistic. The bond stress in the quasi-static case is for this type of concrete between 15-20 MPa.

Chapter 4

Results and discussion

4.1 Quasi-static results

Quasi-static bond stress-slip relationships were measured as a reference for the relationships measured under impact loading. In this chapter, interesting findings from the quasi-static experimental phase will be presented. More than 100 single tests were performed, and several influences were compared. For instance the reinforcement bar diameter influence, the influence of the specimen size and bond zone location as well as the effect of loading direction. In this chapter mainly average curves will be presented. In most of the cases, the average was constructed from four measurements. The average curves were calculated as an average bond stress at a given slip value (see Ch. 3.4.3). In case that a larger amount of single results are available, confidence intervals are shown as a shaded area between 5% and upper 95% quantile. It is important to note that 95% confidence interval does not mean that 95% of the data will lie within the interval. It means that if the experiments would be repeated many times, then 95% of the constructed confidence intervals would contain the true average of the population. That means that confidence intervals are getting narrower with increasing number of single experiments because the calculated average is closer to the actual average.

It is crucial to bear in mind that the normal variation of bond strength test results is relatively high when comparing quasi-static to impact results. The normal variation of pull-out tests as presented in the literature is as high as 20% and is in more detail discussed in Chapter 2.1.5.

4.1.1 Bar diameter influence

During the experimental investigation bars with a diameter of 10 mm were used with a bond length of 20 mm ($2d_s$). It was found out, that the average bond stress is lower in comparison to the results found in the literature. For this reason, a sensitivity study was conducted in order to investigate the reinforcement bar diameter influence, which is theoretically discussed in Chapter 2.1.4.2. In a homogenous material and with the same relative rib area, the bond stress should be independent of the reinforcement bar diameter. Because concrete is not homogenous and the relative rib area also varies with rebar diameter the bond stress is not constant. It is believed, that smaller bar diameters have better bond strength in comparison to the larger bar diameters. The reason for that is that bars with larger diameters have usually smaller relative rib area. This premise would indicate that bars with a diameter of 10 mm should have better bond strength in comparison with the bond strength of 16 mm bars which is mostly presented in the literature. In this chapter, pull-out test results of bars with a diameter from 8 to 28 mm are presented. The average concrete compressive strength was $f_{cm,c} = 59.7\ MPa$. Cubes with an edge size of 200 mm were used for steels Ø8 to Ø25, for the Ø28 rebar a cube with an edge of 300 mm was used. The relative rib areas of the used steel are presented in Table 3-6. The test setup, concrete material properties as well as the casting procedure are described in Chapter 3. The resulting bond stress-slip relationships are shown in Figure 4-1. The curves in Figure 4-1 represent average results from 3 measurements. The maximal bond strength and standard deviations are shown in Figure 4-2. From the Figure 4-1 and 4-2, it can be seen that the bond stress-slip relationship is quite significantly influenced by the rebar diameter. The residual bond stress is decreasing slower for bars with a larger diameter. However, this is to be expected as the friction between the ribs and concrete increases with longer absolute bond lengths. The length of the descending branch of the bond stress-slip relationship is dependent on the clear rib spacing.

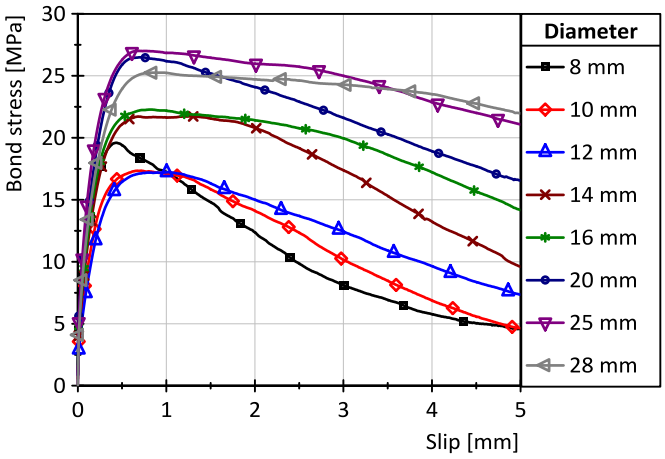

Figure 4-1: Influence of the rebar diameter on the bond stress-slip relationship.

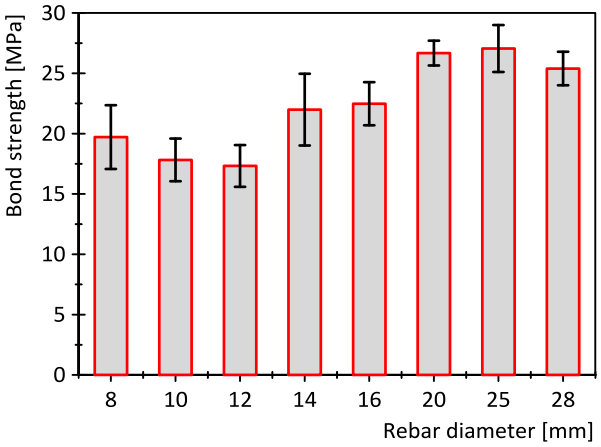

Figure 4-2: Maximal bond stress for various rebar diameters.

What is much more interesting is the value of the maximal bond stress. The bars can be divided into three categories based on the bar diameter. Relatively low bond stress under 20 MPa achieved bars with a diameter of 8-12 mm. Intermediate bond stress (20-25 MPa) achieved bars with a diameter of 14-16 mm. The highest bond strength over 25 MPa was measured for the group of bars with diameters 20-28 mm. These results suggest that the bond strength increases with increasing bar diameter and it will probably decrease for bars with a diameter larger than 25 mm. These results are very interesting and somewhat contradictory to the general belief. They are connected with two phenomena. Firstly, it is the relationship between the aggregate size in the concrete mix and the rib spacing. For instance bars with a diameter of 10 mm have rib spacing approximately 6 mm, and the maximal aggregate size of the concrete used in this research was 8 mm. That means that the larger aggregates cannot get between the ribs a thus increase the local bond strength. Secondly, the distance between the support

plate and bond zone can play a significant role. Although PTFE sheet was placed between the concrete cube and the support plate the contact friction cannot be eliminated. This means that the concrete near to the support is additionally confined because of the Poisson effect. Because the size of the concrete cubes was constant (except the Ø28 rebar) and because the bond length is dependent on the rebar diameter, the distance between the bond zone and the support decreased with increasing bar diameter, as shown in Table 4-1. Steel with Ø25 has the shortest distance between the support and the bond zone, that means that the confinement influence is the highest and indeed it also has the highest measured bond strength.

Table 4-1: Distance from the support to the beginning of the bond zone.

Bar diameter [mm]	**8**	**10**	**12**	**14**	**16**	**20**	**25**	**28**
Cube edge length [mm]	200	200	200	200	200	200	200	300
Bond length [mm]	16	20	24	28	32	40	50	56
Distance to the support [mm]	92	90	88	86	84	80	75	122
Bond strength [MPa]	19.7	17.8	17.3	22.0	22.5	26.7	27.1	25.4

In addition, the pull-out force grows with a second root of the diameter. This is shown in Figure 4-3 where force-rebar diameter dependency is shown for a constant bond stress of 1 MPa. Larger force results in a larger lateral expansion. The lateral expansion is limited by the support friction, and this results in higher confinement effect for bars of large diameters.

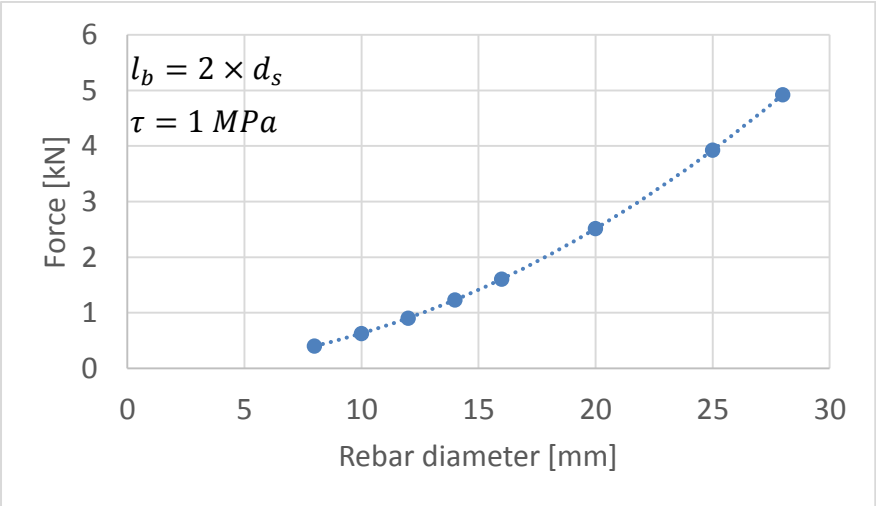

Figure 4-3: Pull-out force against bar diameter by constant bond stress and bond length.

4.1.2 *Specimen shape influence*

In this thesis, two shapes of specimens, cubes and cylinders, were used as described in detail in Chapter 3.2.1. Cubes were used to provide a comparison to the standard RILEM tests, and cylinders were used for their suitability for impact testing, especially in the split Hopkinson bar. When quasi-static tests were compared to the impact tests always the same type of specimen was used. However, it is interesting to look how the specimen size and shape influenced the bond stress-slip relationships. For the pull-out type of test, as shown in Figure 4-4, 200 mm cubes were compared with 100 mm cylinders. Reinforcing steel of a diameter 10 mm was used. In the case of cubes, an average of 17 single measurements is shown as well as the lower 5% and upper 95% confidence interval. The maximal bond strength is different to that presented in Figure 4-1 for Ø10. The reason for that is that averages from only three specimens are shown in Figure 4-1. In addition, the average results from 22 cylindrical specimens including the lower 5% and upper 95% confidence interval are shown in Figure 4-4.

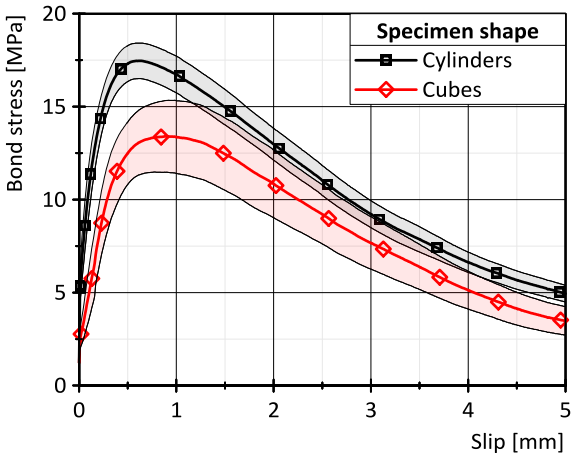

Figure 4-4: Influence of specimen size and shape on the bond stress-slip relationship.

Based on the bond stress-slip relationship presented in Figure 4-4 it can be stated that the size of the specimen has a role on the measured maximal bond strength as well as the stiffness of the bond zone. This is caused by the fact, that in the case of cylinders the distance to the support plate is only 40 mm whereas in the case of the cubes this distance is 90 mm. The concrete cover is also smaller for cylinders in comparison to the cubes, but it still provides satisfactory confinement which demonstrates itself through the typical pull-out failure pattern. Because the specimen shape has a significant influence on the results, in the following work, only cubes will be compared with cubes and cylinders with cylinders. Many cubes had the bond zone damaged even before the

testing. Because of the bar diameter and bond zone length only small force is required to damage the bond zone. Such force can accidentally be induced into the rebar during demoulding and handling of the cubes as their mass is nearly 20 kg.

4.1.3 Bond zone length influence

The influence of bond length on the bond stress-slip relationships was discussed in detail in Chapter 2.1.4.5. The majority of researchers reported that the maximal bond stress decreases with increasing bond length. However, the results of this experimental work show opposite trend. That means that the maximal bond stress increases with the increasing bond length. A similar tendency was observed by Martin and Noakowski [56] who observed an increase in bond stress for slip values of 0.01 mm, 0.1 mm as well as for the maximal slip. The diameter influence as measured on cubes and cylinders during this research is presented in Figure 4-5 and Figure 4-6 respectively. In both types of samples, the shorter bond length of $2\times d_s$ has clearly lower maximal bond stress in comparison to specimens with a longer bond zone of $5\times d_s$. Also, the scattering of the results for short bond lengths seems to be more severe. One of the reasons why the bond stress is lower for shorter bond lengths could be the fact that an imperfection such as an air pore or weak matrix has a much larger influence on shorter bond lengths. The reason for that is that the actual area on which the force is working is much smaller compared to the nominal area as assumed by Eq. (1). Another reason is that the short bond length is more dependent on the amount and position of the ribs in the bond zone. In addition, the differences in the manufacturing process have a larger influence on smaller bond lengths.

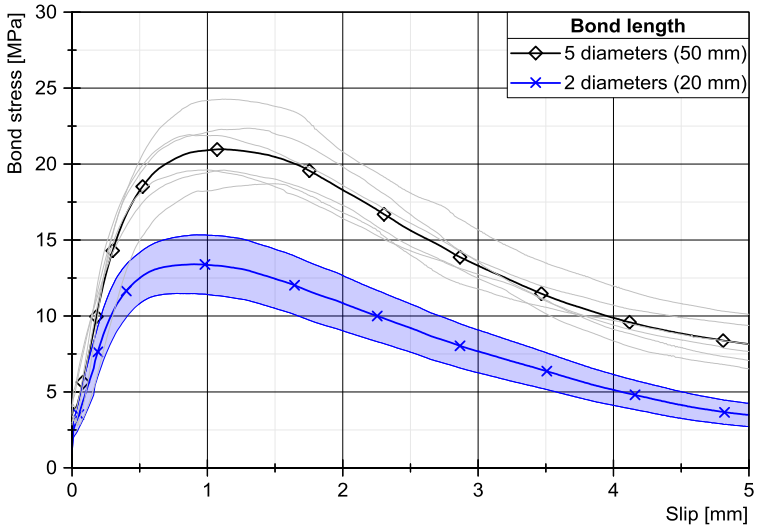

Figure 4-5: Bond length influence measured on cubes. Grey lines are results of single specimens.

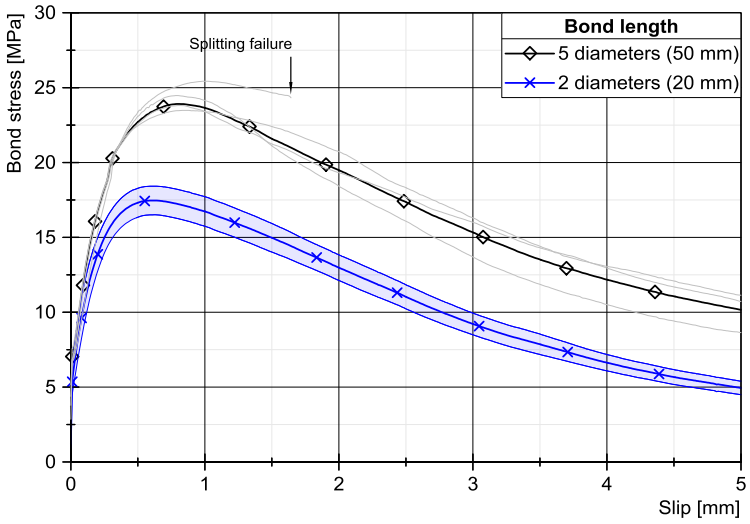

Figure 4-6: Bond length influence measured on cylinders. Grey lines are results of single spec.

4.1.4 Bond zone location influence

In addition to the bond zone length, its location within the specimen was tested. Specimens with the bond zone in the middle were compared to specimens with a bond zone located on top. This was done only for samples with a bond length of ($5\times d_s$). Figure 4-7 shows the influence of the bond zone location on the bond stress-slip relationships for cubes. It can be seen that the difference is minimal and within normal scatter. The reason for that is that the distance of 85 mm between the support and the bond zone located in the middle of the specimen is large enough. Therefore the effect of lateral strain confinement by the friction at the support plate is minimal.

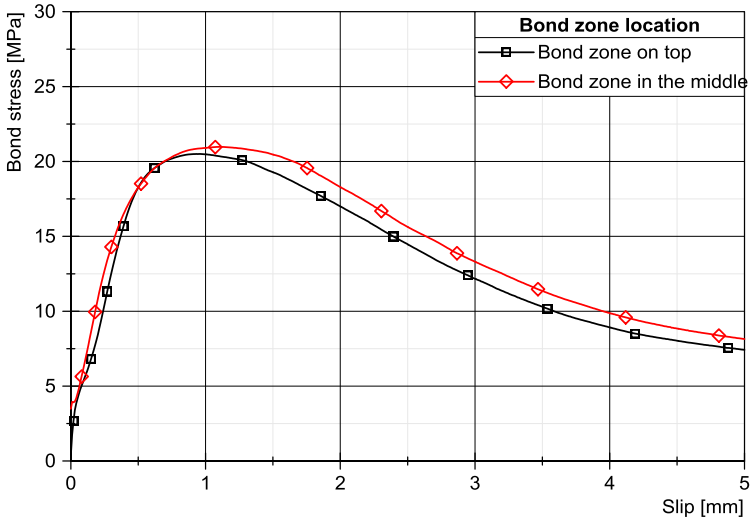

Figure 4-7: Bond zone ($5d_s$) position influence in cubes.

A different situation arises in the case of cylindrical specimens. In this case, the distance between the support plate and the beginning of the bond zone is only 25 mm for bond zone located in the middle of the specimen. For this reason, the maximal bond stress is higher for specimens with the bond zone positioned in the middle, as shown in Figure 4-8. In addition, the slip at the maximal bond value is smaller making the bond behaviour stiffer. This is again caused by the lateral confinement and the influence of the pressure zone near to the support plate.

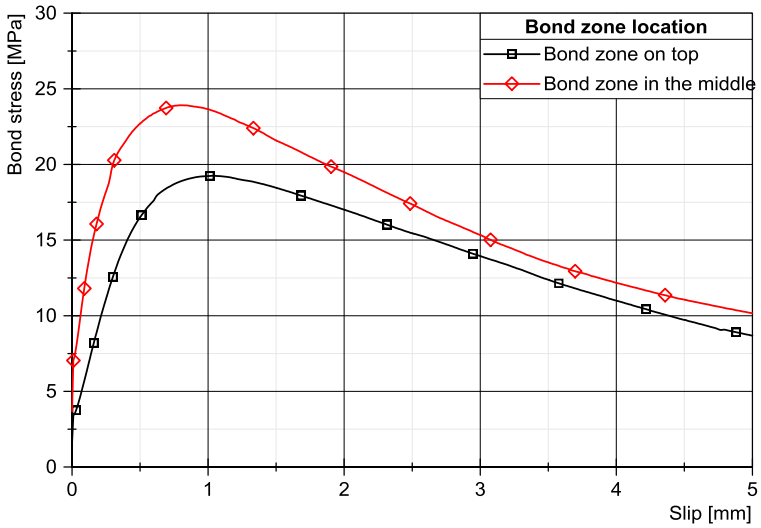

Figure 4-8: Bond zone ($5d_s$) position influence in cylinders

4.1.5 Influence of concrete cover

In the experimental work, the influence of concrete cover was studied as well. It was found that for the pull-out failure mode the concrete cover has minimal influence on the bond stress-slip relationship until the cover value of $2\times d_s$ i.e. 20. This investigation was performed only on cylinders with bond zone located in the middle of the specimen with a length of $2d_s$. The bond stress-slip relationships for cylinder diameters from 100 to 50 mm are presented in Figure 4-9. It can be seen that until the concrete cover of 30 mm ($3d_s$) no splitting failure occurs and the pull-out failure mode is dominant.

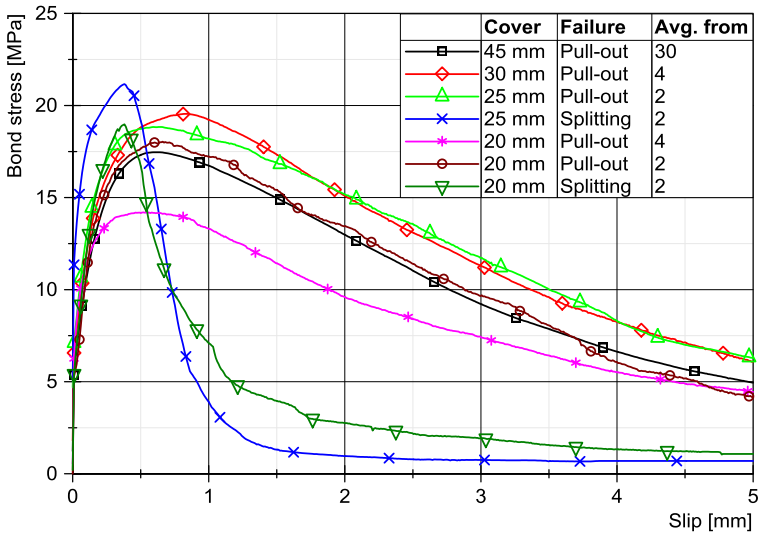

Figure 4-9: Concrete cover influence in cylindrical specimens

For smaller concrete covers between 2.5×d_s to 2×d_s a mixed type of failure exist. If the bond stress is high, splitting failure occurs. However, if the maximal bond strength is low, normal pull-out mode of failure occurs. One series of 4 specimens with a concrete cover of 2×d_s failed exclusively by pull-out. This is represented by the pink bond stress-slip relationship in Figure 4-9. This series had lower maximal bond strength in comparison with other series. That means that the tensile stress in concrete which was developed during the test was smaller in comparison to the other tests and therefore the confinement provided by 20 mm of concrete was satisfactory. The failure mode doesn't have a great influence on the maximal bond strength as it comes to splitting very near to the maximum.

4.1.6 Load direction influence

As already described in Chapters 3.4 and 3.6 about experimental setups two types of experiments were performed based on the loading direction. The first type is a classical pull-out test in which the reinforcement is pulled out of the concrete body. This is the standard test, and it is closer to the reality because steel is predominantly used to transfer tensile forces in structural members. The utilisation of pull-out tests for investigating bond stress under high loading rates is rather complicated because most of the high loading rate experimental machines such as SHBs and drop-towers produce compressive loading pulse. That means that in such a machine a load reversal system needs to be used. Using such systems for impact type of testing is however very complicated, especially because of the unavoidable reflections of the compressive wave.

For that reason, it was decided to perform the push-in type of tests. In order to provide a reference for the impact testing, the push-in tests were also performed under quasi-static conditions. The principle of the push-in test is, that the steel reinforcement bar is pressed (pushed) into the concrete body. It is expected that the bond stress during the test could be higher in comparison to the bond stress measured during a pull-out test because of the Poisson's effect. The bar under compression gets thicker due to the lateral strains and thus the friction between the concrete and steel increases. However, this effect is nearly negligible for small loads such as those that are required to pull-out or push-in a bar with a bond length of only $2\times d_s$. In Figure 4-10 the comparison of the bond stress-slip relationships for pull-out and push-in type is presented.

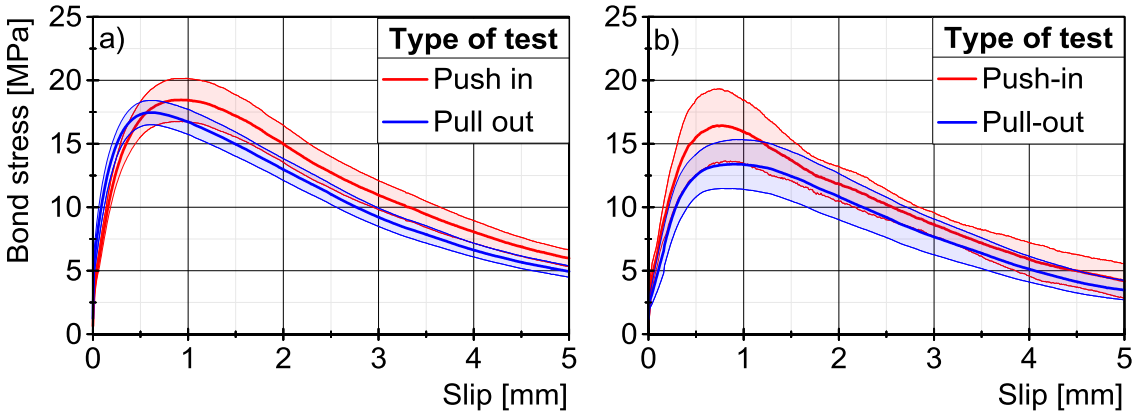

Figure 4-10: Comparison of bond stress-slip relationships for push-in and pull-out type of test for a) cylindrical and b) cubical specimens.

4.1.7 Concrete compressive and tensile strength influence

Although the concrete compressive strength alteration was not a primary goal of the work, it was impossible to avoid its variance due to the heterogeneity of concrete. Throughout the experimental work, the concrete compressive strength oscillated between 40 and 60 MPa with an average of 51.7 MPa. The coefficient of variation was 8%. In Figure 4-11a) the dependence of the average bond strength on the concrete compressive strength is depicted. Only quasi-static push-in and pull-out average maximal bond strengths measured on cylindrical specimens were taken into consideration. In addition, the theoretical bond strength dependency on the mean concrete compressive strength as calculated according to the Model Code 2010 Equation (78) for good bond conditions [16] is presented in Figure 4-11a).

$$\tau_{max} = 2.5 \cdot \sqrt{f_{cm}} \tag{78}$$

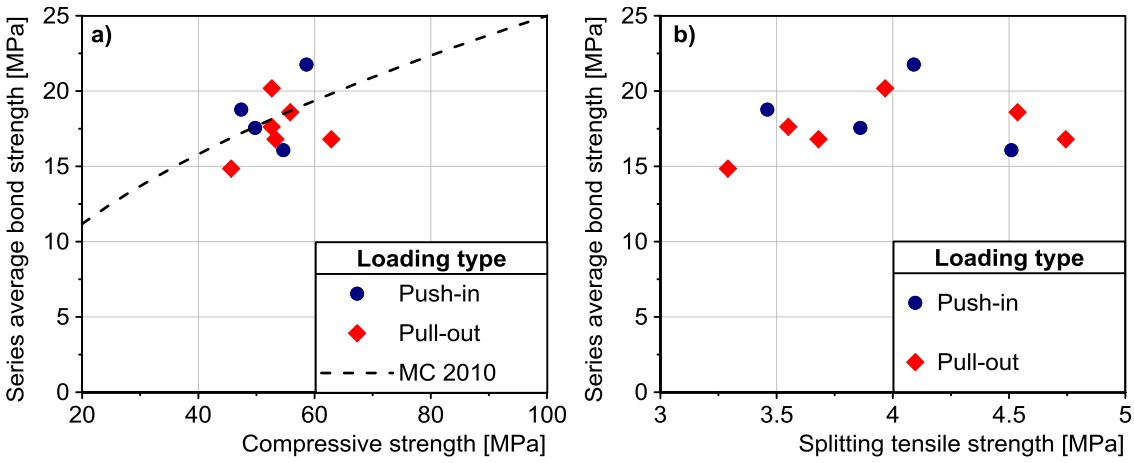

Figure 4-11: Dependency of the bond strength on the a) concrete compressive strength and b) concrete tensile splitting strength.

The relationship between tensile splitting strength the average bond strength is presented in Figure 4-11b). Based on the Figure 4-11a), it can be stated that Eq. (78) for good bond conditions gives a good estimate of the expected bond strength based on the concrete mean compressive strength. After reviewing the Figure 4-11b), it can be stated that in the investigated range of tensile splitting strength no clear dependency between the bond strength and the splitting tensile strength was observed. This is caused by the scattering of the data, and a wider range of splitting tensile strength values would be necessary. Theoretically, a linear relationship can be expected.

4.2 Medium rate and impact loading results

4.2.1 Approaches to loading rate definition

To be able to evaluate the bond stress-slip relationships under impact loading it is very important to define the actual loading rate. Normally in dynamic testing of materials, a strain rate is used to define a loading rate of the impact incident. This works very well for materials where the strains throughout the experiment can be calculated. However, in the case of pull-out or push-in experiments, it would be extremely complicated to measure the strain fields in the bond zone. In addition, several failure mechanisms take place during pull-out testing, such as concrete cantilevers failure and micro-cracking in the tension ring. The failure mechanisms are in detail described in Chapter 2.1.2. It is, therefore, important to define the loading rate in another way. There are three main approaches to doing this.

The first approach involves the definition based on the initial loading velocity, which coincides with the initial impactor velocity in the case of impact and with the machine crosshead velocity in the case of quasi-static experiments. In both cases, it can be non-ambiguously defined to a precise value. For this research, these velocities are presented in Table 3-7, and they are used to categorise the experimental data. However, in the case of bond testing, this velocity does not necessarily correspond to the rate at which the bond zone is loaded. For instance when the impact incident is soft the rising time of the force is longer, and the bond stress or slip rate is lower in comparison to the hard impact. However, the impactor velocities could be the same. On the other hand, it is possible to use the impactor velocities to compare one hard impact to another hard impact as it was done in this work.

The second approach is to define the loading rate based on the bond stress rate. This was done by many authors [103, 104, 110, 126] in the past. The problem with this approach is that the bond stress rate is not constant during the experiment. It varies widely over time, and the determination of a representative single bond stress rate value is at times difficult. The bond stress rate is calculated as:

$$\dot{\tau} = \frac{\dot{F}(t)}{\pi \cdot d_s \cdot l_b} \tag{79}$$

The bond stress rate in time calculated for a representative specimen according to Eq. (79) is shown in Figure 4-12 a). It can be seen that until the chemical adhesion is reached, the bond stress rate is relatively high. After that, the bond stress increases nearly linearly which is pronounced as a plateau in the bond stress rate-time graph. This constant bond stress rate is approximately 0.25 MPa/s. Before the bond stress reaches its maximum, the bond stress rate slowly decreases to zero. It is clear from Figure 4-12 a) that specifying the bond stress rate as one number can be misleading. In this work, the value of average bond stress rate until the maximal bond stress is reached was considered as representative. In this case, the average bond stress rate is $\dot{\tau} = 0.17\ \mathrm{MPa/s}$ and it is marked as dashed red line in Figure 4-12 a). Another way how to determine $\dot{\tau}$ is to calculate the increase of bond stress in time between specified levels of bond stress. The procedure is similar to the way how the modulus of elasticity is determined. The lower level of 2 MPa and upper level of 12 MPa was used in my previous paper [127]. This approach is shown in Figure 4-12 b) and the calculated bond stress rate is 0.26 MPa/s. In other cases, in which the bond stress time rise is not so linear, the difference between the average bond stress rate and the tangential bond stress rate is more significant.

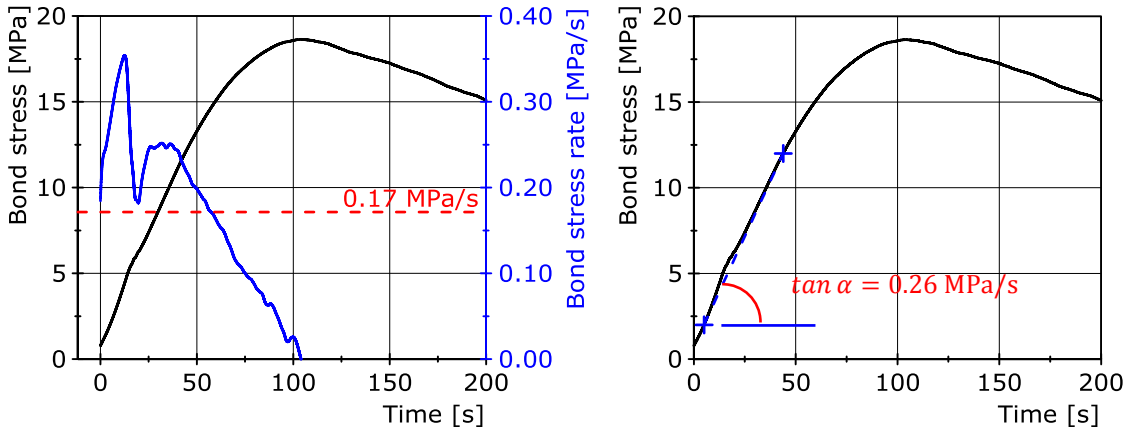

Figure 4-12: Ways to determine the bond stress rate for quasi-static loading: a) as the average bond stress rate until maximal bond stress is reached, b) from the time that is needed to increase the bond stress from 2 to 12 MPa.

The bond stress rate during medium rate loading can be derived analogically to the quasi-static loading, and it is presented in Figure 4-13 a) and b). The constant bond stress rate corresponding to the plateau in the bond stress rate time relationship is 375 MPa/s. The situation gets even more complicated for the case of impact loading because the bond stress rate changes all the time. There is no apparent section where the bond stress rate would be constant. The two possibilities how to determine the bond stress rate for impact loading are shown in Figure 4-14 a) and b). Even though the order of the result is the same the value differs significantly. One of the problems is to determine the exact position of the maximal bond stress as it is not apparent at first sight. A numerical model developed by Ms Panteki [128] was used to locate the maximum, and it is marked with a red cross in Figure 4-13 a).

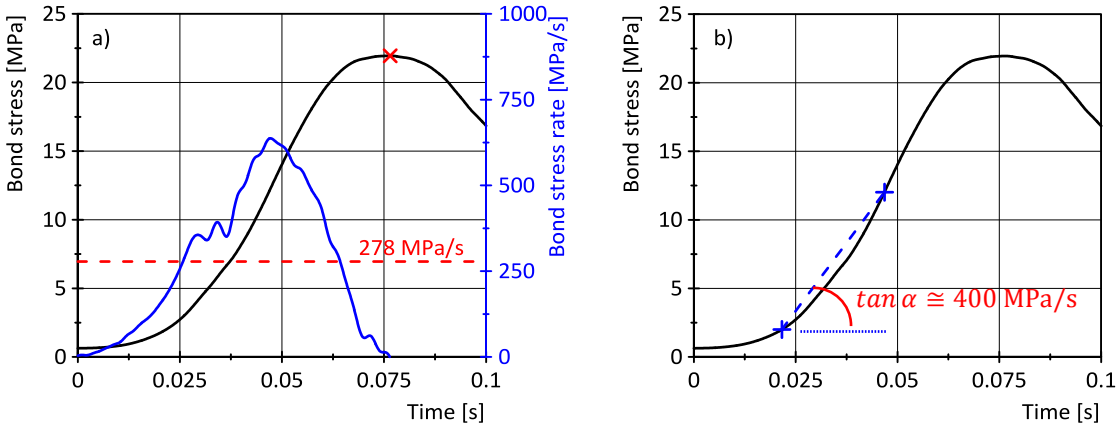

Figure 4-13: Ways to determine the bond stress rate for medium rate loading: a) as the average bond stress rate until maximum, b) between 2 and 12 MPa.

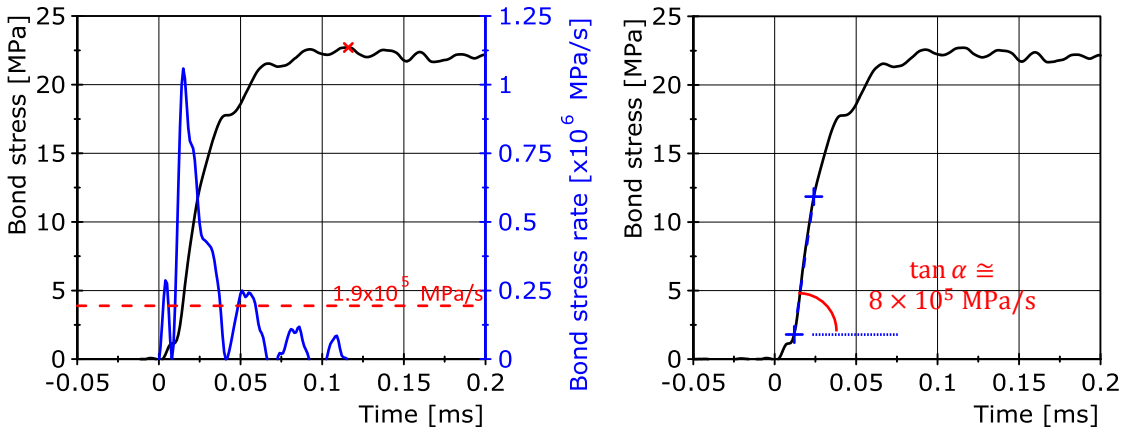

Figure 4-14: Ways to determine the bond stress rate for impact loading: a) until maximal bond stress, b) from the time between 2 and 12 MPa.

Another possibility how to determine the bond stress rate is to calculate it the from the time that is needed to reach a slip value of 0.01 mm and from the corresponding bond stress as shown in Figure 4-15 for the quasi-static loading case. The bond stress rate, in this case, is 0.34 MPa/s which is higher than the bond stress rates determined in Figure 4-12. The reason for that is that in this region the bond stress-slip relationship is relatively stiff due to the influence of chemical bond between the steel and concrete. This definition of $\dot{\tau}$ was used by for instance Vos and Reinhardt in their work [106, 126].

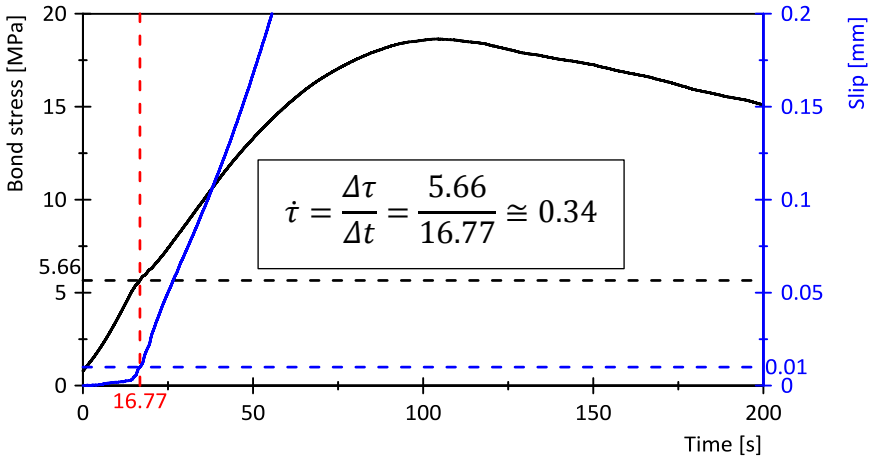

Figure 4-15: Bond stress corresponding to the time that is needed to reach the slip of 0.01 mm. Example on quasi-static loading.

The third approach is to define the loading rate by using the slip rate. Similarly to the bond stress rate, the slip rate is not constant during the loading process. The slip rate can be calculated by derivating the slip over time, and it has the units of velocity. For

quasi-static and medium rate loadings the slip rate gradually increases up to the predefined machine crosshead velocity, which is reached at the maximal bond strength, i.e. failure of the bond zone. In contrast to the bond stress rate that is highest until the chemical adhesion capacity is depleted, the slip rate is nearly zero in this region. In the case of impact loading, the slip rate is not only dependent on the impactor velocity but also on the position where the slip is measured. During the impact experiment, a long longitudinal wave is travelling through the specimen, and as already explained in Chapter 2.2.1 it comes to both displacement and velocity doubling at the free end of the rebar. This needs to be carefully taken into consideration when interpreting the data. For instance, in the SHB tests presented in this work, the slip of the rebar was measured 100 mm from the centre of the bond zone with an optical extensometer. In addition, the movement of the free end of the rebar was measured with a vibrometer. The corresponding results are presented in Figure 4-16 a). For a better comparability, the time lag of 0.13 ms between the two signals was eliminated according to the procedure described in Chapter 3.4.2. The movement of the bar is typical for impulse loading. The bar comes to the complete stop after the wave passes through the measuring point. This is caused by the different length of the impactor and the rebar. After some time this effect is smoothed out due to slight damping of the bar, and all particles have the same velocity. This is, however, much longer after the incident under investigation. It can also be seen, that the signal at the free end of the rebar (vibrometer data) is twice as steep as the signal measured near the bond zone (extensometer data). This is in accordance with the theory of wave propagation through long thin bars as presented e.g. in Graff [89] since doubling of the deflection takes place at the free end of the rebar. With these data it can be shown how important it is, in the case of dynamic loading, to choose the place of slip measurement correctly.

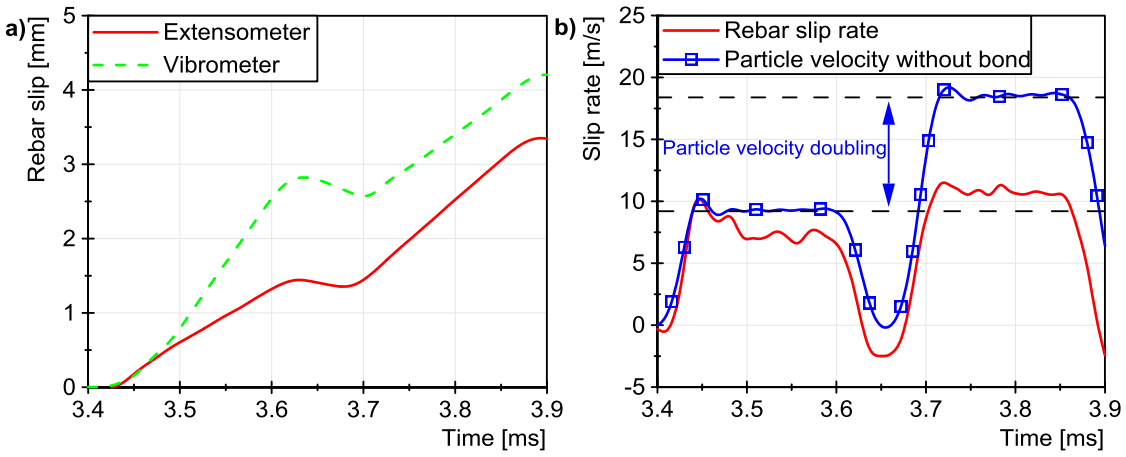

Figure 4-16: a) experimentally determined slip, b) slip rate and particle velocity.

The corresponding slip rate derived from Figure 4-16 a) is shown in Figure 4-16 b) together with a particle velocity as measured on a reinforcement bar without any bond. When comparing the red and blue curve, it can be seen that at the beginning of the loading process and before the bond is fully activated, the slip rate is 9.2 m/s. Afterwards, it is reduced to approximately 7.5 m/s. During the first load wave pass, the influence of the bond on the slip rate can be clearly seen. There is no friction to slow down the rebar movement in the case of no bond (blue line). It is equally interesting to see the doubling of the slip rate (from approx. 9.2 m/s to 18.4 m/s) after the wave is reflected from the free end (at ~ 3.7 ms) and is returning back. It is important to note, that the fact that the initial slip rate of 9.2 m/s more or less corresponds to the initial impactor velocity of 10 m/s is not a rule. For instance, in the case of softer impact, the slip rate will be lower than the impactor velocity and vice versa. The slip rate is also dependent on the experimental setup and the impedance differences between the incident and reinforcement. Therefore, it could be misleading to compare experimental results from two testing rigs based just on the impactor velocity. On the other hand, the impactor velocity is ideal to compare the results coming from one testing rig, as it can be easily and unambiguously measured.

Comparison between loading rates and the range of bond stress and slip rates is shown in Table 4-2 as determined by the three approaches presented in this chapter. For the good readability, the loading velocities will be used for the presentation of the results. For comparison with other research papers and reports the corresponding slip rate ranges should be looked up in Table 4-2. **Based on reasons provided in this chapter, using slip rate instead of bond stress rate to characterise dynamic bond experiments is highly recommended.** Special considerations need to be made about the place of the slip measurement, mainly because of the velocity and displacement doubling at the free end of the bar in case of impact experimental work.

Table 4-2: Categorisation and comparison of different loading rates.

Loading type	Loading velocity [mm/s]	Bond stress rate [MPa/s]	Slip rate [mm/s]
Quasi-static	0.01	0.2-0.4	0.005-0.01
Medium rate	50	300-400	10-30
Impact - drop-tower	8.3×10^3	$2\text{-}8\times10^5$	$5\text{-}8\times10^3$
Impact - SHB	10×10^3	$3\text{-}9\times10^5$	$7\text{-}10\times10^3$

4.2.2 Discussion of the drop-tower results

This chapter will provide results and discussion of the specific aspects of the drop-tower impact testing. The experimental configuration is described in Chapter 3.6.1. Both pull-out and push-in tests were performed in the drop-tower. For the clarity, they will be presented separately because for each type of test the stress wave progresses differently through the specimen. The progress of the wave is dependent on the experimental setup. Stress wave reflections along the load path cannot be avoided because impedance differences exist between the impactor and the reinforcement bar.

4.2.2.1 Push-in results

As already described in Chapter 3.6.1 the primary method for determining the bond stress between the rebar and the concrete was to measure strain histories on the rebar after an impact incident. The strains were measured before and after the bond zone. The development of average strains in time for a representative series of the cylindrical specimen is shown in Figure 4-17. The strain signals are an average of two strain gauges that were attached against each other on the longitudinal ribs of the reinforcing bar, as shown in Figure 3-37. The time lag between the signals was corrected to the centre of the bond zone as described in Chapter 3.4.2.

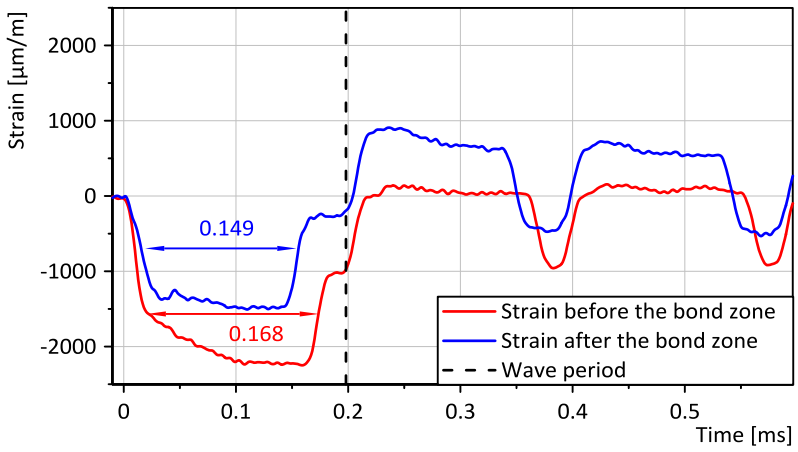

Figure 4-17: Typical strain history of a push-in test.

The evaluation of the measured curves as presented in Figure 4-17 needs to be done with respect to the fundamentals of wave propagation theory as described in Chapter 2.2.1. The loading duration Eq. (35), the velocity of elastic wave propagation Eq. (20) as well as the initial stress Eq. (39) and strain for the impactor can be calculated. The

results for the used impactor and for the impact velocity of 8.3 m/s are presented in Table 4-3.

Table 4-3: The characteristics of a compressive pulse induced by 500 mm long impactor.

T [ms]	c [m/s]	σ_0 [MPa]	ε_0 $[\mu m/m]$
0.198	5048	-164.45	-822

The results presented in Table 4-3 are valid only for the case when the impactor and reinforcement bar have the same impedance. The theoretical background under impedance calculation is presented in Chapter 2.2.1.2. While there is no difference in the material, the difference in the cross-sectional area between impactor and rebar is considerable. That means that the initial momentum p of the impactor calculated according to Eq. (80) cannot be transferred completely into the reinforcement bar during the first reflection cycle in the impactor.

$$p = m_{imp} v_0 \tag{80}$$

That means that the bar is loaded by several impulses, each of which is coming with a stress of lower intensity. At the interface between impactor and rebar an equilibrium of forces must exist which can be expressed as:

$$A_1(\sigma_i + \sigma_r) = A_2 \sigma_t \tag{81}$$

By utilising Eq. (28) and (29) the transmitted and reflected pulses can be calculated as:

$$\sigma_{t1} = \frac{2\frac{A_1}{A_2} I_2}{I_1 + I_2} \cdot \frac{1}{2} \rho_1 c_1 v_0 \tag{82}$$

and

$$\sigma_{r1} = \frac{I_2 - I_1}{I_1 + I_2} \cdot \frac{1}{2} \rho_1 c_1 v_0 \tag{83}$$

With the use of $I_1 = \rho_1 c_1 A_1$ the equations above can be simplified to:

$$\sigma_{t1} = \frac{I_1 I_2}{I_1 + I_2} \cdot \frac{1}{A_2} \cdot v_0 \qquad \sigma_{r1} = \frac{I_2 - I_1}{I_1 + I_2} \cdot \frac{1}{2A_1} v_0 \tag{84}$$

The reflected pulse σ_{r1} is travelling in the impactor where it gets reflected at its free end and travels back as the second impulse. This second impulse then becomes a new incoming pulse in the bar and it can be written:

$$\sigma_{i2} = \sigma_{r1} \tag{85}$$

For the second and n-th loading impulse the stress intensity of the pulse that is transmitted into the bar can be calculated analytically:

$$\sigma_{tn} = \frac{I_1 I_2}{I_1 + I_2} \cdot \left(\frac{I_2 - I_1}{I_1 + I_2}\right)^{n-1} \cdot \frac{1}{A_2} \cdot v_0 \tag{86}$$

where n stands for the n-th reflection cycle in the impactor. The sketch of a semi-infinite reinforcement bar with all other dimensions as in the push-in drop-tower test is shown in Figure 4-18.

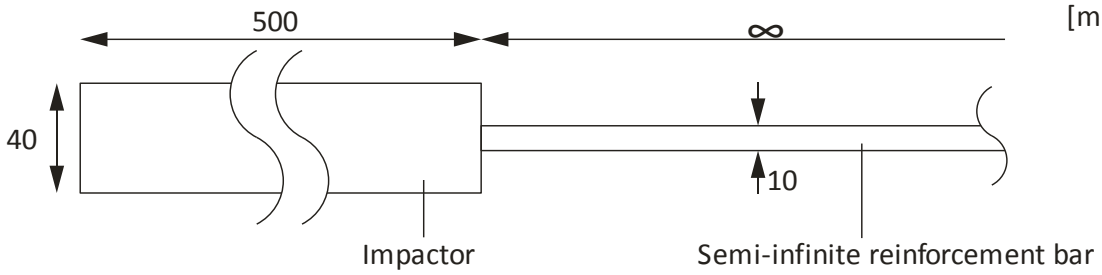

A_1 = 1257 mm^2 A_2 = 78.54 mm^2
v_0 = 8.3 m/s v_2 = 0 m/s
I_1 = 49 800 kg/s I_2 = 3 112 kg/s

Figure 4-18: Impact of an impactor on semi-infinite reinforcement bar.

Using the Hook's law, the stresses can be calculated into strains:

$$\varepsilon = \frac{\sigma_{tn}}{E_s} \tag{87}$$

The analytically calculated strains in semi-infinite reinforcement bar are shown for the first ten reflections in Figure 4-19. Eq. (86) and (87) were used. The length of the compressive pulse was 0.198 ms as calculated in Table 4-3.

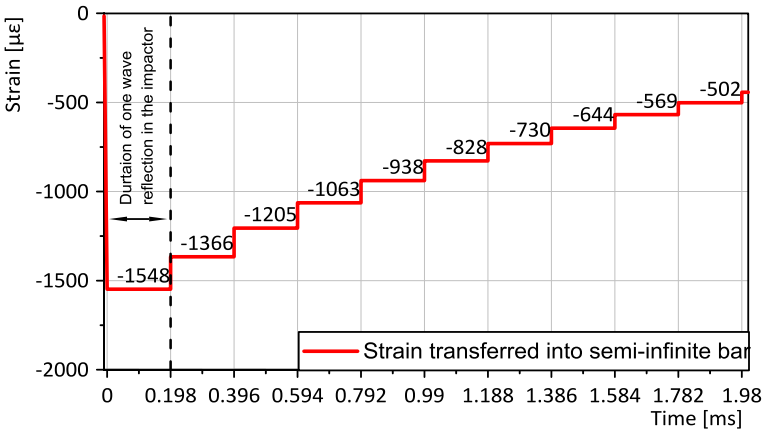

Figure 4-19: Analytically calculated strain transferred into semi-infinite reinforcement bar.

The analytical results presented in Figure 4-19 show that if the rebar were semi-infinite, the loading would have a stair characteristics. That means that the rebar would be loaded by several compressive pulses, which is a direct result of the different impedance between the impactor and the bar. The pulse loading would continue until the whole momentum of the impactor is transferred. However, in reality, the reinforcement bar is not semi-infinite. That means that the first compressive pulse of -1548 µm/m travels through the rebar, it is reflected from its free end and travels back in the form of a tensile pulse. This creates a very complicated situation in the reinforcement bar because during this time the rebar is loaded by the second compressive pulse of -1366 µm/m which comes from the impactor. For this reason, it was decided, that the bond stress-slip relationships will be studied only during the first compressive pulse, which corresponds to 0.198 ms after the first contact. During this time the bar moves for the distance of more than 1 mm as seen in Figure 4-20.

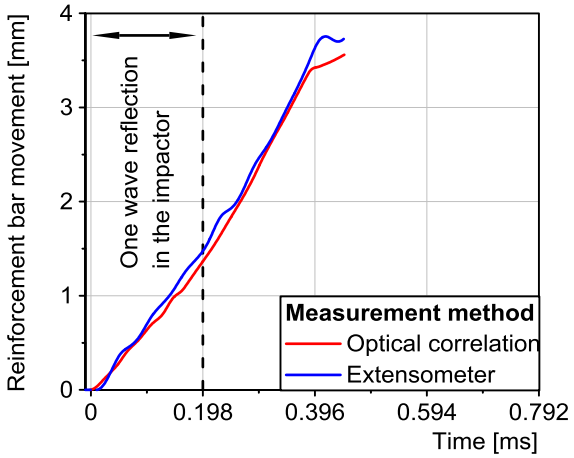

Figure 4-20: Displacement of the bar during the first compressive pulse.

It is assumed that failure is achieved during the bar movement of more than 1 mm and the bond is considered as failed. The comparison of different measuring methods is also shown in Figure 4-20. These methods are digital image correlation (DIC) of high-speed camera footage and the displacement measured by an extensometer. It can be seen an excellent correspondence of the two methods. The signal from the DIC appears smoother because the resolution of the camera under high sampling rates is not very good. It is also important to note that movement of the rebar and not the actual slip are shown in Figure 4-20. For the slip calculation, the rebar displacement is corrected by the sample displacement as described in more detail in Chapter 3.6.3.

Measured strain signals in time of a representative example of a push-in test are shown in Figure 4-22. In addition, the analytically calculated compressive pulse is depicted in Figure 4-22. Only one compressive pulse of a magnitude of -1548 µm/m is assumed, and only the signal of a strain gauge after the bond zone is modelled as it is not so heavily influenced by the wave reflection from the bond zone. In the analytical model, it is assumed that during the reflection from the free end 20% of the pulse dissipates. Because the wave passes through the bond zone for the second time (at a 0.2 ms mark) a loss of 30% is assumed due to friction in the bond zone. It is clear that such analytical model is not very accurate, but it gives a nice perception of the wave propagation and interferences. From Figure 4-22 it can also be seen, that the strains before the bond zone are higher than the theoretical signal. This is caused by the partial reflection of the incoming compressive impact pulse at the bond zone area. The reflected pulse is also compressive but travels from the bond zone towards the impactor. At the strain gauge location, this signal is superimposed on the original incoming pulse travelling in the direction from the impactor. Because the distance between the impactor and the bond zone is very small (100 mm) the pulse that is reflected from the bond zone reflects again from the interface impactor-rebar and influences again the strain gauge readings. This disadvantage of the drop-tower testing was then eliminated in the split Hopkinson bar by introducing the incident bar two (IB2) into the design, compare Figure 3-27. The push-in specimen sketch with the location of the strain gauges is shown in Figure 4-21.

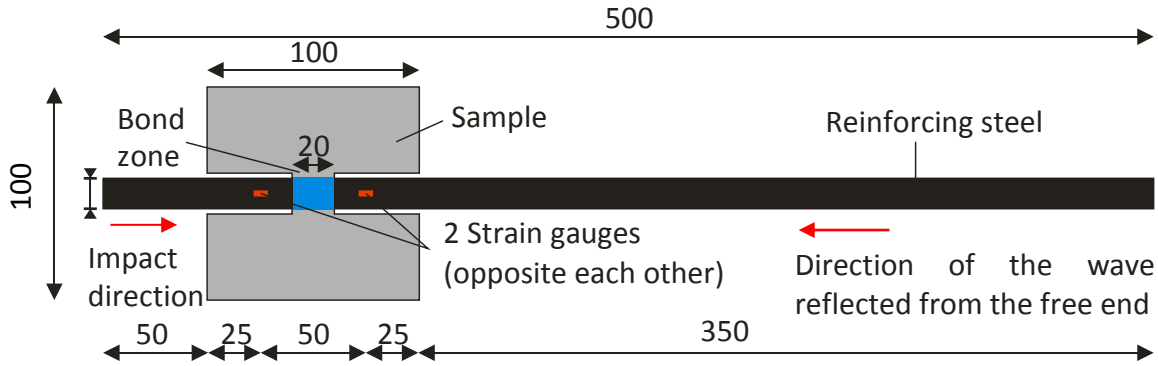

Figure 4-21: Location of strain gauges in the specimen for drop-tower push-in testing.

The strain gauge which is before the bond zone is at the distance of 425 mm from the free end and the strain gauge which is located after the bond zone is only 375 mm from the free end. That means that the reflected wave will reach first the strain gauge located after the bond zone after 0.149 ms and second the strain gauge located before the bond zone at a time of 168 ms after the impact. This can be seen as small plateaus in Figure 4-22. If there weren't any bond, the strain at these plateaus would be zero.

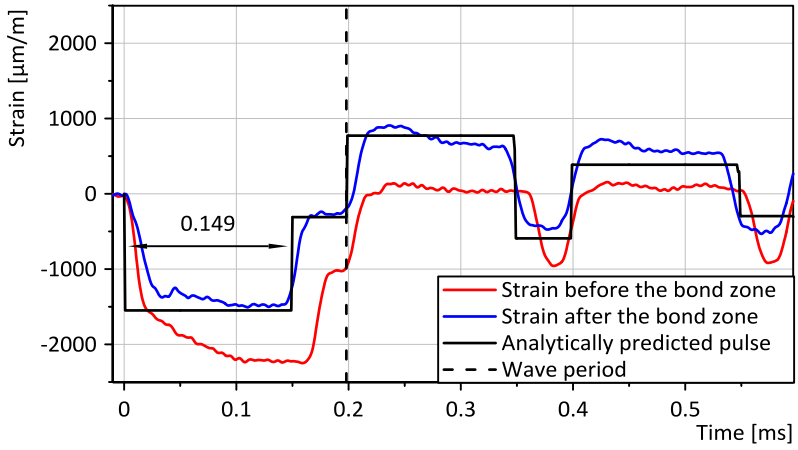

Figure 4-22: Strain history and analytical model of wave interference in the push-in test.

By subtracting the strain gauge signals and utilising Equation (75), it is possible to get the bond stress in time. It is important to note, that because the signals are influenced by the reflected waves, it comes to doubling of the bond stress. This is well documented in Figure 4-23 where the red and blue arrows from Figure 4-22 nicely illustrate the start and end of the stress doubling. **This doubling is caused by measurement method and does not correspond to the stress state in the bond zone.** The doubling is repeated at intervals which correspond to the rebar length, i.e. 0.198 ms

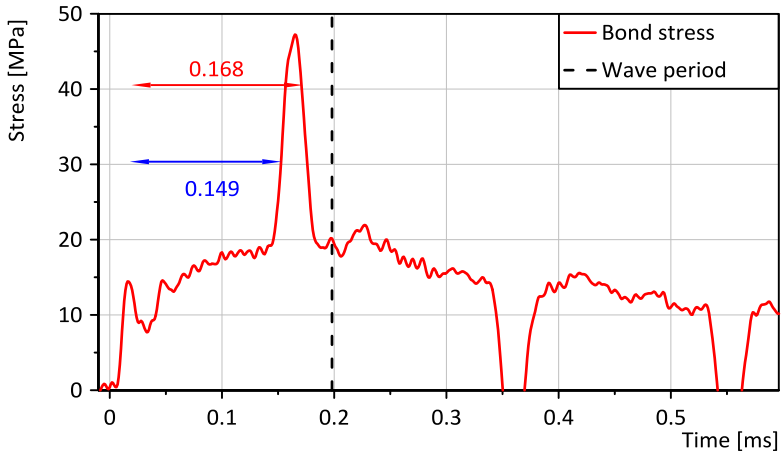

Figure 4-23: Bond stress development in time.

After having data for the movement of the rebar, movement of the sample and bond stress from the strain gauges, it is possible to construct bond stress-slip relationships. The average results from the quasi-static phase of the research were used as a reference for evaluating the effects of loading rate. The quasi-static bond stress-slip relationship until the slip of 5 mm is shown in Figure 4-24a). It can be seen that the maximal bond stress is reached at a slip of 0.9 mm. For this reason in Figure 4-24b) the bond stress-slip relationship is shown only until failure, i.e. 0.9 mm.

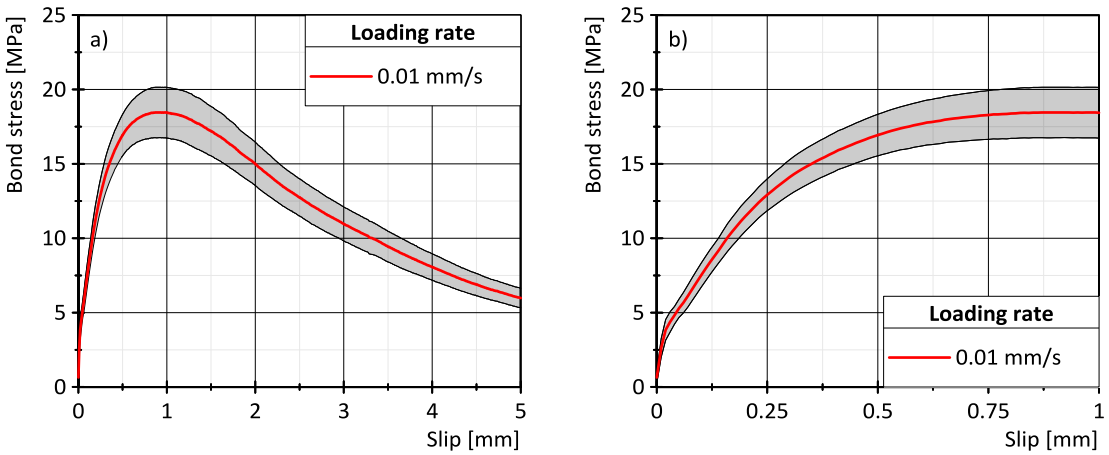

Figure 4-24: Results of quasi-static push-in tests: a) complete bond stress-slip relationship, b) stress-slip relationship until the peak bond stress.

In a similar way the bond stress-slip relationships can be shown for medium rate loading -Figure 4-25a) and for drop-tower impact loading-Figure 4-25b). The bond stress-slip curves presented in Figure 4-24 and Figure 4-25 represent average bond stresses from 16 and 12 specimens for quasi-static and dynamic tests respectively. The averages were

evaluated at a defined slip increment of 0.01 mm according to the procedure described in Chapter 3.4.1. The shaded areas represent the confidence range for the calculated average between 5 % and 95 %. The push-in failure mode was in all cases caused by shearing of the concrete cantilevers between the ribs. During the experimental work splitting of the specimens never occurred. After the push-in tests were finished the specimens were cut into two halves, and the bond zone was examined. The area between the ribs was completely smooth, and no cracking pattern in the concrete body could be macroscopically observed. A comparison of a cut specimen loaded under quasi-static conditions to a specimen loaded under impact is shown in Figure 4-26. The specimens are from the same series to provide a direct comparison. It was found that there was no visual difference in the state of the bond zone based on the loading rate.

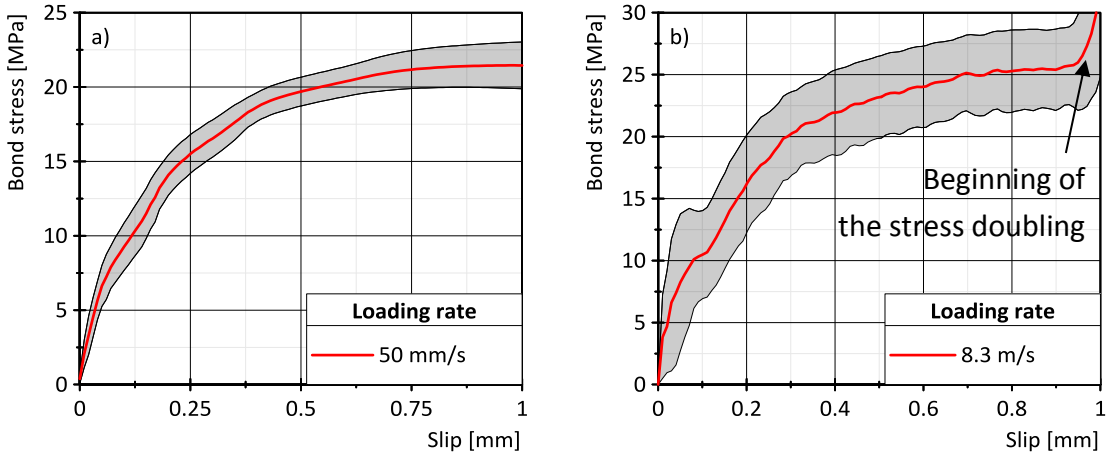

Figure 4-25: Bond stress-slip relationships for a) medium and b) impact loading rates.

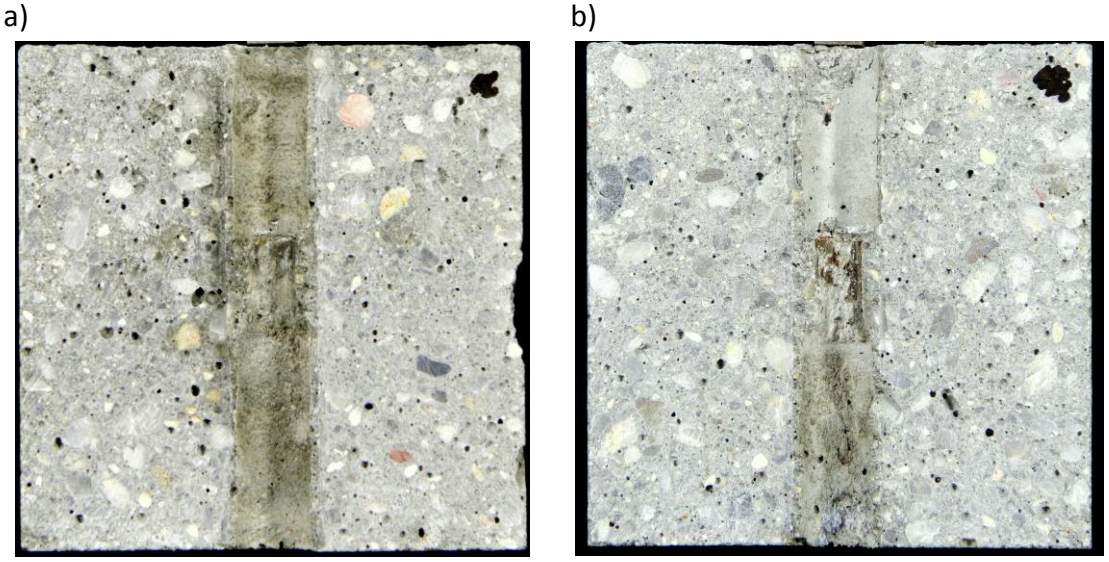

Figure 4-26: Cross-section of a specimen tested under a) quasi-static and b) impact loading rates.

4.2.2.2 Pull-out results

The experimental setup of the pull-out tests is presented in Chapter 3.6.1. The characteristics of the loading pulse are presented in Table 4-3. The main difference in comparison to the push-in type of loading is, that the loading pulse is not compressive but tensile. In addition, the impactor was hollow, but the parameters were chosen in a way that the cross-section, as well as the mass of the impactor, are comparable to the push-in loading. The same Equations (80) to (87) are valid for pull-out loading. In the case of pull-out loading two changes in diameter exist. Firstly it is the change from impactor to the 5 m long transfer bar. Secondly, it is the change between the diameter of the transfer bar and the reinforcement bar. The second change in the diameter is, however, gradual which causes many reflections of the wave in the joint which is shown in Figure 3-22. The cross-sectional areas, values of impedance and strain of these parts are given in Table 4-4. Even though the drop-tower has a height of 6 m the available drop height for pull-out testing was due to the length of the impactor and the hoist mechanism only 3.5 m. The strains presented in Table 4-4 are theoretical values for the first tensile wave that is induced by an impactor falling from the height of 3.5 m. The impactor velocity was reduced due to friction by 6% to 7.8 m/s. The tensile wave travels from the impactor through the transfer bar to the reinforcement bar. This wave is then partially reflected from the bond zone, and the rest is reflected from the free end of the reinforcement bar. After reviewing the data in Table 4-4, it can be seen that the strain in the reinforcement bar is 1982 µm/m.

Table 4-4: Properties of parts used for impulse transfer between the impactor and the concrete specimen. Impactor velocity $v_0 = 7.8\ m/s$.

	Impactor	**Transfer bar**	**Reinforcement bar**
Area [mm^2]	1.271×10^3	314.2	78.5
Mass [kg]	4.99	12.3	0.3
Impedance [kg/s]	51.6×10^3	12.8×10^3	3.1×10^3
Transferred strain [µm/m]	N/A	1239	1982

In the case of pull-out testing, the strains were additionally measured in the middle of the transfer bar. It is, therefore, possible to compare the measured values with the theoretical strains calculated according to Equations (86) and (87). This is shown in Figure 4-27 where the stair characteristics of the loading pulse caused by the impedance difference between the impactor and the transfer bar can be seen. When it comes to

the maximal strain in the transfer bar a very good agreement can be seen between the analytically expected value and the actual strain in the transfer bar. It can also be seen that the measured real loading pulse is not ideally rectangular. The distortion of the loading wave happens on the interface between the stopper and the transfer bar. Also with time the signal becomes smoother and loses its “stair characteristics”.

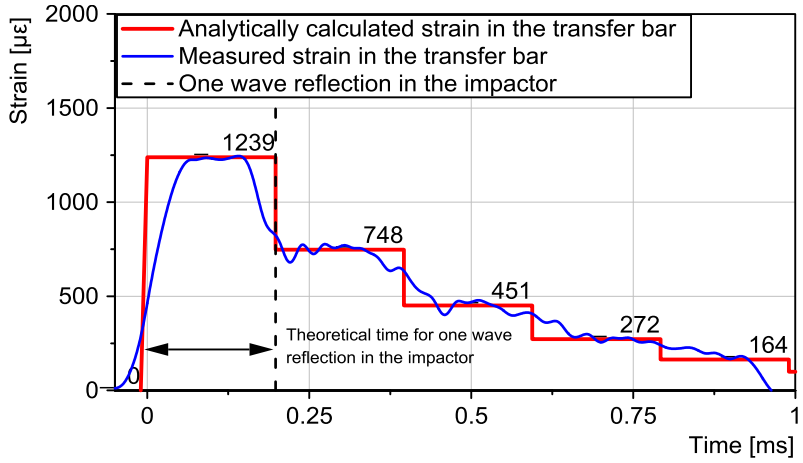

Figure 4-27: Comparison of the analytically calculated and measured loading pulse characteristics for impact velocity of 7.8 m/s.

The bond stress-slip evaluation is very similar to push-in tests. Strain histories before and after the bond zone are measured. Afterwards, the time lag between the strain measurements is corrected to the middle of the bond zone as described in Chapter 3.4.2. By utilising Equation (75), bond stress is calculated. The main difference is in the slip measurement. In pull-out testing, the experimental setup allows measuring the movement of the reinforcement bar on the unloaded section, approximately 50 mm above the concrete surface. The movement of concrete is measured on its surface. The slip is then calculated by subtracting the concrete displacement from the rebar movement. Such slip evaluation procedure exactly corresponds to the quasi-static standart pull-out test. An optical extensometer is used for slip measurement. High-speed video footage is used for visual control, and the DIC of selected points is used as an alternative method to the optical extensometer. Similarly to push-in tests, a very good agreement between these two methods was observed. The time lag of the slip signal is corrected to the middle of the bond zone. The results of average bond stress-slip relationships for the quasi-static type of loading are presented in Figure 4-28. These can be compared with the results for pull-out testing as measured under medium and impact rates. This is presented in Figure 4-29.

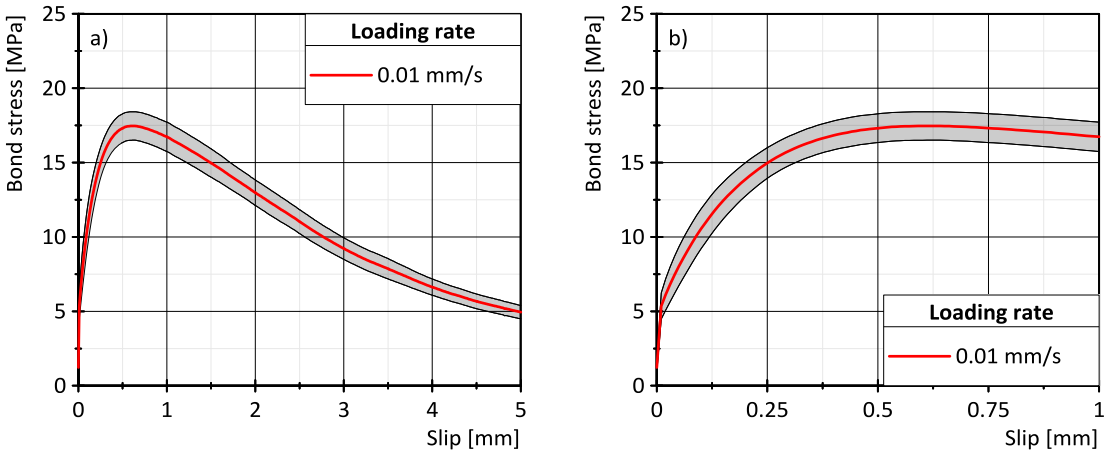

Figure 4-28: Results of quasi-static pull-out tests: a) complete bond stress-slip relationship, b) stress-slip relationship until the peak bond stress.

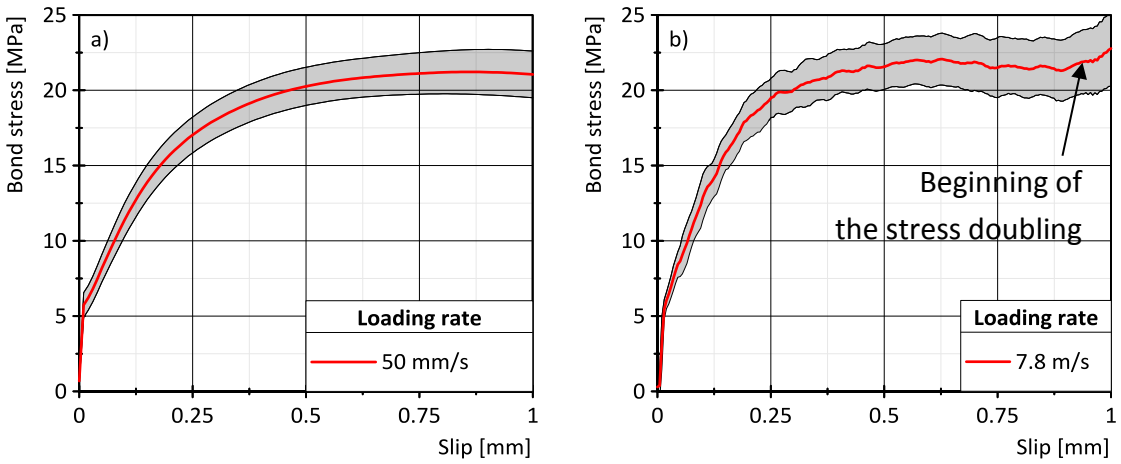

Figure 4-29: Pull-out bond stress-slip relationships for a) medium and b) impact loading rates.

4.2.3 Discussion of the split Hopkinson bar results

The experimental setup of the split Hopkinson bar (SHB) is presented in Chapter 3.6.2. Due to the fact that SHB is in pressure configuration, **only push-in tests were performed.** By introducing the incident bar 2 (IB2) as shown in Figure 3-27 it was possible to eliminate the wave reflection on the impactor reinforcement bar interface because there is no impedance difference between the rebar and the IB2. The analysis of the measured signals was analogous to the procedures described in Chapter 4.2.2:

1. Strains before and after the bond zone were measured.
2. The time lag between the signals was corrected to the centre of the bond zone.
3. Movement of the reinforcement bar and sample were measured.

4. The time lag was corrected for each signal based on its distance from the centre of the bond zone.
5. The relative slip was calculated.
6. Bond stress-slip relationships were constructed.

The main difference was that the experiment was performed horizontally. Also, only one compressive wave loaded the specimen because the whole compressive impulse from the impactor was transferred to IB1. A part of this impulse was reflected from the interface between IB1 and IB2 due to the impedance difference. However, this reflected pulse had to travel all the way back in IB1, reflect from the free end and then travel back. The compressive wavefront travel distance was therefore 6 m until the reflected wave reached the IB1-IB2 interface. This happened much later after the bond zone failure and therefore did not influence the result in any way. The properties of each part together with the analytically calculated strains caused by the compressive pulse are shown in Table 4-5.

Table 4-5: Properties of parts used for impulse transfer between the impactor and the concrete specimen. Impactor velocity $v_0 = 10\ m/s$.

	Impactor	**IB1**	**IB2**	**RB**
Area [mm^2]	1.963×10^3	1.963×10^3	78.5	78.5
Mass [kg]	7.71	46.24	0.62	0.43
Impedance [kg/s]	77.8×10^3	77.8×10^3	3.11×10^3	3.11×10^3
Transferred strain [µm/m]	N/A	-990.6	-1900	-1900

Strains, as measured during an experiment, are presented in Figure 4-30 and compared with the analytically calculated limits presented in Table 4-5. For good readability, the time lag between the signals was not corrected. The trapezoidal shape of the signals was observed. The measured strain in IB1 matched very well the predicted values. Measured strains in IB2 are slightly higher in comparison with the predicted value. This can be explained by deviation in the bar diameter. It is also interesting to see that the signal in the reinforcement bar (RB) was higher in comparison to the theoretical value. This increase in the negative strain was caused by the part of the compressive wave which is reflected from the bond zone and is superimposed on the original signal and will be discussed further on.

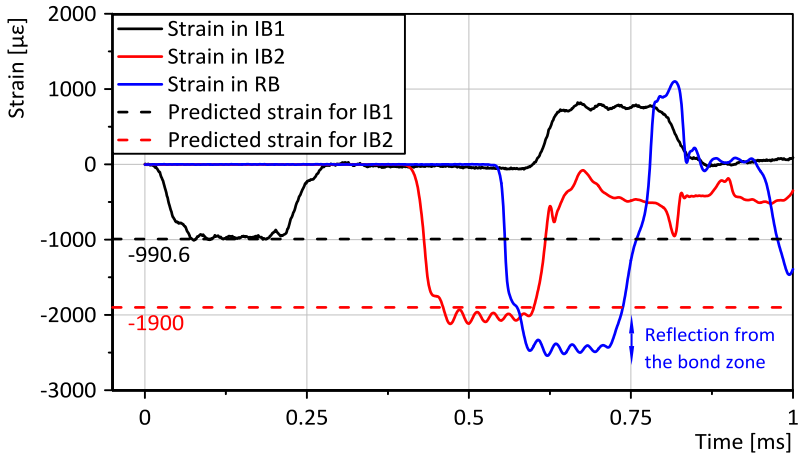

Figure 4-30: Strain signal as measured in incident bar 1(IB1), incident bar 2 (IB2) and in the reinforcement bar (RB).

Strain signals before and after the bond zone are presented in Figure 4-31 for a representative push-in test in the split Hopkinson bar. The time lag between the two signals was corrected to the middle of the bond zone. The correction of the time lag for the first compressive wave has the disadvantage that in the case of the returning tensile wave the time lag is doubled. This area is marked in the Figure 4-31. The first half of the time lag is caused by shifting the blue curve in time by the time that is needed for the signal to travel from the first gauge to the second one. The second half of the time lag is caused by the time that the signal needs to travel from the second gauge to the first because the direction of the reflected wave is from the end to the front. This signal doubling is, therefore, a result of evaluation and measurement method, and it does not correspond to the real contact bond stress. This theory was proven by the numerical model which was developed by Panteki et al.[124]. When comparing Figure 4-31 to the strain histories as measured during drop-tower experiment (see Figure 4-22) a significant difference after the first wave pass can be noticed. This difference is caused by the fact that in the case of drop-tower experiment the loading wave has a stair characteristics as shown in Figure 4-19 and that the reinforcement bar is only 500 mm long. That means that the wave which is reflected from the rebar free end reaches the strain gauge after the bond zone earlier.

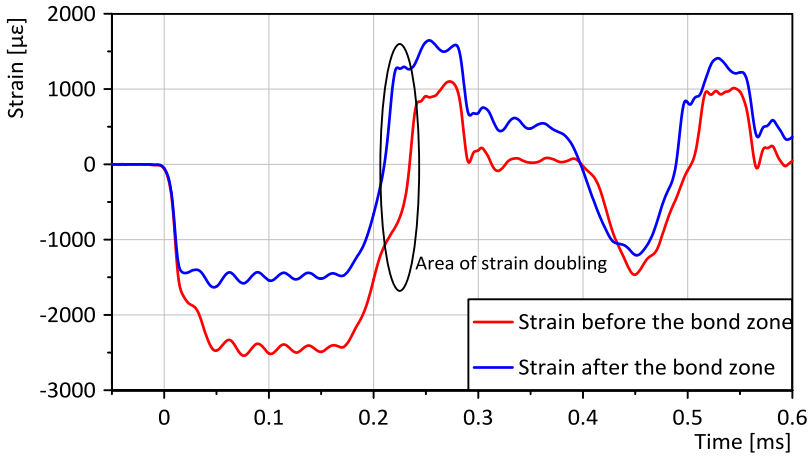

Figure 4-31: Strain signals for representative push-in SHB test before and after the bond zone.

By using Equation (75), it is possible to calculate the bond stress from the difference of the strain measured before and after the bond zone. The resulting bond stress is shown in Figure 4-32. In addition, the numerically calculated bond stress and experimentally measured slip development in time are shown in Figure 4-32. During the time when it comes to the apparent stress doubling (0.2-0.22 ms) caused by the wave interference, the slip increase is zero. In contrast to the experimental measurements, the numerical simulation of the bond contact force shows a decrease in the bond stress during the zero slip increase. During this time it comes to the bond stress relaxation. Afterwards, the bond stress slightly increases with a rise of the slip curve. It is reasonable to assume that the numerical model during this time corresponds to the real bond stress behaviour. For this reason, when constructing the bond stress-slip relationship, it is possible to delete the area where it comes to the apparent doubling in the signal.

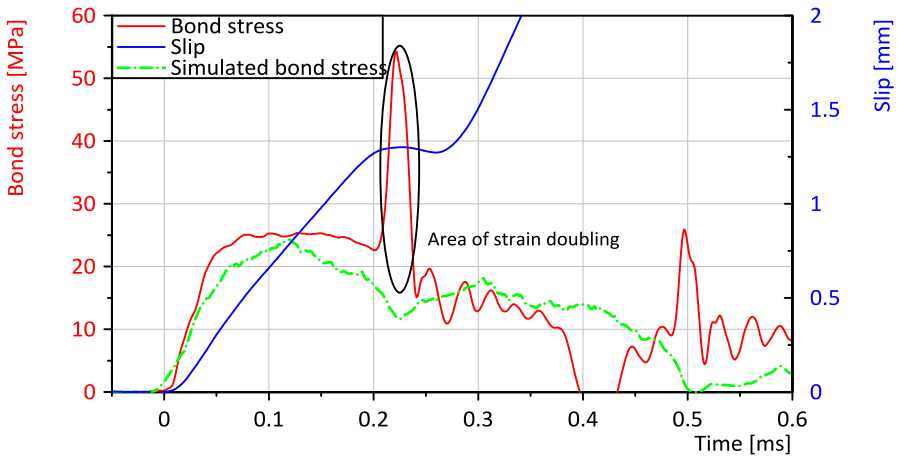

Figure 4-32: Bond stress and slip in time.

The resulting bond stress-slip relationship for the investigated specimen is shown in Figure 4-33. The area where the strain doubling occurs is marked in the figure. It can be seen that the SHB method provides better results also for slip values larger than 0.9 mm, which was the limit for the drop-tower method.

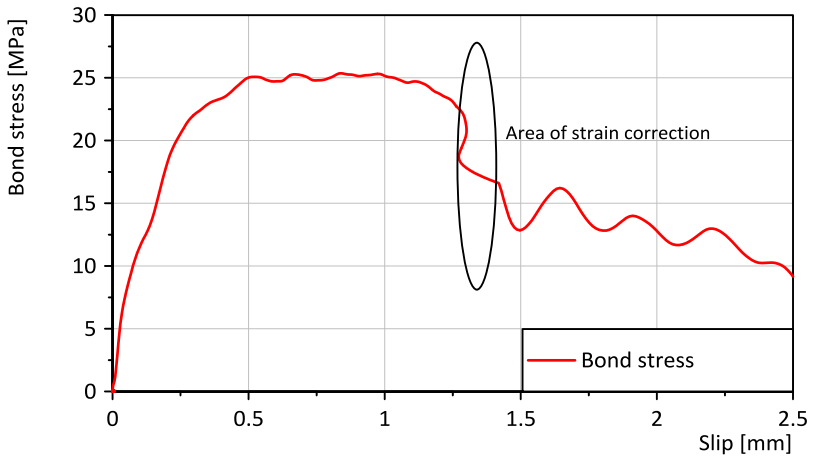

Figure 4-33: Bond stress-slip relationship for representative push-in SHB test.

All other specimens that were tested in the split Hopkinson bar were evaluated according to the method described above. The comparison between the quasi-static average push-in tests and the split Hopkinson bar results is presented in Figure 4-34. Average curves with 5% and 95% confidence intervals are shown. Due to the improved SHB configuration, the bond stress-slip relationships until the slip value of 2 mm can be depicted. This is a significant advantage in comparison to the drop-tower test where only bond stress values until the slip of 0.9 mm could be reliably measured.

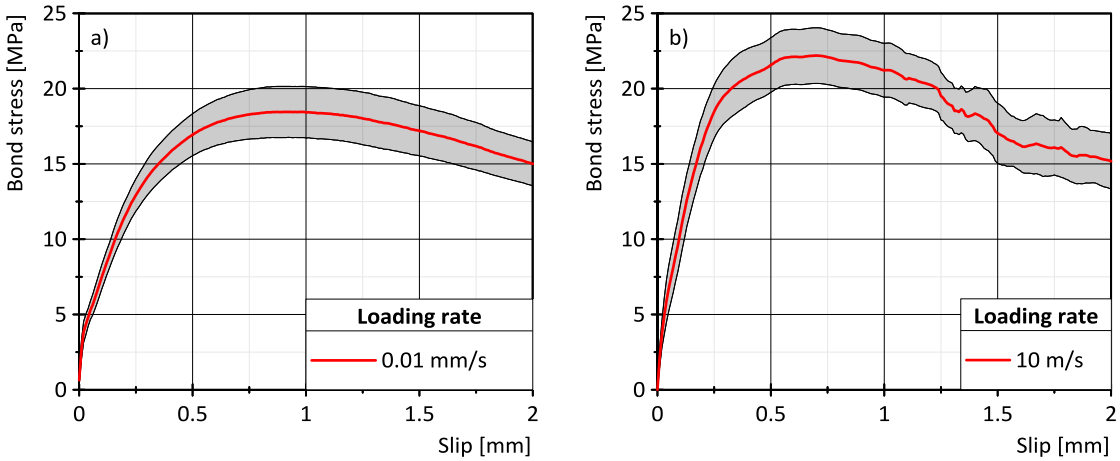

Figure 4-34: Bond stress-slip relationships for a) quasi-static and b) SHB loading.

4.3 Summary on the loading rate influence

In this chapter quasi-static bond stress-slip relationships are compared. This is done separately for push-in and pull-out type of specimen. Only results for cylindrical specimens are shown. For every series of specimens for bond strength determination concrete compressive and tensile splitting strength were measured. The results are presented in Table A-2 and Table A-3 for push-in and pull-out specimens respectively. The comparison to the quasi-static bond stress-slip relationship as measured on cubes is presented in Figure 4-4. When comparing the results of this work to the literature, where cubical specimens are predominantly used, it needs to be taken into consideration that the cubical specimens have lower bond stress because the bond conditions are not as good as in the case of cylindrical specimens. This is connected with the concreting direction and position of the rebar during concreting.

The average bond stress-slip relationships for pull-out loading type are presented in Figure 4-35. The average curves were constructed from bond stress-slip relationships of individual specimens that are presented in Appendix B, Figures B-5 to B-7. The bond stress at slip of 0.1 mm, the maximal bond stress as well as the slip at maximal bond stress are presented in Tables B-5 to B-7. It is important to note, that average maximal bond stress as presented in Tables B-5 to B-7 is calculated from individual specimens. On the other hand, the maximal bond stress calculated from the average curves is slightly different (Table 4-6). The reason for that is that the maximal bond stress is reached at different values of slip. For more details about averaging the results, Chapter 3.4.3 can be referred to.

From Figure 4-35, it can be seen that the maximal bond stress increases with increasing loading rate. The increase is, however, not very significant. It also appears that the most significant bond stress increase happens between quasi-static and medium loading rates. This is in agreement with Yan and Chen [33] who observed on similar specimens a DIF of 1.28 when the loading rates were increased from 0.004 mm/s to 1.65 mm/s. It is also important to note that results presented in Figure 4-35 need to be interpreted carefully with respect to the usual scattering for pull-out tests. The comparison of maximal bond stress τ_{max}, the value of slip at maximal bond stress s_{max} and the dynamic increase factor (DIF) for the average results of pull-out and push-in type of loading are presented in Table 4-6.

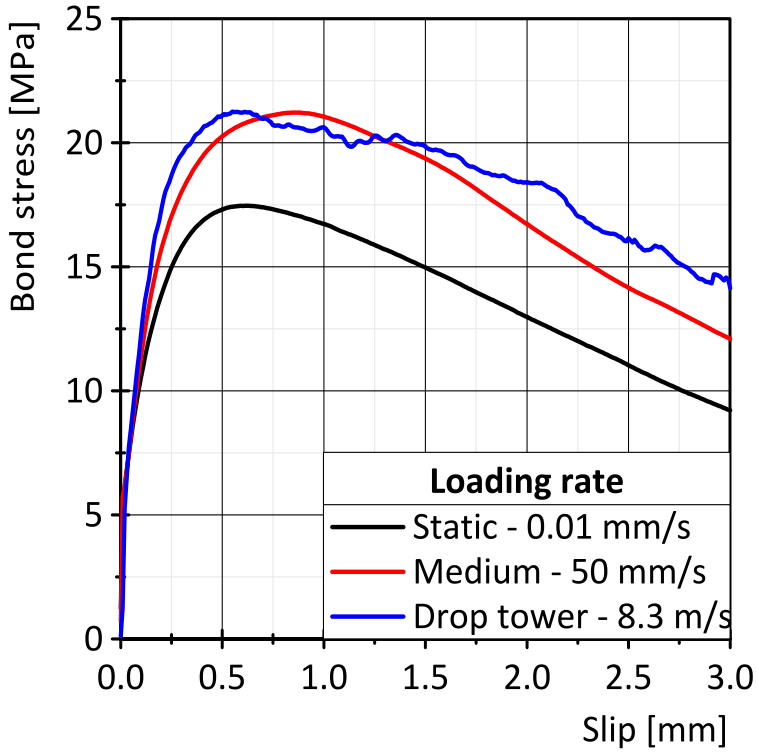

Figure 4-35: Loading rate effect on pull-out average results.

Table 4-6: Maximal bond stress, slip and DIF.

Loading rate [mm/s]	Type of loading	$s_{max}\,[mm]$	$\tau_{max}[mm]$	DIF
0.01	pull-out	0.59	17.46	1
	push-in	0.80	19.14	1
50	pull-out	0.86	21.22	1.22
	push-in	0.84	21.58	1.13
8.3	pull-out	0.55	21.26	1.22
	push-in	0.86	23.19	1.21
10	pull-out	N/A	N/A	N/A
	push-in	0.67	23.92	1.25

The average bond stress-slip relationships for the push-in type of loading are presented in Figure 4-36. The average curves were constructed from bond stress-slip relationships of individual specimens that are presented in Appendix B, Figures B-1 to B-4. The bond stress at slip of 0.1 mm, the maximal bond stress as well as the slip at maximal bond stress are presented in Tables B-1 to B-4. Similarly as in the case of pull-out specimens, the average of bond strength for each specimen differs to the bond strength of the average curve. A similar trend of increase in bond strength with increasing loading rate as for the pull-out type of testing (Figure 4-35) was observed. The bond strength increase between the medium and drop-tower loading rate is more pronounced than in the case of pull-out testing. The difference between the drop-tower and SHB type of loading is nearly negligible, which is to be expected as the loading rates, as well as the slip rates, are very near to each other. It is not possible to increase the SHB loading rate because the yielding of the steel works as an upper limit to the bond stress increase. In the numerical simulation presented in a paper from Panteki et al. [129] the yielding of the steel has been switched off by assigning an elastic material to the rebar. This allowed to increase the loading rates as high as 50,000 mm/s, and DIF up to 1.73 was reached.

In case of push-in type of loading it is important to review the results from the drop-tower in more detail as they can be influenced by the experimental setup. In the case of push-in experiments, the impactor is directly hitting the reinforcement steel. This is shown in Figure 3-24. As already discussed in Chapter 4.2 a part of the compressive wave which reaches the bond zone gets reflected from it and travels in the direction of the impactor. That means that this reflection gets superimposed on the original compressive wave. A similar situation arises after the reflected part of the wave reaches the impactor-rebar interface. Because of the difference in impedance, a large part of the reflected wave gets reflected from the impactor-rebar interface for the second time and travels back in the direction of the bond zone. It gets again superimposed on the strain measurements of the original wave and the first bond zone reflection. The result is that the strain gauge in front of the bond zone measures the original wave, reflection from the bond zone and reflection from the impactor-rebar interface. This could be theoretically eliminated by prolonging the reinforcement bar in front of the bond zone. Practically it is not possible because of the possible buckling and other stability issues of such a long rebar. This effect is eliminated in the SHB experimental setup where incident bar 2 with the same impedance as the reinforcement bar is used. This is in more detail explained in Chapter 3.6.2.

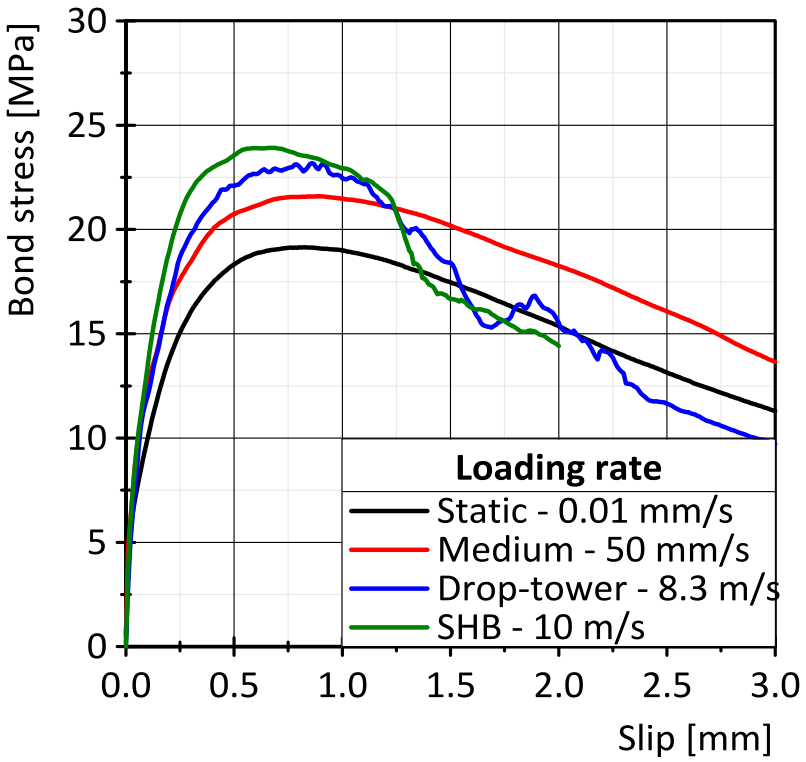

Figure 4-36: Loading rate effect on push-in average results.

Chapter 5

Conclusions

5.1 Validation of the hypothesis

The goal of this work was to answer the question if the bond strength between steel reinforcement and concrete increases with impact loading. **Based on the results presented in Chapter 4 it can be concluded that an influence of the loading rate was observed. However, the measured dynamic increase factor is lower than expected.** It is very hard to separate the loading rate effects from other influencing factors, such as concrete quality, the presence of imperfections in the bond zone, and uncertainties arising from the data acquisition. An increase in dynamic bond strength can be seen already at moderate loading rates achievable in the servo-hydraulic loading machine. The author believes that this increase in bond strength arises mostly from material inertia. During the test at moderate loading rates, the bond strength is calculated from the reaction force. From the working principle of the load cell, it is clear that the specimen needs to move so that force can be measured. That means that the specimen needs to accelerate and subsequently decelerate. Because the load cell is relatively stiff, the accelerations are very high, and the inertia of the specimen can, therefore, influence the measured reaction force. The faster we pull, the larger this influence is.

The situation gets even more complicated when it comes to push-in tests in the SHB. Actually, the SHB is meant for investigation of material properties such as compressive and tensile strength with respect to loading rate. In the case of the bond testing, material properties influence is combined with the contact and friction between steel and concrete. Therefore it is very hard to measure the actual strain rate during the test. For the purpose of this research, the SHB had to be modified through a series of iterative

modifications to provide reliable and repeatable results. In the case of the SHB, the bond stress is measured directly on the reinforcing steel as a stress loss of the loading pulse. This eliminates inertial effects that can be observed at the loading cell. Unfortunately, another inertial effect influences the results. During the SHB test, the concrete has a tendency to expand in the lateral direction. That means that the concrete surrounding the rebar needs to be accelerated to a certain velocity. Before this happens, this mass of concrete provides additional confinement to the steel rebar, thus influencing the result. The question is if the additional confinement provided by the inertial effect should be considered as a material behaviour. According to one opinion, it is irrelevant where the dynamic increase effect comes from. Important is that the specimen can carry more load. The other opinion is that the inner inertia influence is not a real material behaviour and thus should be subtracted from the results. This is, however, very problematic as the acceleration inside of the specimen varies widely with location and time.

5.2 Most important conclusions from impact testing

Throughout this work, a new method of measuring bond stress-strain relationships under high loading rates was shown. The novelty of this approach is that the bond stress is calculated from the stress loss inside of the bond zone during the first loading pulse pass. As already described in the above chapter, the inertial effects of the concrete body can be significantly reduced by utilising this method. The main disadvantage is that the bond zone needs to be short so that even stress distribution can be assumed. Although the bond zone length influences the bond strength minimally, the force required for the bond failure is relatively low, and therefore especially large specimens, such as the standard cubes, are susceptible to pre-damage during manipulation. In addition, the scattering of the results is higher because all imperfections have a larger influence on the results.

Four loading rates were compared in this research, i.e.: quasi-static, medium, drop-tower impact and SHB impact rate. Throughout the research, the scattering of the results was very high. This was attributed to a number of ribs that are in the bond zone. Very mild dynamic increase factor of 1.2 to 1.3 was observed in this work. It is, however, important to note the difference in between the slow and high loading rates is very low and lies in the scatter range of the individual results.

Based on the results presented in this work answers to the questions as presented in Chapter 1.3 are as follows:

1. The standard RILEM cubes are inappropriate for high loading rate tests. Cylindrical specimens without sharp edges are much more suitable. It can come to unexpected wave reflections around the edges. Additionally, the cubical specimens are hard to test in the SHB. In case a pure pull-out failure is desirable, the minimal concrete cover, as well as the bond free length, should be $4\times d_s$. For smaller concrete covers a splitting failure will occur as reported for instance by Michal et al. [23]. In their work, they also recommended the use of cylindrical specimens. During the impact tests, it is theoretically possible to calculate the bond stress from the reaction measured under the specimen in a similar manner to RILEM recommendations. However, the inertial force caused by the mass of the sample needs to be subtracted from the results. For this, an acceleration throughout the whole specimen needs to be known. The assumption that the acceleration measured on top of the specimen corresponds to the volumetric acceleration is very unprecise, because of the multiple wave reflections inside of the specimen.
2. The definition of loading rate for the impact tests is rather complicated. There is no standardised procedure how to come up with one value. The different approaches for the determination of the loading rate are discussed in Chapter 4.2.1. The classification of the bond stress-slip tests based on the slip rate seems to be more reasonable as the slip rate is nearly constant during the loading phase. For a very quick comparison of results measured in the same loading machines, it is possible to use the loading velocity. When comparing the results to the other authors, the hardness of the impact and the losses in the testing rig need to be considered.
3. Based on the results presented in Chapter 4.1.6 there is minimal difference between pull-out and push-in type of loading independently of the loading rate. The reason for that is very short bond length used in this research and relatively low force that is needed for reaching the maximal bond stress. Because the longitudinal stress in rebar is low, the lateral contraction or expansion caused by the Poisson effect is nearly negligible.
4. The bond stress-slip relationship is sensitive to the loading rate. However, this sensitivity is lower than expected. The increase in maximal bond strength is proportional to the second root of the concrete compressive strength increase. In all studied cases, the stiffness of the rising part of the bond stress-slip curve is

increased with increasing loading rate. Steel yielding limits the maximal loading rate. The behaviour under loading rates higher than 10 m/s can be studied numerically. It is equally important to note that it is hard to separate the loading rate effects from other influences because of the relatively high scattering of the results.

5. The influence of concrete compressive and tensile strength on the measurements is in good agreement with models presented in the literature. The bond strength can be calculated by using the MC 2010 formulas. The higher DIF for tensile strength doesn't seem to have a significant influence on the results. No change in failure mode depending on the loading rate was observed during the experimental work
6. It was found out, that reinforcing steel with larger diameter has higher bond strength in comparison to the steel with a smaller diameter. Based on the experimental results of this work, it can be concluded that it is not true that the bond strength is independent of the reinforcement diameter. It is important to note that this result is not consistent with some findings presented in the literature and should be investigated in a separate research program.

In addition to the answers to the main questions in objectives, the following interesting conclusions can be drawn:

a. It is possible to measure bond stress-slip relationships during impact loading with the most inertial effects eliminated. Both drop-tower and split Hopkinson type of test are suitable experimental equipment.
b. After comparing the experimental results to the numerical model developed by Panteki et al. [124] a very good agreement was reached Figure 4-32.
c. Sampling frequencies higher than 100 kHz should be used to measure bond stress-slip relationships under impact loading. Effect of any filter needs to be investigated.
d. There is a difference between cylindrical and cubical specimens. The bond strength of steel to concrete is higher for cylindrical specimens. This lies probably on the concreting direction which is vertical and thus more favourable in case of the cylinders.
e. The maximal bond stress in case of a short bond zone of $2 \times d_s$ is very sensitive to the position of ribs in the bond zone. The difference between the most and least favourable ribs position is as high as 20%

5.3 Future research needs

The loading rates presented in this work were limited by the yielding threshold of the used steel. In the future research, different steel diameters, as well as high strength steels, should be investigated. This should allow achieving higher loading rates. In the presented research only small portion of the loading impulse was used for loading the bond zone. The rest of the energy was stored as an elastic pulse in the rebar. By increasing the bond stress, a higher percentage of the loading pulse can be utilised until the failure of the bond zone. The bond stress can be increased for instance by increasing the concrete compressive strength. This disadvantage of increasing the bond strength is that the wave reflected from the bond is increased as well. That means that the steel before the bond zone can get into yielding and thus distort the readings. To increase the slip rate a longer impactor or a long pre-stressed bar can be used. The long pre-stressed bar can be suddenly released, and the stored elastic energy will induce a long loading pulse which will increase the deformation of the reinforcement bar and thus the slip. However, also the distance to the free end of the rebar needs to be very long so that the overlapping of the incoming and reflected pulse is avoided. Using such a long bar is unfortunately very impractical. A new type of joint that will be capable of transferring both tensile and compressive stress from the rebar to some sort of extension bar needs to be developed. Special attention needs to be paid that no part of the wave gets reflected inside of the joint as that would negatively influence the results. In addition, in the future research, the applicability of the developed method should be checked for reinforcing steels of larger diameters that are used more frequently in construction.

Because the method described in this work does not provide any information about the local stress state of concrete in the vicinity of the reinforcement, there is a need for a more detailed numerical model. This model can be calibrated on the results provided in this work, and it can be used to analyse the multiaxial stress state under the ribs during the high-rate loading. Such model is currently being developed by E. Panteki as a part of her Ph.D. thesis [128]. In addition, the numerical model can be used to predict the behaviour of whole structural parts. It can also be possible to simulate parameters which are very hard to measure experimentally. For instance, it would be of great advantage if the steel rebar would be much longer. This is, however, impossible to achieve in reality for bars with a diameter of 10 mm because they tend to bend very easily. Also, the short bond zone is very sensitive to any bending moments induced by the manipulation with the specimen.

Lastly, the bond stresses arising during impact loading of reinforced concrete structures such as beams and plates need to be measured. Strain gauges glued directly on the reinforcement can be used in a similar way as in this research work. It must be made sure that the measured strain will not be influenced by the surrounding concrete in any way. The measured results can be then compared with the local bond stress-slip behaviour as presented in this research work.

List of Figures

List of Tables

References

[1] RILEM RC 6: *Bond Test for Reinforcement Steel. 2. Pull-Out Test*. London: E & FN Spon, . 1994

[2] Bischoff, P.: *Stress-strain relationship of reinforced concrete subjected to biaxial tension*. In: ACI Structural Journal 102 (2005), pp. 169–170

[3] Malvar, L. J.: *Review of Static and Dynamic Properties of Steel Reinforcing Bars*. In: ACI Materials Journal 95 (1998) 5, pp. 609–614

[4] Cadoni, E.; Fenu, L.; Forni, D.: *Strain rate behaviour in tension of austenitic stainless steel used for reinforcing bars*. In: Construction and Building Materials 35 (2012), pp. 399–407

[5] ACI Committee 466: *Report on Dynamic Fracture of Concrete*. 2004

[6] Comité euro-international du béton: *Concrete Structures under Impact and Impulsive Loading*. 1988

[7] Bischoff, P. H.; Perry, S. H.: *Compressive behaviour of concrete at high strain rates*. In: Materials and Structures 24 (1991) 6, pp. 425–450

[8] Quast, M.; Curbach, M.: *Behaviour of Concrete under Biaxial Dynamic Loading*. In: Fifth International Workshop on Performance, Protection & Strengthening of Structures under Extreme Loading. East Lansing, 2015, p. 8

[9] Ožbolt, J.; Sharma, A.; Reinhardt, H.-W.: *Dynamic fracture of concrete – compact tension specimen*. In: International Journal of Solids and Structures 48 (2011) 10, pp. 1534–1543

[10] Ožbolt, J.; Bošnjak, J.; Sola, E.: *Dynamic fracture of concrete compact tension specimen: Experimental and numerical study*. In: International Journal of Solids and Structures 50 (2013) 25, pp. 4270–4278

[11] DIN 488-2: 2009-08: *Betonstahl-Betonstabstahl*. Beuth Verlag GmbH, 2009

[12] Eurocode 2: Teil 1-1: 1992-1-1:2004 + AC:2010: *Bemessung und Konstruktion von Stahlbeton- und Spannbetontragwerken. Allgemeine Bemessungsregeln und Regeln für den Hochbau*. Beuth Verlag GmbH, 2011. Deutsche Fassung.

[13] Manning, D. G.: *Corrosion performance of epoxy-coated reinforcing steel: North American experience*. In: Construction and Building Materials 10 (1996) 5, pp. 349–365

[14] Shang, H.; Zhao, T.; Cao, W.: *Bond behavior between steel bar and recycled aggregate concrete after freeze-thaw cycles*. In: Cold Regions Science and Technology 118 (2015), pp. 38–44

[15] Cook, R. A.; Doerr, G. T.; Klingner, R. E.: *Bond Stress Model for Design of Adhesive Anchors*. In: ACI Structural Journal 90 (1993) 5, pp. 514–524

[16] fib – fédération internationale du béton: *Model Code for Concrete Structures 2010. First complete draft. Volume 1, fib Bulletin 55*. 2010

[17] Plizzari, G.; Russo, G.; Gambarova, P.; Rosati, G.: *Bond mechanics including pull-out and splitting failures*. . In: Chapter I of FIB State-of-Art Report "Bond of Reinforcement in Concrete" (Bull. n. 10) : FIB, 2000, pp. 1–98

[18] Rostásy, F. S.; Scheuermann, J.: *Verbundverhalten einbetonierten Betonrippenstahls bei extrem tiefer Temperatur*. In: Deutscher Ausschuß für Stahlbeton 280 (1987) 2, p. 144

[19] Ritter, L.: *Der Einfluss von Querzug auf den Verbund zwischen Beton und Betonstahl.* TU Dresden, Diss., 2014

[20] DIN Deutsches Institut für Normung: *DIN EN 10080, Stahl für die Bewehrung von Beton - Schweißgeeigneter Betonstahl - Allgemeines*. Beuth Verlag GmbH, 2005

[21] Wildermuth, A.: *Untersuchungen zum Verbundverhalten von Bewehrungsstäben mittels vereinfachter Versuchskörper*. Berlin: Beuth, 2013 - ISBN 978-3-410-65251-9

[22] Yan, C.: *Bond Between Reinforcing Bars and Concrete Under Impact Loading.* The University of British Columbia, Ph.D. Thesis, 1992

[23] Michal, M.; Keuser, M.; Millon, O.: *Verbund von Beton und Bewehrungsstahl bei hoch-dynamischer Belastung*. In: Beton- und Stahlbetonbau 111 (2016) 1, pp. 32–40

[24] Martin, H.; Noakowski, P.: *Verbundverhalten von Betonstählen: Auswertung von Ausziehversuchen*. TU München, . Research report, 1978

[25] Torre-Casanova, A.; Jason, L.; Davenne, L.; Pinelli, X.: *Confinement effects on the steel–concrete bond strength and pull-out failure*. In: Engineering Fracture Mechanics 97 (2013), pp. 92–104

[26] Tepfers, R.; Olsson, P.-Å.: *Ring Test for Evaluation of Bond Properties of Reinforcing Bars*. In: Bond in Concrete - From Research to Practice. Riga, Latvia, 1992, p. 12

[27] Lundgren, K.: *Bond between ribbed bars and concrete. Part 1: Modified model*. In: ConRes 57 (2005) 7, pp. 371–382

[28] Metelli, G.; Plizzari, G. a.: *Influence of the relative rib area on bond behaviour*. In: Magazine of Concrete Research 66 (2014) 6, pp. 277–294

[29] den Uijl, J. A.; Bigaj, A. J.: *A bond model for ribbed bars based on concrete confinement*. In: Heron 41 (1996) 3, pp. 201–226

[30] Hong, S.; Park, S. K.: *Uniaxial bond stress-slip relationship of reinforcing bars in concrete*. In: Advances in Materials Science and Engineering 2012 (2012)

[31] Tassios, T. P.: *Properties of bond between concrete and steel under load cycles idealising seismic action*. In: CEB Bulletin d'Information 1 (1979) 131

[32] Wensauer, R.: *Zum Einfluss hochdynamischer Einwirkungen auf das Verbundverhalten von Stahlbeton.* Universität der Bundeswehr München, Diss., 2013

[33] Michal, M.; Keuser, M.; Solomos, G.; Peroni, M.; Larcher, M.; Esteban, B.: *Experimental investigation of bond strength under high loading rates*. In: Cadoni, E. (Ed.): EPJ Web of Conferences, DYMAT 2015 - 11th International Conference on the Mechanical and Physical Behaviour of Materials under Dynamic Loading. Lugano, 2015, p. 5

[34] Eligehausen, R.; Popov, E. P.; Bertero, V. V.: *Local bond stress-slip relationships of deformed bars under generalized excitations*. In: Proceedings of the 7th European Conference on Earthquake Engineering. Athens, 1982, pp. 69–80

[35] Ruiz, M. F.; Muttoni, A.; Gambarova, P. G.: *Analytical Modeling of the Pre- and Postyield Behavior of Bond in Reinforced Concrete*. In: ASCE Journal of Structural Engineering 133 (2007) 10, pp. 1364–1372

[36] American Concrete Institutue: *ACI 408R-03: Bond and Development of Straight Reinforcing Bars in Tension*. 2008

[37] Rehm, G.: *Über die Grundlagen des verbundes zwischen Stahl und Beton*. In: Deutscher Ausschuss für Stahlbeton 138 (1961)

[38] Cairns, J.; Plizzari, G. A.: *Towards a harmonised European bond test*. In: Materials and Structures 36 (2003) 8, pp. 498–506

[39] CEB: *RC elements under cyclic loading*. In: Bulletin d' Information No. 230. London, 1996

[40] Rehm, G.; Eligehausen, R.: *Einfluß einer nicht ruhenden Belastung auf das Verbundverhalten von Rippenstählen*. In: Betonwerk + Fertigteil-Technik 43 (1977) 6, pp. 295–299

[41] Balázs, G. L.: *Fatigue of Bond*. In: ACI Materials Journal 88 (1991) 6, pp. 620–629

[42] Zuo, J.; Darwin, D.: *Bond Slip of High Relative Rib Area Bars under Cyclic Loading*. In: ACI Structural Journal 97 (2000) 2, pp. 331–334

[43] Lindorf, A.: *Ermüdung des Verbundes von Stahlbeton unter Querzug.* Technische Universität Dresden, Diss., 2011

[44] Leonhardt, F.: *Vorlesungen über Massivbau-Teil 2: Sonderfälle der Bemessung im Stahlbetonbau*. 3. ed. Berlin-Heidelberg-New York: Springer Verlag, 1986

[45] Gylltoft, K.; Krister Cederwall, L. E.; Nilsson, larsgunnar: *Bond Failure in Reinforced Concrete Under Monotonic and Cyclic loading: A Fracture Mechanics Approach*. In: Special Publication 75 (1982), pp. 269–288

[46] Rehm, G.; Eligehausen, R.: *Verbundverhalten gerippter Betonstähle mit kurzer Einbettungslänge bei nicht ruhender Belastung*. Stuttgart, Germany. Technical report 75/17, 1975

[47] Rehm, G.; Eligehausen, R.: *Verbundverhalten von Rippenstäben mit langer Einbettungslänge bei nicht ruhender Belastung*. Stuttgart, Germany. Technical report 75/2, 1975

[48] Darwin, D.; Graham, E. K.: *Effect of Deformation Height and Spacing on Bond Strength of Reinforcing Bars*. In: ACI Structural Journal 90 (1993) 6, pp. 646–657

[49] Soleymani Ashtiani, M.; Dhakal, R. P.; Scott, A. N.; Bull, D. K.: *Cyclic beam bending test for assessment of bond–slip behaviour*. In: Engineering Structures 56 (2013), pp. 1684–1697

[50] König, G.; Danielewicz, I.: *Ermüdungsfestigkeit von Stahlbeton- und Spannbetonbauteilen mit Erläuterungen zu den Nachweisen gemäß CEB-FIP Model Code 1990*. In: DAfStb 439 (1994)

[51] Schütz, W.: *Zur Geschichte der Schwingfestigkeit*. In: Materialwissenschaft und Werkstofftechnik 24 (1993), pp. 203–232

[52] Koch, R.; Balázs, G. L.: *Verbund unter nicht ruhender Beanspruchung*. In: DFG (Ed.): Abschlusskolloquium zum Schwerpunktprogramm: Bewehrte Betonbauteile unter Betriebsbedingungen. Stuttgart, 1997

[53] Koch, R. G.; Balázs, G. L.: *Verbund unter nicht ruhender Beanspruchung*. In: Beton - und Stahlbetonbau 93 (1998) 7 & 8, pp. 177-181-223

[54] Mainz, J.: *Modellierung des Verbundtragverhaltens von Betonrippenstahl.* München: TU München, Diss., 1993

[55] Martin, H.: *Zusammenhang zwischen Oberflächenbeschaffenheit, Verbund und Sprengwirkung von Bewehrungsstählen unter Kurzzeitbelastung*. . In: Deutscher Ausschuss für Stahlbeton. 228 : Wilhelm Ernst & Sohn, Berlin, 1973, p. 50

[56] Martin, H.; Noakowski, P.: *Verbundverhalten von Betonstählen - Untersuchung auf der Grundlage von Ausziehversuchen*. In: Deutscher Ausschuß für Stahlbeton 319 (1981)

[57] CEB: *Bond Action and Bond Behaviour of Reinforcement. State of the Art Report*. In: Bulletin d'Information No. 151. Paris, 1982

[58] Martin, H.: *Bond Performance of Ribbed Bars (Pull-out-test) - Influence of Concrete and Consistency*. In: Bartos, P. (Ed.): Bond in Concrete, 1982, pp. 289–299

[59] Martin, H.: *Einfluß der Betonzusammensetzung auf das Verbundverhalten von Bewehrungsstählen*. In: Eligehausen, R. (Ed.): Fortschritte im Konstruktiven Ingenieurbau, Gallus Rehm zum 60. Geburtstag, 1984, pp. 161–166

[60] Paschen, H.; Steinert, J.; Hjorth, O.: *Untersuchung über das Verbundverhalten von Betonstählen bei Kurzzeitbeanspruchung*. 1974

[61] Untrauer, R. E.; Henry, R. L.: *Influence of Normal Pressure on Bond Strength*. In: Journal of the American Concrete Institute 62 (1965) 5, pp. 577–586

[62] Robins, P. J.; Standish, I. G.: *The influence of lateral pressure upon anchorage bond*. In: Magazine of Concrete Research 36 (1984) 129, pp. 195–202

[63] Soroushian, P.; Choi, K.; Park, G.; Aslani, F.: *Bond of deformed bars to concrete: Effects of confinement and strength of concrete*. In: ACI Materials Journal 88 (1991) 3, pp. 227–232

[64] Nagatomo, K.; Kaku, T.: *Experimental and analytical study on bond characteristics of reinforcing bars with only a single transverse rib*. In: Transactions of the Japan Concrete Institute 7 (1985), pp. 333–340

[65] Nykyri, P.: *Bond behaviour- Recent research projects at the concrete and silicate laboratory*. In: Technical Research Centre of Finnland (Ed.): Bond and Anchorage of Rein- forcement in Concrete. Göteborg, 1986, pp. 10–24

[66] DIN EN 1992-1-1: *Eurocode 2: Bemessung und Konstruktion von Stahlbeton- und Spannbetontragwerken - Teil 1-1: Allgemeine Bemessungsregeln und Regeln für den Hochbau*. Beuth Verlag GmbH, 2011

[67] Huang, Z.; Engström, B.; Magnusson, J.: *Experimental and analytical studies of the bond behaviour of deformed bars in high strength concrete*. In: 4th International Symposium on Utilization of High-strength/High-performance concrete. Paris, 1996

[68] fib – fédération internationale du béton: *Interface Characteristics*. . In: fib Model Code for Concrete Structures 2010 : Wiley-VCH Verlag GmbH & Co. KGaA, 2013. – ISBN 9783433604090, pp. 152–189

[69] Barbosa, M. T. G.; Sánchez Filho, E. D. S.; Oliveira, T. M. De; Santos, W. J. Dos: *Analysis of the relative rib area of reinforcing bars pull out tests*. In: Materials Research 11 (2008) 4, pp. 453–457

[70] Mathey, R. G.; Watstein, D.: *Investigation of Bond in Beam and Pull-out Specimens with High-Yield-Strength Deformed Bars*. In: ACI Journal 57 (1961) 9, pp. 1057–1090

[71] Richter, T.: *Untersuchung zur Verankerung von Betonrippenstahl.* TU Dresden, Diss., 1984

[72] Abrams, D. A.: *Tests of bond between concrete and steel*. 1913

[73] Clark, A. P.: *Comparative Bond Efficiency of Deformed Concrete reinforcing Bars*. In: ACI Journal Proceedings V. 43 (1946) 11

[74] Clark, A. P.: *Bond of Concrete Reinforcing Bars*. In: ACI Journal Proceedings 46 (1949) 3, pp. 161–184

[75] Rehm, G.; Martin, H.: *Zur Frage der Rißbegrenzung im Stahlbetonbau*. In: Beton- und Stahlbetonbau 63 (1968) 8, pp. 175–182

[76] Bach, C.: *Versuche über den Gleitwiderstand einbetonierten Eisens*. In: VDI (Ed.) Mitteilungen über Forschungsarbeiten Heft 22 (1905), pp. 1–41

[77] Rehm, G.; Eligehausen, R.: *Bond of Ribbed Bars Under High Cycle Repeated Loads*. In: ACI Journal Proceedings 76 (1979) 2, pp. 297–310

[78] Fédération Internationale du Béton: *Bond of reinforcement in concrete: state-of-art report*. 2000

[79] Abrishami, H. H.; Mitchell, D.: *Influence of Splitting Cracks on Tension Stiffening*. In: ACI Structural Journal 93 (1996), pp. 703–710

[80] Eckfeldt, L.: *Möglichkeiten und Grenzen der Berechnung von Rissbreiten in veränderlichen Verbundsituationen.* Dresden: Technische Universität Dresden, Diss., 2008

[81] Eligehausen, R.; Mayer, U.; Lettow, S.: *Mitwirkung des Betons zwischen den Rissen Stahlbetonbauteilen. Abschlussbericht zum DFG-Forschungsvorhaben EL 72/8-1+2*. 2000

[82] Losberg, A.; Olsson, P. A.: *Bond Failure of Deformed Reinforcing Bars Based on the Longitudinal Splitting Effect of the Bars*. In: ACI Journal 76 (1979) 1, pp. 5–18

[83] fib – fédération internationale du béton; Cairns, J.: *Bond and anchorage of embedded reinforcement: Background to the fib Model Code for Concrete Structures 2010*. fib - Fédération internationale du béton, . 2014

[84] Hawkins, N. M.; Lin, I. J.; Jeang, F. L.: *Local Bond Strength of Concrete for Cyclic Reversed Loadings*. In: Bond of Concrete, 1982, pp. 151–161

[85] Idda, K.: *Verbundverhalten von Betonrippenstählen bei Querzug.* Karlsruhe: Universität Karlsruhe, Diss., 1999

[86] Solomos, G.; Berra, M.: *Rebar pullout testing under dynamic Hopkinson bar induced impulsive loading*. In: Materials and Structures 43 (2010), pp. 247–260

[87] Eligehausen, R.; Popov, E. P.; Bertero, V. V: *Local Bond Stress-Slip Relationships of Deformed Bars under Generalized Excitations - Report No. UCB/EERC-83/23*. 1983

[88] Ruina, A. L.; Pratap, R.: *Introduction to Statics and Dynamics*. Oxford University Press (Preprint), 2015

[89] Graff, K.: *Wave motion in elastic solids*. New York: Dover Publications, 1991 - ISBN 9780486139579

[90] Meyers, M. A.: *Dynamic Behavior of Materials*. Hoboken, NJ, USA: John Wiley & Sons, Inc., 1994 - ISBN 9780470172278

[91] Mechtcherine, V.; Millon, O.; Butler, M.; Thoma, K.: *Mechanical behaviour of strain hardening cement-based composites under impact loading*. In: Cement and Concrete Composites 33 (2011) 1, pp. 1–11

[92] Pochhammer, L.: *Ueber die Fortpflanzungsgeschwindigkeiten kleiner Schwingungen in einem unbegrenzten isotropen Kreiscylinder*. In: Journal für die reine und angewandte Mathematik (Crelle's Journal) 1876 (1876) 81, pp. 324–336

[93] Chree, C.: *The Equations of an Isotropic Elastic Solid in Polar and Cylindrical Co-ordinates their Solution and Application*. In: Transactions of the Cambridge Philosophical Society 14 (1889), pp. 250–396

[94] Rayleigh, S. J. W. B.: *The Theory of Sound*. London, UK: Macmillan, 1877 - ISBN 978-1-108-03221-9

[95] Banthia, N. P.; Mindess, S.; Bentur, A.: *Impact behaviour of concrete beams*. In: Materials and Structures 20 (1987) 4, pp. 293–302

[96] Suaris, W.; Shah, S. P.: *Properties of Concrete Subjected to Impact*. In: Journal of Structural Engineering 109 (1983) 7, pp. 1727–1741

[97] Curbach, M.; Quast, M.: *Concrete under biaxial impact loading*. In: Hiermaier, S. (Ed.): Hopkinson Centenary Conference Cambridge. Cambridge (UK), 2014, pp. 117–139

[98] Bischoff, P. H.: *Compressive Response of Concrete to Hard Impact.* University of London Imperial College, Ph.D. Thesis, 1988

[99] Takeda, J.: *Strain Rate Effects on Concrete and Reinforcements, and their Contributions to Structures*. In: MRS Proceedings 64 (1985), p. 15

[100] Bentur, A.; Mindess, S.; Banthia, N.: *The behaviour of concrete under impact loading: Experimental procedures and method of analysis*. In: Materials and Structures 19 (1986) 5, pp. 371–378

[101] Banthia, N. P.: *Impact resistance of concrete.* Vancouver, B. C., Canada: University of British Columbia, Ph.D. Thesis, 1987

[102] Lin, F.: *Materialmodelle und Querschnittsverhalten von Stahlbetonbauteilen unter extrem dynamischer Beanspruchung.* Ruhr-Universität Bochum, Diss., 2005

[103] Hjorth, O.: *Ein Beitrag zur Frage der Festigkeiten und des Verbundverhaltens von Stahl und Beton bei hohen Beanspruchungsgeschwindigkeiten.* Techische Universität Braunschweig, Diss., 1976

[104] Hansen, R. J.; Liepins, A. A.: *Behavior of Bond Under Dynamic Loading*. In: ACI Journal 59 (1962) 4, pp. 563–584

[105] Shah, I. K.: *Behavior of Bond Under Dynamic Loading*. Massachusetts: Massachusetts Institute of Technology, . Research report, 1963

[106] Vos, E.; Reinhardt, H. W.: *Influence of loading rate on bond behaviour of reinforcing steel and prestressing strands*. In: Matériaux et Constructions 15 (1982) 1, pp. 3–10

[107] Vos, E.: *Influence of Loading Rate and Radial Pressure on Bond in Reinforced Concrete - A Numerical and Experimental Approach.* Delft, The Netherlands: Technical University Delft, Ph.D. Thesis, 1983

[108] Reinhardt, H. W.: *Concrete under impact loading, tensile strength and bond*. In: Heron 27 (1982) 3, pp. 1–48

[109] Rußwurm, D.: *Betonstähle für den Stahlbetonbau: Eigenschaften und Verwendung*. Wiesbaden Berlin: Bauverlag BV GmbH, 1993 - ISBN 978-3762530787

[110] Yan, C.; Mindess, S.: *Effect of Loading Rate on Bond Behavior Under Dynamic Loading*. In: ACI Special Publication 175 (1998), pp. 179–198

[111] Yan, C.; Mindess, S.: *Bond between epoxy-coated reinforcing bars and concrete under impact loading*. In: Canadian Journal of Civil Engineering 21 (1994) 1, pp. 89–100

[112] Mindess, S.; Yan, C.: *Fracture Mechanics Analysis of Bond Behavior Under Dynamic Loading*. In: Special Publication 156 (1995), pp. 107–124

[113] Weathersby, J. H.: *Investigation of Bond Slip between Concrete and Steel Reinforcement under Dynamic Loading Conditions.* Louisiana State University, Ph.D. thesis, 2003

[114] Hartmann, T.: *Zur mesomechanischen Modellierung von Beton und ihrer Anwendung zur makromechanischen Modellbildung.* Universität der Bundeswehr München, Diss., 2009

[115] Michal, M.; Keuser, M.: *Bond of steel and concrete under high loading rates*. In: Proceedings of the 9th International Conference on Structural Dynamics, 2014, pp. 3491–3496

[116] DIN Deutsches Institut für Normung: *DIN EN 12350-5: Prüfung von Frischbeton - Teil 5: Ausbreitmaß*. Berlin: Beuth Verlag GmbH, August 2009

[117] Müller, H. S.; Anders, I.; Breiner, R.; Vogel, M.: *Concrete: treatment of types and properties in fib Model Code 2010*. In: Structural Concrete 14 (2013) 4, pp. 320–334

[118] Comité euro-international du béton: *CEB-FIP Model Code 1990. Design Code.* London: Thomas Telford, 1993

[119] Malárics, V.; Müller, H. S.: *Evaluation of the splitting tension test for concrete from a fracture mechanical point of view the*. In: Proceedings of the Fracture Mechanics of Concrete and Concrete Structures - Assessment, Durability, Monitoring and Retrofitting of Concrete Structures (2010), pp. 709–716

[120] DIN EN ISO 6892-1: *Metallische Werkstoffe - Zugversuch - Teil 1: Prüfverfahren bei Raumtemperatur*. Berlin: Beuth Verlag GmbH, . 2009

[121] Chen, W. W.; Song, B.: *Split Hopkinson (Kolsky) bar: design, testing and applications*. Berlin: Springer Science & Business Media, 2010 - ISBN 1441979824

[122] Nabih, A.; Matthew, P.: *Design of Digital Low-pass Filters for Time-Domain Recursive Filtering of Impact Acceleration Signals*. Fort Rucker, Alabama: USAARL, . 1995

[123] Society of Automotive Engineers: *SAE J211/1: Instrumentation for Impact Test, Part 1, Electronic Instrumentation*. Warrendale, PA: SAE International, . 1995

[124] Panteki, E.; Máca, P.; Häussler-Combe, U.: *Finite element analysis of dynamic concrete-to-rebar bond experiments in the push-in configuration*. In: International Journal of Impact Engineering 106 (2017), pp. 155–170

[125] Krips, M.: *Rißbreitenbeschränkung im Stahlbeton und Spannbeton*. In: Mitteilungen aus dem Institut für Massivbau der Technischen Hochschule Darmstadt. Heft 33, 1985

[126] Vos, E.; Reinhardt, H. W.: *Bond Resistance of Deformed Bars, Plain Bars and Strands Under Impact Loading*. Delft: Delft University of Technology, . Technical report, 1980

[127] Máca, P.; Panteki, E.; Curbach, M.: *Bond Stress-slip Behaviour of Concrete and Steel Under High-loading Rates*. In: International Journal of Computational Methods and Experimental Measurements 4 (2016) 3, pp. 221–230

[128] Panteki, E.: *A finite element investigation of the influence of high loading rates on the bond of reinforcement in concrete.* Germany: TU Dresden, Diss., 2017 – in press

[129] Panteki, E.; Máca, P.; Häussler-Combe, U.: *Finite element parametric study on the effect of loading rate on the bond of reinforcement in concrete*. In: 6th International Workshop on Performance, Protection & Strengthening of Structures under Extreme Loading, PROTECT2017. Guangzhou, 2017. In press.

Appendix

The following naming convention was used:

type of test | specimen geometry | - series No. | - loading type | -specimen No.

where:

type of test: push-in PI or pull-out PO

specimen geometry: Cylinder Z* or cube C

Loading type: Quasi-static Q, medium rate M, drop-tower F†, SHB SHB

The resulting code can look for instance as PI | Z | 1 | -F | -1 which gives PIZ-1-F-1

* To distinguish between cubes and cylinders, the letter Z was used for cylinders (from German *Zylinder*)
† From German *Fallturm*

A. Material parameters

Table A-1: Mechanical properties of the used concrete.

Sample Nr.	$f_{c,cube}$ [MPa]	$f_{c,cyl}$ [MPa]	ρ [kg/m^3]	$f_{ct,f}$ [MPa]	$f_{ct,sp}$ [MPa]	E_c [GPa]
1	53.2	48.0	2310	4.7	3.91	31.8
2	55.2	48.6	2310	4.7	3.61	33.5
3	54.4	45.5	2280	4.6	3.97	34.1
4	45.6	46.2	2290	4.5	3.14	33.7
5	50.1	48.5	2310	5.0	2.89	34.9
Average	51.7	47.4	2300	4.7	3.5	33.6
St. dev.*	3.9	1.4	14.1	0.2	0.5	1.1
COV†	8%	3%	1%	4%	14%	3%

Table A-2: Average‡ properties of control specimens casted with the specimens for push-in bond stress tests.

Series name	Age [days]	Flowability [mm]	$f_{c,cube}$ [MPa]	$f_{ct,sp}$ [MPa]
PIZ-1	14	440	47.4	3.5
PIZ-2	15	460	43.0	3.7
PIZ-3	33	470	49.3	3.9
PIZ-4	28	520	49.4	4.0
PIZ-5	28	450	58.6	4.1
PIZ-6	28	540	49.8	3.9
PIZ-7	28	440	52.4	4.2
PIZ-8	31	410	54.6	4.5
PIZ-9	28	390	56.0	4.6
PIZ-10§	28	385	58.2	3.8
PIZ-10§	39	385	58.1	3.5
PIZ-11	28	400	55.8	4.2

* Standard deviation
† Coefficient of variation
‡ Average from 3 specimens
§ In some cases, it was not possible to preform static and impact tests at the same time. Therefore 6 cubes (per property) were casted. Three were tested at the time of quasi-static bond test and 3 at the time of impact bond test.

PIZ-12	27	420	53.4	4.0
PIZ-13	28	395	50.5	3.9
PIZ-13	27	395	47.8	3.4
PIZ-14	28	385	56.8	4.2
PIZ-15	28	400	45.6	3.5
PIZ-15	104	400	58.7	3.6
PIZ-16	28	400	48.1	3.8
PIZ-17	28	400	52.7	-
PIZ-18	28	400	49.6	3.5
PIZ-18	140	400	57.8	3.7
PIZ-19	28	400	52.4	3.8
PIZ-19	139	400	66.2	3.9
PIZ-20	28	-	49.6	3.5
PIZ-27	35	390	53.2	3.6
PIZ-28	31	400	47.8	3.9
PIZ-29	35	400	54.4	3.6
Average	-	-	52.8	3.8
St. dev.	-	-	5	0.3
COV			9%	8%

Table A-3: Average properties of control specimens casted with the specimens for pull-out bond stress tests.

Series name	**Age [days]**	**Flowability [mm]**	$f_{c,cube}$ **[MPa]**	$f_{ct,sp}$ **[MPa]**
POZ-1	28	-	52.6	3.6
POZ-2	18	-	53.3	3.7
POZ-3	18	400	45.6	3.3
POZ-4	28	500	52.6	4.0
POZ-5	28	405	58.7	4.3
POZ-6	53	400	62.9	4.7
POZ-7	32	400	61.6	4.2
POZ-8	28	405	55.8	4.5
POZ-9	28	400	55.7	4.2
Average	-	-	55.4	4.1
St. dev.	-	-	5.3	0.5
COV			10%	12%

B. Bond stress-slip relationships

Table B-1: Results of push-in quasi-static tests.

Specimen name	$\tau_{0.1}$* [MPa]	τ_{max} [MPa]	s_{max} [MPa]
PIZ1-Q-1	4.85	20.86	1.06
PIZ1-Q-2	7.16	17.45	0.70
PIZ1-Q-3	9.36	19.70	0.98
PIZ1-Q-4	6.58	18.25	1.22
PIZ5-Q-1	9.42	23.66	0.89
PIZ5-Q-2	7.12	17.25	0.70
PIZ5-Q-3	7.30	25.93	0.91
PIZ5-Q-4	8.56	20.74	0.77
PIZ6-Q-1	8.43	17.03	1.11
PIZ6-Q-2	8.56	14.88	0.77
PIZ6-Q-3	8.74	19.59	1.13
PIZ6-Q-4	9.24	19.42	0.90
PIZ8-Q-1	6.01	15.05	0.69
PIZ8-Q-2	4.83	15.77	1.10
PIZ8-Q-3	7.47	15.58	0.64
PIZ8-Q-4	6.36	19.08	1.22
PIZ27-Q-1	12.44	22.46	0.65
PIZ27-Q-2	16.81	23.24	0.52
PIZ27-Q-3	23.15	28.73	0.47
PIZ27-Q-4	16.79	23.24	0.48
PIZ28-Q-1	12.97	19.03	0.94
PIZ28-Q-2	11.53	16.26	0.56
PIZ28-Q-3	13.05	17.81	0.57
PIZ28-Q-4	12.67	19.95	0.55
Average	9.97	19.62	0.81
St. dev.	4.34	3.52	0.24
COV	43%	18%	30%

* Bond stress at a slip of 0.1 mm

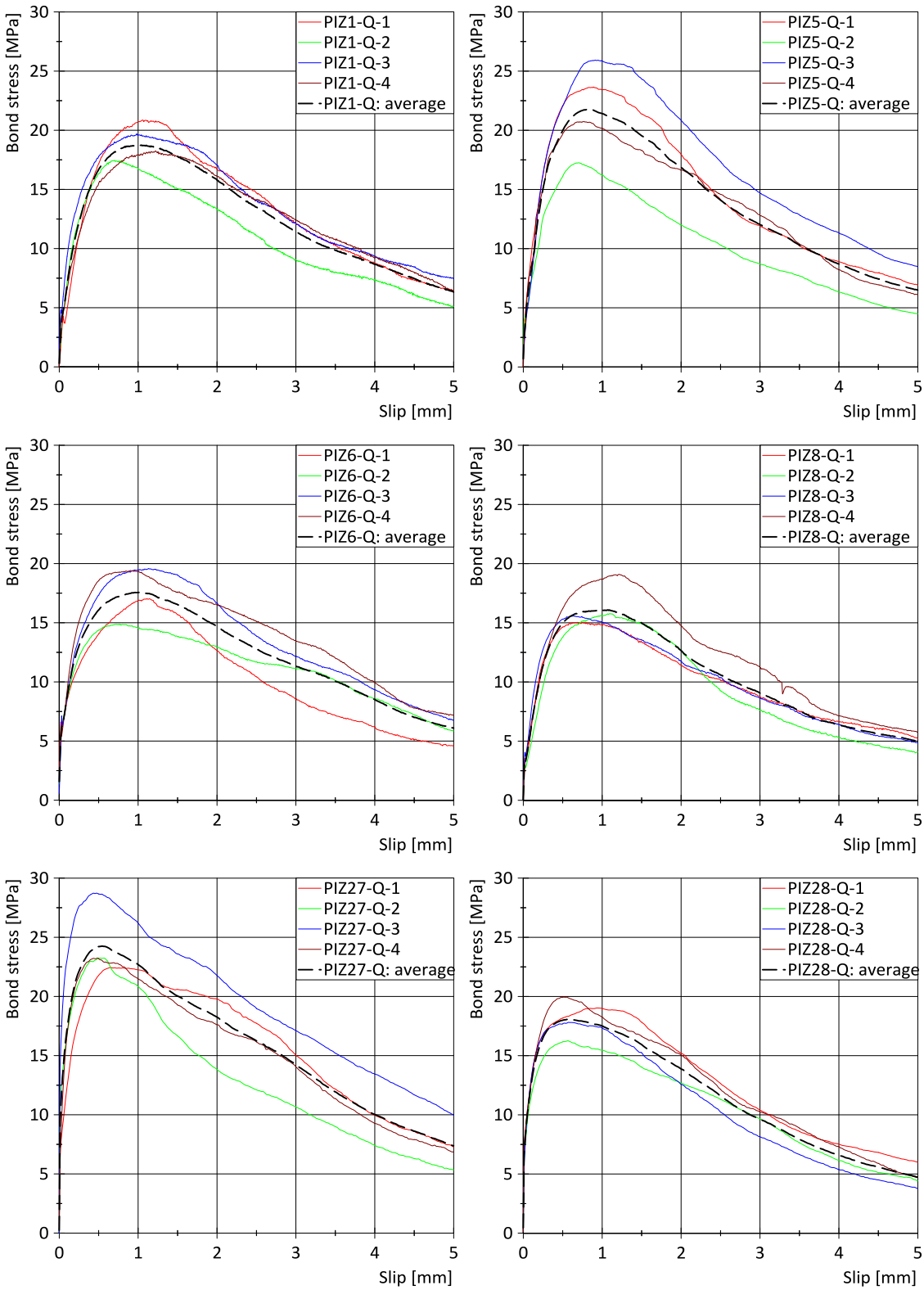

Figure B-1: Bond stress-slip relationships of push-in quasi-static tests.

Table B-2: Results of push-in medium loading rate tests.

Specimen name	$\tau_{0.1}$ [MPa]	τ_{max} [MPa]	s_{max} [MPa]
PIZ4-M-1	9.99	24.92	1.03
PIZ4-M-2	7.26	21.65	1.29
PIZ4-M-3	5.60	26.60	1.10
PIZ4-M-4	7.55	23.73	1.05
PIZ7-M-1	10.16	21.59	1.87
PIZ7-M-2	10.50	22.69	0.96
PIZ7-M-3	15.75	21.19	0.80
PIZ7-M-4	10.09	21.32	1.45
PIZ9-M-1	7.86	19.49	0.74
PIZ9-M-2	8.90	18.46	0.64
PIZ9-M-3	9.27	20.74	0.97
PIZ9-M-4	8.26	20.01	0.85
PIZ27-M-5	18.79	25.52	1.19
PIZ27-M-6	23.13	25.03	0.37
PIZ27-M-7	24.31	29.89	0.32
PIZ27-M-8	14.27	19.46	0.66
PIZ28-M-5	12.99	19.37	0.60
PIZ28-M-6	18.95	24.91	0.52
PIZ28-M-7	9.89	18.09	0.69
PIZ28-M-8	15.95	21.21	0.83
Average	12.47	22.29	0.90
St. dev.	5.38	3.07	0.37
COV	43%	14%	42%

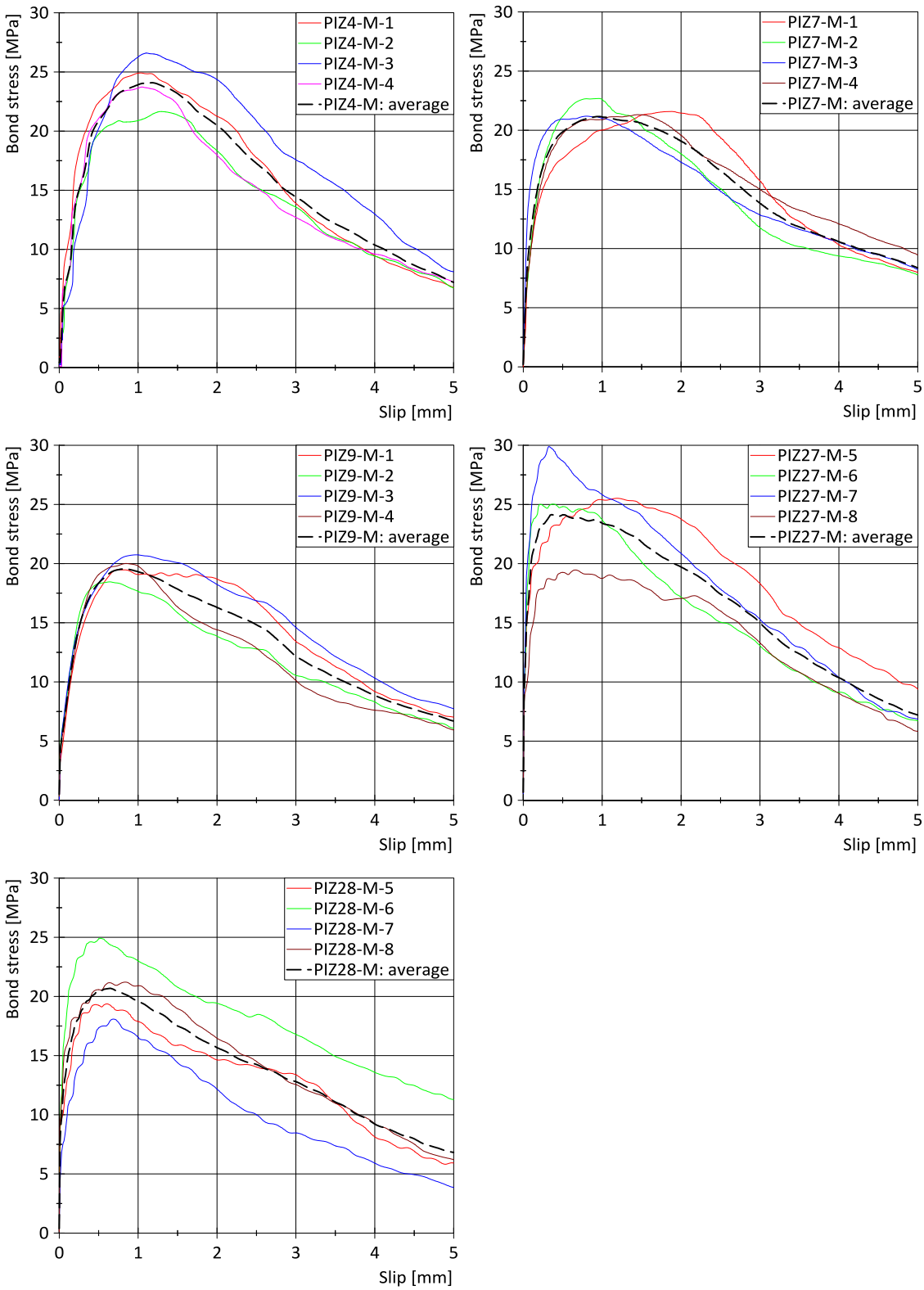

Figure B-2: Bond stress-slip relationships of push-in medium rate tests.

Table B-3: Results of push-in drop-tower tests.

Specimen name	$\tau_{0.1}$ [MPa]	τ_{max} [MPa]	s_{max} [MPa]
PIZ5-F-6	12.60	20.93	0.48
PIZ5-F-7	6.52	28.72	1.13
PIZ5-F-8	15.05	25.40	0.86
PIZ6-F-6	15.46	22.85	0.44
PIZ6-F-7	17.48	25.74	0.46
PIZ6-F-8	17.49	24.06	0.50
PIZ7-F-5	4.45	18.73	0.83
PIZ7-F-6	9.78	20.55	0.77
PIZ7-F-7	5.39	23.12	0.74
PIZ8-F-5	2.45	23.64	1.05
PIZ8-F-6	16.44	24.26	0.80
PIZ8-F-7	5.33	29.08	1.08
PIZ8-F-8	8.40	25.78	1.38
PIZ9-F-5	11.53	25.58	0.91
PIZ9-F-6	17.95	30.96	1.00
PIZ9-F-7	9.23	20.77	0.83
PIZ9-F-8	8.18	25.25	0.83
PIZ29-F-2	16.38	24.35	0.46
PIZ29-F-4	13.81	24.01	0.56
PIZ29-F-5	18.25	28.13	0.50
PIZ29-F-6	13.87	25.25	0.83
PIZ29-F-9	13.90	21.34	1.31
PIZ29-F-12	16.01	25.36	0.60
Average	12.00	24.52	0.80
St. dev.	4.90	2.96	0.27
COV	41%	12%	34%

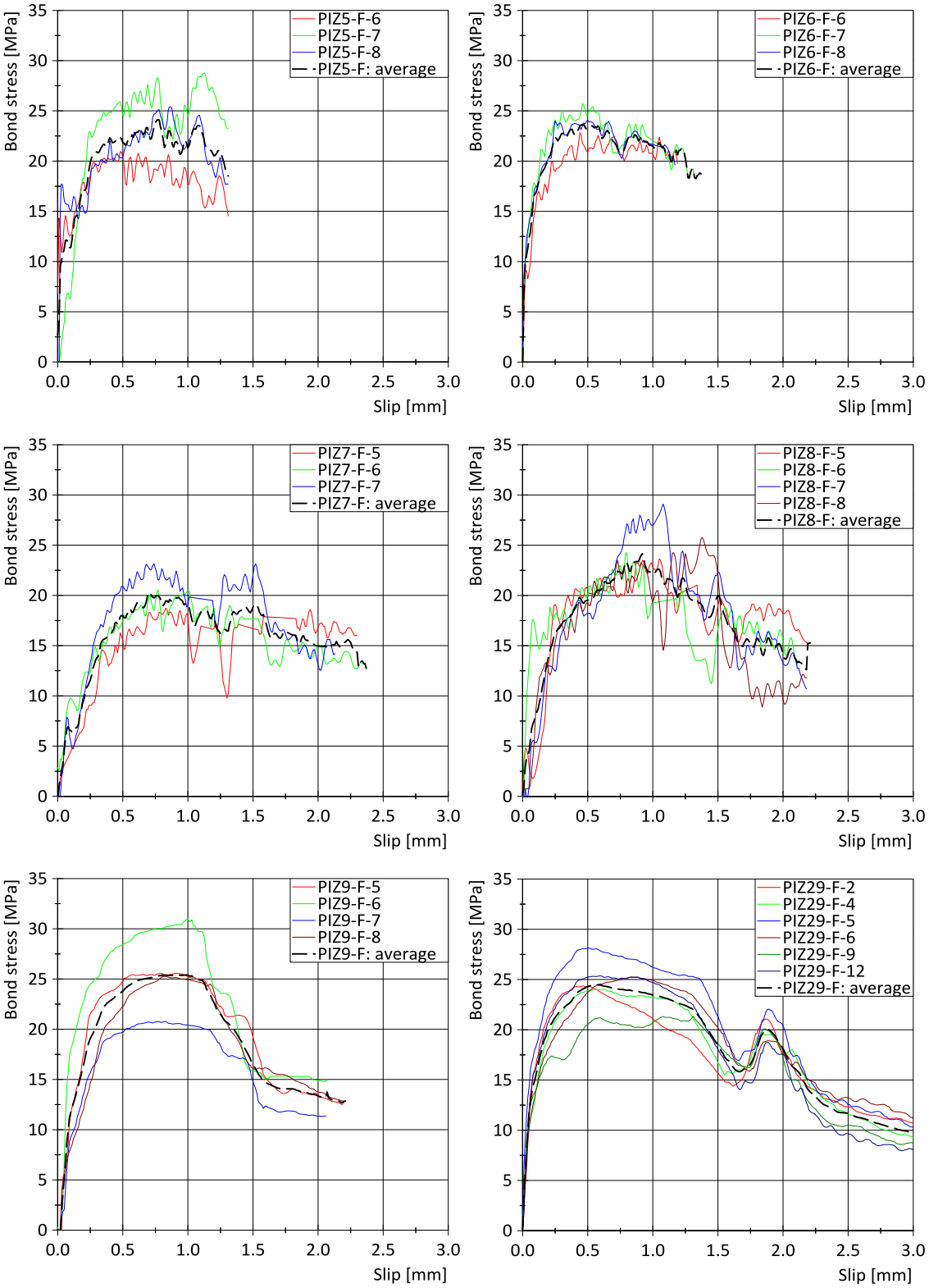

Figure B-3: Bond stress-slip relationships of push-in drop-tower tests.

Table B-4: Results of push-in SHB tests.

Specimen name	$\tau_{0.1}$ [MPa]	τ_{max} [MPa]	s_{max} [MPa]
PIZ10-SHB-1	14.15	33.38	0.69
PIZ10-SHB-2	11.22	25.61	0.68
PIZ10-SHB-3	9.21	31.90	1.00
PIZ11-SHB-1	11.75	25.25	0.42
PIZ11-SHB-3	11.40	26.39	1.47
PIZ11-SHB-4	10.81	27.56	0.71
PIZ12-SHB-1	6.79	19.47	0.56
PIZ13-SHB-1	3.92	17.76	0.78
PIZ14-SHB-5	11.30	22.84	0.25
PIZ14-SHB-8	17.70	28.67	0.66
PIZ15-SHB-2	6.52	23.56	1.37
PIZ15-SHB-3	16.33	26.80	0.57
PIZ15-SHB-4	9.41	19.91	1.21
PIZ15-SHB-5	16.96	24.72	0.39
PIZ15-SHB-6	14.97	27.14	0.37
PIZ15-SHB-7	24.45	30.95	0.55
PIZ16-SHB-2	3.82	15.89	0.96
PIZ17-SHB-3	8.84	17.55	0.81
PIZ17-SHB-4	15.70	18.32	0.69
PIZ17-SHB-5	10.48	22.71	0.82
PIZ17-SHB-7	4.40	19.40	0.84
PIZ20-SHB-1	11.83	25.36	0.84
PIZ20-SHB-2	11.58	25.94	0.92
PIZ20-SHB-3	5.93	18.57	0.58
PIZ20-SHB-5	10.87	24.67	0.89
PIZ20-SHB-6	8.61	24.93	0.54
PIZ20-SHB-7	6.12	15.58	0.53
PIZ20-SHB-8	11.67	25.13	0.33
PIZ27-SHB-9	7.60	24.22	1.42
PIZ27-SHB-10	12.24	24.05	0.66
PIZ27-SHB-11	17.77	26.73	0.62
PIZ27-SHB-12	15.60	20.35	1.55
PIZ27-SHB-13	17.06	29.23	0.87
PIZ27-SHB-14	18.72	28.95	0.65
PIZ27-SHB-15	19.48	29.92	0.56

PIZ27-SHB-16	19.44	32.67	0.66
PIZ-28-SHB-9	14.48	20.81	0.54
PIZ-28-SHB-10	22.16	28.42	0.31
PIZ-28-SHB-11	18.15	28.52	0.48
PIZ-28-SHB-13	20.65	27.38	0.55
PIZ-28-SHB-14	24.82	30.46	0.85
PIZ-28-SHB-16	28.72	33.69	0.31
Average	13.42	25.03	0.73
St. dev.	5.87	4.75	0.31
COV	44%	19%	43%

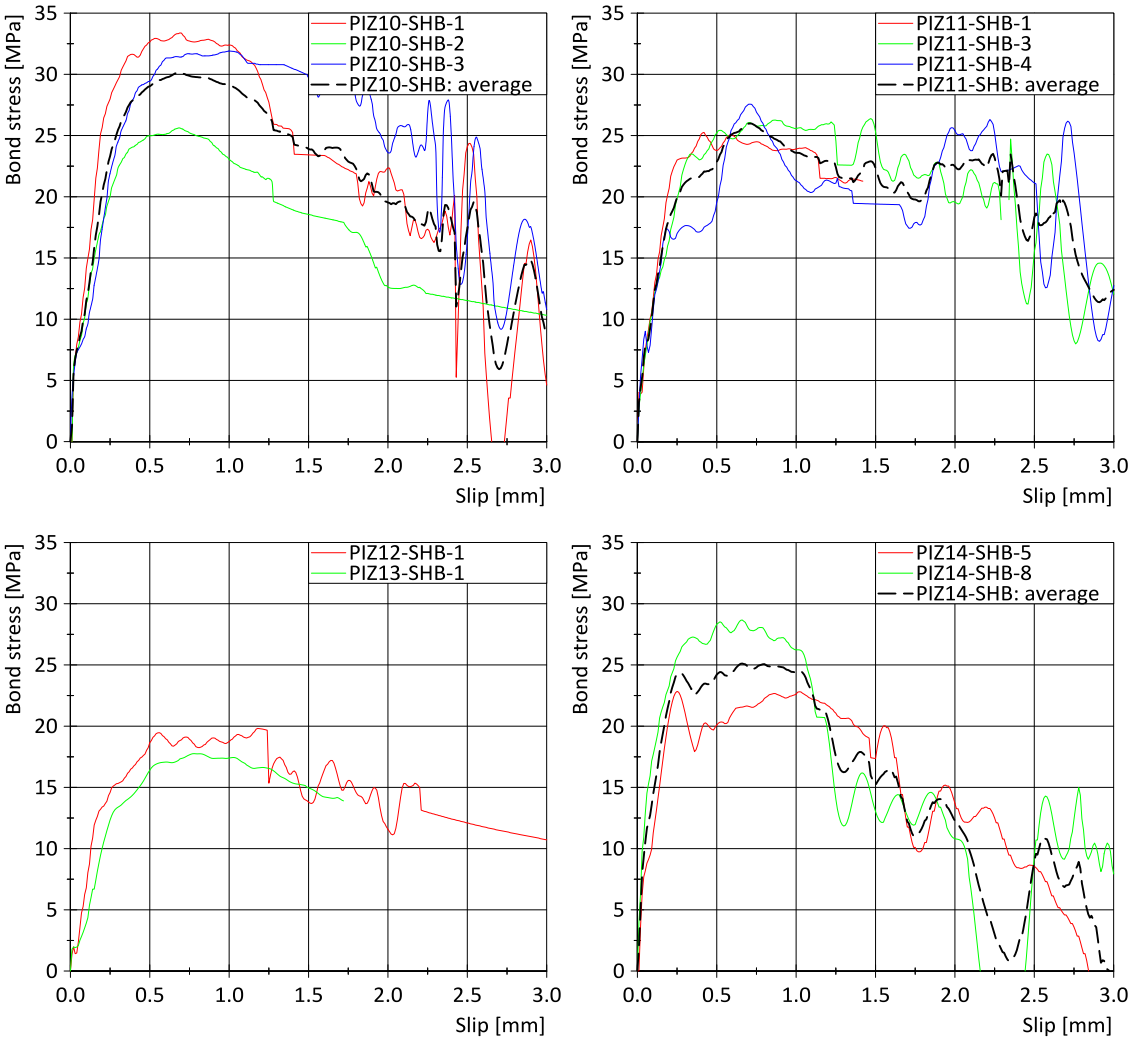

Figure B-4: Bond stress-slip relationships of push-in SHB tests.

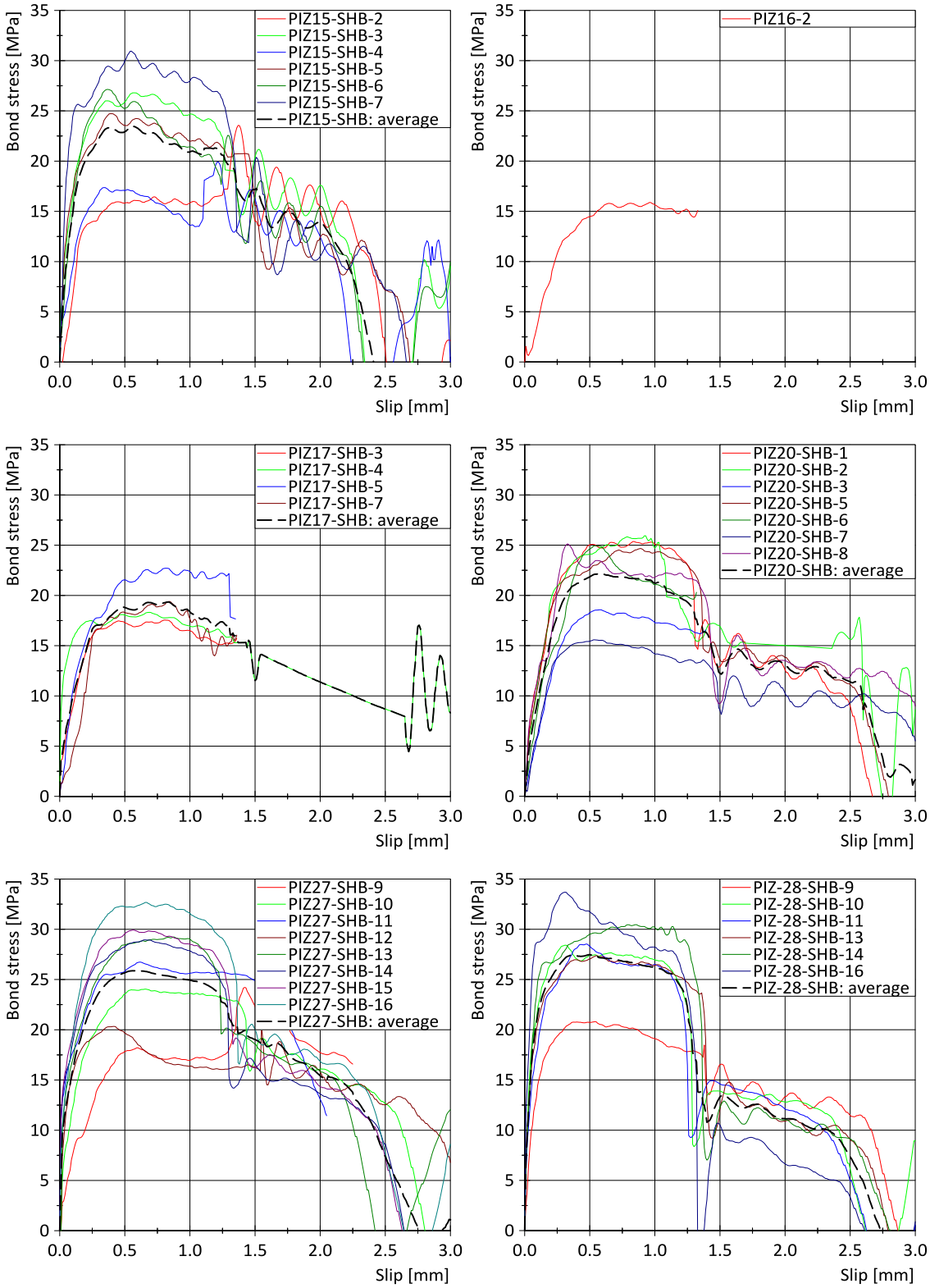

Continuation of Figure B-4: Bond stress-slip relationships of push-in SHB tests.

Table B-5: Results of pull-out quasi-static tests.

Specimen name	$\tau_{0.1}$ [MPa]	τ_{max} [MPa]	s_{max} [MPa]
POZ1-Q-1	14.59	19.05	0.64
POZ1-Q-2	14.50	18.27	0.68
POZ1-Q-3	12.43	15.93	0.40
POZ2-Q-1	14.57	18.43	0.52
POZ2-Q-2	13.15	16.14	0.52
POZ2-Q-3	11.88	15.87	0.49
POZ3-Q-1	6.95	13.33	0.64
POZ3-Q-2	7.87	16.02	0.83
POZ3-Q-3	7.40	13.69	0.56
POZ3-Q-4	9.44	17.07	0.80
POZ4-Q-1	13.23	20.83	0.48
POZ4-Q-2	14.80	20.96	0.52
POZ4-Q-3	12.46	20.03	0.68
POZ4-Q-4	11.40	19.34	0.55
POZ6-Q-1	6.75	16.69	0.53
POZ6-Q-2	6.14	17.41	1.03
POZ6-Q-3	7.01	18.13	1.00
POZ6-Q-4	6.15	16.22	0.80
POZ8-Q-1	12.06	19.45	0.72
POZ8-Q-2	9.88	20.77	0.76
POZ8-Q-3	9.02	16.95	0.45
POZ8-Q-4	10.53	18.30	0.60
Average	10.56	17.68	0.65
St. dev.	3.02	2.13	0.17
COV	29%	12%	26%

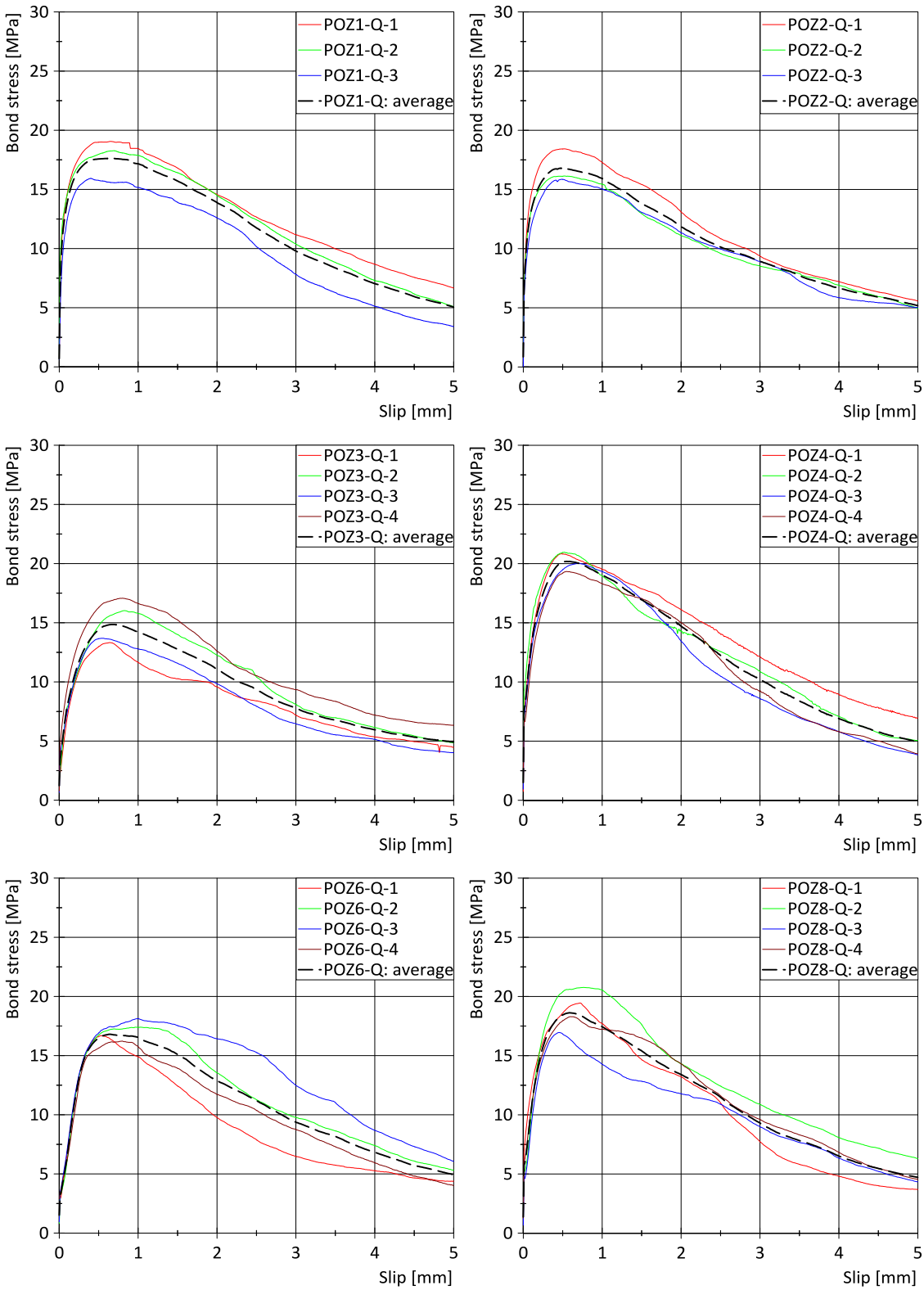

Figure B-5: Bond stress-slip relationships of pull-out quasi-static tests.

Table B-6: Results of pull-out medium loading rate tests.

Specimen name	$\tau_{0.1}$ **[MPa]**	τ_{max} **[MPa]**	s_{max} **[MPa]**
POZ3-M-5	12.32	26.46	0.97
POZ3-M-6	9.09	21.57	0.94
POZ3-M-7	10.60	17.16	0.62
POZ3-M-8	9.33	17.65	1.09
POZ5-M-1	12.68	21.43	0.93
POZ5-M-3	11.53	19.94	1.26
POZ5-M-4	11.34	21.35	0.78
POZ7-M-2	11.68	18.96	0.72
POZ7-M-3	13.25	23.23	0.87
POZ7-M-4	8.92	22.12	0.91
POZ9-M-1	16.10	23.89	0.49
POZ9-M-2	10.82	20.41	1.09
POZ9-M-3	12.07	24.06	0.98
POZ9-M-4	9.71	23.19	0.88
Average	11.39	21.53	0.90
St. dev.	1.93	2.59	0.20
COV	17%	12%	22%

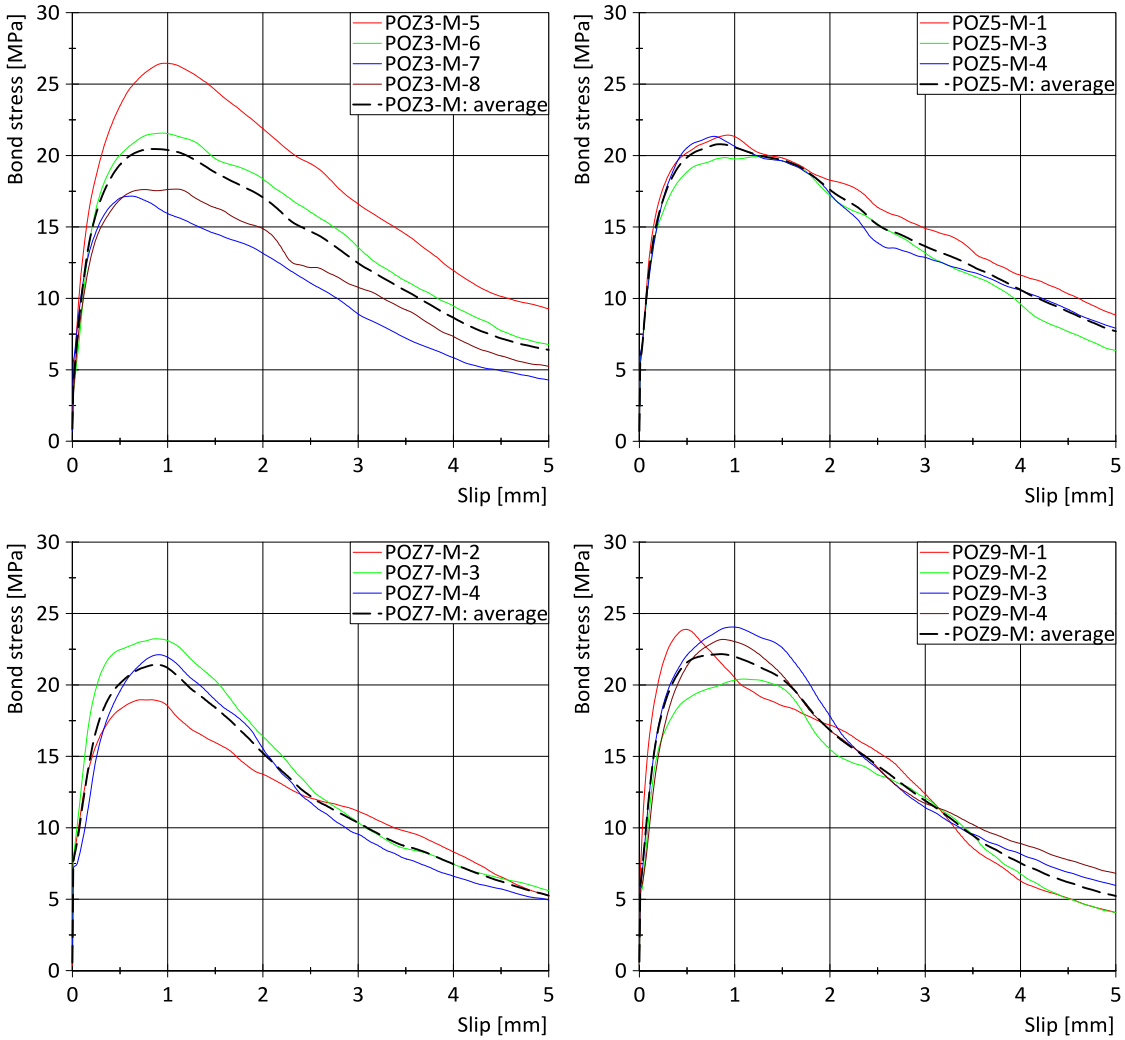

Figure B-6: Bond stress-slip relationships of pull-out medium loading rate tests.

Table B-7: Results of pull-out drop-tower tests.

Specimen name	$\tau_{0.1}$ [MPa]	τ_{max} [MPa]	s_{max} [MPa]
POZ4-F-6	16.54	23.69	0.91
POZ4-F-7	14.19	25.16	1.88
POZ4-F-8	15.00	22.61	0.46
POZ5-F-5	14.16	20.85	0.48
POZ5-F-6	13.40	18.60	0.54
POZ5-F-7	13.81	26.50	0.81
POZ6-F-5	10.48	19.15	0.57
POZ6-F-6	12.71	21.09	0.41
POZ6-F-7	7.53	23.23	0.70
POZ7-F-5	9.87	20.28	1.05
POZ7-F-6	15.09	25.98	1.38
POZ7-F-7	11.94	24.61	0.80
POZ7-F-8	12.21	21.15	0.59
POZ8-F-8	9.32	20.85	0.53
POZ9-F-6	12.27	22.73	0.51
POZ9-F-7	13.20	20.78	0.49
POZ9-F-8	10.57	24.70	0.65
Average	12.49	22.47	0.75
St. dev.	2.34	2.37	0.38
COV	19%	11%	51%

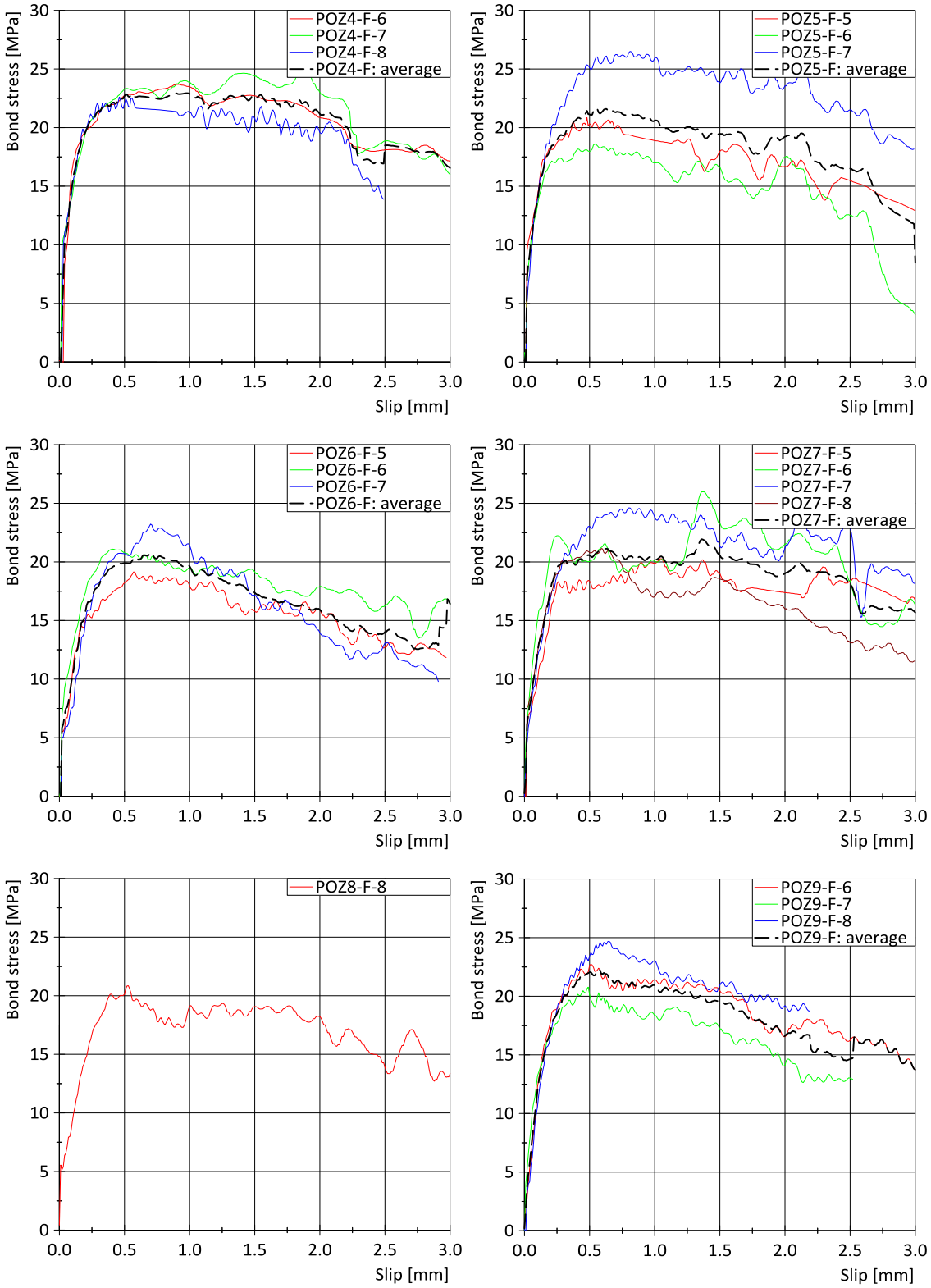

Figure B-7: Bond stress-slip relationships of pull-out drop-tower tests.

C. Used steel

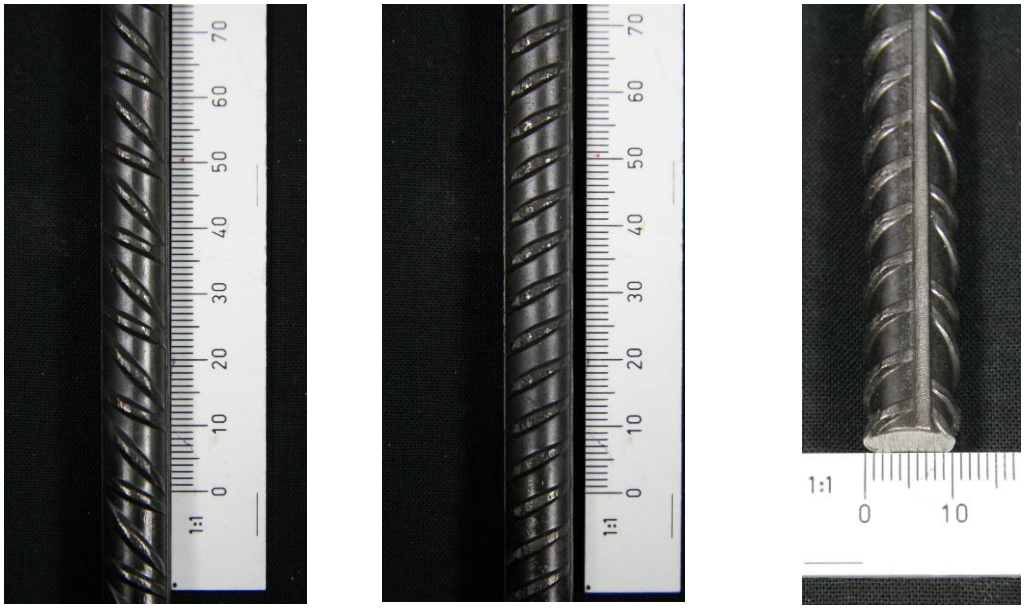

Side 1 Side 2 Longitudinal rib

Figure C-1: Detail of ribs of the used steel: d_s = 10 mm